Process Design and Scale-up of Counter-Current Chromatography for the Fractionation and Recovery of Polyketide Antibiotics

A thesis submitted to the University of London

for the degree of

Doctor of Philosophy

by

Andrew Jason Booth B.Sc (Hons)

Department of Biochemical Engineering, University College London,

Torrington Place, London, WC1E 7JE.

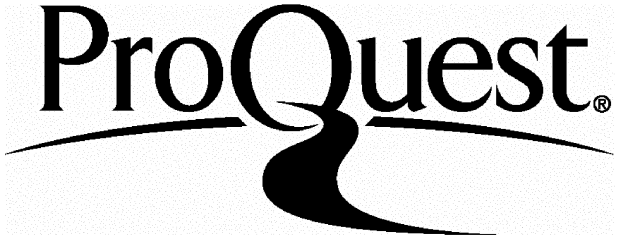

Abstract

Regulatory constraints on products of the modern biotechnology industry require final dosage forms to exhibit high and consistent levels of purity. At the same time, financial constraints on process development require cost-effective purification methods to be found. Counter-current chromatography (CCC) is a liquid-liquid chromatographic technique, in which solutes are fractionated based on their selective partitioning between two immiscible liquid phases. The absence of a solid support, as in conventional HPLC, overcomes problems of irreversible adsorption and pore diffusion, and ensures that CCC is a low pressure operation. Although an established analytical scale technique, widespread use of CCC has been hampered by the lack of generic and robust method development strategies and well-engineered industrial scale machines.

This project has examined the operation and scale-up of novel J-type CCC devices for application as a generic and scalable high-resolution purification technique. The fractionation of the chemical pharmaceutical erythromycin A (EA) from its structurally similar analogues was used as a test system since this provides a difficult and realistic separation challenge. Initial research addressed the need for a generic method development strategy to increase the speed of CCC phase system selection and identification of the optimal run mode. For the purification of EA, a broad polarity quaternary phase system consisting of hexane/ethyl acetate/methanol/water was identified. Results from a matrix of simple equilibrium partition experiments were used to identify a suitable solvent system for use firstly in gradient elution mode. Based on these results, an optimised reverse phase isocratic separation was then selected which enabled the separation of EA from all of its closely related biosynthetic analogues.

Subsequent optimisation studies, using a model erythromycin mixture, addressed the impact of solute loading and mobile phase flow rate on EA purity, column efficiency and throughput in a laboratory scale J-type CCC device. Under optimal conditions (8 $mL.min^{-1}$; 0.6 g solute loading) a maximum throughput of 0.097 $kg.day^{-1}$ could be achieved, with an EA purity and yield of 97% (w/w) and 100% (w/w) respectively. Further research focused on the feasibility of using CCC for the purification of EA from real *Saccharopolyspora erythraea* fermentation broths. Studies here examined the degree of pre-purification required prior to CCC separation. These used feeds consisting of either clarified broth or solvent extracts having undergone either forward or back extraction processes to determine the degree of impurity

removal required to ensure a reproducible elution profile of EA. Further studies using a back extracted feed stream examined the effects of CCC mobile phase flow and solute loading on the attainable EA purity and yield. The results in all cases demonstrated a high attainable EA purity (>97% w/w).

The results for both model and real systems were subsequently scaled-up using a novel, pilot scale CCC machine. From an understanding of the phase system hydrodynamics, a predictive scale-up model of the separation was established, to describe how solute fractionation at the pilot scale varied with changes in operating variables, such as feed type, mobile phase flow rate and solute loading. Linear scale-up was successfully demonstrated with both model and real erythromycin feed streams, based on the parameters taken from a single laboratory scale CCC chromatogram. Scale-up predictions were accurate to within 5-13% (model system) and 6-10% (real system) depending on the actual operating conditions.

Finally, this research explored the successful application of 'Fractionation Diagram theory' as a graphical tool to allow quantification of the trade-off between product purity and solute yield in CCC separations. Combined with a new generation of robust industrial scale machines currently under construction, this work has demonstrated the potential of CCC as a generic and flexible high-resolution separation technique for the modern biotechnology industry.

Acknowledgements

First and foremost I would like to express my gratitude to my supervisor, Dr Gary Lye for providing me with this opportunity to read for a PhD in Biochemical Engineering, and for his continual and invaluable support, guidance, and encouragement throughout my studies.

I would like to thank Dr Les Brown of AECS Ltd for his greatly appreciated assistance in method development and initial familiarisation of the CCC machine used during this study. My thanks also goes out to the research team at the Brunel Institute for Bioengineering for their continued support and expert tutoring on the operation and maintenance of the Brunel CCC machine (the fitting of the quieter motor couldn't have come sooner!!!) and for the loan of the pilot scale coils.

Within the Department of Biochemical Engineering, I would firstly like to thank Drs Andreas Stein, Frank Baganz, and Angela Scholtzovà for their support regarding HPLC analysis, and Billy Doyle for his technical assistance with the fermentations. With regards the application of the Fractionation diagram theory and subsequent result analysis, I would like to express my deepest thank to Dr Sheau-Huey Ngiam. To all my friends in the department and the 'lads' back home, especially Stu, thank you all for your friendship and support!

Finally, to my parents, sis and Donna, thank you all so much for your love and support through all the hard times.

Table of Contents

List of Figures

List of Tables

List of Abbreviations

Å	Anstrom
ACP	Acyl carrier protein
Abs	Absorbance (nm)
AECS	Agricultural and Environmental Services
AT	Acyl-transferase
ATF	Anti-trypanosomal factor
BIB	Brunel Institute for Bioengineering
CCC	Counter-current chromatography
CCD	Countercurrent distribution
CCE	Countercurrent extractor
CER	Carbon dioxide evolution rate
CPC	Coil planet centrifuge
Da	Daltons
DAP	Diaminopimelic acid
DCCC	Droplet counter-current Chromatography
DEBS	6-deoxyerythonylide B synthase
DNA	Deoxyribonucleic acid
DOT	Dissolved oxygen tension
DWC	Dry cell weight
EA	Erythromycin A
EB	Erythromycin B
EC	Erythromycin C
ED	Erythromycin D
EDTA	Ethylenediaminetetraacetic acid
EEA	Enol ether of erythromycin A
EF	Erythromycin F
ELSD	Evaporative light scattering detector
EtOAc	Ethyl acetate
GLCCC	Gyration locular countercurrent chromatography
H_2O	Water
Hex	Hexane
HFTCPC	Horizontal flow-through coil planet centrifuge
HIV	Human immunodeficiency virus
HPLC	High performance liquid chromatography
KS	Ketosynthase
LCCC	Locular countercurrent chromatography
LLC	Liquid-Liquid Chromatography
MeOH	Methanol
MLCPC	Multilayer coil planet centrifuge
MPBV	Mobile phase bed volume
OBM	Oil based media
OLCCC	Oscillation locular countercurrent chromatography
OUR	Oxygen uptake rate
pH	Hydrogen ion concentration
pK_a	$-\log_{10}$ (acid dissociation constant)
PKS	Polyketide Synthase
PLRP-S	Poly(styrene-divinylbenzene)
PPG	Polypropylene glycol

Psu-EEA	Ring-contracted enol ether of erythromycin A
PTFE	Polytetrafluoroethylene
RLCCC	Rotating locular countercurrent chromatography
rpm	Revolutions per minute
RQ	Respiratory quotient
SLPM	Standard litres per minute
SS	Stainless steel
TMIF	Total Mass In Fraction (mg)
UV	Ultra Violet
VTFCPC	Vertical flow-through coil planet centrifuge

Nomenclature

A	Cross-sectional area of the CCC coil
C_{aq}	Solute concentration in the aqueous phase ($mg.mL^{-1}$)
C_m	Solute concentration in the lower mobile phase ($mg.mL^{-1}$)
C_{org}	Solute concentration in the organic phase ($mg.mL^{-1}$)
C_s	Solute concentration in the upper stationary phase ($mg.mL^{-1}$)
d	Internal coil (tubing) diameter (mm)
Δt_m	Variation in t_m between two CCC runs performed at the same mobile phase flow rate (minutes)
EA_{max}	Maximum EA concentration corresponding to the peak maxima ($mg.mL^{-1}$)
F	Mobile phase flow rate ($mL.min^{-1}$)
$F_{m\text{-}actual}$	Square root of actual measured mobile phase flow rate
H	Height equivalent to a theoretical plate (cm/plate)
H_{min}	Minimum height equivalent to a theoretical plate (cm/plate)
i.d.	Internal coil (tubing) diameter (mm)
K	Distribution ratio
K_{EA}	Distribution ratio of erythromycin A
$K_{EB/psu\text{-}EEA}$	Distribution ratio of erythromycin B/psu-EEA
$K_{EC/ED}$	Distribution ratio of erythromycin C/D
k	Retention factor
k_{EA}	Retention factor of erythromycin A
$k_{EB/psu\text{-}EEA}$	Retention factor of erythromycin B/psu-EEA
$k_{EC/ED}$	Retention factor of erythromycin C/D
L	Coil length (cm)
M_{Ai}	Concentration of impurity, A, in a specific collected fraction at the *i*-th time interval ($mg.mL^{-1}$)
M_{Bi}	Concentration of impurity, B, in a specific collected fraction at the *i*-th time interval ($mg.mL^{-1}$)
M_o	Initial target solute concentration in the feed ($mg.mL^{-1}$)
M_{Pi}	Concentration of target product, P, in a specific collected fraction at the *i*-th time interval ($mg.mL^{-1}$)
M_s	Amount of sample target solute injected ($mg.mL^{-1}$)
M_{Ti}	Total concentration of all solutes in a particular fraction at the *i*-th time interval ($mg.mL^{-1}$)
N	Column efficiency (theoretical plate number)
N_{eff}	Effective theoretical plate number
N_{op}	Number of operational CCC runs achievable per day (24 hours)
o.d.	Outer coil (tubing) diameter (mm)
P'	Rohrschneider solvent polarity parameter
PF	Purification factor
PF_{max}	Maximum purification factor
$PurEA_{final}$	Purity of EA in fractions collected after processing by CCC
Q_m	Number of molecules of a solute in the mobile phase per unit volume (mg)
Q_r	Mass of recovered erythromycin (mg)
Q_s	Number of molecules of a solute in the stationary phase per unit volume (mg)
r_i	Inner coil radius (mm)
r_o	Outer coil radius (mm)
R	Rotor radius (mm)

R_s	Resolution (measure of zone overlap between two adjacent solute peaks)
S_f	Stationary phase retention within the CCC coil (% v/v)
t_c	Time from sample injection to elution of the K=1 peak (minutes)
t_c'	Time from solvent front to elution of the K = 1 peak (minutes)
t_k	Retention time of peak (K) of interest from sample injection (minutes)
t_k'	Time from solvent front to elution of K peak (minutes)
$t_{k\text{-anal}}$	Elution time of the peak of interest from an analytical scale CCC sample volume experiment (minutes)
$t_{k\text{-start}}$	Beginning of elution of a peak with a distribution ratio of K (minutes)
$t_{k\text{-end}}$	End of elution of a peak with a distribution ratio of K (minutes)
t_i	Time for injection of solute of known volume at a set mobile phase flow rate ($mL.min^{-1}$)
t_m	Time from sample injection to the solvent front (K = 0) (minutes)
TMIF	Total mass of erythromycins in a collected fraction (mg)
t_R	Retention time for a peak of interest from sample injection
$\bar{u}$	Average linear mobile phase velocity ($cm.s^{-1}$)
V_c	System volume (mL)
V_c	Volume of eluted stationary phase volume originally in the coil that has been displaced by the mobile phase during phase equilibrium (mL)
$V_{c\text{-corrected}}$	Corrected volume of eluted stationary phase obtained by subtracting the volumes of the inlet (V_{in}) and outlet (V_{out}) flying leads (mL)
V_i	Solute injection volume (mL)
V_{in}	Volume of the coil inlet flying lead (mL)
V_m	Mobile phase volume within the CCC coil (mL)
V_{out}	Volume of the coil outlet flying lead (mL)
V_R	Retention volume for a peak
V_s	Stationary phase volume within the CCC coil (mL)
$V_{s\text{-start}}$	Recorded volume of stationary phase in the graduated measuring cylinder prior to hydrodynamic equilibrium (mL).
$V_{s\text{-end}}$	Recorded volume of stationary phase in the graduated measuring cylinder after hydrodynamic equilibrium (mL).
w_B, w_A	Baseline bandwidth of two adjacent peaks, B and A (minutes or cm)
$W_{h/2}$	Peak width at one half the peak height
w_k	Width of a peak with a distribution ratio K (minutes)

Greek Symbols

α	Separation factor
β-ratio	Ratio of inner (r_i) or outer (r_o) coil radius to the rotor (R) radius
μ_u μ_l	Viscosity of upper and lower phases (cP)
ρ_u ρ_l	Density of upper and lower phases ($kg.m^{-3}$)
σ_s	Interfacial tension ($mN.m^{-1}$)
σ	Standard deviation of the Gaussian peak
Φ	Volume fraction of pure solvent
ω	Rotational speed of the bobbins (rpm)

1. Introduction

1.1. Taxonomy

1.1.1. Actinomycetes

Actinomycetes are among the most widely distributed groups of micro-organisms, with the members of this extensive class considered as chemo-organotrophs, requiring a form of organic carbon for growth. The extent of their growth on an artificial medium is regulated by the availability of oxygen, inorganic nitrogen source, other additional nutrients and an approximately neutral pH (Gusek and Kinsella, 1992). Until thirty years ago, there was not a clear consensus as to the classification of actinomycetes. Bacteriologists considered them to be bacteria due to the presence of elongated cells or filaments exhibiting some degree of branching (Goodfellow *et al.*, 1983), while mycologists classified them as fungi due to characteristics such as their growth on a solid substrate. Nowadays, actinomycetes are generally accepted as bacteria, more specifically gram positive, sporalating, saprohytic bacteria (Goodfellow *et al.*, 1988). A common feature of this class is hyphae formation during growth. These hyphae, consisting of numerous tubular cells, obtain nutrients required for growth and replication by solubilising the organic media via the secretion of hydrolytic enzymes. It is this morphology that plays a crucial role in antibiotic production, with many factors, such as the species strain, growth media and conditions influencing product titers. Actinomycetes, therefore potentially exhibit a wide range of morphological structures from simple rods and cocci to complex mycelia (Goodfellow *et al.*, 1983), with the stuctures changing due to variations in their environment, from cell growth, through to primary and secondary metabolism, where the production of bioactive metabolites occurs.

1.1.2. Streptomyces

Streptomyces are members of the family streptomycetaceaes and are considered to be the most common Gram-positive bacteria, belonging to the order of Actinomycetales.

They are abundant in soil, degrading a variety of organic materials with the ability to produce numerous bioactive products, such as antibiotics, vitamins, enzymes and immuno-suppressors (Gilbert *et al.*, 1995). This classifies them among the most industrially important micro-organisms (Gilbert *et al.*, 1995). Specifically, in the context of this study, 60% of all microbially produced antibiotics (Table 1-1) are produced from Streptomyces (Queener *et al.*, 1986).

Strain	Antibiotic	Antibiotic group
Streptomyces aureofaciens	Chlorotetracycline	Tetracyclines
Streptomyces rimosus	Oxytetracycline	
Streptomyces griseus	Streptomycins	Aminoglycosides
Streptomyces fradiae	Neomycin & Tylosin	
Streptomyces kanamycetius	Kanamycin	
Streptomyces clavuligerus	Clavams	β-lactams
Streptomyces venezuelae	Chloramphenicol	Chloramphenicols
Streptomyces ambofaciens	Spiramcin	Macrolides
Streptomyces narbonensis	Narbomycin	

Table 1-1 Antibiotics produced by Streptomyces (from Queener *et al.*, 1986).

1.1.3. *Saccharopolyspora erythraea*

Saccharopolyspora erythraea, was first discovered in 1952 in a soil sample from Iloiol City in the Philippines, with the wild type strain known as NRRL 2338 (Northern Utilisation Research and Development Division, US Department of Agriculture). Prior to its reclassification (Labeda, 1987), it was originally known as *Streptomyces erythreus*. The reason for its reclassification was due to the differences in the cell wall structure. The Streptomyces possess a type-I cell wall (Holt *et al.*, 1994), containing L-diaminopimelic acid (DAP) and mycolic acids, whereas the *Saccharopolyspora* genus possess a type IV cell wall (Holt *et al.*, 1994) containing meso-DAP and no mycolic acids. One of the most abundant secondary microbial products of the *Saccharopolyspora* fermentations is the macrolide class of antibiotics, whose biosynthesis and structural classification is discussed later in Sections 1.1.4 and 1.1.6.

1.1.4. Biosynthesis of both natural and recombinant polyketides

The formation of polyketides, such as erythromycin, occurs by the sequential activity of a number of enzymes and carrier proteins, collectively termed polyketide synthase or PKSs. These giant (> 300kDa) modular multi-enzyme complexes are multifunctional proteins, possessing different active sites, or modules for each successive step of polyketide chain assembly. The PKSs contains six of these modules, which can be segregated from the amino to the carboxylic termini into a loading domain, four modules, and finally a releasing domain, as illustrated in Figure 1-1.

The loading domain of the PKS consists of the enzyme acyl-transferase (AT) and an acyl carrier protein (ACP). The intermediate modules are responsible for the extension of the polyketide chain and contain a ketosynthase (KS), AT and ACP. Finally the off-loading domain contains a thioesterase that also possess a degree of cyclase activity and acts by thiolysis or acyltransfer. In this biosynthetic process, the PKSs not only contain the numerous required active sites for synthesis, but also acts as the platform for it. As shown in Figure 1-2, the polyketide chain traverses each module, where it increases in length by two carbon atoms whilst being covalently attached to the enzyme as a thiol ester. Each module contains the minimum set of domains required for the formation of carbon-carbon bonds, and therefore the number of modules present dictates the size of the polyketide.

In addition to the presence of domains dedicated to the formation of the carbon-carbon bonds, additional domains are present, performing the function of encoding the oxidation state of the β-carbon of each two-carbon unit. Together with this, modules can contain up to three addition enzymes, modifying the resulting β-keto group following each cycle of chain elongation prior to its transfer to the next module. From this arises the concept that the structure of the polyketide is dependent on the order in which the various modules are arranged along the PKS. Together with the specificity of the enzyme, AT, and the presence of these β-modified enzymes, the order of these domains within modules, modifying the structure of the polyketide produces a diverse range of both polyketide chains and recombinant polyketide products.

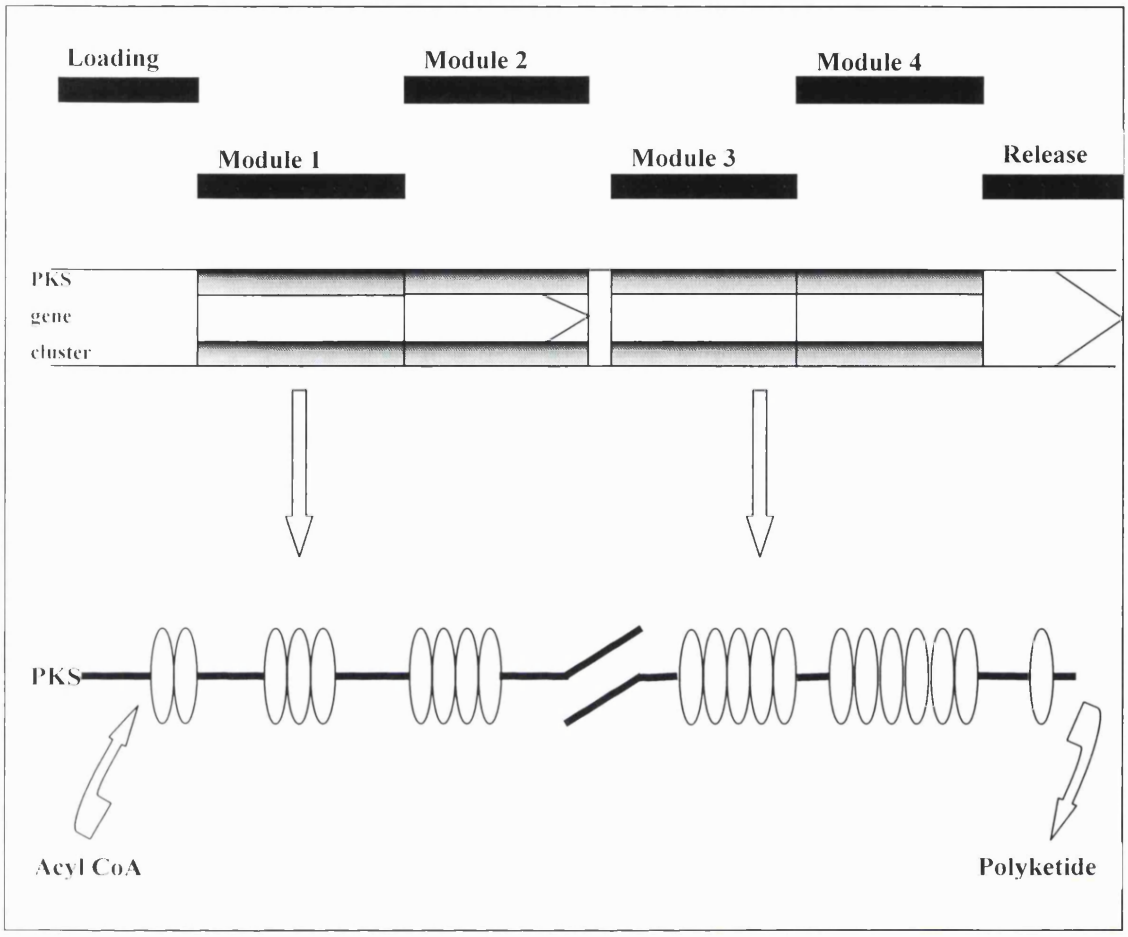

Figure 1-1 Illustration of the modular PKS gene cluster and enzyme assembly (redrawn from Carreras and Santi, 1998).

Manipulation of the polyketide chain length, as developed by Kao *et al.* (1994), uses a plasmid-based expression system for 6-deoxyerythonylide B synthase (DEBS) in *Streptomyces coelicolor*. As a result of this research, truncated PKSs were generated by the deletion of modules late in the biosynthetic pathway by the use of the natural thioesterase, resulting in the production of novel triketide, tetraketide and hexaketide lactones from 2-, 3- and 5-module derivatives of DEBS, respectively. An example of the structural form of the triketide lactone can be seen in Figure 1-3, where truncation by the thioesterase occurs at the point between modules two and three (Figure 1-2).

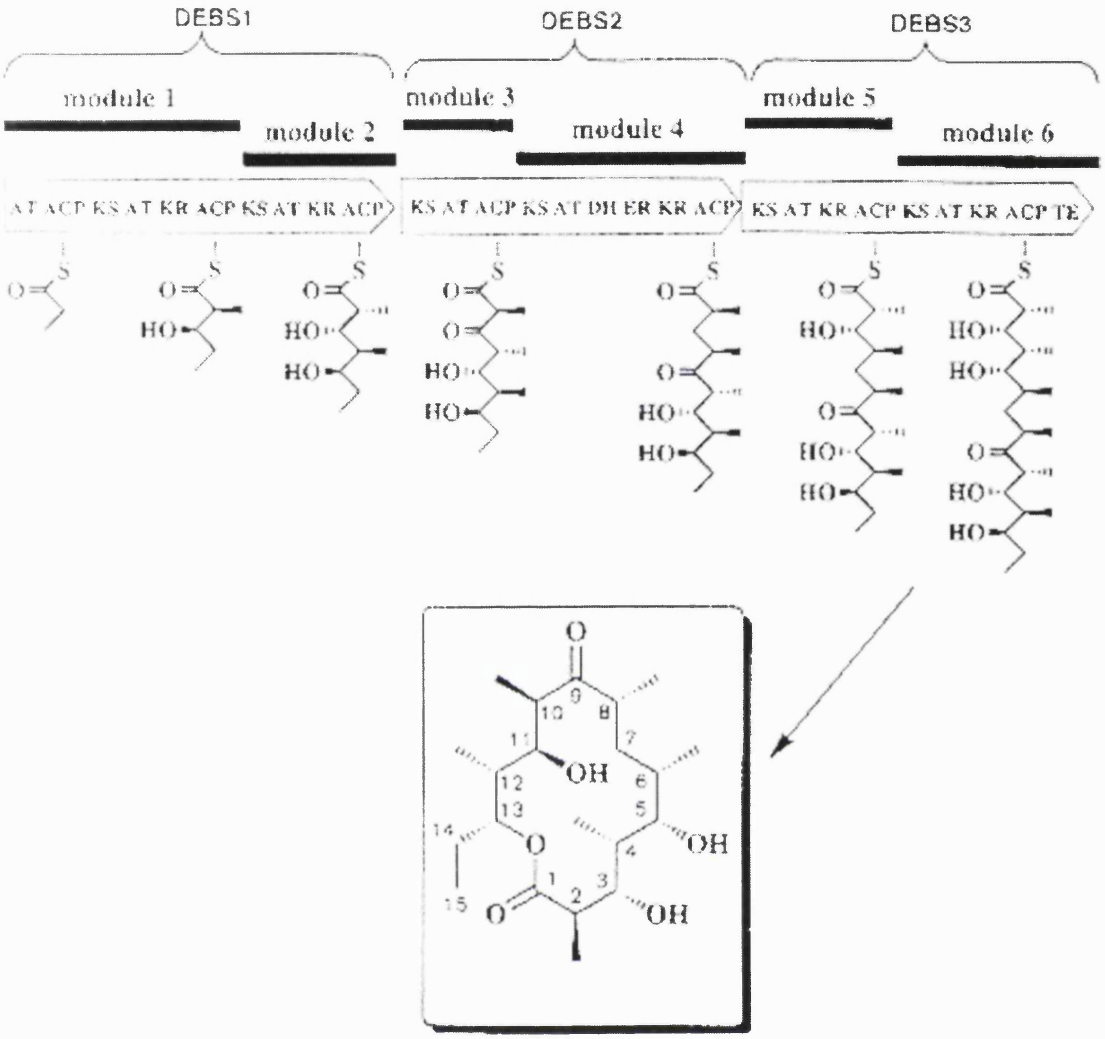

Figure 1-2 **Illustration of the PKS template which catalyses the biosynthesis of the erythromycin aglycone (Carreras and Santi, 1998).**

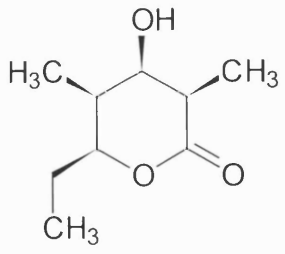

Figure 1-3 **Structure of a recombinant polyketide (triketide lactone).**

1.1.5. Macrolide Antibiotics

The macrolide antibiotics are a diverse range of compounds which include erythromycin, oleandomycin, leucomycin (kitasamycin), spiramycin, midecamycin and tylosin. The first reported macrolide antibiotic was pikromycin (Brockmann and Henkel, 1950), then erythromycin (McGuire *et al.*, 1952), leucomycin (Hata *et al.*, 1953), spiramycin (Pinnert-Sindico *et al.*, 1954), and oleandomycin (Sobin *et al.*, 1955). These macrolides are members of a large and diverse range of natural compounds called polyketides, which include aromatic, polyether and macrolactone compounds. Of these antibiotics, erythromycin was the first commercially produced antibiotic, with annual figures for the production of polyketides in the region of 2000 tonnes (Schuler, 1987). The market value of these microbial secondary metabolites has exceeded annual sales of $10 billion (Carreras & Santi, 1998). The production of erythromycin, its structure and function is described in the sections to follow.

1.1.6. Erythromycin

1.1.6.1. The structure of erythromycin

Clinically useful macrolide antibiotics are classified into three distinct groups based on the size of the macrocyclic lactone ring, i.e. containing 14, 15, or 16 membered rings with sugars linked via glycosidic bonds (Elks and Ganellin, 1991). Within the 14-membered group, erythromycin is one of the most industrially important compounds. Structurally, this class of antibiotic can be characterised by 1) large lactone rings, 2) keto groups and 3) amino sugars in glycosidic linkages as shown in Figure 1-4.

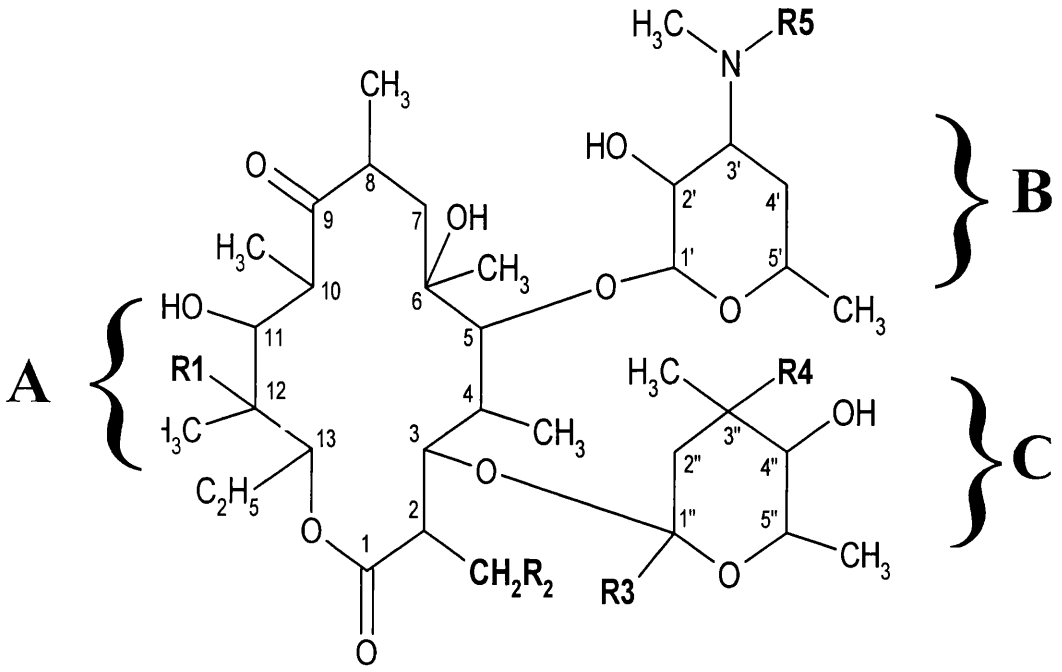

Figure 1-4 **Structure of erythromycin. Section (A) corresponds to the 14-membered lactone ring. (B) corresponds to the amino sugar moiety (*D*-desosamine). (C) corresponds to the secondary sugar *L*-caladinose. R_x represents specific points on the molecule where the erythromycin analogues vary, as illustrated in Table 1-2.**

The large polyhydroxylactone ring of erythromycin, illustrated in Figure 1-4 (A) has, in addition to it one or more sugar residues substituted into the ring (Figure 1-4 (B) and 1-4 (C)). These sugar residues can also, with the addition of a nitrogen atom, take the form of an amino sugar moiety (*D*-desosamine), as illustrated in Figure 1-4 (B). The fermentation process for erythromycin manufacture results in the formation of small quantities of erythromycins B (EB), C (EC), D (ED), E (EE) and F (EF) in addition to EA (Kanfer *et al.*, 1998). In commercially produced erythromycin preparations there are also small quantities of both acid and basic degradation products derived from erythromycin A, namely the enol ether of erythromycin A (EEA) and the ring-contracted enol ether of erythromycin A (Psu-EEA) respectively (Kanfer *et al.*, 1998).

All of these analogues of erythromycin possess the *D*-desosamine ring, but vary at specific points on the erythromycin molecule, labelled as R_1 to R_5 in Figure 1-4. Table 1-2 illustrates the structural variations that exist between the different forms of erythromycin.

As can be seen from Table 1-2, the erythromycin analogues are structurally and chemically very similar, differing in some cases by only a single hydroxyl or methyl group. The biosynthetic pathway leading to the production of erythromycin A and its analogues is shown in Figure 1-5.

	R_1	R_2	R_3	R_4	R_5	**Molecular formula**	**Mw**
Erythromycin A (EA)	OH	H	H	OCH_3	CH_3	$C_{37}H_{67}NO_{13}$	734
Erythromycin B (EB)	H	H	H	OCH_3	CH_3	$C_{37}H_{67}NO_{12}$	718
Erythromycin C (EC)	OH	H	H	OH	CH_3	$C_{37}H_{65}NO_{13}$	720
Erythromycin D (ED)	H	H	H	OH	CH_3	$C_{37}H_{67}NO_{14}$	750

Table 1-2 Structural variations of the erythromycins (from Kanfer *et al.*, 1998).

1.1.6.2. Properties of erythromycin and its mode of action.

Erythromycin A, with the empirical formula: $C_{37}H_{67}NO_{13}$ has a molecular weight of 734 Da, and a maximum UV absorbance at 278 nm. It is slightly soluble in water, but more soluble in organic solvents and has a pK_a of 8.8, with its basic character conferred through the D-desosamine sugar moiety (Kanfer *et al.*, 1998). Maximum stability is in the pH range 6–9.5 (Kavanagh and Dennin, 1963), with it losing its biological activity at a pH<5 (Hahn, 1967). The erythromycins are bacteriostatic agents whose biological activity is dependent on intracellular accretion and ribosome binding. More specifically, the erythromycins act by binding to the 50S ribosomal subunit and stimulate dissociation of peptidyl-tRNA from the ribosome during the translocation process (Brisson-Noel *et al.*, 1988). Gram-positive bacteria are more sensitive to erythromycin A than Gram-negative forms. This is due to the Gram-positive forms accumulating greater intracellular levels of the antibiotic.

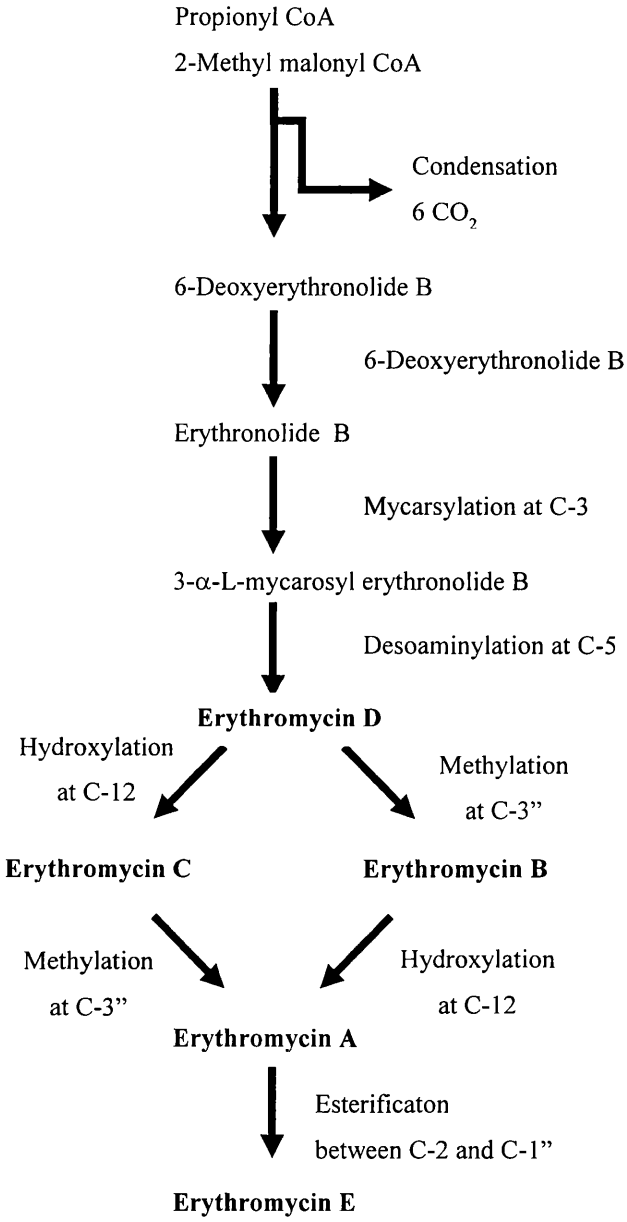

Figure 1-5 Biosysnthesis of the various forms of erythromycin analogues.

1.1.6.3. Clinical uses of erythromycin

Erythromycin, as with other macrolides is very effective against Gram-positive bacteria, in particular staphylococci, and mycoplasmas. Other clinical applications of erythromycin include:

1) Active against *Legionella* species.
2) Active against *Campylobacter* species.
3) A useful substitute for penicillin and flucloxacillin in hypersensitive patients (e.g. upper respiratory, skin and soft tissue infections).
4) Clinically useful against atypical pneumonia, severe Campylobacter infections, non-gonococcal genital infections.
5) Erythromycin is the antibiotic of choice for diphtheria.
6) As a combined treatment for HIV.

1.1.6.4. Industrial production of erythromycin.

This section aims to outline the industrial production by fermentation and the downstream recovery and purification operations of the target product. The industrial production of natural products, such as antibiotics incorporates a number of unit operations, from the fermentation, with its continual optimisation, through to recovery from initial clarification of the whole broth, primary extraction/concentration by the technique of liquid-liquid partitioning, and finally drying and formulation.

1.1.6.4.1. Fermentation

In the production of secondary metabolites the first stage involves the growth of the selected strain of micro-organism, specifically *Sacchropolyspora erythraea.* At this point, upon the addition of the inoculum to the fermenter, the process can last for anything up to seven days, with the continuous or intermittent addition of extra nutrients, chemical precursors, acid or alkali to maintain a successful level of microbial growth within the operational constraints of the process, such as pH, OUR, DOT or

temperature. As already discussed in Section 1.1, *Sacchropolyspora erythraea* possesses a distinctive morphological feature of forming branched filaments, or hyphae.

Requirement	Source
Carbon	Glucose, sucrose, starch, molasses, soya bean oil, rapeseed oil, animal fats
Nitrogen	Soya meal, blood meal, corn steep liquor, casein, yeast extract, meat extract
Inorganics	Calcium salts, ammonium salts, Sulphides, phosphorus salts, trace elements
Antifoam	Polypropylene glycol (PPG)

Table 1-3 Source(s) of nutrient and antifoam requirements for the fermentation

Research within our laboratories studies the optimisation of erythromycin production using both soluble complex media (SCM) and a more industrially relevant oil based media (OBM), in addition to the interactions of the fermentation with initial product recovery by microfiltration (Davies *et al.*, 2000). The filtered fermentation broth used during this study was produced using the soluble complex medium formulation (Table 2-1).

During the final fermentation phase, the biosynthesised product will either be associated with the microbial cells, or in solution. In the case of erythromycin, the latter process occurs. The resultant fermentation broth, the 'whole broth', is composed of the biomass in a dilute aqueous solution containing unused nutrients, undefined impurities such as unwanted metabolites, surfactants (antifoaming agents) and the target product. The typical constituents of an antibiotic fermentation broth are shown below in Table 1-4.

Broth constituent	% by weight
Water	75-95
Cells	2-6
Product	0-10
Residual raw materials	1-5
Proteins /polysaccharides	0-5

Table 1-4 Typical constituents of a harvested antibiotic fermentation broth (Carrington, 1986).

During the course of process development and continual process optimisation, with the aim being to increase the product titers and reduce media costs, the fermentation scientist will be continually modifying the fermentation media formulations. These modifications can be in the form of the chosen carbon or nitrogen sources (Table 1-3) and their relative amounts. However, the effects of these media changes on subsequent downstream processing operations are rarely considered, with the result of this being that any increase in product titre can be compromised by product loss during recovery operations (Davies *et al.*, 2000). The main objective of downstream processing is to successfully recovery the target product from the initial fermentation broth at an acceptable purity and yield. This objective can be considered as a number of stages; cell removal, product concentration, purification and finally isolation.

1.1.6.5. Primary recovery

This section aims to give an overview of the primary recovery steps employed by industry and their relative merits. The harvested broth from a fermentation process can be considered to consist of a number of phases, namely the continuous-aqueous and solid-medium phases, consisting of the microbial cells, residual raw materials such as soya bean flour and insoluble organic elements e.g. oil. As the erythromycin is produced extracellularly, there is no need for prior cell disruption techniques such as homogenisation to be employed. The first step is to condition the broth by either acidification or the addition of flocculation aids to remove cells. Acidification further assists in preparing the product in a form suitable for solvent extraction. There are then a number of unit operations for mycelia removal, such as:

1) **Filtration**
    a. Rotary drum vacuum filters – robust, reliable and can handle a wide range of broths. However, the addition of the filter aid may cause problems with downstream equipment, e.g. pumps.
    b. Cross flow filtration – enables complete removal of suspended solids.

2) **Solvent extraction**
    a. Whole broth extraction – enables significant volume reduction and process integration by removing the upstream solids removal process.
    b. Clarified filtrate solvent extraction – eliminates problems of emulsion formation with whole broth (2a).

3) **Ultrafiltration** – smaller pore sizes could enable greater product selectivity, hence enable a larger volume reduction and a more clarified broth.

4) **Adsorption** – combines cell separation, volume reduction and a degree of purification in one step. However, fouling of the adsorbent is a major issue at this early stage in the process.

1.1.6.6. Purification

Following cell removal, there are a number of unit operations available. Their relative merits are discussed below:

1. **Precipitation**. This operation is composed of three distinct stages, precipitation, filtration and then drying. It can only be applied to the isolation of compounds that form highly insoluble salts or complexes. This purification technique is an economic means of product recovery, but the final product can often be rather crude, hence a low achievable product purity.

2. **Crystallisation**. Achieves higher degrees of product purity than precipitation, with the separation achieved by the formation of crystal structures. The advantages of this technique are its low start-up and operational costs, important factors for large volume antibiotic production.

3. **High performance liquid chromatography (HPLC).** Reverse phase HPLC has demonstrated its ability to successfully resolve the erythromycin analogues at the analytical scale (Paesen *et al.,* 1994). Large scale separation of erythromycin has been extensively studied in our laboratories with the application of the Prochrom preparative chromatography column (Champigneulles, France), investigating the effects of injection volume and mobile phase flow rate on the achievable separation and column efficiency (Scholtzová, 2000).

1.1.6.7. Drying

For the production of pharmaceuticals such as antibiotics, drying is used as a means of processing heat labile formulations under aseptic conditions to remove excess water, ensuring minimal loss in viability or activity. Different types of drying processes can be utilised with the main technique briefly described below (discussed in detail by Coulson and Richardson, 1991):

Spray drying. Produces a powder by firstly atomizing the liquid into small droplets and then contacting them with a steam heated drum (drum drier) or directly with an upward spiralling stream of hot gas (counter-current spray drier). As a result of the atomisation of the liquid, the high area:volume ratio results in a rapid evaporation rate. The counter-current spray drier is the most economical method for drying large volumes.

1.2. Theoretical aspects and the development of CCC

1.2.1. Introduction

Counter-current chromatography (CCC) is a form of liquid-liquid chromatography, bridging the gap between equilibrium counter-current distribution (CCD) and conventional liquid-liquid chromatography (LLC) (Conway, 1990). The principle of chromatography in CCC is analogous to LLC, in that the separation of molecules is

based on their selective partitioning between two immiscible liquid phases (Conway, 1990). Where these techniques differ is in the mechanism by which one of the liquid phases is retained in the column. In conventional LLC the chosen 'stationary' phase is retained in the column by immobilising it on the surface of solid porous packing material. In CCC, which for this particular study employed a rotating coil, adequate retention of the chosen stationary phase is achieved by rotating the coil to develop the required 'g' fields. The development of CCC machines, in terms of their design, through a greater understanding of the solvent system hydrodynamics within the coil, has focused on maximising the volume of stationary phase retention, termed S_f, to optimise the chromatographic separation, i.e. the resolution. The aims of this section are to firstly explain the principles behind liquid two-phase distribution in a rotating coil under both unit gravity and an applied centrifugal force. In addition, the further development of both coil configurations, and a greater theoretical understanding of phase system hydrodynamics have enabled rapid, high-resolution chromatographic separations to be achieved. This section will therefore in addition focus on the design and operation of CCC machines.

The observations of the applied solvent system hydrodynamics that occur as a result of the coil motion generated when using this J-type rotational configuration (Ito, 1991) will be examined in terms of:

- Hypotheses that have been developed and experimentally verified to describe hydrodynamic distribution, specifically the mechanisms by which both stationary phase retention and phase mixing are achieved.

- The effects of physico-chemical properties of biphasic systems on stationary phase retention. This will identify the optimal choice of operational conditions, i.e. directions of both column rotation and mobile phase pumping, in order to achieve the most satisfactory degree of stationary retention.

1.2.2. Phase distribution within a spirally wound coil

Since the 1970s, a great deal of pioneering work has been performed by Ito (1991), both in the development of novel coil and rotational configurations, as discussed in Section 1.2.2, but also in the development of hypotheses describing the mechanisms of phase distribution. The first experimental observations by Ito using a sealed helical coil containing equal volumes of two immiscible 'heavy' and 'light' solvents, were that, when rotated clockwise in a unit gravitational field, both phases travelled through the coil in the same direction, establishing a hydrodynamic distribution in each coil turn. Figure 1-6 illustrates this phenomenon, with the light and heavy solvent phases depicted by a bubble and bead respectively. Due to the gravitational force, the light and heavy phases in any helical turn occupy the outer and inner portions respectively.

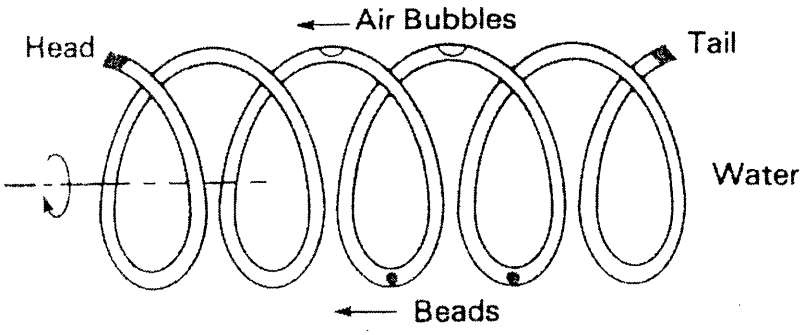

Figure 1-6 Illustration of the Archimedean screw principle in a helical coil. Light and heavy phases are depicted by air bubbles and beads respectively. Both solvent phases have a tendancy to move in the same direction towards the 'head' of the coil (Ito, 1992).

As can be seen (Figure 1-6) both phases competitively move towards the 'Head' of the coil, with the other end labelled as the 'Tail'. Ito then generalised his experimental observations into two categories to describe phase distribution patterns (Ito, 1992):

1) **Unilateral hydrodynamic equilibrium** – here both phases are distributed along the length of the coil, so that one phase occupies the head and the other the tail in an approximately 50:50 ratio.

2) **Uniform radial distribution** – here both phase are uniformly distributed along the length of the coil occupying at each helical turn equal volumes.

Two phase distribution data presented by Ito (1992) showed that for a range of solvent systems the effects of further increases in rotational speed (100 - 400 rpm) resulted in the phases moving from a unilateral configuration (Figure 1-7 (B)), to one in which, due to the stronger generated radial forces, there was an even distribution of both solvent phases throughout the length of the coil. As a result the heavier and lighter phases occupy the outer and inner portions of the coil respectively (Figure 1-7 (C)).

Berthod (1991) also studied the effects of increased rotational speed on phase volume distribution, finding a critical rotational speed (60-100 rpm) where the immiscible solvents are completely separated along the coil length.

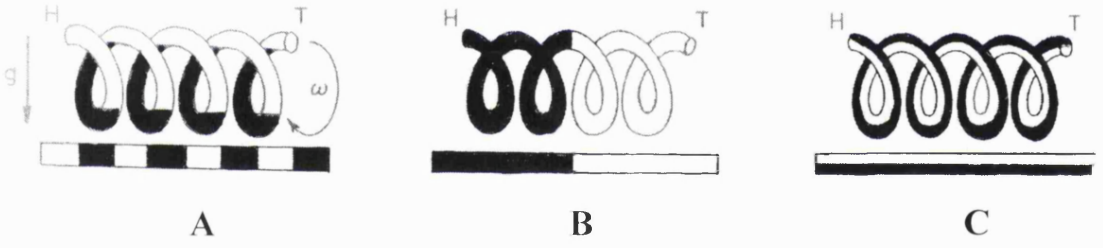

Figure 1-7 **Representation of the variation in the distribution of the heavy (▬) and light (▭) solvent phases within a helically wound coil. (A) slow rotation (10 rpm) illustrating Archimedean distribution. (B) intermediate rotation (10 – 160 rpm) illustrating unilateral distribution. (C) high rotation (~300 rpm) where uniform, radial distribution is achieved. H = 'Head' of coil; T = 'Tail' of coil (Conway, 1990).**

1.2.3. Hydrodynamic phase distribution within a flow through coil

The application of the simple CCC system as described in Section 1.2.2, had the disadvantage, due to the low Archimedean screw forces generated under gravity, of a low degree of stationary phase retention. As a result, long processing times and lack of sufficient resolution rendered these devices unsuitable for use.

Ito (1992) postulated that, by applying a centrifugal force to the helically wound coil, the tangential force component, responsible for generating the Archimedean screw effect, would act against the radial forces to generate a hydrostatic phase distribution. This finding led to the development of a series of synchronous devices, which, as illustrated in Figure 1-8, involved orientating the column (the holder around which the length of coil is wound) to achieve a high degree of stationary phase retention.

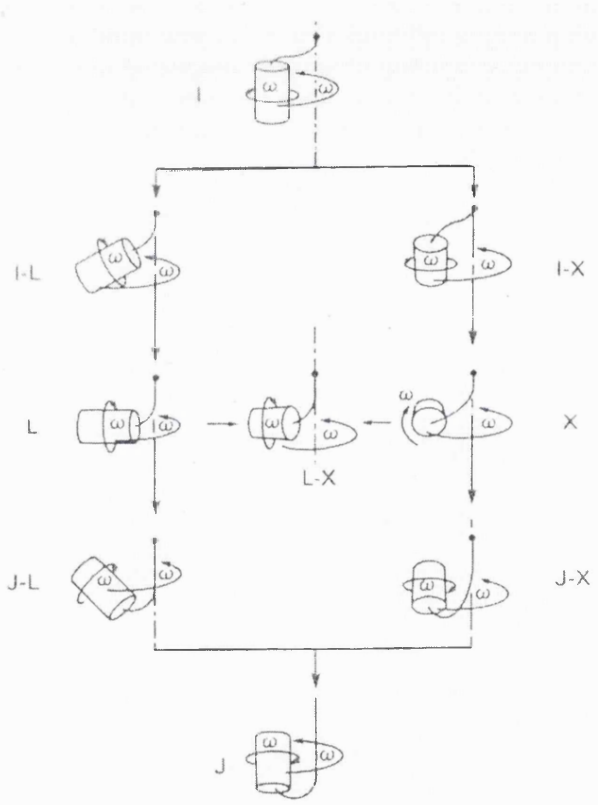

Figure 1-8 Schematic representation of various coil orientations investigated by Ito. Each diagram illustrates the motion of coil holder in relation to the direction of the centre of revolution (Ito, 1996).

The two typical configurations were the Type I and J designs. As can be seen from Figure 1-9, in the Type I configuration, the coil rotates in a planetary motion around the central axis of revolution, and simultaneously counter-rotates around its own axis. In the Type J configuration in contrast, the direction of revolution (around the central axis) and column rotation are in the same direction.

Figure 1-10 (A) and (B) schematically illustrate the directions and magnitude of the generated centrifugal forces for both I and J-type configuration respectively.

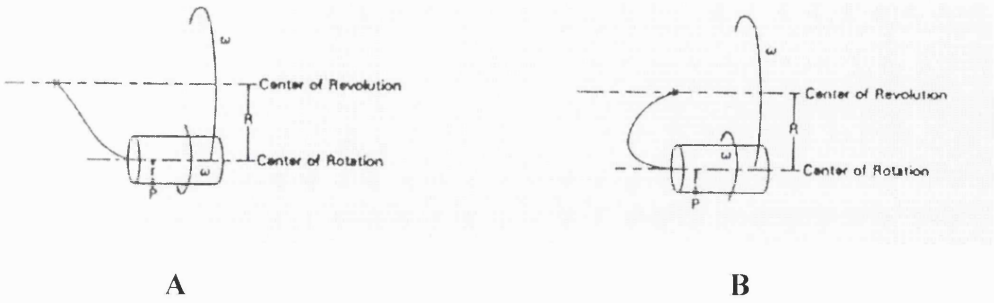

Figure 1-9 Representation of the synchronous planetary motion of the I and J-type CCC configurations, illustrated by (A) and (B) respectively (Ito, 1992).

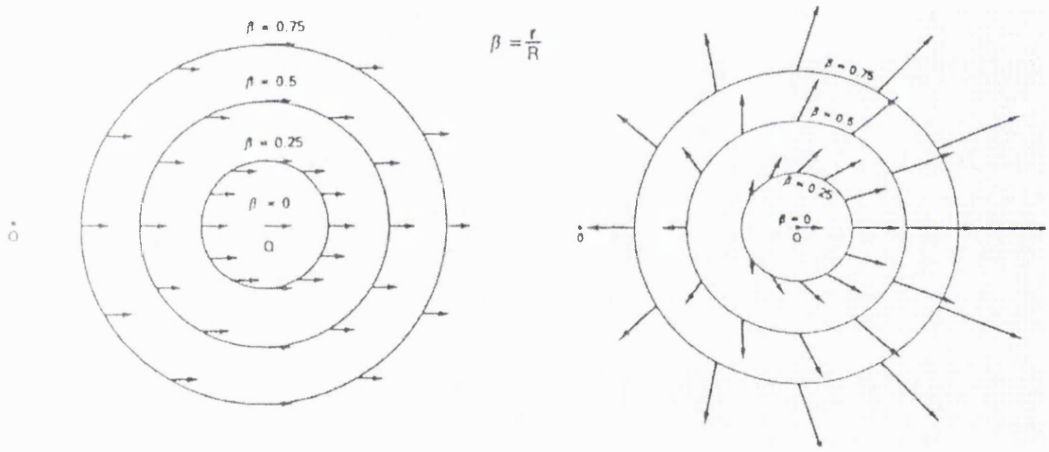

Figure 1-10 Vector maps of the centrifugal force fields generated during coil rotation in Type I (A) and Type J (B) CCC configurations. Points O and Q correspond to the centre of revolution and rotation respectively (Ito, 1992).

From the schematic drawings in Figure 1-10, the centrifugal forces generated by rotation in the I-Type configuration (Figure 1-10 (A)) occur in the same direction and with a similar magnitude, resulting in a unilateral distribution of the phases, as illustrated in Figure 1-7 (B). However, considering the J-Type CCC configuration (Figure 1-10 (B)), the first point that must be made is with regard the direction and magnitude of the centrifugal forces, which are always found to extend outwards from

the centre of rotation. In addition, an important operational parameter termed the β-ratio has a major effect on the magnitude and direction of the centrifugal forces. This ratio term can be described and calculated by the following equation:

$$\beta = r/R \qquad 1.1$$

where 'r' corresponds to the rotational radius, i.e. the distance from any point on the coil to the centre of rotation (centre of the column holder). 'R' corresponds to the revolution radius, i.e. the distance between the axis of the holder and central axis of the apparatus. This parameter, as illustrated in Figure 1-10 (B), plays an important role in the magnitude of the centrifugal forces. As the β-ratio increases, the magnitude of these centrifugal forces also increases.

1.2.4. Mechanism of chromatography in the J-Type CCC machine

The hydrodynamic motion and distribution of two immiscible phases in a rotating CCC coil was first reported by Conway and Ito (1984), who observed distinct zones of rapid phase mixing and settling. The generation of these mixing and settling zones is the result of the cardiodial motion which every location on the column follows. Ito's experimental observations (1992) concluded that for each helical turn of the coil, there are two key points on the coil, termed nodes, where the Archimedean force reverses its direction with respect to the coil. These are the proximal and distal key nodes, and are positioned at the centre of revolution and the point furthest from the centre of rotation respectively. Upon coil rotation, at the proximal key node the lighter phase moves towards the coil 'Head', and at the distal key node, the heavier phase moves towards the coil 'Head'.

Figure 1-11 (A) illustrates the planet (column) and sun (centre of revolution) gears, with (B) illustrating the cardiodial motion generated as a result of the coil configuration. Relating Figure 1-11 (B) to the corresponding centrifugal forces (Figure 1-10 (B)), Sutherland *et al.* (2000b) have shown from stroboscopic studies of a single spirally wound coil mounted in the J-type configuration, that phase mixing (mass transfer step) occurs at the proximal key node, where the centrifugal forces are low. Phase settling, i.e. the formation of two distinct immiscible phases, occurs at the distal key node.

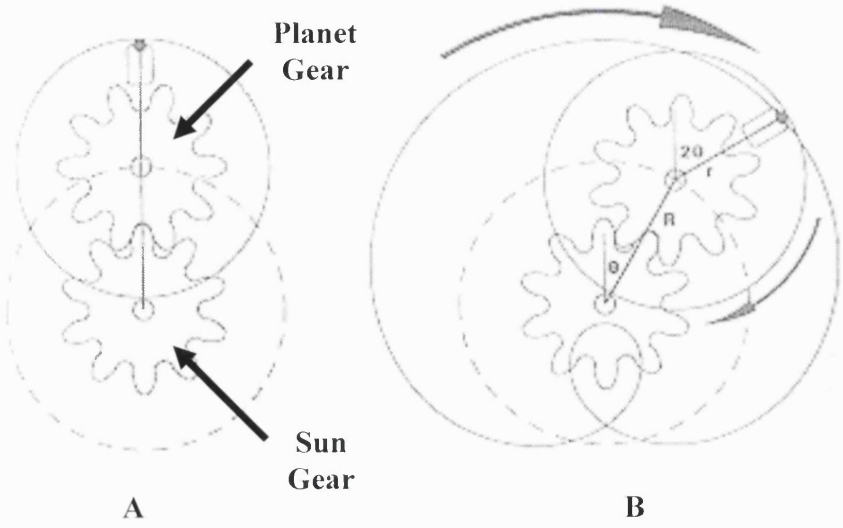

Figure 1-11 **Representation of coil motion in the J-Type CCC machine. (A) illustrates the planet and sun gears corresponding to the points of rotation and revolution respectively. (B) illustrates the cardiodial path taken by any point on the column (Sutherland *et al.*, 2000b).**

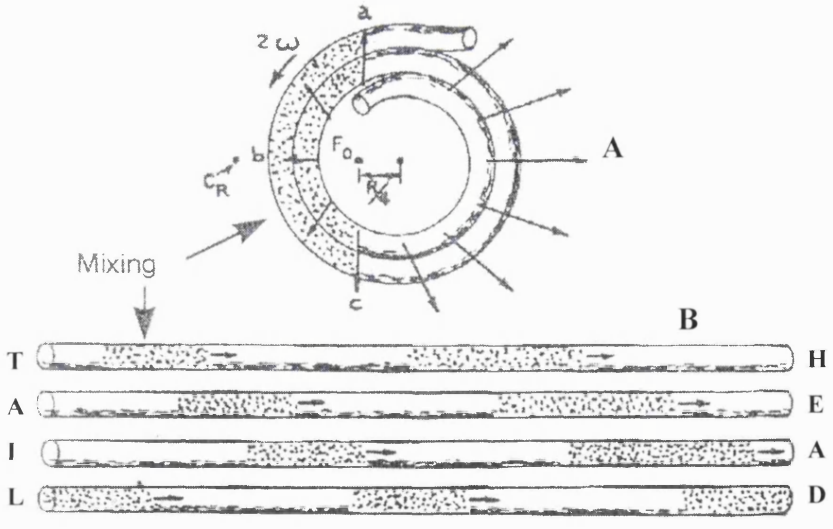

Figure 1-12 **(A) Representation of the mixing (agitation) and settling zones in a spirally wound coil mounted in a J-type CCC machine together with the corresponding centrifugal forces. (B) Movement of mixing and settling zones from the column head to the tail (Sutherland *et al.*, 2000b).**

Figure 1-12 (A) schematically illustrates the previously described areas of phase mixing and settling, illustrating them occurring where the centrifugal forces are at their lowest and highest respectively. Figure 1-12 (B) represents an unwound coil, illustrating the movement of the mixing zone travelling from the column tail to the head at a rate equal to the speed of revolution.

1.2.3.1. Determination of optimal elution mode

Phase distribution studies with the J-Type CCC device by Ito (1996) classified the retention profile findings into three groups dependent on the phase system used and operating conditions.

1) Hydrophobic binary solvent systems, e.g. hexane/water, ethyl acetate/water. High phase retention was observed if the lower or upper phase were eluted from head to tail, or tail to head respectively.
2) Hydrophilic solvent systems. High phase retention was achieved if the upper or lower phases were eluted from head to tail, or tail to head respectively.
3) Intermediate solvent system. These phase systems possessed moderate hydrophobicity of the organic phase, with the retention characteristics greatly affected by the β-ratio (Section 1.2.3). At low β values (0.25) hydrodynamic phase distribution showed similar profiles to those with the hydrophilic systems. At β values greater than 0.5, the hydrodynamic phase distribution showed similar profiles to those with the hydrophobic systems.

Ito's hypothesis was further validated and expanded upon by Sutherland and co-workers (2000b). This group experimentally verified two hypotheses:

1) The Archimedean screw action always forces the heavy phase towards the tail end of the coil.
2) Hydrostatic pressure forces the heavy phase to the periphery in multilayer coils.

The experiments performed by Sutherland and co-workers (2000b) in the first instance mimicked those by Ito (1996), but also investigated the retention characteristics of the quaternary heptane/ethyl acetate/methanol/water system, similar to that used during this work. The conclusions were that:

1) When rotating in the clockwise direction, the Archimedean and hydrostatic forces are additive, placing the coil "Head" at the centre, and the "Tail" at the periphery. In this operating mode, the denser (lower) phase always travels towards the "Tail" of the coil.
2) When rotating in the counter-clockwise direction, i.e. the opposite direction to which the coils are wound on to the bobbin, the Archimedean and hydrostatic forces oppose each other, placing the coil head at the periphery and the tail at the centre. When the phase density ratio (ρ_u/ρ_l) is > 1.15, the denser phase moves towards the "Tail". For a phase density ratio < 1.15, the denser phase moves towards the "Head".
3) Under counter-clockwise rotation, for high density ratio phase systems the Archimedean forces dictates the movement of the phases. For low density ratio phase systems the hydrostatic forces dictate the movement of the phases.

From the experimental findings of Sutherland and co-workers (2000b), an important coil construction and operating rule was proposed, stating that "all CCC instruments should be marketed with only one direction of rotation, which is the same direction as the coils are wound, so that the "Tail" is at the periphery. The lower, heavy phase, will always want to go to the "Tail" (Periphery) and the upper, lighter phase, to the "Head" (Centre)". As a result of this rule, this group also stated the correct mobile phase pumping direction to ensure optimal stationary phase retention for effective chromatography as "always flow the mobile phase in the direction it wants to go – lower, heavy phase towards the "Tail" (Head (Centre) > Tail (Periphery)) and the upper, lighter phase towards the "Head" (Tail (Periphery) > Head (Centre))".

Further hydrodynamic investigations by this group (Wood *et al.*, 2001) identified wave mixing as the primary method of mass transfer between the mobile and stationary phases in the J-type CCC device.

The development of a basic model enabled accurate prediction of the range of flow instabilities, i.e. mixing, with their results demonstrating the formation of waves at the proximal key node due to the movement of the interface, causing an increased linear velocity of the mobile phase.

1.3. History of CCC development

The development of CCC machines can be separated into two distinct groups, these being non-helical and helical forms of CCC. The first conceptual development of CCC, related to countercurrent distribution (CCD), began with the discovery of the liquid-liquid distribution train by Jantzen (1932), and then Tavel and Bollinger (1968) as illustrated in Figure 1-13 (A) and (B) respectively. The Jantzen device typically consisted of 20 U-tubes connected by plastic tubing and arranged in a pseudohelical manner. Mixing of the solvents took place by rotation of the train around its axis. Rotation was then stopped and the solvents allowed to equilibrate before transferral of the second phase from tube 1 to 2 and the addition of fresh solvent into 1 by inclining the train.

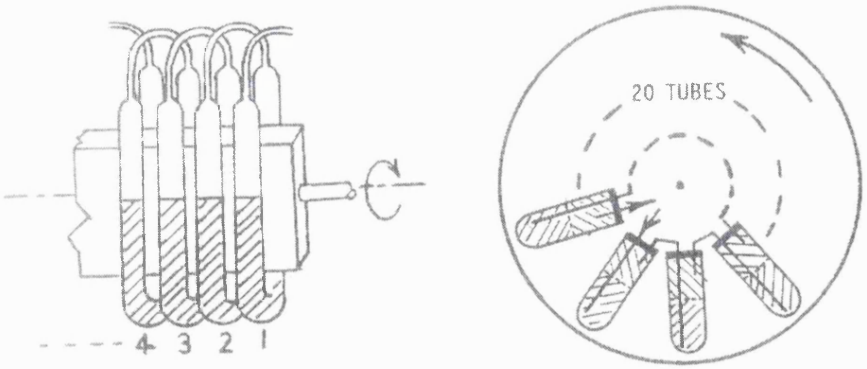

A B

Figure 1-13 (A) Jantzen CCD apparatus (B) Countercurrent distribution centrifuge (Tavel and Bollinger, 1968).

The analogous device to the Jantzen distribution train, named the countercurrent extractor (CCE) was developed by Martin and Synge (1941) and consisted of a number of tubes connected by both inlets and outlets, with mixing being performed by pulsation

from pumping and the reduction in rotor speed (Figure 1-14). This device employed both aqueous two-phase polymer and aqueous-organic systems.

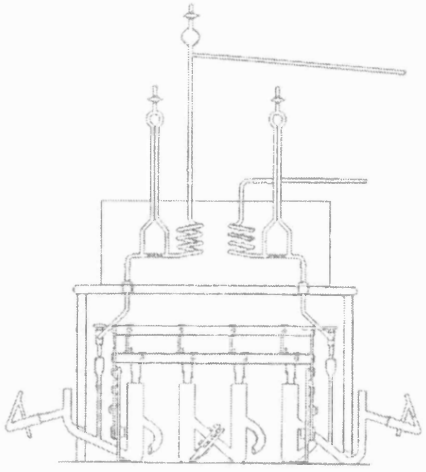

Figure 1-14 The countercurrent extractor (CCE) developed by Martin and Synge (1941).

The discovery of devices related to present day CCC began with the development of the tubular rotating locular CCC (RLCCC) by Cornish (1934). The RLCCC consist of perforated compartments (locules), with alternate ones containing stirring rods providing the mixing process (Figure 1-15). Sample injection occurred at the centre of the tubular structure, with gravity assisted solvent flow achieved by the inclination of the column. The main drawback of this system was the lengthy running time of 2 days and the several hours needed for equilibrium of the phases prior to extraction.

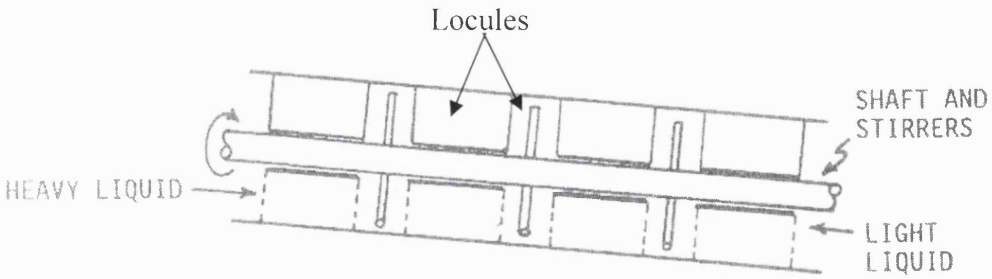

Figure 1-15 The rotating locular CCC (RLCCC) device developed by Cornish (1934).

Further development of this extraction technique took place by Synder between 1952-1967. Variations included incorporating rotating baffles into each locule, rapidly reducing the time for phase equilibration and preventing emulsification or droplet formation.

An analogous development to the RLCCC (1967) resulted in the marketing of a RLCCC, the 'Ronor Column' by Brinkman Instruments. This device succeeded previous RLCCC design by rotating the whole column at 20 rpm, resulting in the stationary phase being retained within the column, whilst the mobile phase cascaded down through these locules by gravity. Further development of the locular devices were in the areas of oscillation (OLCCC) and gyration (GLCCC), where the mixing techniques employed were vibrational and non-rotational gyratory motion respectively. OLCCC, in terms of processing time, was slower than RLCCC, but enabled larger samples to be loaded onto the column at any one time and could utilise a wide variety of solvent systems. The advantage GLCCC has over RLCCC is that there is no requirement for the rotating seal, therefore eliminating product contamination problems, but its mechanistic action does not provide, in terms of efficiency, the same number of theoretical plates.

The final form of non-helical CCC, is droplet CCC (DCCC) as illustrated in Figure 1-16. The evolution of DCCC machines began in 1951 (Kies and Davis), with the development of a cascading train, consisting of up to 25 stages. DCCC is primarily a non-centrifugal technique using gravitational forces to induce mixing between the phases. These devices, as described by Tanimura, Pisano, Ito and Bowman in 1970, consisted of numerous glass tubes connected in series by PTFE tubing. By reducing the diameter of the inlet tubing, a small stream of droplets were permitted into the glass tubes and travelled through the tubing by gravity.

Commercial DCCC devices were produced firstly in 1972 by Tokyo Rikakikai, and then in 1982 by Buchi Laboratory-Techniques Ltd. DCCC has become the most successful, to date, of all forms of CCC despite the slow operating times and the limited number of applicable solvents due to the requirements of the solvent systems to firstly form discrete droplets which neither adhere to the tubing wall or coalesce whilst traversing the vertical columns.

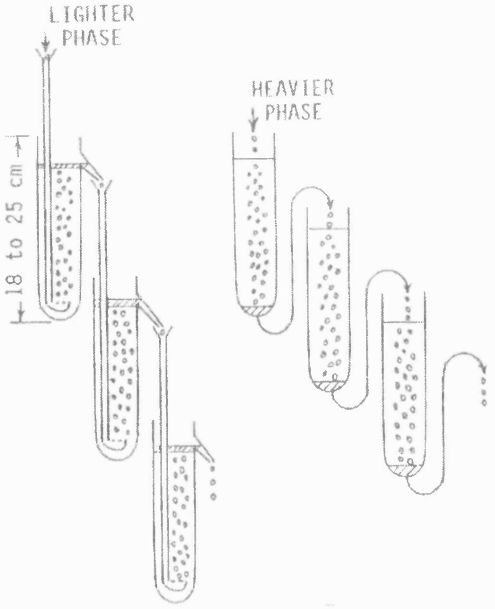

Figure 1-16 **A droplet CCC device, illustrating the configuration for using the lighter (A) and heavier (B) phase as mobile phase (Conway, 1990).**

An exception to this is the centrifugal droplet CCC device (CDCCC) developed by Murayama and commercialised in 1982 by Sanki Engineering, which, unlike conventional DCCC, can employ a wider variety of solvents and does not specifically depend on the formation of droplets in order to function effectively.

The main developmental work in helical CCC, branching off from previous research into locular CCC and DCCC, began in 1965 by Ito and his collaborators. Before summarising the developmental work in helical CCC to date, it is firstly important to provide a logical means of generic classification, due to diverse variations of devices constructed simply by changing the type or position of the column and driving mechanism (Conway, 1990). Classification is achieved in terms of (1) type of column holder, i.e. solar, planet, angle rotor, (2) the driving mechanism, i.e. pulley, gear, forward, reverse, nonsynchronous, (3) the geometrical relationship between the column and the holder, i.e. coaxial or eccentric, and (4) the type of column configuration, i.e. linear, helix, toroidal coil, multilayered coil. The first coil planet centrifuge (CPC) was developed in 1966 by Ito and co-workers. The driving mechanism employed was the worm gear that transmitted power to two column holders via a central shaft.

This device was further developed, replacing the worm drive for the spur driving unit and commercially sold by Sanki Engineering Ltd. as the CPC Analyzer. These devices were closed systems, where the column was first filled with both the stationary and mobile phase in a 50:50 ratio, with the sample placed in the column between the two immiscible phases prior to separation. Limitations of these helical devices such as the low sample loading capacity and the fact that it is a closed system, led to the development of flow-through CCC devices. The first of these to be developed was the helix CCC (Ito and Bowman, 1970), with a toroidal coil column constructed by winding narrow bore PTFE tubing onto a flexible bobbin and mounted in a solar coaxial position inside a helixtractor bowl.

The column was initially filled with stationary phase, upon which sample (5μl) entered the column inlet by suction. Delivery of the mobile phase by injection via a high-pressure syringe through a thrust bearing at 16 to 20 atm, only occurred once rotation of the coil had begun. Effluent collection was through a rotary seal at atmospheric pressure. Efficiency studies with the helix CCC in the separation of DNP-amino acids indicated that it increased with increasing tubing length, smaller bore-size and slower mobile flow rates.

However although helix CCC provided greater efficiency, the run time was still slow and due to the small bore tubing employed in these devices the sample loading capacity was small. Further development of these devices to the commercially available units of today began in 1971 with the development of the vertical flow-through coil plant centrifuge (VFTCPC) by Ito and Bowman (Figure 1-17). The advantages of these devices over earlier ones was due to the gyratory motion developed from the use of the planet pulley drive, thus eliminating the need for the rotating seal. The drawback of this system was, although stationary phase retention in aqueous-organic systems was high, when aqueous two-phase polymer systems were employed, upon vigorous mixing, emulsification of these low-interfacial tension systems occurred.

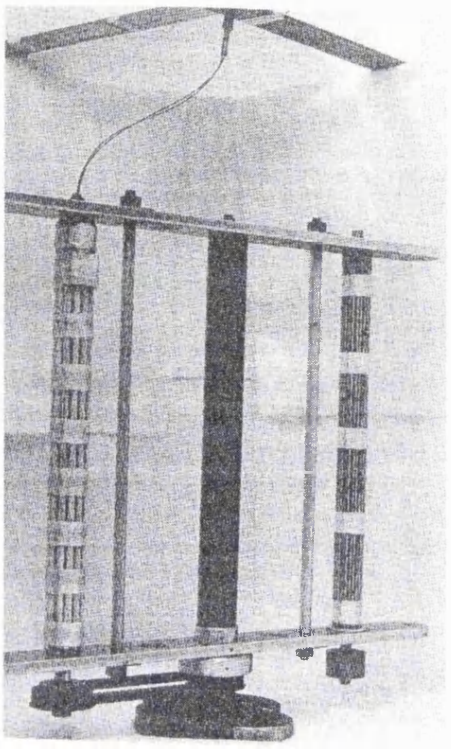

Figure 1-17 The vertical flow through CPC device (VFTCPC) developed by Ito and Bowman in 1971 (from Conway, 1990).

This led to the development of angle rotor centrifuges by Ito and Bowman in 1972. These devices specifically looked at optimising the efficiency of systems consisting of aqueous two-phase polymers by determining the critical angle of column inclination. The most effective angles of inclination were at 30° and 45°, where at 45° with narrow-bore tubing 2000-4000 theoretical plates were achieved. A further development in 1975 by Ito, Suandeau and Bowman expanded on the work performed by Adams in 1971. The incorporation of the anti-twisting inlet and outlet lead mechanism into subsequent flow through CCC devices after 1975 (Ito and Bowman, 1978), provided great advantages over devices designed with rotary seals, where in these devices, damage of the feed material, leading to contamination in sterile systems, localised heating of volatile solvents coupled with the possible risk of denaturation of heat liable products and leakage, could all occur.

The application of the anti-twisting mechanism, coupled with the introduction of the planet gear drive (Ito and Bowman, 1978) led to the formation of the horizontal flow-through coil planet centrifuge (HFTCPC) as illustrated in Figure 1-18. Compared

to the VFTCPC, HFTCPC was more versatile, as the centrifugal forces that the column was subjected to were dependent on the radius of the planetary column holder (r), and hence the β-ratio (r/R), whose operational importance is discussed in Section 1.2.3.

Also, in 1978 the helix CCC was developed to incorporate the anti-twisting mechanism. The HFTCPC was further developed to be used on a preparative scale by using larger internal diameter (d_i) tubing wound onto a bobbin of small radius, increasing the number of coil turns.

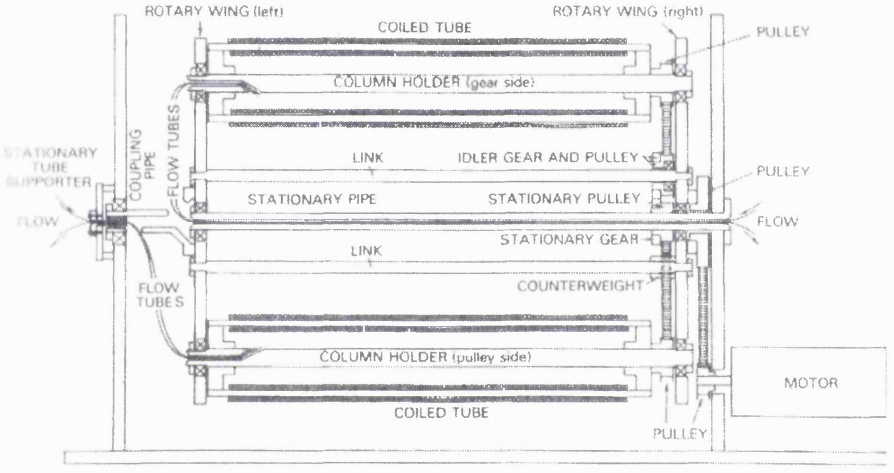

Figure 1-18 The horizontal flow through CPC (HFTCPC) device illustrating the combined gear and pulley drive system developed by Ito and Bowman in 1978 (from Conway, 1990).

In 1980, Ito developed the toroidal coil planet centrifuge (Figure 1-19) from the combination of the helix CCC, a static device with the toroidal coil setup, and the gear driven CPC, a dynamic device. This combination resulted in the dimensions of the toroidal CPC being significantly smaller than the mechanically similar HFTCPC. Optimum resolution conditions, using test mixtures of DNP-glutaminc acid and DNP-alanine in a chloroform system ($CHCl_3$/HOAc/0.1N HCL - 2:2:1), were found to be in the rotational speed range 800-1000 with 0.55 mm bore PTFE tubing. However, despite this development of the torodial CPC in 1980, with such dynamic devices, due to the rapid coil motion relative to the centrifugal force field, emulsification of aqueous two-phase polymer systems occurred, resulting in low stationary phase retention.

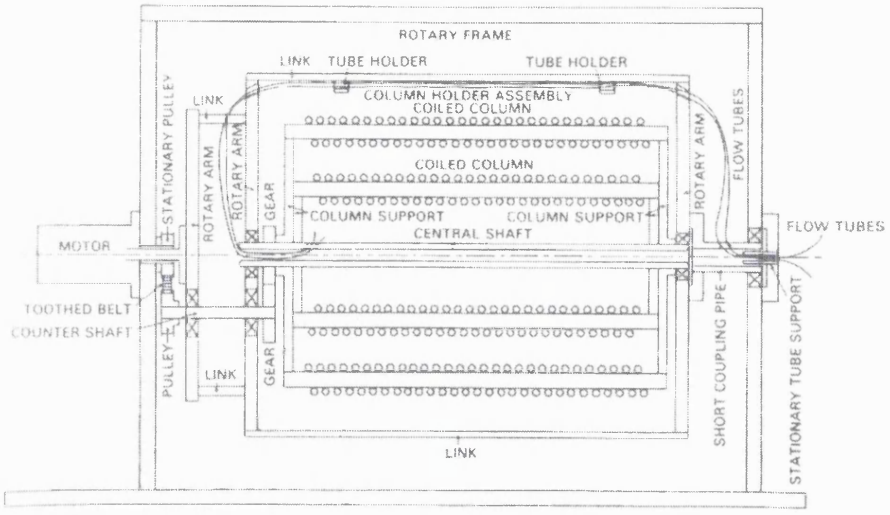

Figure 1-19 The torodial CCC device developed by Ito in 1980 (from Conway, 1990).

Going back to 1979, Ito, Carmeci and Sutherland developed the non-synchronous CCC that operated under slow column rotation, but still produced the high g-fields needed for successful mixing of aqueous two-phase polymer systems, by enabling the ratio of column rotation relative to the acceleration field to be altered, something that was fixed in dynamic CCC devices. However, the drawback of this device was that it employed dual rotary seals, and with these came the previously described problems associated with their use. This drawback was overcome in 1980 by the incorporation of the anti-twisting mechanism, producing the first nonsynchronous flow-through coil planet centrifuge. Improvements in the construction of these devices took place in 1983 by Ito and co-workers.

Prior to 1982, the hydrodynamic behaviour of solvent systems, such as EtOAc/H_2O in single-layer helical gear driven CPC's, as observed by Ito, was of a unilateral nature, where the heavy phase occupies the 'Tail' end of the coil, and the lighter phase occupies the 'Head' end of the coil (Section 1.2.2). In solvent systems where the lighter phase has a greater viscosity, the unilateral distribution observed in the coil is not equal between the two phases, resulting of stationary phase stripping. This drawback led to the development of the multilayer-CPC (Ito *et al.*, 1982) as illustrated in Figure 1-20. Ito postulated that in the multilayer coil successive coil layers would be exposed to greater centrifugal forces.

By positioning the 'Head' of the coil at the centre and the 'Tail' at the periphery, these increasing centrifugal forces could assist in the flow of the heavy mobile phase to the 'Tail' or periphery, and thus allow a wider range of solvents to be used. The advantage of the multilayer CPC over prior devices, such as the HFTCPC was the greater degree of stationary phase retention, which in turn provided greater resolution of multi-component samples.

Up to the present day, further developments in the field of CCC have concentrated on variations of the multilayer CPC. These variations include the development of preparative multilayer CPC for the fractionation of multigram quantities of DNP-amino acids in both rotating solar coaxial coil (Ito and Bhatnagar, 1984) and planet gear coaxial (Sandlin and Ito, 1985) configurations. The latter employed a larger-volume two layer helical coil, in comparison to the three layer helical coil orientated in the solar coaxial position by using a larger diameter spool.

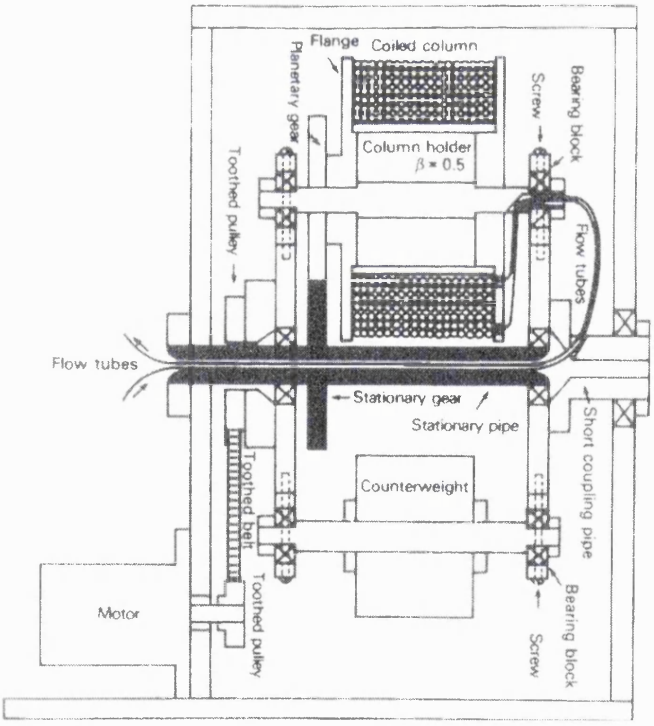

Figure 1-20 The multilayer CCC device developed by Ito *et al.*, 1982 (from Conway, 1990).

More recently, the development of the laboratory scale Brunel J-Type CCC device, whose construction is described in detail in Section 2.3, has resulted in the successful purification of a range of polar and non-polar products (Sutherland *et al.*,

1998; Wang-fan *et al.*, 1999; Wang-fan *et al.*, 2001). In addition, the Brunel group have constructed a novel J-type pilot scale CCC machine (1 L nominal coil volume), which has successfully been applied to the purification of an active pharmaceutical intermediate (API) by Graham *et al.* (2001).

1.4. Applications of CCC

As a result of the wide range of possible biphasic solvent systems for application in CCC (Conway, 1990) the technology has successfully been applied to a range of purification challenges. Within the literature there are numerous detailed reviews of both analytical and preparative applications (Conway, 1990; Marston and Hostettmann, 1994; Maillard *et al.*, 1996) including:

- Polar plant extracts, such as flavonoids and tannins.
- Agricultural chemicals – plant hormones and pesticides.
- Amino acids, peptides (Knight *et al.*, 1986) and proteins (Shibusawa and Ito, 1998).
- Inorganics (Maryutina *et al.*, 1999).
- Antimalarial drug, artemisinin isolation from the contaminant artemisitene (Acton, *et al.*, 1986).
- Anti-Trypanosomal Factor (ATF-II) produced from *Pseudomonas fluorescens* (Mercado, *et al.*, 1988).
- Integrated reaction and separation process (Van Der Wielen *et al.*, 1990; Berthod *et al.*, 1998; Lye and Woodley, 1999).
- Different forms of plasmid DNA (Kendall *et al.*, 2001).

In the context of this work, the application of CCC to the purification and recovery of antibiotics at the laboratory scale has been well exploited and documented, with a selection of these applications given in Table 1-5.

Compound	References
2-Norerythromycin A, B, C & D Niaddamycin Tiacumicin Coloradocin	Chen *et al.* (1988)
Erythromycin E	Stecher (1968)
Siderochelin A Efrotomycin Pentalenolactone Bu 2313B A201 E Tirandamycin A & B	Brill *et al.* (1985)
Valinomycin Piericidin Concanamycin C Quinomycin A & C Tomaymycin Toyocamycin	Martin *et al.* (1986a)
Actinomycins C_1, C_2, and C_3	Martin, Peltonen and Nielsen (1986b)
Sporaviridins	Harada *et al.* (1990) Oka *et al.* (1998)

Table 1-5 Antibiotics fractionated by CCC.

Studies by Brill *et al.* (1985), Chen *et al.* (1988) and Oka *et al.* (1998) have all successfully separated fermentation derived antibiotics, with varying degrees of pre-purification prior to solute injection. With regard to the work performed by Harada *et al.* (1990), the sporaviridins, which are water-soluble glycoside antibiotics existing as a mixture of closely related compounds, were separated on the Shimadzu CCC instrument (total capacity of 325 mL at 800 rpm) using a sample injection method known as "sandwich" injection. This is where the sample is injected after the coil is filled with stationary phase, and before elution with the mobile phase. The chosen solvent system, after initial work based on solute partition coefficient data, was n-BuOH/diethyl ether/H_2O, in the ratios 10:4:12. With this phase system, separation of the six components occurred in 3.5 hours, with a total elution volume of 500 mL.

Recent research by Oka *et al.* (2000) has successfully separated the main components of the macrolide antibiotic, spiramycin (25 mg), using the quaternary hexane/ethyl acetate/methanol/water solvent system, in the reverse phase mode, i.e. organic stationary phase, at an aqueous mobile phase flow rate of 1 $mL.min^{-1}$. The purity of the main spiramycin fractions (I-III) ranged from 92.3% to 98.2%. The total

process time in this case was found to be 6.9 hours, with a total mobile phase elution volume of 380 mL. Harada *et al.* (2001) have further demonstrated the successful application of CCC at the laboratory scale for the purification and recovery of WAP-8294A components, achieving high resolution of a 25 mg sample size, at a mobile phase flow rate of 0.5 $mL.min^{-1}$ (total process time of 13.3 hours), and total solute recovery of 85.5%.

Detailed investigations by Wang-fan *et al.* (1999) for the macrolide antibiotics ascomycin and FK-506 established a methodology for selecting suitable solvent systems based on solubility and distribution ratios. Their findings resulted in an optimised quaternary phase system comprising of hexane/tert.-butyl methyl ether/methanol/water enabling a baseline separation of these two 23-membered macrolides in the J-Type counter-current chromatograph, again in the reverse phase mode (aqueous mobile phase), at a mobile phase flow rate of 1 $mL.min^{-1}$. The total process time was found to be approximately 5.5 hours. The same group have also investigated the effects of mobile phase flow rate, mass loading and column rotational speed on peak resolution (Wang-fan *et al.*, 2001) for a range of six closely related macrolide antibiotics consisting of ascomycin and rapamycin analogues.

1.5. Project Aims.

Based on the previous research described above, the aims of this project are as follows:

1) To evaluate CCC as a novel chromatographic technique for the high-resolution fractionation and recovery of EA from its structurally similar analogues. This will involve the development of an effective solvent system and operating run mode, initially with the 'model' erythromycin preparation, as described in Chapter 4.
2) Process optimisation (model system), investigating the effects of solute loading and mobile phase flow rate on separation performance. This will be described in Chapter 6.

3) To examine the feasibility of using CCC for the purification of fermentation derived EA 'real system', together with subsequent optimisation studies. This will be described in Chapter 7.

4) To evaluate the scale-up of CCC for both the model and real systems by (a) investigating the effects of feed impurity, mobile phase flow rate, solute loading and column rotational speed on the separation performance and (b) demonstrating the predictive nature of the technology upon scale-up by the application of a model to enable the determination of product elution times over a range of operating conditions. This will be described in Chapter 8.

5) To evaluate the use of 'Fractionation diagram theory' to visually determine the effects, at both scales of operation, of operational conditions studied on separation performance, ultimately identifying the optimal trade-off between product purity and solute yield, together with respective cut-point determinations. This will be described in Chapter 9.

2. Materials and Methods

2.1. Chemicals

2.1.1. Fermentation components

A soluble complex medium (SCM) was used for the production of erythromycin. The various components of this medium together with their initial concentrations are given in Table 2-1.

Component	Concentration ($g.L^{-1}$)	Supplier
Glucose	30.0	BDH
Yeast extract	6.0	Oxoid
Bacto-peptone	4.0	Oxoid
Glycine	2.0	Sigma-Aldrich Company
$MgSO_4.7H_2O$	0.5	Sigma-Aldrich Company
KH_2PO_4	0.7	Sigma-Aldrich Company
Antifoam (PPG)	2.5	Sigma-Aldrich Company

Table 2-1 Composition of the soluble complex medium (SCM) used.

Other fermentation components used for pH control were phosphoric acid and alkaline phosphate (KH_2PO_4) from Merck (Lutterworth, Leicestershire, U.K.) and BDH (Poole, Dorset, U.K.) respectively. Reverse osmosis (R.O) water was used for all media preparation. The strain used during this study was *Saccharpolyspora erythraea* CA340, kindly supplied by Abbott Laboratories (N. Chicago, U.S.A.). A 20% (v/v) glycerol (Sigma-Aldrich Company, Gillingham, Dorset, U.K.) solution was used for storage of spore stocks.

2.1.2. Chemicals used in other unit operations and assays

2.1.2.1. Microfiltration

R.O. water and 5% hypochlorite at 50°C were used for the initial cleaning of the membrane prior to use. Redphos Special SN557, a phosphoric acid based cleaner (Kleancare Hygiene, Cheshire, U.K.) was used for final cleaning of the membrane after use.

2.1.2.2. Solvent extraction of clarified fermentation broth

The solvent used for extraction of erythromycin from fermentation broths was butyl acetate (VWR International Ltd, Lutterworth, Leicestershire, U.K.). Prior to addition of the butyl acetate, the clarified fermentation broth was adjusted to pH 10 using a 4M sodium hydroxide (NaOH) solution. Back extraction from the butyl acetate phase, into a fresh aqueous phase was performed using 25 mM KH_2PO_4 solution buffered to pH 7 using a 10 mM potassium phosphate solution.

2.1.2.3. Chemicals for CCC

The biphasic solvent system used in CCC experiments consisted of hexane, ethyl acetate, methanol and water. The organic solvents were of HPLC grade (purity >99.9%), from Fisher Scientific, Loughborough, U.K. R.O. water was used in all experiments.

2.1.2.4. Chemicals for off-line assays

For HPLC analyses acetonitrile used was of HPLC grade (purity >99.9%, from Fisher Scientific), as was the buffer K_2HPO_4 and H_3PO_4, both prepared using R.O. water. Sulphuric acid (H_2SO_4) used for the colorimetric assay was from Fisher

Scientific (Loughborough, U.K.), again prepared in R.O. water. Isopropanol used in forming a single phase from collected fractions during gradient CCC operation was of HPLC grade (purity >99.9%, from Fisher Scientific).

2.1.2.5. Erythromycin

The crude, commercial erythromycin preparation used was kindly supplied by Abbott Laboratories (N.Chicago, U.S.A.) and was between 75 and 80% (w/w) pure erythromycin A.

2.2. Production and partial purification of broth-derived erythromycin

2.2.1. Strain and culture storage

S. erythraea spore stocks were prepared using a medium consisting of glucose (2 $g.L^{-1}$), sucrose (1 $g.L^{-1}$), yeast extract (20 $g.L^{-1}$), soy peptone (2.5 $g.L^{-1}$), agar (Technical no. 1) and ethylenediaminetetraacetic acid, EDTA (0.036 $g.L^{-1}$). The pH of the medium was adjusted to 7.0 using 0.1M NaOH before being sterilised by autoclaving for 20 minutes at 121°C. The Petri dishes inoculated with the vegetative organism were incubated at 28°C for three weeks, after which time aerial spores were removed by scouring the agar surface with a loop and transferring the collected spores to a solution consisting of 20% (v/v) glycerol and 0.1% (v/v) Tween 80. This spore suspension was then stored at -20°C.

Prior to inoculation of the fermenter, several seed stages were performed. The first of these was the aseptic addition of 1 mL of thawed stock suspension to 50 mL of nutrient broth (8 $g.L^{-1}$) in a 500 mL baffled shake flask. Seven separate 500 mL shake flasks were inoculated to allow for any potential contamination. The broth was then incubated for 48 hours at 28°C and continually agitated at 200 rpm using an orbital shaker (model G25, New Brunswick Scientific Co. Inc. N.J. U.S.A.). The second seed stage involved the aseptic transfer of the total culture volume in five of the 500 mL shake flasks to five 2 L shake flasks containing 450 mL of sterile SCM. Once inoculated, the 2 L shake flasks were incubated for 30 hours at 28°C, again agitated at 200 rpm. The final seed stage involved the inoculation of the fermenter with the contents of the 2 L flasks. The inoculum volume used was 10% (v/v) of the final

working volume of the fermenter. At each of the seed stages, culture samples were examined under a light microscope to check for any possible contamination.

2.2.2. Fermenter design and auxillary equipment

The fermenter used during this study was a LH2000 series vessel (Inceltech Ltd., Pangbourne, U.K.). It had a total volume of 20 L, and an operating volume of 14 L. The dimensions of the fermenter are given in Table 2-2.

Dimensions	LH 20 L Vessel
Total volume (L)	20
Working volume (L)	14
Vessel height (mm)	510
Vessel diameter (mm)	230
Shaft height (mm)	490
Shaft diameter (mm)	12.7
Number of impellers	3
Impeller diameter (mm)	68.7
Impeller position from base (mm)	
1	75
2	155
3	245
Impeller tip dimensions (mm)	
Length	16
Width	14.4
Height	2
Baffle dimensions (mm)	
Height	355
Width	22
Depth	1.8
Sparger dimensions (mm)	
Diameter	9.5
Diameter of sparging holes	22
Number of sparging holes	6

Table 2-2 Dimensions of the 20 L fermenter used during this study.

The fermentation vessel used was constructed from glass and contained four equally spaced baffles, with a stainless steel top and bottom plate. The impeller was constructed from stainless steel and consisted of three 6-bladed Rushton turbine impellers and was rotated using a top driven motor. Filtered air was supplied to the ring sparger from a dedicated air supply fitted with a cartridge-type filter. Temperature control of the fermenter was achieved using an electric element and cooling water supplied to coils within the fermentation vessel.

The dissolved oxygen tension of the fermentation broth (DOT) was measured during the fermentation using a pre-calibrated probe (Ingold Messtechnik AG, Urdorf, Switzerland). The pH was measured using a Mettler Toledo probe (Mettler Toledo GmbH, Urdork, Switzerland). Control of the pH was achieved using two pre-autoclaved plastic vessels (1 L), containing 5M NaOH or H_3PO_4, the required solution being added by a peristaltic pump. The composition of the inlet and outlet gas from the fermenter was measured on-line using a MM8-80S mass spectrometer (VG Gas Analysis Ltd., Winsworth, U.K.). Control of the fermenter and data logging was achieved using Bioview software (Adaptive Biosystems Ltd., Luton, U.K.).

2.2.3. Fermenter operation

Prior to inoculation, the fermenter was steam sterilised and simultaneously pressure tested. Initially all media components, auxillary holding vessels, probes and any external connecting tubing with attached connectors were sterilised. Sterilisation was performed in two ways. Firstly yeast, bactopeptone, glycine and KH_2PO_4 were sterilised together *in situ* in the fermenter. Glucose and $MgSO_4.7H_2O$ were autoclaved separately at 121°C (1 Bar) for 20 minutes, as were any holding vessels, probes or external connecting tubing. Prior to the insertion of the DOT and pH probes into the fermenter, both were calibrated. The DOT probe was first calibrated to 0% by passing oxygen free nitrogen gas (BOC, Surrey, U.K) over the membrane. *In situ* sterilisation of the DOT probe was also performed by sparging air at the desired flow rate through the sterile medium to obtain a 100% oxygen reading. The pH probe was calibrated outside the fermenter using standards at 4.01 and 7.00. Once all probes and feed lines had been fitted to the fermenter, the agitation rate and temperature were increased to

750 rpm and 28°C respectively, with the pH set to 7. With all operating conditions set, the fermenter was aseptically inoculated with the 10% (v/v) culture described in Section 2.2.1. Sampling from the fermenter was performed at pre-determined time intervals during the 75 hour operating period, with the dry cell weight (DCW) measured each time as described in Section 2.2.3.1. Final harvesting of the fermentation broth yielded 13 litres, with 10 litres used for further downstream processing.

2.2.3.1. Dry cell weight determination

Broth samples of 5 mL were loaded onto dry pre-weighted glass microfilters (0.2 μm) (Whatman Ind. Ltd) and washed with an equal volume of R.O. water. Dead-end vacuum filtration was used for the removal of liquid broth and water from the surface of the filter. The filter paper was then dried using a HG53 Halogen moisture analyser (Mettler-Toledo, Leicester, U.K.) at 95°C until the weight of the filter paper remained constant. The dried filter paper was then reweighed using the same micro balance to 5 d.p (Sartorius, Germany). All measurements were performed in triplicate.

2.2.4. Downstream processing

2.2.4.1. Broth clarification by cross-flow microfiltration

Broth clarification was performed using a Pellicon Mini microfiltration rig (Millipore, MA, U.S.A.). This consisted of a Pellicon mini cartridge holder, which held four Pellicon-2 0.1 m^2 membrane cartridges. These microporous membranes were made of a hydrophilic Durapore membrane, with a nominal pore size of 0.2 μm. This type of membrane has been extensively used in our laboratories, as it has been shown to minimise fouling by proteins (Zhang et *al.*, 1998) and antifoaming agents, such as PPG (Liew *et al.*, 1997). The membrane holder was connected to a Millipore Proflux M12 self-contained microfiltration rig (Millipore, MA, U.S.A.), which consisted of a peristaltic pump, three pressure transducers and a baffled reservoir.

Filtration was performed in a concentration mode, the permeate collected being aliquoted into 500 mL fractions and frozen at -5°C until required for further use.

2.2.4.2. Erythromycin isolation by solvent extraction

Solvent extraction of the clarified broth (see Section 2.2.4.1) was performed based on the description of an industrial extraction process by Baker-Perkins (in Verrall, 1992). In this case two equilibrium batch-wise extractions were performed. Firstly, forward extraction was performed using butyl acetate (BA) as the extractant. The volume ratio of BA to clarified broth was 1:4 respectively and extraction was performed at an aqueous phase pH of 10, the pH being adjusted using 4M NaOH. Phase mixing was performed using a Heildoph REAX 2 Mixer (Labplant, Huddlesfield, U.K.) at approximately 40 rpm for 30 minutes at room temperature. At 5 minute intervals, the aqueous phase pH was monitored and adjusted back to 10 as required. Phases were then allowed to equilibrate overnight at room temperature prior to further use.

Prior to back extraction, the settled erythromycin-rich BA phase from the forward extraction step was removed and centrifuged at 3500 rpm (30°C) for 30 minutes to produce a clear solvent phase. Back extraction of erythromycin from the BA phase into an aqueous phase was then performed by mixing for 30 minutes (as described above) at a 1:1 volume ratio of BA to 25 mM $K_2HPO_4 \cdot 3H_2O$ solution buffered to pH 7 using 10 mM H_3PO_4. Monitoring and adjustment of the pH back to 7 was performed at 5 minute intervals for the duration of the extraction. Again, at the end of the 30 minute mixing period the phases were allowed to equilibrate overnight. The resultant aqueous solution was cloudy and so was separated by centrifugation at 3500 rpm (30°C) for 30 minutes prior to use in CCC experiments.

Sample preparation prior to use for CCC experiments in all cases, regardless of whether the feed was clarified broth, or had undergone forward and backward extraction stages, involved drying of the sample using a SpeedVac SC100 (Life Science International, U.K) at 40°C for between 1.5 and 2 hours depending on the feed type. The dried fractions were then resuspended in an equal volume of the aqueous mobile phase prior to use in CCC experiments as described in Section 2.4.1.2.

2.3. CCC instrumentation and auxillary equipment

2.3.1. Laboratory scale CCC instrument

The laboratory scale CCC instrument used was a Brunel Labprep (J-type design) (Rhomulus Technologies Ltd, Uxbridge, U.K.). This coil planet centrifuge is shown in Figure 2-1.

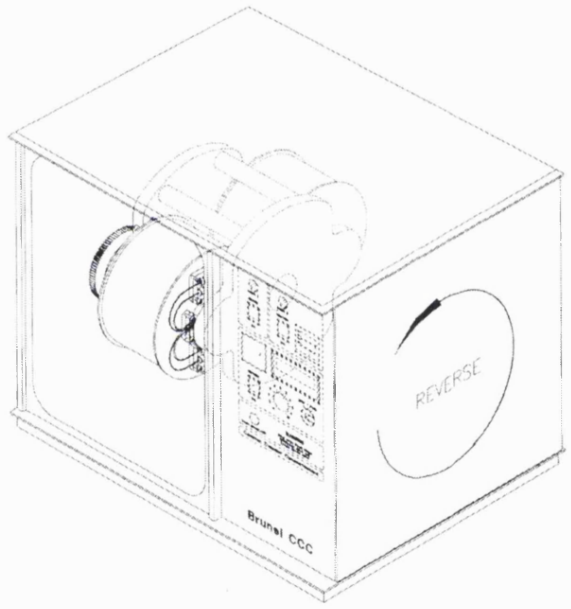

Figure 2-1 **The Brunel CCC instrument illustrating the mounting positions of the two bobbins in the rotor housing (Brunel CCC manual).**

This device was fitted with two equivalent bobbins, each containing coils prepared from either polytetrafluoroethylene (PTFE) or stainless steel (SS) tubing of varying diameters. The bobbins accommodating the PTFE coils were labelled as 'Bobbin 7/1' and 'Bobbin 7/2'. The bobbins accommodating the SS coils were labelled as 'Bobbin 6/1' and 'Bobbin 6/2'. Each bobbin consisted of an inner and outer coil, shown in Figure 2-2. The coil was spirally wound from the centre of the bobbin to its periphery in an anticlockwise manner, forming a multilayered configuration. Once the tubing was wound onto the bobbin, an outer stainless steel sleeve was put in place and

the whole internal structure potted together using an epoxy resin, to prevent any lateral movement of the multilayered coils during rotation. The dimensions of the coils for both sets of bobbins are given in Tables 2-3 and 2-4.

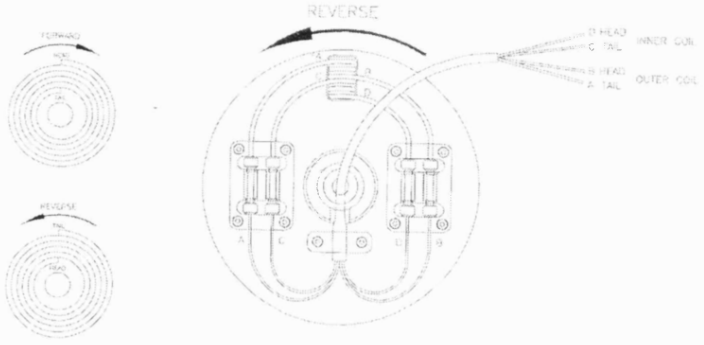

Figure 2-2 **Coil winding illustrating the entrance and exit of the two sets of flying lead arrangements (Brunel CCC manual).**

Measurement	Bobbin 7/1		Bobbin 7/2	
	Inner coil	Outer coil	Inner coil	Outer coil
Coil o.d. (mm)	3.13	3.13	3.13	3.13
Coil i.d.(mm)	1.56	1.56	1.56	1.56
Coil length (m)	82.1	47.6	84.5	46.6
Number of loops	162	81	162	81
Coil volume (mL)	162.5	94.3	167.2	92.3
Inner coil radius (r_i) (mm)	75.5	88.2	75.5	88.2
Outer coil radius (r_o) (mm)	88.2	94.6	88.2	94.6
Rotor radius (R) (mm)	110	110	110	110
β ratio range ($r_i/R - r_o/R$)	0.69 – 0.80	0.80 – 0.86	0.69 – 0.80	0.80 – 0.86

Table 2-3 **Dimensions of both the inner and outer PTFE coils on bobbins 7/1 and 7/2 together with their respective Beta ratio ranges (β).**

Measurement	Bobbin 6/1		Bobbin 6/2	
	Inner coil	**Outer coil**	**Inner coil**	**Outer coil**
Coil o.d. (mm)	3.13	4.69	3.13	4.69
Coil i.d.(mm)	1.75	3.35	1.75	3.35
Coil length (m)	35.4	9.7	37.6	10.7
Number of loops	64	20	64	20
Coil volume (mL)	85.5	85.3	90.7	94.7
Inner coil radius (r_i) (mm)	75.5	75.5	75.5	75.5
Outer coil radius (r_o) (mm)	101	101	101	101
Rotor radius (R) (mm)	110	110	110	110
β ratio range ($r_i/R - r_o/R$)	0.69-0.92	0.69-0.92	0.69-0.92	0.69-0.92

Table 2-4 Dimensions of both inner and outer stainless steel coils on bobbins 6/1 and 6/2 together with their respective Beta ratio ranges (β).

The flying lead volumes for the PTFE and SS coils were 0.35 mL and 0.85 mL per lead respectively, i.e. 0.7 mL and 1.7 mL per PTFE and SS coil respectively. This Brunel CCC device differs from other coil planet centrifuges in the novel design of the flying lead arrangement (Figure 2-3), enabling a higher β value to be generated.

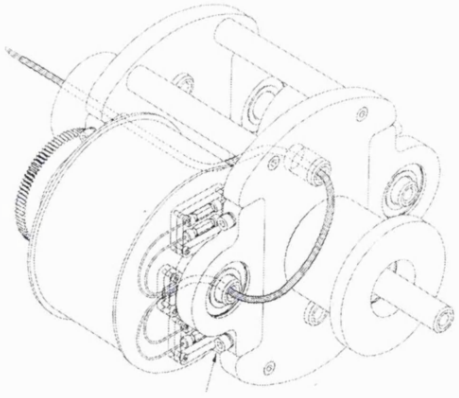

Figure 2-3 Bobbin mounting between two rotor plates together with the novel flying lead arrangement (Brunel CCC manual).

The bobbins were rotated at 800 rpm in the reverse direction, placing the 'Head' of the coil at the centre of the bobbin. The internal operating temperature of the machine was controlled at 30°C with an internal fan and a water-cooled jacket. The stationary and mobile phases were pumped using Dionex P580 high-pressure isocratic and gradient pumps (Dionex, U.K.).

These pumps provide a pulse-free flow of the phases and therefore accurate flow rates even at low backpressures. This is of great importance for this investigation as the backpressure developed and measured (500 – 4000 $kN.m^{-1}$) in CCC is far lower than that encountered in other techniques such as HPLC, and any pulsating flow could influence phase hydrodynamics (Section 1.2). Sample injection was performed using a Rheodyne 7725i valve fitted with either a 1 or 2 mL loop (Rheodyne, Rohnert Park, USA).

2.3.2. Pilot-scale CCC instrument

The pilot-scale CCC instrument used during this study was a modified Labprep coil planet centrifuge (Rhomulus Technology Ltd, Uxbridge, U.K.) designed as part of a BBSRC/DTI LINK programme examining the industrial scale up of CCC. This consisted of two equivalent coils, each constructed from 3.68 mm i.d. stainless steel tubing with 84 loops (Figure 2-4) providing a capacity of 464 mL per bobbin. Both coils were connected in series resulting in a total capacity of 928 mL, with a total coil length of 91.15 metres. In addition the coil consisted of two flying leads (inlet and outlet) each with a volume of 2.4 and 1.4 mL respectively. The coils on both bobbins were helically wound clockwise from the centre to the periphery forming a multilayer coil configuration, with a corresponding β-ratio range of 0.63-0.87.

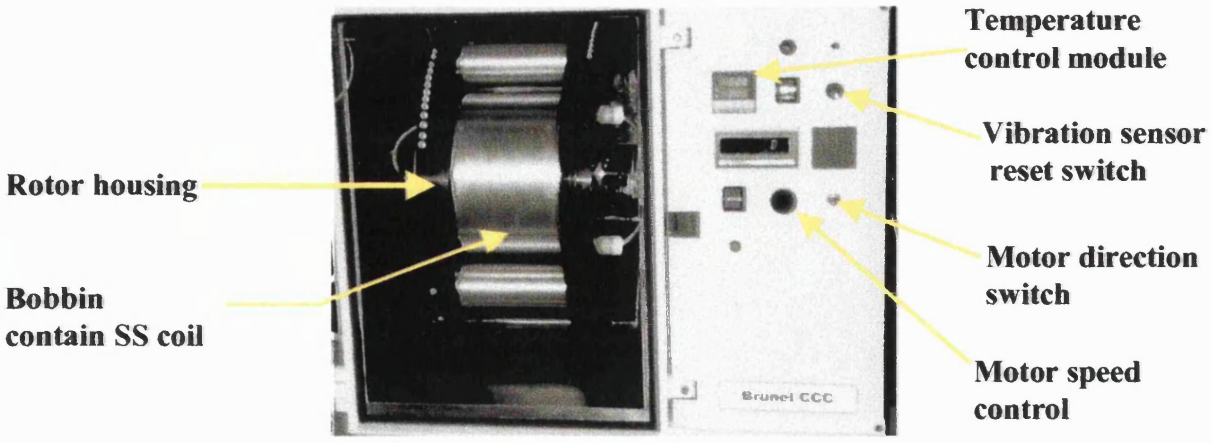

Figure 2-4 **Photograph of the Brunel pilot-scale CCC machine showing the stainless steel bobbins.**

The rotational speed of this device was from 0-1400 rpm. The rotor housing of the CCC machine was temperature controlled at 30 ± 2°C during all experiments via an internal cooling fan and a water/glycol-cooled jacket. The coolant was supplied by a Grant cooler, type RC14006 (Grant Instruments Cambridge Ltd, Herts, U.K.). Stationary and mobile phases were pumped using a Gilson HPLC pump (model 302) fitted with a 100SC head (Anachem, Luton, U.K.), and preheated to 30°C via an external stainless steel coil submersed in a Grant waterbath (Grant Instruments Cambridge Ltd, Herts, U.K.). Samples were manually injected using a Rheodyne sample valve (Rheodyne, Ronhert Park, U.S.A.) fitted with a 100 mL PTFE loop.

2.3.3. Comparison between laboratory and pilot scale CCC devices

Table 2-5 below provides, from the description of the two CCC machines given in Sections 2.3.1 and 2.3.2, a direct comparison between the two scales of operation in terms of coil geometry, materials of construction for the coils used, mode of operation and hydrodynamics.

	Laboratory scale CCC	**Pilot scale CCC**
Coil volume (mL)	94.3	928
Material of construction of coils	PTFE	SS
Coil internal diameter (mm)	1.56	3.68
Total coil length (m)	47.6	91.15
Direction of coil winding	From centre to periphery – anticlockwise	From centre to periphery - clockwise
Number of coil loops around bobbin	81	84
β-ratio range	0.80 – 0.86	0.63 - 0.87
Direction of bobbin rotation	Reverse (anticlockwise)	Forward (clockwise)
Direction of mobile phase flow for optimal S_f	Head (centre) to Tail (periphery)	Head (centre) to Tail (periphery)

Table 2-5 Comparison between the two scales of CCC.

2.3.4. Detection Methods

For this study colormetric and HPLC assays were used for quantitative and qualitative analysis of eluted CCC fractions. In addition, two types of detector were used to continually monitor the eluent stream from the CCC machine, those being the UV-visible detector and an evaporative light scattering detector (ELSD). Their principle of operation, together with their operating conditions, will be discussed in the following sections.

2.3.4.1. UV-visible absorbance detector

A Beckman System Gold model 166 (Beckman Instruments Inc., CA, U.S.A.) UV-visible detector was used during laboratory scale studies for identifying the presence of eluting compounds from CCC separations. Determination of the optimal wavelength to operate the UV-visible detector at, in order to be confident of detecting all sample components, was initially achieved by performing a wavelength scan of the crude commercial Abbott erythromycin preparation. The maximum absorbance was found to be at a wavelength of 290 nm, and was therefore used for all subsequent CCC experiments. The detector was fitted with an analytical flow cell, enabling mobile phase flow rates of up to 10 $mL.min^{-1}$ to be used. For pilot scale studies with the model system, solute detection was performed again at a wavelength of 290 nm, but using a Cecil CE272 UV spectrophotometer (Cambridge, U.K.).

2.3.4.2. Evaporative Light Scattering Detector

For on-line monitoring of erythromycin from broth-derived studies, due to the presence of numerous pigmented compounds, erythromycin detection using UV-visible absorption was not feasible. Based on published applications of using an evaporative light scattering detector (ELSD) coupled to a CCC device in such cases (Drogue *et al.*, 1991; Schaufelberger *et al.*, 1991) a model 500 ELSD (Alltech Associates Inc., IL., U.S.A.) was used for real broth experiments. The principle of detection in ELSD is that firstly the volatile component of the eluent from the CCC machine is nebulised by contact with the nitrogen 'carrier' gas, and is then immediately vaporised within the drift tube. The remaining non-volatile solute then passes down the drift tube in the carrier gas and is contacted with a laser beam, whose scattered light is then detected. The generated electrical response is a function of solute mass, hence a larger detector response signifies the presence of more of a specific solute.

Determination of the optimal operating conditions, i.e. the drift tube temperature and oxygen-free nitrogen gas (B.O.C) flow rate (SLPM) for this application was calculated from knowledge of the solvent ratios (% v/v) constituting the chosen CCC mobile phase and the manufactures corresponding temperature and gas flow rate tables specific for a range of solvents. For the aqueous methanol mobile phase (Section 4.1.3.2) used for all CCC experiments, the optimal drift tube temperature and gas flow rate used were 84 ± 0.2°C and 2.20 ± 0.01 SLPM respectively. The ELSD attenuation in all experiments was set to 2^8.

2.3.4.3. Data capture and construction of CCC chromatograms

Data capture of the analogue signals generated by either the UV-visible or ELSD detectors was performed using Beckman System Gold software (Beckman Instruments Inc., CA, U.S.A.) at a set frequency of 2 Hz. Data generated and stored during on-line monitoring was transferred initially into a Microsoft Excel™ spreadsheet package, with the respective data then copied across to the Microcal Origin software for the final construction of the CCC and HPLC chromatograms. For initial pilot scale studies (model system), data capture was performed using a Gould model BS272 chart recorder (Servoscript Instrument Services, U.K.). From the elution traces, the relative

absorbances were plotted by directly measuring the corresponding peak heights (cm) at set time intervals, with final construction of the CCC chromatograms performed using the Microcal Origin software.

2.3.4.4. Off-line fraction analysis

2.3.4.4.1. Quantitative determination of total erythromycin concentration

Off-line analysis of the total erythromycin concentration in collected CCC fractions was performed using a colorimetric assay proposed by Ford *et al.* (1953) and further developed by Danielson *et al.* (1993). The method is based on the reaction of concentrated sulphuric acid with the two sugar moieties attached to the main 14-membered ring of the erythromycin molecule (Figure 1-4). The reaction generates an intense yellow colour which can be measured spectrophotometrically at 470 nm. Sample preparation involved pipetting equal volumes of the sample and water into a test tube (to give the required dilution), followed by the addition of an equal volume of 15N H_2SO_4. The reaction mixture was then left overnight. Analysis of the resultant assay mixture was performed using a Beckman DU®-70 spectrophotometer (Beckman Instruments Inc., C.A, U.S.A.). The calibration curve was constructed over the range 0.15 to 1 $mg.mL^{-1}$ (Appendix 13.1.1). All assays were performed in triplicate and the maximum coefficient of variance for this assay was 10%.

2.3.4.4.2. HPLC analysis of CCC fraction

HPLC analysis of collected CCC fractions was performed using a C-18 reverse phase column (150 x 4.6 mm i.d.) packed with 8 μm PLRP-S [poly(styrene-divinylbenzene)] particles having a 1000Å pore size (Polymer Laboratories, Church Stretton, U.K.). The column was connected to a Beckman HPLC system (Beckman Instruments Inc., C.A., U.S.A.) comprising of an autosampler (model 507) and solvent pumps (model 126). Prior to HPLC analysis, 0.5 mL aliquots of collected CCC fractions were dried using a Speedvac SC100 (Life Science International, U.K.) at 40°C for 2 hours, or until the vial weight had stabilised. The dried fractions were then

redissolved in 1 mL of methanol before being injected onto the HPLC column (20 μL). The mobile phase used consisted of 45% acetonitrile, 55% 10 mM dipotassium hydrogen phosphate (v/v) buffered to pH 7 using a 1% H_3PO_4 solution and pumped isocratically at a flow rate of 1 $mL.min^{-1}$. The column temperature was 70 ± 0.1°C. Erythromycin analogues were detected by UV absorption at 215 nm and were identified from the known retention times of the various species present in the commercial erythromycin preparation. Quantification of the erythromycin concentration in collected fractions was achieved using calibration curves of peak area against injected concentration of the various erythromycin analogues (Appendix 13.1.2) and was performed in triplicate, the maximum coefficient of variance being 10%.

2.4. CCC setup and operation

2.4.1. Laboratory scale setup and operation

2.4.1.1. Bobbin balancing and rotation

As the CCC machine is a dynamic piece of equipment, in order to ensure both vibration free and reproducible operation, balancing of both bobbins is essential. The manufacturer of the bobbins ensure that all 'flying leads' are correctly labelled, identifying for both the inner and outer coils which is the 'Head' and 'Tail' end. The laboratory scale coils used during this study were helically wound anticlockwise from the bobbins centre to its periphery. It is therefore, at this point, important to stress the effect of rotational direction on the positioning of the 'Head' and 'Tail'. Sutherland *et al.* (2000b) have shown that by rotating the bobbins in the same direction as they are wound, the 'Head' of the coil will therefore always be situated at the centre of the coil (Figure 2-2). As in the laboratory scale CCC device used in this work, when the rotational direction is set to either FORWARD or REVERSE, the coils rotate clockwise and anticlockwise respectively. In order to position the 'Head' of the coil at the centre of the bobbins to obtain the highest degree of stationary phase retention, the coil should be rotated with the rotating switch set to REVERSE. It is therefore apparent that if, as in the work described here, the denser aqueous phase is the chosen mobile phase, the direction of mobile phase pumping should always be set from 'Head' to 'Tail'. A stepwise procedure for the setup and operation of the Brunel Lab-prep machine is given in Table 2-6. The procedure in Table 2-6 is applicable for the balancing of all coils

(Tables 2-3 and 2-4). Prior to any phase pumping, the equilibrated biphasic solvent system (achieved by vigorous mixing and equilibration overnight at room temperature) was degassed by bubbling through oxygen-free helium for a period of 10 minutes. In all cases the densities of the upper (ρ_u) and lower (ρ_l) phases were 0.657 ± 0.006 g.cm^{-3} and 0.903 ± 0.007 g.cm^{-3} respectively, determined by weighing, in triplicate, 1 mL of the respective phase on a microbalance. The average kinematic viscosities of the upper (μ_u) and lower (μ_l) phases at 30°C, obtained in triplicate, were 0.434 ± 0.002 cP and 1.087 ± 0.001 cP respectively. The average interfacial tension (σ_s) of the equilibrated two phase system, obtained by measuring in triplicate, was found to be 0.45 ± 0.02 mN.m^{-1}.

2.4.1.2. Sample preparation and injection

Once the bobbins are balanced with the required phase system, as described in Section 2.4.1.1, the CCC device is ready for sample injection. Sample preparation, for model system studies, involved weighing of the crude erythromycin solute on a microbalance, and the addition of the required volume of the degassed aqueous mobile phase used during the balancing procedure (Table 2-6). In all cases, a standardised solute injection procedure was applied. This, in the case of laboratory scale CCC experiments involved using a 1 mL, 1000 series luer tipped 'Gastight' Hamilton syringe fitted with a luer point style 3, 26 gauge needle (Fisher Scientific Ltd., Loughborough, U.K.). A volume required to completely fill the respective injection loop (1-2 mL), with Rheodyne valve in the 'load position', was carefully injected to ensure the air bubble present within the syringe would not also be injected. An additional 1 mL of the sample solution was then injected into the rheodyne injection loop, ensuring a uniform dispersion of the solute solution within the injection loop. Once a steady mobile phase flow rate through the detection device was measured, simultaneous sample injection, on-line detection/data capture and fraction collection began. Fraction collection, into 28 mL screw top glass vials (VWR International Ltd, Lutterworth, Leicestershire, U.K.), was performed at 0.5-2 minute intervals depending upon operating scale and mobile phase flow rate. These were subsequently analysed for total erythromycin and erythromycin A concentrations as described in Sections 2.3.3.4.1 and 2.3.3.4.2 respectively.

Step number	Operation
1	Connect the 'Head' end, outer coil flying lead, labelled as HO of bobbin 7/1, to the outlet of the 'stationary' phase pump.
2	Connect the 'Tail' end, outer coil flying lead on bobbin 7/1, labelled as TO, to the 'Head' end of the inner coil flying lead (HI) on bobbin 7/1.
3	Connect the 'Tail end, inner coil on bobbin 7/1 to the 'Head' end, outer coil flying lead (HO) on bobbin 7/2.
4	Connect the 'Tail' end, outer coil flying lead on bobbin 7/2 to the 'Head' end, inner coil flying lead (HI) on bobbin 7/2.
5	The 'Tail' end, inner coil flying lead (TI) on bobbin 7/2 should then be placed in a graduated measuring cylinder and secured to enable the accurate measurement of stationary phase retention.
6	The inlet solvent tubing from the isocratic pump can now be placed into the degassed phase system, i.e. the chosen stationary phase and secured. Pumping of the solvent at 10 $mL.min^{-1}$ can then be initiated.
7	Once a steady solvent stream is seen eluting from the TI flying lead of bobbin 7/2, indicating the coils are completely filled, stationary phase pumping can be stopped.
8	Using either the same isocratic pump, or a separate one, prime with the corresponding mobile phase, and connect the outlet from that pump to the HO flying lead from bobbin 7/1. Set the required mobile phase flow and start bobbin rotation in the REVERSE direction. Switch on the heater control switch ensuring operating temperature is set to 30°C.
9	Increase bobbin rotation up to 800 rpm as displayed on the tachometer. Ensure the operating temperature of the bobbin housing chamber is at 30°C before continuing.
10	Once at 800 rpm, ensure that the outlet flying lead TI from bobbin 7/2 is securely connected to the graduated measuring cylinder and that the relative volumes of both the lower mobile and upper stationary phases in the measuring cylinder have been recorded. Simultaneously start the pumping of the mobile phase and a stop watch.
11	At regular time intervals, e.g. 2 minutes, record the new relative volumes of both the upper and lower phases in the measuring cylinder, together with the operating temperature, making adjustments to the circulating cooling water rate as required to maintain the operating temperature at 30°C.
12	Continue to record the relative volumes of the eluting phases from the CCC machine until a constant stationary phase volume is obtained. This now constitutes hydrodynamic phase equilibrium across the whole system and the corresponding degree of stationary phase retention can then be calculated as described in Section 3.1.1.
13	Switch off the mobile phase pump and bobbin rotation. Once bobbin rotation has ceased, reconnect the corresponding head and tail flying leads for both the inner and outer coils on both bobbins, enabling only the required coil(s) to be used independently or in series for subsequent experimentation.

Table 2-6 Step-wise procedure for bobbin balancing and determination of S_f in the Brunel J-type counter-current chromatograph.

2.4.2. Pilot scale setup and operation

2.4.2.1. Bobbin balancing and rotation

The procedure for setup and operation of the pilot scale CCC machine was similar to that described in Section 2.4.1. The main difference was in specifying the direction of bobbin rotation and hence mobile phase flow direction. For pilot scale model and real system experiments, the stainless steel pilot coils (Section 2.3.2) due to their winding configuration were rotated in the forward (clockwise) direction, placing the 'Head' and 'Tail' end of the both coils at the centre and periphery respectively.

2.4.2.2. Sample preparation and injection

Sample preparation at the pilot scale was the same as described for the laboratory scale studies in Section 2.4.1.2. Solute injection at this operating scale was performed manually using a Rheodyne valve (Rheodyne, Ronhert Park, U.S.A.) fitted with a 100 mL loop.

2.5. Method development and CCC operation

2.5.1. Method development

The protocol for development of an effective solvent system for this study was based on a proposed generic method development strategy (Brown L. personal communication). For this specific application a broad polarity solvent system, consisting of hexane/ethyl acetate/methanol/water was first chosen. There are many published examples of the use of this phase system for the purification of antibiotics (Hochlowski *et al.*, 1991; Oka *et al.*, 1996). Having selected this phase system, the next step was distribution ratio screening by variation of the volume ratio of the four solvents, as described in Section 2.5.1.1.

2.5.1.1 Equilibrium distribution ratio experiments

Screening of the solute distribution ratio was performed by varying the volume ratio of the various solvents in the quaternary solvent system and also the aqueous phase pH. Table 2-7 lists the conditions used. For each equilibrium distribution experiment, a total system volume of 8 mL was prepared, mixed for 30 minutes and allowed to equilibrate overnight at room temperature. In all experiments (Table 2-7), the mixed solvents all formed a two phase system.

Experiment number	Ratio of phase system components Hex / EtOAc / MeOH / H_2O (v/v)
1	1.4 / 0.1 / 0.5 / 1.0
2	1.4 / 0.6 / 0.1 / 1.0
3*	1.4 / 4.5 / 1.0 / 1.0
4	1.4 / 0.6 / 3.5 / 1.0
5	1.4 / 2.0 / 0.1 / 1.0
6	1.4 / 2.0 / 2.0 / 1.0
7	1.4 / 2.0 / 3.5 / 1.0
8	1.4 / 0.6 / 2.0 / 1.0
9	1.4 / 0.6 / 1.0 / 1.0
10	pH 6
11	pH 7
12	pH 8
13	pH 9
14	pH 10

Table 2-7 Distribution ratio experiments performed with the hexane/ethyl acetate/methanol/water (v/v) biphasic solvent system. * indicates phase system used to investigate the effect of aqueous phase pH on erythromycin distribution.

To 5 mL of the aqueous phase, 2.5 mg of the crude erythromycin was added and allowed to dissolve, with 1 mL removed for initial concentration determination. To the remaining erythromycin-rich solution (4 mL), an equal volume of the upper organic phase was added. Each system was then mixed at room temperature for a period of 30 minutes using a Heildoph REAX 2 Mixer (Labplant, Huddlesfield, U.K.) at a speed setting of 4 (~40 rpm) and then left to equilibrate overnight, again at room temperature. 1 mL aliquots of both the upper and lower phases were then taken and dried under vacuum using a SpeedVac SC100 (Life Science International, U.K.) at 40°C for 1.5 hours, or until the vial weight had stabilised. The dried fractions were then redissolved

in 1 mL of methanol before being assayed for erythromycin concentration, as described in Section 2.3.3.4.1. From the results, corresponding distribution ratio values (K) were calculated as described in Section 3.1.2.

2.5.1.2. Choice of operating strategy

Based on the results from the distribution ratio experiments, as described in Section 2.4.1.1, the next stage in the method development strategy was to perform either or both normal and reverse phase gradient CCC runs. Various options for normal and reverse phase gradients have been proposed (Brown L., personal communication), those employed during this study are shown in Table 2-8.

Solvent gradient	Stationary phase type
Ethyl Acetate	Aqueous
Ethyl Acetate	Organic
Methanol	Aqueous
Methanol	Organic

Table 2-8 Normal and reverse phase CCC gradient options.

The most effective gradient elution mode using a reverse phase CCC system is through the modification of methanol content. Initially a CCC run is performed running this methanol gradient from the solvent system (A) to (B) as shown in Table 2-9. The protocol for this initial gradient run is schematically represented in Figure 2-5. These preliminary studies were performed on the laboratory scale CCC machine (as described in Section 2.3.1, initially with a 101.1 mL coil volume at a mobile phase flow rate of 2 $mL.min^{-1}$).

The final phase system composition for use in later experiments was determined based upon where on the methanol gradient the erythromycin eluted.

Phase system	Solvent ratios Hex / EtOAc / MeOH / H_2O (v/v)
A	1.4 / 2.0 / 0.05 / 1.0
B	1.4 / 2.0 / 2.0 / 1.0

Table 2-9 **Solvent phase compositions used to perform a reverse phase methanol gradient. Phase system (A) corresponds to the beginning of the gradient where the mobile phase composition is 100% (A), 0% (B). Phase system (B) corresponds to end of the gradient, where the mobile phase composition is 0% (A), 100% (B).**

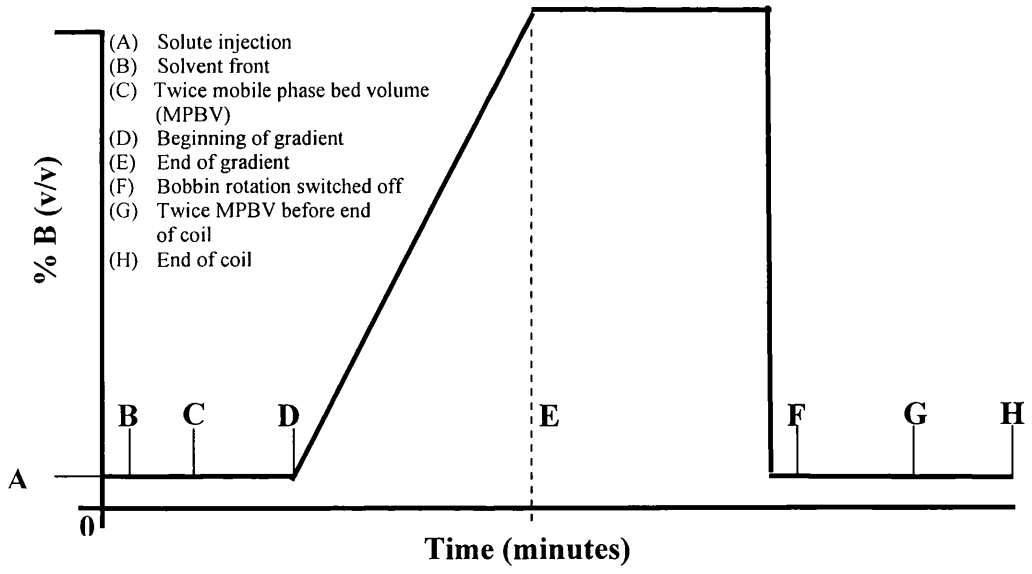

Figure 2-5 **CCC operating conditions for a reverse phase methanol gradient used in the CCC method development.**

3. Chromatography and Fractionation diagram theory

3.1. Chromatographic parameters for CCC

The formulae used to calculate the various chromatographic parameters associated with CCC technology are somewhat different to those for conventional HPLC, and hence are briefly summarised here along with the theory used for the construction of fractionation diagrams from CCC chromatograms.

3.1.1. Stationary phase retention

An important hydrodynamic parameter in CCC is the volume of stationary phase retained (S_f) in the CCC column. S_f determines not only the degree of solute retention but also the achievable resolution between two feed components (Conway, 1990). The initial stage in determining S_f requires accurate volumetric measurement of the chosen stationary phase eluting from the coil prior to establishment of a hydrodynamic equilibrium under the chosen operating conditions, i.e. mobile phase flow rate, pumping direction and bobbin rotational speed/direction. The experimental approach to determining S_f is described in Sections 2.4.1.1 and 2.4.2.1.

Let $V_{s\text{-}start}$ and $V_{s\text{-}end}$ correspond to the recorded volumes of the organic stationary phase within the graduated measuring cylinder prior to and after hydrodynamic phase equilibrium is achieved. V_e is the volume of stationary phase originally in the coil that has been displaced by the aqueous mobile phase (Section 2.4) and is equal to $V_{s\text{-}end} - V_{s\text{-}start}$. This experimental data, together with knowledge of the volumes of the coil inlet (V_{in}) and outlet (V_{out}) flying leads (Tables 2-3 and 2-4) enables the corrected V_e values to be calculated according to:

$$V_{e-corrected} = V_e - (V_{in} + V_{out}) \qquad 3.1$$

Since the content of the CCC coil at hydrodynamic equilibrium is comprised entirely of the biphasic solvent system in a ratio (S_f) determined by the operating conditions employed, it can therefore be deduced that the total coil volume (V_c) is equal to the sum of stationary and mobile phase volumes within the coil:

$$V_c = V_s + V_m \qquad 3.2$$

If $V_m = V_e$, with $V_{e\text{-corrected}}$ being equal to the actual volume of stationary phase displaced from the column, Equation 3.2 can be rewritten as:

$$V_c = V_s + V_{e-corrected} \qquad 3.3$$

By rearranging Equation 3.3, together with knowledge of V_c from the manufacturer's data, as presented in Table 2-3 and 2-4 for the laboratory scale coils, and in Section 2.3.2 for the pilot scale coil, the volume of the stationary phase can be calculated:

$$V_s = V_c - V_{e-corrected} \qquad 3.4$$

Stationary phase retention is the fraction of stationary phase within the coil and is commonly represented as the stationary phase fraction or a percentage ($100.S_f$):

$$S_f = \frac{V_s}{V_c} \qquad 3.5$$

3.1.2. Solute distribution ratio

The distribution ratio represents the underlying basis of separation in CCC where, due to the lack of a conventional solid support, solute distribution is entirely dependent upon its partitioning between the two liquid phases. In batch partitioning studies the distribution ratio (K) is calculated according to:

$$K = \frac{C_s}{C_m} \qquad 3.6$$

where C_s and C_m correspond to the solute concentration at equilibrium in the stationary and mobile phases respectively. The relationship between K and a CCC chromatogram has been described by Schaufelberger (1996) and is illustrated in Figure 3-1.

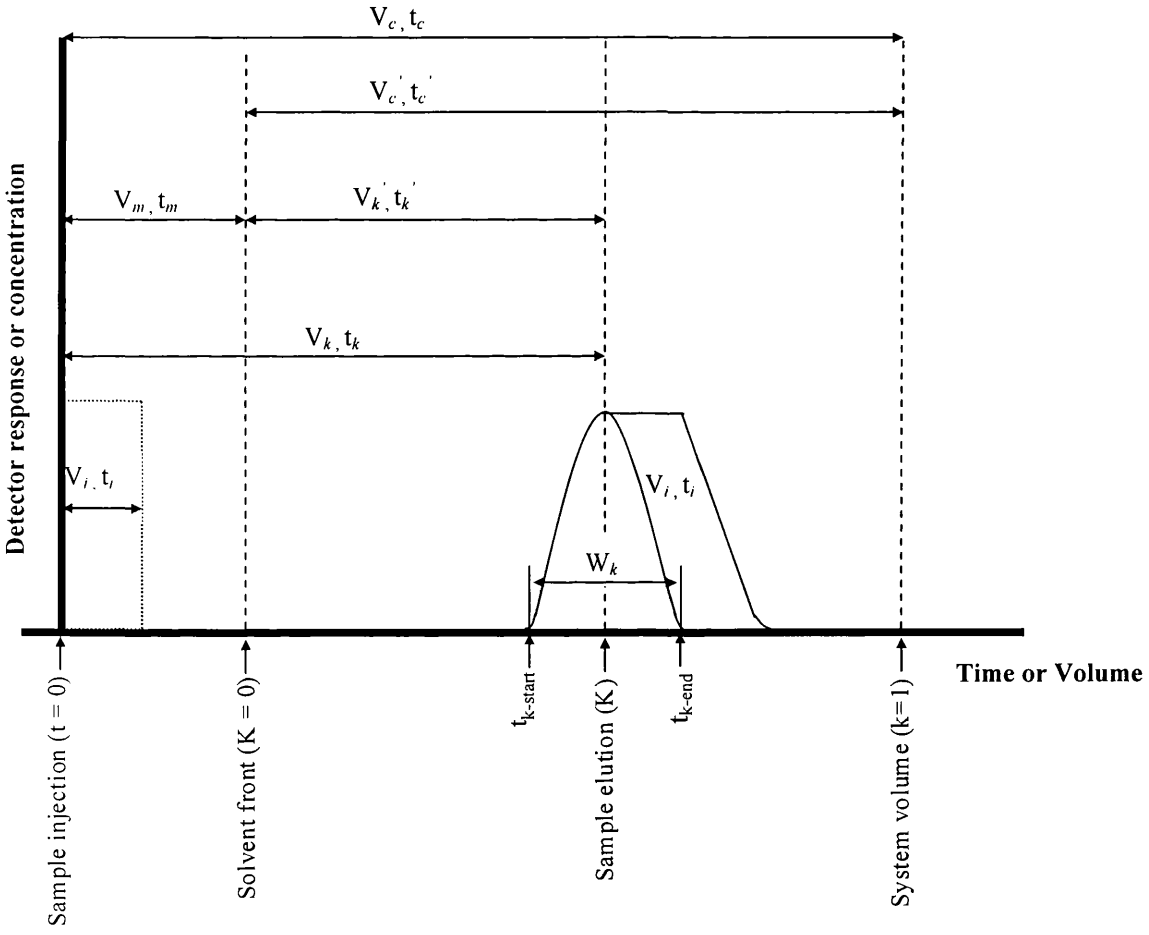

Figure 3-1 Schematic represention of a CCC chromatogram illustrating the relationship between the solvent front (K = 0), the elution of a sample (K) and the system volume (K = 1). Also shown is the effect of increasing sample injection volume (V_i) on peak broadening. Redrawn from Sutherland *et al.*, 2001a.

K values can be calculated directly from Figure 3-1 from knowledge of the solute elution time (t_k) and phase volumes (V_s and V_m) within the CCC coil under stable

hydrodynamic equilibrium as described in Section 3.1.1. Firstly, in order to derive K from the CCC chromatogram, accurate knowledge of the time for the K = 0 and K = 1 points to elute is required. The K = 0 and K = 1 points correspond to the mobile phase and system volume respectively and can be calculated using.

$$t_m = \frac{V_m}{F} \qquad t_c = \frac{V_c}{F} \qquad 3.7$$

where F corresponds to the mobile phase flow rate ($mL.min^{-1}$), with the units of t_m and t_c being in minutes. The K value for the eluting solute is calculated from the solvent front (K = 0), i.e. correcting for the volume of mobile phase already present in the coil under hydrodynamic equilibrium as shown below:

$$K = \frac{t_k - t_m}{t_c - t_m} = \frac{t_k'}{t_c'} \qquad 3.8$$

3.1.3. Retention factor

The retention factor (k) is a more practical quantity than the distribution ratio (K) for describing the retention characteristics of feed components. It can be considered to be the number of molecules of a solute in the stationary phase (Q_s) compared to the number of solute molecules in the mobile phase (Q_m) per unit volume:

$$k = \frac{Q_s}{Q_m} \qquad 3.9$$

This parameter therefore describes the ability of the stationary phase to retain feed components, and as such is a dimensionless measure of the actual retention properties of the stationary phase in the CCC coil. The retention factor (k) is related to the distribution ratio by the phase volume ratio (Conway, 1990) as follows:

$$k = \frac{C_s V_s}{C_m V_m} = K \frac{V_s}{V_m} = K\left(\frac{S_F}{1-S_F}\right) \qquad 3.10$$

3.1.4. Separation factor

The ability of the stationary phase to separate two feed components, for example erythromycin B/psu-EEA (EB/psu-EEA) and erythromycin A (EA), where EB is the more strongly retained component, can be determined directly from the relative distribution ratios, retention factors (k) or the corrected retention times, t_k' (Equation 3.8) as shown below:

$$\alpha = \frac{K_{EB\,/\,psu-EEA}}{K_{EA}} = \frac{k_{EB\,/\,psu-EEA}}{k_{EA}} = \frac{t'_{k-EB\,/\,psu-EEA}}{t'_{k-EA}} \qquad 3.11$$

As the larger value of the two terms is set as the nominator, the resultant value for α will always be greater than unity, i.e. greater than one for both normal and reverse phase modes of operation.

3.1.5. Resolution

This is another dimensionless number enabling the degree of separation between two feed components to be determination; the resolution (R_s). R_s is a measure of zone overlap, and as such acts as a indication of column efficiency (Section 3.1.6). In order for resolution to be accurately calculated, adjacent peaks must be sufficiently resolved so that accurate measurement of the peak areas can be obtained (Braithwaite and Smith, 1996). In chromatography a minimum R_s of 1 is deemed acceptable and corresponds to a 4σ separation, i.e. 95.5% of a Gaussian distribution is contained within $\pm 2\sigma$ (σ corresponds to the standard deviation of the Gaussian peak describing the degree of band spreading). Calculation of R_s within this σ range involves the determination of the corresponding peak widths (w_B and w_A) according to:

$$R_s = \frac{2(t_{kB} - t_{kA})}{w_B + w_A} = \frac{2\Delta_t}{w_B + w_A} \qquad 3.12$$

The achievable peak resolution is dependent upon a number of factors, namely the retention characteristics of each component (k), the degree of selectivity of the stationary phase to retain the solute components (α) and the overall efficiency of the column (*N*). The derivation of Equation 3.13, which relates all the above factors, is discussed by Braithwaite and Smith (1996), where k_2 corresponds to the retention factor for the second peak, i.e. the peak with the larger retention factor, calculated using Equation 3.10. The separation factor (α) is calculated using Equation 3.11, with *N* calculated using $N = 16.(t_R/w_B)^2$.

$$R_s = \frac{\sqrt{N}}{4}\left(\frac{k_2}{k_2+1}\right)\left(\frac{\alpha-1}{\alpha}\right) \qquad 3.13$$

3.1.6. Column efficiency

Column efficiency, or the number of theoretical plates (*N*), was estimated using an alternative formula to $N = 16.(t_R/w_B)^2$ (Equation 3.14) based on the geometry of the normal curve but using the peak width at one half the peak height, $W_{h/2}$. This is less susceptible to error in drawing tangents and is more appropriate for use with peaks that exhibit significant tailing or that slightly overlap the adjacent peaks (Synder and Kirkland, 1979). The quantities V_R, and $W_{h/2}$ are usually measured as distances (d_R and $d_{h/2}$) on the chromatogram. At a constant flow rate, the units of either time or volume on the horizontal axis of a CCC chromatogram will be proportional and therefore either can be used to provide a value for d_R and $d_{h/2}$.

$$N = 5.54\left(\frac{V_R}{W_{h/2}}\right)^2 = 5.54\left(\frac{d_R}{d_{h/2}}\right)^2 \qquad 3.14$$

However, Conway (1990) suggests that the use of this conventional equation for calculating N (Equation 3.14) for a Gaussian peak, can lead to large overestimations of column efficiency, since in CCC the t_m value is relatively large compared to that in solid-phase chromatography. It has been advocated that the effective theoretical plate number, N_{eff} (Equation 3.15), is a more accurate means of comparing column performance where there are variations in the phase volume ratio, as it incorporates the contribution of the phase volume ratio and varies less than N as a function of k (Synder and Kirkland, 1979):

$$N_{eff} = N\left(\frac{k}{k+1}\right)^2 \qquad 3.15$$

3.1.7. Throughput

Throughput of the solute through the CCC machine (T) was estimated in terms of kilograms of purified erythromycin per day and was based on the continuous operation of a CCC instrument fitted with parallel columns as shown below:

$$T = Q_r \times N_{op} \qquad 3.16$$

where Q_r is the mass of recovered erythromycin (mg) and N_{op} corresponds to the number of operational runs achievable per day (24 hours). Note that the time required for input of the stationary phase is neglected in throughput calculations, as this would become insignificant over extended periods of operation.

3.2. CCC scale-up theory

The basic theory related to the scale-up of CCC has previously been described by Sutherland *et al.* (2001a). The extended theory is presented here in two parts. The first deals with the prediction of solute elution time based on knowledge of the solute distribution ratio (Section 3.1.2) from a laboratory scale machine and knowledge of the hydrodynamics (Section 3.1.1) of the pilot scale machine. This assumes that for a given

separation, performed at an equivalent mobile phase flow rate and solute loading with the same biphasic solvent system, the solute distribution ratio (Equation 3.6) remains constant. The second part of the extended theory deals with prediction of the start and end points of a peak upon increased sample injection volume.

3.2.1. Pilot scale predictions based on a laboratory scale separation

The first stage in the predictive scale-up methodology is to perform a laboratory scale CCC separation of the target compound. This allows initial calculation of the solute distribution ratio, K. From the schematic chromatogram shown in Figure 3-1, the distribution ratio for the centre of the target compound peak (K) is calculated according to Equation 3.8, where all values used are in units of time (minutes). The t_k term is obtained directly from the CCC chromatogram (Figure 3-1), while t_m and t_c are calculated according to Equation 3.7.

Once the laboratory scale distribution ratio for the peak of interest is known, the next step is to experimentally determine the relationship between the degree of stationary phase retention (S_f) and the mobile phase flow rate at the pilot scale using the same biphasic solvent system. Du *et al.* (1999) have shown that there is a linear relationship between S_f and the square root of the mobile phase flow rate ($F^{0.5}$). This enables, simple and reliable prediction of S_f based on only two retention tests, and therefore the corresponding volumes of mobile (V_m) and stationary (V_s) phase. The equations used to calculate S_f are described in Section 3.1.1.

By rearranging Equation 3.8 and assuming K is constant at the two scales of operation, it is possible to determine t_k at the larger scale, as shown below:

$$t_k = Kt_c^{'} + t_m \qquad 3.17$$

The significantly longer sample injection time at the larger scale can also be accounted for as shown in Equation 3.18:

$$t_k = Kt_c^{'} + (t_m + t_i) \qquad 3.18$$

where t_i corresponds to the time required for solute introduction. A similar procedure to that described above can also be used to predict $t_{k\text{-start}}$ and $t_{k\text{-end}}$ for the peak of interest.

3.2.2. Prediction of peak elution times with increased injection volume

At the pilot scale, in order to further increase throughput, larger sample injection volumes must be used. The CCC model, as described in Section 3.2.1, also enables predictions of the elution time for the start ($t_{k\text{-start}}$) , centre (t_k) and end ($t_{k\text{-end}}$) of a peak of interest. Figure 3-1 illustrates schematically the effect of an increase in injection volume (V_i) on band broadening. It can be seen that increasing the injection volume by V_i results in the peak width increasing by V_i and hence alters $t_{k\text{-end}}$. In order to account for this, the first step is to perform a pilot scale separation using an equivalent injection volume (e.g. 10 mL injection onto a 1000 mL coil) to that used at the laboratory scale, and directly measure from the resultant chromatogram the corresponding peak width (W_k) and value of t_k. The start, centre and end of peak elution can then be calculated using:

$$t_{k-start} = t_{k-anal} - \frac{w_k}{2} \qquad 3.19$$

$$t_{k-centre} = t_{k-anal} + t_i \qquad 3.20$$

$$t_{k-end} = t_{k-anal} + \frac{w_k}{2} + t_i \qquad 3.21$$

The CCC scale-up model (Sutherland *et al.*, 2001a) assumes that for a given separation at a constant mobile phase flow rate, regardless of the size of the solute loading volume used, the start of peak elution remains constant. For repeated injection

schedules however, or in cases where there is gradual leakage of the stationary phase during operation (Graham *et al.*, 2001), t_m may vary between runs. This can be accounted for by incorporating a Δt_m term as described in Equations 3.22 to 3.24 as described below:

$$t_{k-start} = t_{k-anal} - \frac{w_k}{2} - \Delta t_m \qquad 3.22$$

$$t_{k-centre} = t_{k-anal} + t_i - \Delta t_m \qquad 3.23$$

$$t_{k-end} = t_{k-anal} + \frac{w_k}{2} + t_i - \Delta t_m \qquad 3.24$$

The t_k values on the left hand side of Equations 3.22 to 3.24 correspond to the predicted elution times as a result of increasing loading volume. The $t_{k\text{-anal}}$ values corresponding to the solute retention times of the peak of interest determined from a pilot scale analytical injection volume experiment. The value of Δt_m is obtained from the difference in the t_m values for two operational runs.

3.3. Fractionation diagram theory

The determination of chromatographic performance to changes in operating conditions have previously been evaluated directly from resultant chromatograms (Ngiam *et al.*, 2001). A model should enable the determination of the cut points, i.e. to consistently identify the start and end points for sample collection to obtain the target product at the maximum purity and yield. Research within our laboratories has focused on the development of a fractionation diagram approach, initially to investigate fractional protein precipitation (Richardson *et al.*, 1989, 1990), and more recently as a graphical method for determining chromatographic performance in terms of the process trade-off between purity and yield (Ngiam *et al.*, 2001). The stages involved in this modelling technique are visually provided in Figure 3-2.

3.3.1. Construction of fractionation diagrams

To construct a fractionation diagram the whole process is simplified into a three component system, the target product (labelled 'P') and the contaminants, labelled as 'A' and 'B'. The contaminants are treated as two pseudo-components, i.e. the contaminant(s) eluting just before and just after the solute of interest. The CCC chromatogram is then divided into *N* steps with equal widths of time or volume (mL), determined prior to the separation. From fractions collected at each of the specified intervals off-line HPLC determination of the erythromycin concentration can then be performed to determine the amount of product (M_p), impurities A (M_A) and B (M_B). Hence for the *i*-th interval, defined as the arithmetic mean time (t_{am}) between the upper and lower limit of the interval, each of the fraction components would be donated as being to the *i*-th term, with the total amount of solute in a particular fraction (M_T) being the sum of all components:

$$M_{Ti} = M_{Pi} + M_{Ai} + M_{Bi} \qquad 3.25$$

The next stage is to calculate the cumulative fraction of total solute components (Cum. fraction P + (A + B)), i.e. cumulative fractional mass of solute components at a time interval 't' over the total mass of solute components at t = ∞, and the cumulative fraction of the target product (Cum. fraction P). From this one can plot the cumulative fractional mass of total solutes eluted on the *x*-axis and the cumulative fraction of product on the ordinate to generate the sigmodial fractionation diagram (Figure 3-2; Stage 3). Since both axes are expressed as fractions, the scales in all cases will range between 0 and 1.

3.3.2. Construction of purification factor versus yield diagrams

The next stage in cut point determination is the construction of the purification factor (PF) versus yield graph. For demonstrative purposes, if we consider the points 1 and 2 on the fractionation diagram (Figure 3-2; Stage 3), the PF versus yield diagram is achieved by calculating the gradient of the tie line between any combination of two

points, and their corresponding yield. This term can be written as:

$$PF = \left[\frac{M_P^{(2)} - M_P^{(1)}}{\left(M_P^{(2)} + M_I^{(2)}\right) - \left(M_P^{(1)} + M_I^{(1)}\right)}\right] \Big/ \left(\frac{M_o}{M_s}\right) \qquad 3.26$$

Since from Equation 3.25 M_T is equal to $M_P + M_I$, then Equation 3.26 can be rewritten and rearranged as shown below:

$$PF = \left[\frac{M_P^{(2)}}{M_O} - \frac{M_P^{(1)}}{M_O}\right] \Big/ \left[\frac{M_T^{(2)}}{M_S} - \frac{M_T^{(1)}}{M_S}\right] \qquad 3.27$$

The subscripts P and S correspond to the amount of product (total solute mass injected) and sample (target solute). The subscript O corresponds to the initial target solute concentration (EA) in the feed. Hence, from Equation 3.27 the nominator and denominator terms (M_P/M_O) and (M_T/M_S) respectively, corresponds to the *y* and *x*-axis respectively. The superscripts (1) and (2) correspond to the start and end collection times. For any given PF value between any combinations of two collection points there is also a corresponding total target solute yield (%) value which can be calculated. This yield term is expressed as the difference in the *y*-axis values between the collection times (2) and (1), hence is the nominator term of Equation 3.27. The yield values correspond to the percentage of initial total product mass recovered in the fraction collected between two specified cut points.

The outcome of calculating the PF and product yield (%) values for all possible collection time combinations is the generation of a PF versus product yield (%) diagram as shown in Figure 3-3.

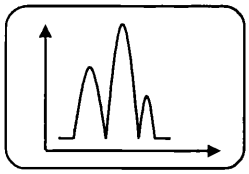

STAGE 1 – On-line CCC chromatogram illustrating elution peaks.

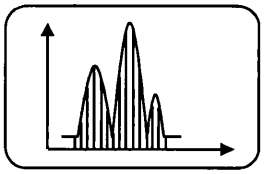

STAGE 2 – Division of chromatogram into predetermined steps of equal time or volume together with quantitative/qualitative analysis.

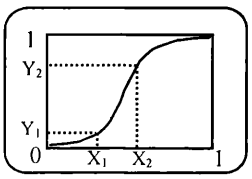

STAGE 3 – Construction of the fractionation diagram.

$$\text{Yield} = Y_2 - Y_1$$

$$PF = \frac{Y_2 - Y_1}{X_2 - X_1}$$

STAGE 4 – Evaluation of PF and product yield (%) for any combination of collection points

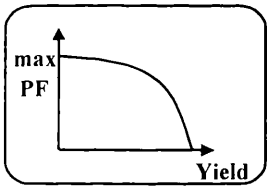

STAGE 5 – Determination of PF_{max} for any required product yield.

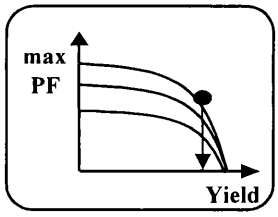

STAGE 6 – Identification of optimal trade off between required product purity (PF_{max}) and product yield.

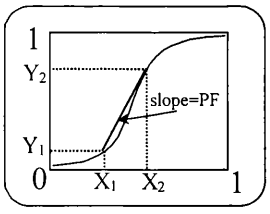

STAGE 7 – Determination of time or volume cut points corresponding to the identified optimal trade off between PF_{max} and product yield from Stage 6.

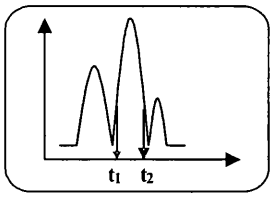

STAGE 8 – Final cut point determination on initial CCC chromatogram from Stage 1.

Figure 3-2 Stages involved in the construction of fractionation and PF_{max} versus product yield diagrams for the identification of collection points for the optimal trade off between product purity and yield. Redrawn from Ngiam *et al.*, 2001.

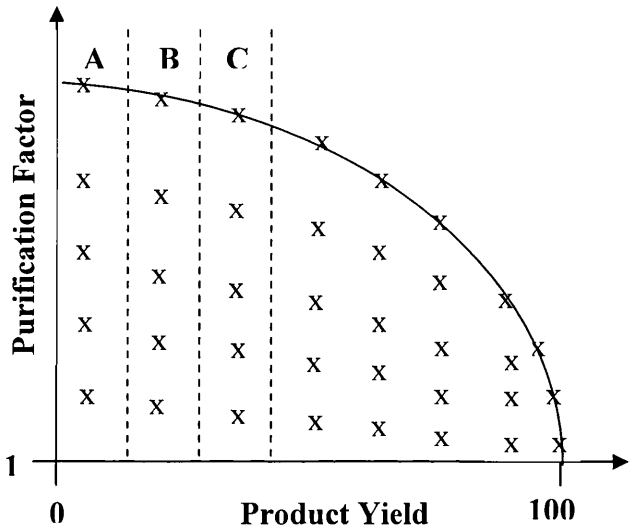

Figure 3-3 Schematic represention of a PF versus product yield diagram. For any given yield value, presented as A, B and C regions, there exists a number of possible PF values. Solid line represents the upper boundary (PF_{max} boundary) where the optimal PF value for a fixed product yield would be achieved. Redrawn from Ngiam *et al.*, 2001.

Finally a 'searching-type' algorithm can be used to determine for each set product yield value the optimal PF value (PF_{max}) that could be obtained, with the corresponding plot of PF_{max} versus product yield generating a single line similar to the upper (PF_{max}) boundary illustrated in Figure 3-3. In addition, during the simulation a set of corresponding data of the PF_{max} for each product yield is recorded for use in later identifying the required start and end collection points to achieve a desired level of product purity and yield (Stages 7 and 8; Figure 3-2).

The final purity of the target product after purification, in an ideal process, where baseline separation is achieved, would be 100% (w/w). This 100% product purity value, at 100% product yield, would constitute the maximum PF value attainable:

$$PF_{max} = \frac{100}{x} \qquad 3.28$$

Hence, from Equation 3.28 it can be deduced that PF_{max} is equal to the ratio of the final product purity, i.e. after purification, to the initial product purity:

$$PF_{max} = \frac{Final\ product\ purity}{Initial\ product\ purity} \qquad 3.29$$

3.4. Performance measures in chromatography (the Van deemter equation)

Band broadening in chromatographic separations is a factor which must be minimized to ensure that high-resolution separation of closely related compounds can be achieved, and is the result of a number of random molecular processes, which can be broadly grouped into non-column and column effects. Non-column effects are the result of solute molecules dispersed within the 'dead volume' of the chromatographic system, comprising of the injector and connections before the column and between the column and the active part of the injector, due to mixing caused by eddy or whirlpool effects. These effects are more pronounced at lower mobile phase flow rates and hence good design of injectors, detectors, tubing and fittings to minimize the dead volume is important to achieve good resolution.

The non-equilibrium theory, referred to as 'random walk theory' for band broadening has been proposed by Giddings and co-workers (1965). This assumes that during the chromatography the solute molecules progress through the column in a succession of steps, where, at each step, random molecular dispersion occurs. At each of these steps, also termed theoretical plates, the solute molecules during phase interaction, i.e. between the organic and aqueous liquid phases in CCC, try to attain an equilibrium. The equilibrium is dictated by the distribution ratio (Equation 3.6; Section 3.1.2), but due to slow mass transfer kinetics, complete equilibrium is not achieved, which ultimately results in broadening of eluting peaks.

Column band broadening in conventional solid phase chromatography has been shown to be the result of three molecular diffusion processes, all related by the Van deemter equation (Equation 3.30):

$$H = A + \frac{B}{\bar{u}} + C_S\bar{u} + C_M\bar{u} \qquad 3.30$$

where the H term, known as the height equivalent to a theoretical plate (HETP), is length of the column available divided by N (Section 3.1.6), i.e. $H = L/N$. ū is the average linear mobile phase velocity ($cm.s^{-1}$). The A-term in Equation 3.30 corresponds to 'eddy diffusion' of the solute molecules, i.e. the number of variable pathways the mobile phase, and hence the solute molecules, could take. The B-term relates to the longitudinal diffusion of the solute molecules in the mobile phase. This type of diffusion takes place along the axis of the column, parallel to the direction of mobile phase flow. This lateral movement (molecular diffusion) contributes to band broadening by the solute molecules either moving ahead or lagging behind the peak maxima. The C-term relates to the mass transfer rate of the solute between the two phases (organic stationary and aqueous mobile). It is therefore greatly influenced by the distribution ratio (Equation 3.6) and hence the relative solubility of the solute in the stationary phase. In addition this C-term is affected firstly by mobile phase flow rate, decreasing with decreasing mobile phase flow, effectively allowing more time for hydrodynamic equilibrium to be achieved. Secondly the C-term is affected in solid phase chromatography by the depth of the stationary liquid-phase film, and can be minimized by keeping this stationary phase film as thin as possible, effectively minimizing diffusional effects within this phase. Since in CCC the stationary phase is liquid, then as shall be shown later (Section 10.4), minimizing this film thickness, i.e. reducing the S_f within the coil, decreases this C-term enabling higher mass transfer rates to be achieved.

In CCC a number of methods have been proposed for calculating the average linear mobile phase velocity (ū). Due to phase retention within the coil, the mobile phase present within the coil at hydrodynamic equilibrium can be viewed as occupying an area of the tubing, where one side is bound by the outer circular tubing wall and the other by the interface with the stationary phase. This semi-circular configuration remains constant along the length of the coil whilst in motion, i.e. rotating. The average linear mobile phase velocity within a circular tubing of known length is calculated by:

$$u = \frac{F}{A} \qquad 3.31$$

where F corresponds to the mobile phase flow rate ($mL.min^{-1}$), A corresponds to the cross-sectional area of the tubing ($\Pi.d^2$), and 'd' corresponding to the internal tubing diameter (mm). Equation 3.31, however, is only true for a system where no retention of the stationary phase is present. Hence, in calculating '$\bar{u}$', a correction must be made for the proportion of the mobile phase occupying the coil at hydrodynamic equilibrium:

$$\bar{u} = \frac{4.(F/60)}{\Pi.d^2 \times \left(\frac{V_M}{V_C}\right)} \qquad 3.32$$

V_M and V_C correspond to the volume of mobile phase and the system volume (mL) respectively. F corresponds to the mobile phase flow rate ($mL.min^{-1}$), with the units of '$\bar{u}$' therefore being $cm.s^{-1}$.

4. Method development

The aim of this Chapter is to demonstrate the principle of a generic method development strategy for CCC to rapidly identify an effective solvent system and operating mode for the successful fractionation and recovery of erythromycin A from its structurally similar analogues.

4.1. Solvent system development

An important prerequisite for any chromatographic technique is the development of an effective, robust solvent system and optimal operating mode for the purification challenge in question. CCC can in principle use any solvent mixture that forms a biphasic system, and with such a wide range of solvent combinations available, determination of the most effective biphasic solvent system for a given separation may be difficult (Berthod, 1991). In CCC the main aim in solvent selection and subsequent optimisation is to form a solvent mixture in which the target solute is readily soluble, with the solvent system ratios then altered to ensure the distribution ratio of the target solute differs enough from the other contaminants (Foucault and Chevolot, 1998) to enable acceptable separation both in terms of resolution and required process time. A study by Oka *et al.* (1991) has identified a number of requirements for successful selection of a suitable two-phase solvent system:

- The equilibrated solvent system should provide nearly equal volumes of the upper and lower phase, enabling either phase to be used as the mobile one without excessive solvent wastage.
- The settling time of the two-phase system should, for HSCCC, be less than 30 seconds to provide satisfactory stationary phase retention in the column.
- The distribution ratio (K) of the desired compound should equal or be close to one.

This group also notes that the search for suitable solvent systems has previously 'entirely relied on a laborious and time-consuming trial and error method which has often discouraged the users of CCC, while the methods for a systematic solvent search have not been reported'. In the context of this work, the emphasis was on the industrial scale application of CCC, and hence any solvent selection methodology would have to be generic, rapid, and sufficiently simplistic for non-experts to successively develop robust solvent systems. The results presented are the outcome of a novel generic method development strategy developed under a BBSRC-LINK initiative comprising of a number of academic institutions and industrialists. Researchers from the Mass Spectrometry Research Unit at the University of Wales (Swansea) under the guidance of Dr Les Brown (AECS Ltd, P.O.Box 80, Bridgend, S.Wales) initially focused on the detailed identification of an initial solvent system, finding that for complex feed streams a broad polarity hexane (Hex), ethyl acetate (EtOAc), methanol (MeOH) and water (H_2O) system was effective.

4.1.1. Equilibrium distribution ratio studies.

The initial screening of distribution ratios for the crude erythromycin preparation was performed as described in Section 2.5.1.1. The results provided are in Table 4-1. Firstly, the biphasic system is established between the pure apolar hexane and polar water due to their immiscibility, i.e. high density and interfacial tension differences. The results of experiments 1-9 indicate that there are a wide range of erythromycin distribution ratios obtained by varying the methanol and ethyl acetate content. In effect, variations in the amount of methanol and ethyl acetate cause changes in solute distribution by varying the polarity across the biphasic solvent system. The term polarity, both in solvent extraction and chromatography designates the rank-order ability of a solvent to extract, or increase the rate of chromatographic migration (Conway, 1990) and it is this collective polarity of the solvent or solvents which determines the magnitude of the solute distribution ratio. In order to understand the effects of polarity variations on the resultant erythromycin distribution ratio, an indexing scheme can be used.

Experiment number	Integer ratios of phase system components Hex / EtOAc / MeOH / H_2O (v/v)	Erythromycin distribution ratio ($K = C_{org}/C_{aq}$)
1	1.4/0.1/0.5/1.0	0.48
2	1.4/0.6/0.1/1.0	0.52
3*	1.4/4.5/1.0/1.0	1.29
4	1.4/0.6/3.5/1.0	1.87
5	1.4/2.0/0.1/1.0	1.05
6	1.4/2.0/2.0/1.0	0.33
7	1.4/2.0/3.5/1.0	0.17
8	1.4/0.6/2.0/1.0	0.14
9	1.4/0.6/1.0/1.0	0.11
10	pH 6	0.42
11	pH 7	0.41
12	pH 8	2.73
13	pH 9	6.41
14	pH 10	3.92

Table 4-1 Variation in equilibrium erythromycin distribution ratio with phase system composition and pH. * indicates phase system number 3 chosen to investigate the effect of pH on K.

4.1.2. Solvent polarity indices.

Numerous polarity indexing schemes for solvent characterisation have been proposed, such as the Hildebrand solubility parameter (δ) which links solvent polarity to its solubilisation capability, defining solubility as the energy necessary to separate two molecules of that solvent (Hildebrand and Scott, 1962). Synder (1979) proposed a polarity scale based on the adsorption strength of the solvent for the solute, identifying four distinct interaction mechanisms: dipole-dipole, dispersion, hydrogen-bonding and dielectric. The larger combination of these four interaction mechanisms, would result in a stronger attraction between the solute and the solvent. Because of the wide range of solvent component variations in the quaternary phase system used during this study however, phase system polarity was determined using the Rohrschneider (1973) solvent polarity parameter, P′. This parameter evaluates a solvent's ability to act either as a hydrogen bond donor or acceptor, or to generate dipole-dipole interactions. Experimental results from Rohrschnedier's studies demonstrate that the polarity of a

solvent mixture, such as those investigated here, is calculated from the arithmetic average of the P′ values of the pure solvents 'a' and 'b' as shown in Equation 4.1, where ϕ is the volume fraction of each solvent.

$$P' = \Phi_a P'_a + \Phi_b P'_b \qquad 4.1$$

For the pure solvents used during this study, Table 4-2 shows the corresponding Rohschneider solvent polarity parameters. These values indicate an increasing P′ value with increasing hydrophilicity, i.e. an increase in solvent polarity.

Solvent	Rohrschneider solvent polarity parameter (P′)
Hexane	0.1
Ethyl Acetate	4.4
Methanol	5.1
Water	10.2

Table 4-2 Rohrschneider solvent polarity parameters (P′) for the pure solvents used in this study. Data from Menet and Rolet-Menet (1999).

The first stage in generating polarity values for the phase systems investigated here is to present the phase compositions in percentage terms. Generally, multi-component phase system composition are presented as integer ratios, which however provides little basis for the comparison of a range of mixtures (Conway, 1990). Table 4-3 presents the volumetric composition (mL) of each solvent in phase systems 1-9 (Table 4-1) and the value for the mixture calculated according to Equation 4.1.

Based on the equilibrium distribution ratio results presented in Table 4-1, five phase systems were selected and again screened to narrow down the search for the phase systems for subsequent gradient CCC operation. The chosen phase system with their calculated distribution ratios and corresponding Rohrschneider phase polarity values (P′) are given in Table 4-4. Experimental data for these specified distribution studies are presented in Appendix 13.2.

Phase system number	Integer ratios of phase system components Hex / EtOAc / MeOH / H_2O (v/v)	Volumetric composition of phase system components Hex / EtOAc / MeOH / H_2O (mL)	Rohrschneider pure solvent polarity (P′) for Hex / EtOAc / MeOH / H_2O	Polarity (P′) of solvent mixture
1	1.4/0.1/0.5/1.0	3.7/0.3/1.3/2.7	0.05/0.15/0.85/3.40	4.44
2	1.4/0.6/0.1/1.0	2.8/1.2/2.0/2.0	0.05/0.85/0.16/3.29	4.35
3	1.4/4.5/1.0/1.0	1.4/4.6/1.0/1.0	0.02/2.51/0.65/1.29	4.46
4	1.4/0.6/3.5/1.0	1.7/0.7/4.3/1.2	0.02/0.41/2.75/1.57	4.74
5	1.4/2.0/0.1/1.0	2.5/3.6/0.2/1.8	0.03/1.96/0.11/2.27	4.37
6	1.4/2.0/2.0/1.0	1.8/2.5/2.5/1.3	0.02/1.38/1.59/1.59	4.58
7	1.4/2.0/3.5/1.0	1.4/2.0/3.5/1.0	0.02/1.11/2.26/1.29	4.68
8	1.4/0.6/2.0/1.0	2.2/1.0/3.2/1.6	0.03/0.53/2.04/2.04	4.64
9	1.4/0.6/1.0/1.0	2.8/1.2/2.0/2.0	0.04/0.66/1.28/2.55	4.52

Table 4-3 **Variation in quaternary solvent system polarity (P′) with variations in volumetric fraction of hexane, ethyl acetate, methanol and water.**

Phase system number	Polarity (P′) of solvent mixture	K Values $= C_{org}/C_{aq}$
1	4.37	1.1
2	4.58	0.3
3	4.68	0.2
4	4.64	0.1
5	4.52	0.1

Table 4-4 **Stage 2 screening study results - Variation in individual distribution ratios and solvent mixture polarity with variations in integer ratios of ethyl acetate and methanol. Experiments 1 to 5 correspond to experiments 5 to 9 (Table 4-3) respectively. Experiments performed as described in Section 2.5.1.1.**

From the results in Table 4-4, a general trend is observed; with an increasing P′, i.e. increase system polarity, there is a decrease in the corresponding erythromycin distribution ratio. From an operational perspective, those phase systems yielding a $K \leq 0.1$ would cause the solute to elute close to t_m ($K = 0$), with a resulting poor degree of resolution.

As previously discussed in this section, representing phase system composition as integer ratios does not provide a detailed means of comparison between modified phase mixtures. By presenting quaternary phase system compositions as pseudo-two-component systems, the effect of solvent modification on solute distribution can be appreciated. Table 4-5 contains, for the second stage quaternary phase systems, the corresponding pseudo-two-component notation, i.e. the percentage composition of both ethyl acetate in hexane (v/v) and methanol in water (v/v), described as aqueous methanol. Analysis of the results in Table 4-5 demonstrates that for experiment 1, the larger proportion of ethyl acetate to methanol present in the system has a two component effect on the distribution ratio of the erythromycin. Ethyl acetate, classed as a hydrogen-bond accepting species will draw a small proportion of methanol from the aqueous CCC mobile phase, lowering its overall phase polarity. This is observed from the presented data in Table 4-3 where the corresponding P' value across the quaternary phase system is 4.37. More specifically considering the P' values in Table 4-2 that corresponds to both ethyl acetate and methanol individually, the polarity of ethyl acetate to methanol is 17 times greater.

Erythromycin is a relatively hydrophobic molecule, i.e. does not readily form either dipole-dipole interactions or hydrogen bonds with water, with its solubility in water increasing in the presence of a water-soluble organic solvent such as methanol. Hence, with respect to the erythromycin distribution over the range of second stage solvent systems investigated (Table 4-5), the effect of the wide polarity difference across the biphasic solvent system, emanating from the non-polar solvent, hexane, is an increase in the distribution ratio of the erythromycin. Considering phase system 1 (Table 4-5) the low system polarity results in an experimentally determined K of 1.1. As the proportion of methanol to ethyl acetate in the quaternary phase system increases (Experiments 2 and 3; Table 4-5) the overall phase system polarity (Table 4-5) increases from 4.37 (Experiment 1) to 4.68 (Experiment 3). Closer inspection of the P' values for the individual solvents ethyl acetate and methanol over this range of experiments demonstrates an increase in the polarity of the methanol to that of the ethyl acetate, culminating in a decrease in the distribution ratio, i.e. increasing eluting strength of the aqueous mobile phase.

Phase system number	Integer ratios of phase system components Hex / EtOAc / MeOH / H_2O (v/v)	% Ethyl acetate in hexane (v/v)	% Aqueous methanol (v/v)	Polarity (P′) of solvent mixture	K Values = C_{org}/C_{aq}
1	1.4/2.0/0.1/1.0	59	9	4.37	1.1
2	1.4/2.0/2.0/1.0	59	67	4.58	0.3
3	1.4/2.0/3.5/1.0	59	78	4.68	0.2
4	1.4/0.6/2.0/1.0	30	67	4.64	0.1
5	1.4/0.6/1.0/1.0	30	50	4.52	0.1

Table 4-5 **Stage 2 screening study results presented in pseudo-two-component notation, signifying the percentage change in aqueous methanol (v/v) and ethyl acetate in hexane (v/v) for the phase system studied, together with the corresponding experimental determined erythromycin distribution ratios. Experiments performed as described in Section 2.5.1.1.**

The effects of percentage aqueous methanol in the CCC mobile phase on the solute distribution ratio over two ranges of percentage ethyl acetate in hexane (v/v) (Table 4-5) are illustrated in Figure 4-1. For the 58% ethyl acetate in hexane phase system, increasing the methanol content results in an apparent linear decrease in the solute distribution ratio. At the lower percentage ethyl acetate in hexane value of 30% (v/v), with the same aqueous methanol content of 67% (v/v) (Experiments 2 and 4; Table 4-5) there is a significant drop in the K value of the erythromycin, due to its reduced affinity of the organic-rich phase. In the context of erythromycin separation by CCC this would result in the compounds eluting close to the solvent front (K = 0), which would result in a greatly reduced degree of resolution between the target product erythromycin A and its analogues.

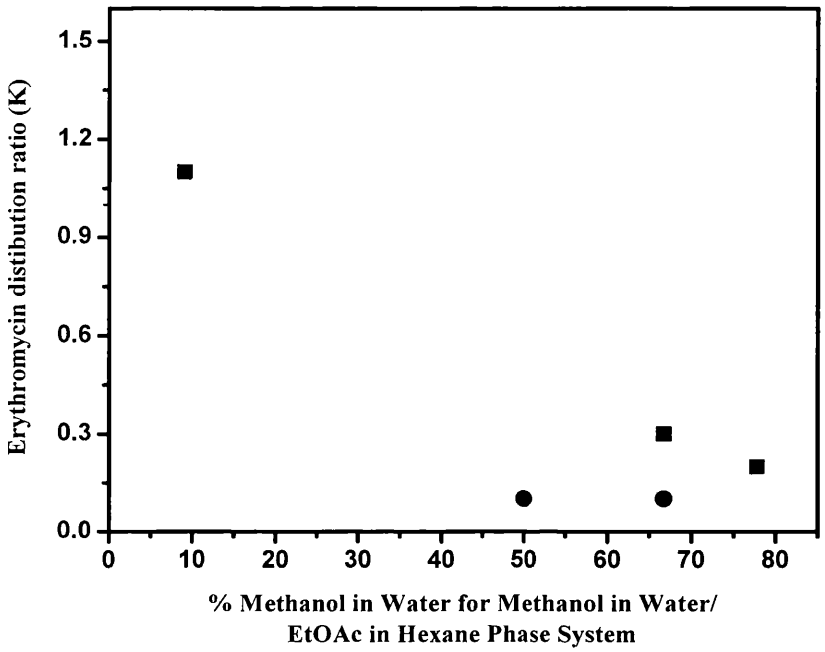

Figure 4-1 Relationship between percentage aqueous methanol content in the CCC mobile phase and erythromycin distribution ratio. (■) partitioning studies performed using a 58% (v/v) ethyl acetate in hexane apolar organic phase. (●) Partitioning studies performed using a 30% (v/v) ethyl acetate in hexane apolar organic phase.

4.1.3. Determination of optimal CCC operating mode

4.1.3.1. Gradient elution of erythromycin

Based on the outcome from batch partitioning studies (Table 4-5), the next stage in the method development strategy is to perform a CCC run with a linear methanol gradient. The gradient CCC operating profile, as illustrated in Figure 4-2, comprises of a number of discrete stages. The first stage, labelled A-B (Section 2.5.1.2; Figure 2-5) involved flowing solvent system (A) with an aqueous methanol content of 4.8% (v/v) isocratically at a mobile phase flow rate of 2 $mL.min^{-1}$. At the beginning of point D (Figure 2-5) the linear methanol gradient was initiated and continued for a period of 60 minutes (Point E; Figure 2-5). During the operation of this linear gradient the aqueous methanol content increased from 4.8% (v/v) up to 66.7% (v/v). The rational for the choice of gradient conditions was to have ethyl acetate in the system to adequately retain the erythromycin sample at the start of the separation. Then by increasing the

methanol content (Solvent B) the stationary phase polarity was reduced by drawing a small proportion of the ethyl acetate out of it, increasing the eluting power of the mobile phase, partitioning erythromycin A and its analogues back into the mobile phase.

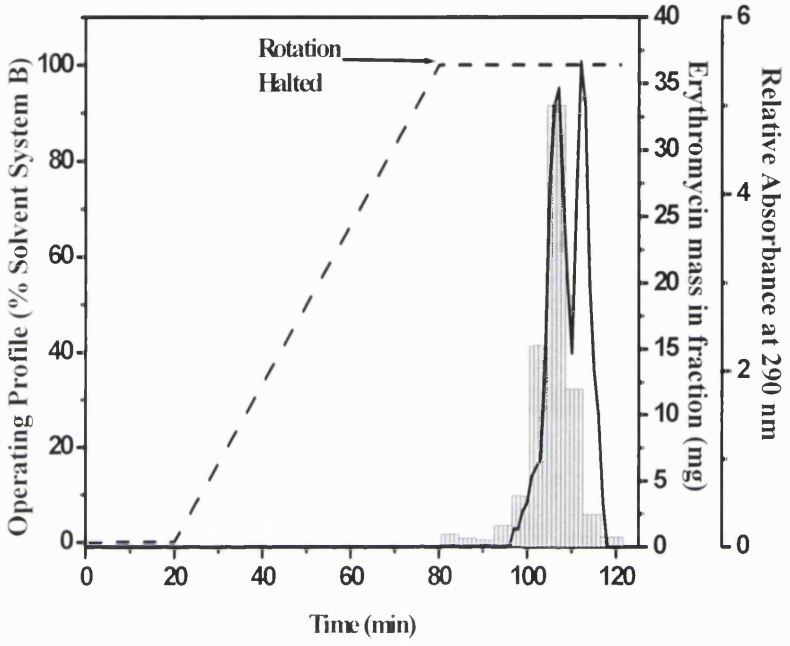

Figure 4-2 **Gradient elution CCC chromatogram. (——) Relative signal from UV detector, ( ) Results from off-line H_2SO_4 assay of collected fractions, (– -) Solvent gradient profile (% B). Experiments performed as described in Section 2.5.1.2. Rotational speed set to 800 rpm, with a mobile phase flow rate of 2 mL.min^{-1}. Sample injection was at t = 0 minutes. Stationary phase retention was 82%.**

Figure 4-2 shows the resultant CCC chromatogram from this gradient run. The relative absorbance profile, illustrated by the solid black line, was reconstructed directly from the on-line UV trace recorded using a chart recorder (Sections 2.3.3.1 and 2.3.3.3). As can be seen from the CCC operation profile in Figure 4-2, coil rotation was halted at 85 minutes and the contents of the coil purged in a plug flow manner in the 'Head' to 'Tail' direction using oxygen free nitrogen at an operating pressure of 40 Bar. Fraction collection (1 minute intervals) began at 85 minutes, and prior to analysis, due to the nature of the collected fractions, i.e. fractions comprising of the biphasic solvent system, isopropanol was added to all collected fractions to form a single phase in all

cases. The erythromycin mass content was determined using the H_2SO_4 colormetric assay as described in Section 2.3.3.4.1. The total mass of the erythromycins in each fraction is plotted on the same CCC chromatogram, presented in Figure 4-2 as a solid bar chart and shows a good correlation between the maximum mass in the fraction collected between 104 and 108 minutes and the corresponding 'relative absorbance trace'.

4.1.3.2. Isocratic elution of erythromycin

Prior to erythromycin fractionation by CCC, it was also necessary to accurately establish the composition of the feed material to be used. An analytical HPLC chromatogram of the commercial erythromycin preparation (2 $mg.mL^{-1}$) is shown in Figure 4-3. This chromatogram provides a qualitative and quantitative comparison with fractions analysed from CCC runs in terms of retention times and peak areas for the various erythromycin analogues. The main component of the feed material is clearly seen to be erythromycin A which has a retention time of 5 minutes. The minor components present i.e. EB, EC, pseudo-EEA and the enol ether of EA, account for approximately 24% w/w of the injected solute.

Based on the results from the reverse phase gradient elution run (Figure 4-2) the next step in the method development strategy was to perform the separation isocratically using the biphasic system at the top of the methanol gradient; 100% solvent B, i.e. hexane/ethyl acetate/methanol/water (1.4/2.0/2.0/1.0 v/v). The operating benefit of this at the industrial scale is two fold. Firstly, the preferred use of an isocratic solvent delivery mode requires less elaborate pumping equipment and would reduce the capital equipment and operational costs. Secondly, by performing the fractionation isocratically with the identified solvent system the whole chromatogram would be transposed into an earlier time frame.

The CCC chromatogram from the reverse phase isocratic separation of the crude erythromycin preparation is illustrated in Figure 4-4 and shows both the UV trace at 290 nm of the eluent from the CCC column together with results from the off-line total erythromycin assay (Section 2.3.3.4.1). For the off-line acid assay results, there is a good correlation between the main fraction and the main UV absorbance peak. The retention time of the main peak was 19.4 minutes. In addition a number of smaller peaks can be observed before and after the main peak.

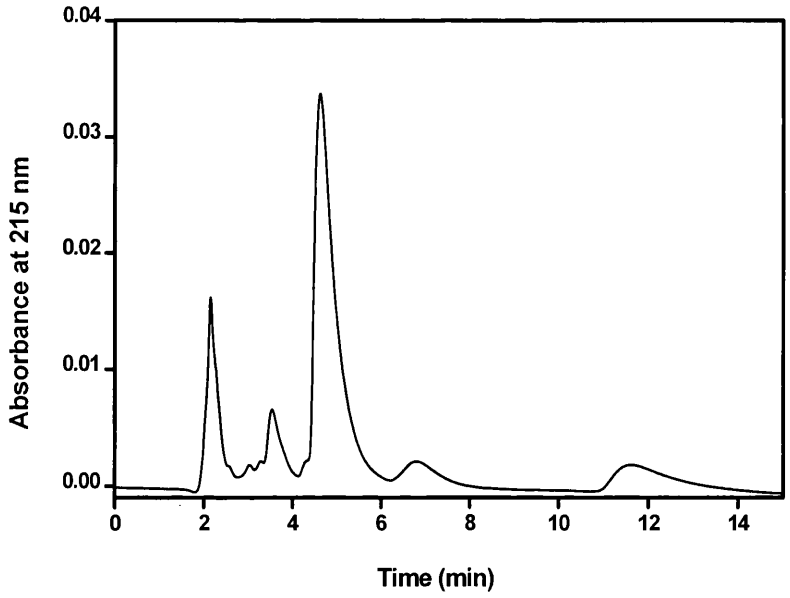

Figure 4-3 Analytical reverse phase HPLC chromatogram of a commercial erythromycin preparation. The retention times of the erythromycin analogues are as follows; EC = 3.5 minutes, EA = 5 minutes, EB and pseudo-EEA = 7 minutes, enol ether of EA = 11.5 minutes. The peak at 2.1 minutes corresponds to the solvent front.

However, due to the somewhat noisy baseline, as is common in CCC fractionations monitored by this type of detection method (Conway, 1990) it is difficult to clearly distinguish between the various erythromycin peaks. In order to overcome this limitation of the on-line detection system and to identify the erythromycins present in each of the observed CCC peaks, eluted fractions were collected and analysed individually by reverse phase HPLC (Section 2.3.3.4.2). Figure 4-5 illustrates the composition of selected fractions collected corresponding to the peaks between 14 and 22 minutes in Figure 4-4. From Figure 4-5(b) it is clear that the main peak in Figure 4-4 corresponds to EA. The peaks either side correspond to EC/ED (Figure 4-5(a)) and EB/psu-EEA (Figure 4-5(c)) respectively. Therefore a good separation by isocratic CCC has been achieved. At this point it should be noted that although the enol ether (EEA) is present in the feed (Figure 4-3), since over the set CCC operating period the EEA compound did not elute from the CCC column, it therefore, as a result, was deemed to be easily separated from the target compound, EA. Based on this observation, for all subsequent studies discussed in later Chapters, EEA was not considered when determining the performance of the CCC separation. However, where

applicable EEA was accounted for when constructing the mass balance across the CCC system.

Using the chromatographic theory described in Section 3.1.2 – 3.1.3 (Figure 3-1), the distribution ratio of the main EA peak (K_{EA}) was calculated to be 0.25, with a retention factor (k_{EA}) of 1.12. In terms of chromatographic performance, column efficiency, based on the main EA peak (Section 3.1.6), was calculated to be 336 theoretical plates, with a total solute and EA yield of 100% (w/w). In relation to the main EA peak, from HPLC analysis (Figure 4-5(b)) the purity was determined to be 100% (w/w). Throughput, as described in Section 3.1.7, was calculated to be 0.0058 $kg.day^{-1}$.

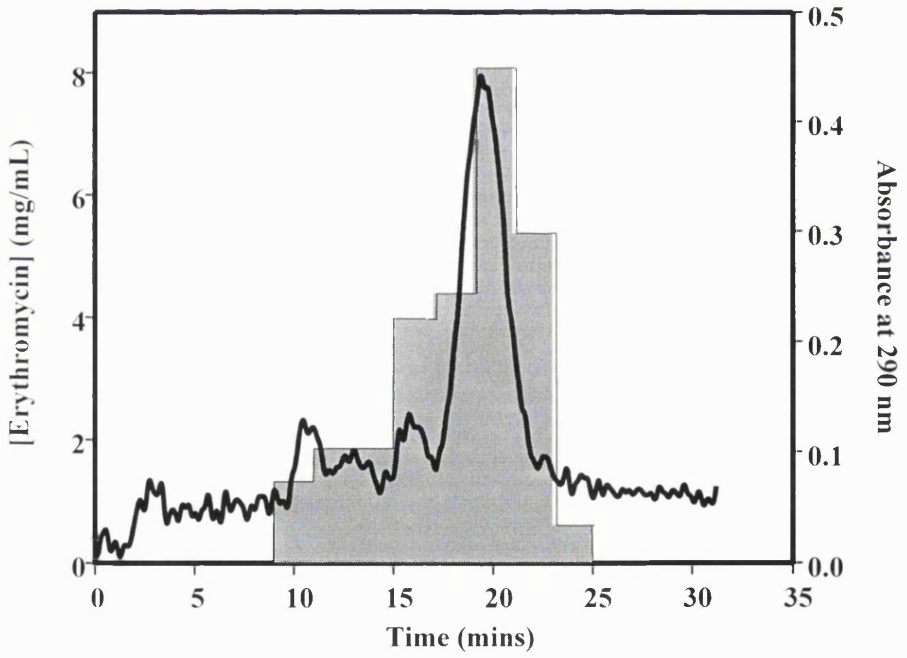

Figure 4-4 **Isocratic CCC chromatogram . (——) absorbance. (▒) results from off-line H_2SO_4 assay. Experiments performed as described in Section 2.5.1.2. Rotational speed of bobbins = 800 rpm, mobile phase flow rate = 2 $mL.min^{-1}$. Stationary phase retention was 82% (v/v).**

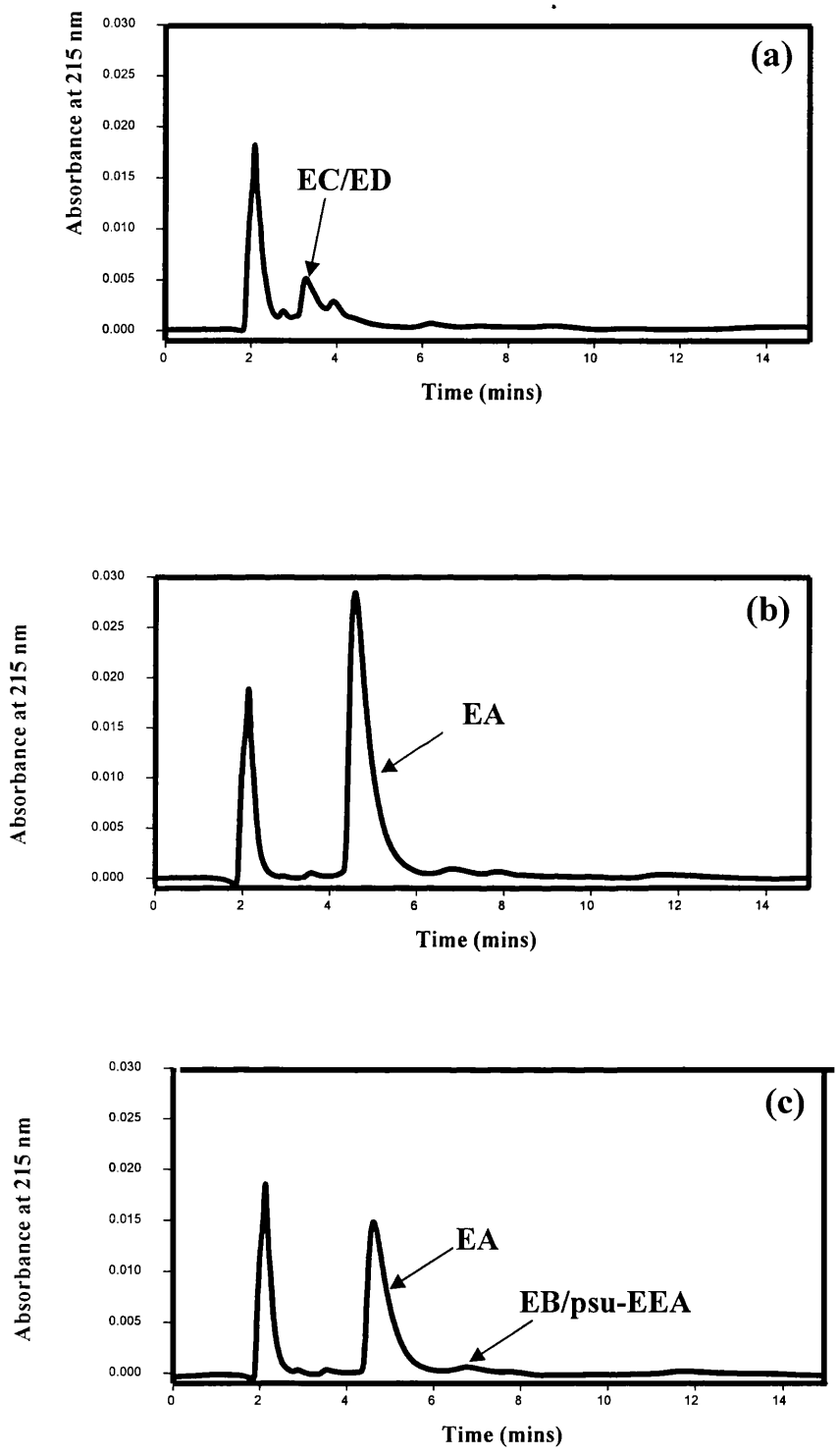

Figure 4-5 **HPLC chromatograms of fractions collected at 2 minute intervals between 14 and 22 minutes from isocratic CCC run (Figure 4-4). (a) = 15-17 min. (b) = 17-19 min. (c) = 21-23 min. The peak observed at 2 minutes is the methanol solvent front.**

4.2. Summary

In this Chapter the principle of a generic method development strategy for phase system selection in CCC has been demonstrated. The results show that based on a broad polarity quaternary phase system, equilibrium solute distribution ratio coefficients can be used to identify suitable conditions for a gradient CCC run (Figure 4-2). This, in turn, rapidly identifies a phase system composition for use in isocratic CCC mode (Figure 4-4). As shown in Figure 4-5 this has enabled the fractionation of EA from its various analogues, which was the initial aim of this Chapter. In Chapter 6 the conditions for the isocratic CCC separation will be optimised in terms of mobile phase flow rate and solute loading to increase throughput.

5. Liquid-Liquid hydrodynamics in J-type CCC machines

5.1. Introduction

Detailed knowledge of the liquid-liquid hydrodynamics in CCC machines is of great importance if accurate calculation of chromatographic parameters, such as solute distribution and column efficiency, is to be achieved. Furthermore, as will be demonstrated in Chapter 8, knowledge of the hydrodynamics at different scales of operation is important if accurate scale-up predictions of the solute elution time are to be achieved. Liquid-liquid hydrodynamics in the J-type CCC machines have been extensively studied for a wide range of binary, ternary and quaternary phase systems, with a linear relationship between the square root of mobile phase flow ($F^{0.5}$) and the degree of stationary phase retention (S_f) shown to apply for all phase systems (Du *et al.*, 1999). This relationship between S_f and $F^{0.5}$ enables the accurate determination of stationary phase retention over the range of operational flow rates investigated simply by performing two retention tests (Sutherland, 2000a). Extended hydrodynamic studies by Sutherland (2000a), based on the observed correlation between retention and flow (Du *et al.*, 1999) have also shown there to be a linear relationship between S_f and the linear mobile phase velocity (u).

The importance of the linear relationship between S_f and $F^{0.5}$ was the impetus for the range of retention tests performed in this work on the particular J-type CCC machine used. Section 5.2 describes results obtained using the PTFE and SS coils in the laboratory scale CCC machine, with Section 5.3 describing the results obtained in the SS coil of the pilot scale CCC machine. All results were obtained using the chosen quaternary phase system hexane / ethyl acetate / methanol / water at the fixed integer ratios of 1.4 / 2.0 / 2.0 / 1.0 (v/v). The experimental protocol used in all retention testing is described in Table 2.5 (Section 2.4.1.1).

5.2. Phase hydrodynamics in the laboratory scale machine

This section demonstrates that the linear relationship between $F^{0.5}$ and S_f holds over the entire range of mobile phase flow rates studied for all PTFE and SS coil volumes available, i.e. bobbins 7/1 and 7/2 and bobbins 6/1 and 6/2 respectively. The results are presented both in a tabular format, and as Du plots of stationary phase retention (S_f) against flow ($F^{0.5}$). The list of retention experiments performed is provided in Table 5-1.

Experiment number	Bobbin number	Coil material	Coil type
1	7/1	PTFE	Outer
2	7/1		Inner
3	7/2		Outer
4	7/2		Inner
5	6/1	SS	Outer
6	6/1		Inner
7	6/2		Outer

Table 5-1 List of hydrodynamic experiments performed. Coil details as described in Section 2.3.1 (Tables 2-3 and Table 2-4). All experiments performed between mobile phase flow rates of 2- 10 mL.min^{-1}, with CCC operation as described in Section 2.4.1.

5.2.1. Retention data and Du plots

For illustrative purposes, Table 5-2 contains the data obtained from the hydrodynamic studies required to generate Du plots (Appendix 13.3). This set of results relates to retention tests performed using the outer coil on bobbin 7/1 with a coil volume (V_c) of 94.3 mL and a β-ratio range of 0.80 – 0.86. All experiments were performed at a bobbin rotational speed (ω) of 800 rpm in the reverse direction, with the direction of mobile phase pumping being from 'Head' (coil centre) to 'Tail' (coil periphery).

Flow rate ($mL.min^{-1}$)	$V_{s\text{-}start}$ (mL)	$V_{s\text{-}end}$ (mL)	V_e (mL)
2	30	48	18
4	48	56	26
6	56	64	34
8	66	70	38
10	70	75	43

Table 5-2 Example of raw data from a retention study performed on the outer coil of bobbin 7/1 indicating for a range of mobile phase flow rates the volume of stationary phase eluted from the coil once a hydrodynamic equilibrium is achieved. Experiments performed using the phase system hexane/ethyl acetate/methanol/water (1.4/2.0/2.0/1.0 v/v) as described in Section 2.4.1.1.

The V_e values shown in Table 5-2 are first corrected, as described in Equation 3.1, to determine the actual volume of mobile phase (V_m) retained within the coil at hydrodynamic phase equilibrium. The coil inlet (V_{in}) and outlet (V_{out}) flying leads volumes are each 0.35 mL. Table 5-2 illustrates the corresponding V_s (mL) values calculated using Equation 3.4 and hence the corresponding calculated S_f values (Equation 3.5). The calculated data presented in Table 5-2 was then used to generate the corresponding Du plot. It should be noted at this point that the mobile phase flow rate values provided in Tables 5-2 were those set on the gradient pump. The actual measured mobile phase flow rates ($F_{m\text{-}actual}$) can be calculated from the raw data obtained (V_e) divided by the time it has taken from the initial collection of eluting stationary phase to when no further stationary phase stripping is detected, i.e. hydrodynamic phase equilibrium is attained. The corrected mobile phase flow rate values, together with the calculated $F_{m\text{-}actual}^{0.5}$ and S_f values are given in Table 5-3.

Actual mobile phase flow rate ($mL.min^{-1}$)	$V_{e\text{-}corrected}$ (mL)	V_s (mL)	$F_{m\text{-}actual}^{0.5}$	S_f (% v/v)
2	17	77	1.41	82
4	25	69	2.00	73
6.22	33	61	2.49	65
8.20	37	57	2.86	61
10.13	42	52	3.18	55

Table 5-3 **S_f values calculated from the experimental data in Table 5-2 for mobile phase flow rates between 2 and 10 $mL.min^{-1}$. Experiments performed using the quaternary phase system Hexane/EtOAc/MeOH/H_2O (1.4/2.0/2.0/1.0 v/v) as described in Section 2.5. $F_{m\text{-}actual}$ corresponds to the corrected mobile phase flow rate. $V_{e\text{-}corrected}$ corresponds to the corrected volume of stationary phase eluted (Section 3.1.1). V_s corresponds to the volume of the chosen organic stationary phase retained within the rotating coil at hydrodynamic equilibrium. V_c used in calculating S_f (% v/v) (Equation 3.5) determined to be 94.3 mL (Table 2-3).**

The results in Table 5-3 were plotted to generate the Du plot, as shown in Figure 5-1. Linear regression analysis of the data is presented as the linear regression approximation by Du *et al.* (1999):

$$S_f = A - B\sqrt{F_c} \qquad 5.1$$

where the term A corresponds to the intercept with the ordinate, B is the gradient of the fitted linear regression line, and F_c corresponds to the $F_{m\text{-}actual}^{0.5}$. The corresponding regression equation for the data in Figure 5-1 is $S_f = 102.9 + 14.6F^{0.5}$, with a correlation coefficient (R^2) of 0.999.

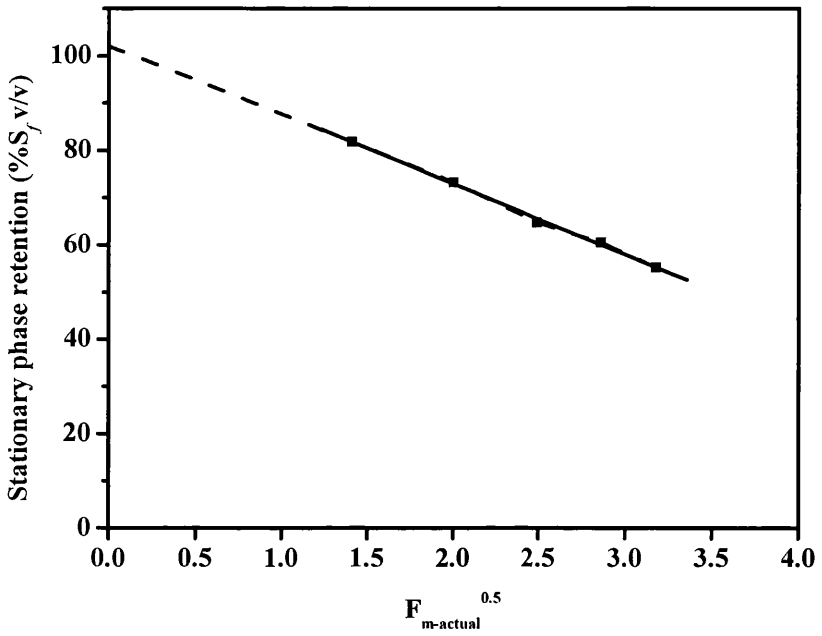

Figure 5-1 **Percentage stationary phase retention against the square root of mobile phase flow rate (2-10 mL.min^{-1}). Solid line fitted by linear regression. Phase system consisted of hexane/ethyl acetate/methanol/water in the ratios 1.4/2.0/2.0/1.0 (v/v). Experiments performed using a Brunel J-Type CCC machine (94.3 mL coil, 800 rpm, 30°C) as described in Section 2.4.1.1.**

From the results in Figure 5-1 there is a good correlation between square root of mobile phase flow rate and the degree of stationary phase retention. This supports the observations by Du and co-workers (Du *et al.*, 1999) for a wide range of solvent systems and mobile phase flow rates in the range 0.5 to 40 mL.min^{-1}. Figure 5-1 demonstrates that with an increase in the mobile phase flow rate, there is a stripping of the stationary phase, resulting in lower S_f values.

During the course of their studies Du *et al.* (1999) observed that the 'A' value substantially exceeds 100 at the point where the linear fit line intercepts the ordinate. For the data presented in Figure 5-1 this was found to be 102.9. This discrepancy between the theoretically expected ordinate intercept (100%) and that observed from actual experimental data is discussed later in this section.

All S_f values corresponding to retention experiments performed as described in Table 5-1 are given in Table 5-4. A representative raw data set corresponding to the retention experiment illustrated in Figure 5-1 can be found in Appendix 13.3. The Du plots from the data in Table 5-4 for bobbin 7/1 Inner is illustrated in Figure 5-2(a), for 7/2 Inner (Figure 5-2(b)) and 7/2 Outer (Figure 5-2(c)). The Du plots for the

SS-coils, bobbins 6/1 Inner and Outer and 6/2 Outer are given in Figure 5-3(a), (b) and (c) respectively. Linear regression analysis of data in Figures 5-2 and 5-3, presented in all case as the solid line, resulted in a number of corresponding equations (Table 5-5). All figures showed the expected decrease in S_f with increasing mobile phase flow rate.

Bobbin number	F_m (mL.min^{-1})	$F_{m\text{-actual}}$ (mL.min^{-1})	$F_{m\text{-actual}}^{0.5}$	V_s (mL)	S_f (% v/v)
7/1 Inner	2	1.9	1.4	134	82
	4	4.0	2.0	118	73
	6	5.9	2.4	104	64
	8	7.5	2.7	100	62
	10	10.5	3.2	92	57
7/2 Outer	2	1.9	1.4	76	83
	4	4.1	2.0	64	70
	6	6.0	2.5	58	62
	8	8.6	2.9	48	52
	10	10	3.2	45	48
7/2 Inner	2	1.9	1.4	138	82
	4	4.0	2.0	122	73
	6	5.9	2.4	108	64
	8	7.5	2.7	103	62
	10	10.5	3.2	95	57
6/1 Outer	2	1.9	1.4	77	90
	4	4.0	2.0	75	88
	6	6.0	2.5	71	83
	8	8.0	2.8	69	81
	10	10.1	3.2	67	79
6/1 Inner	2	1.9	1.4	75	88
	4	4.0	2.0	67	79
	6	6.0	2.5	59	69
	8	8.2	2.9	53	62
	10	10.0	3.2	51	60
6/2 Outer	2	2.0	1.4	85	89
	4	4.0	2.0	83	87
	6	6.0	2.5	81	85
	8	8.3	2.9	79	83
	10	10.1	3.2	77	81

Table 5-4 **Corrected mobile phase flow rates ($F_{m\text{-actual}}$), together with the square root of mobile phase flow ($F_{m\text{-actual}}^{0.5}$) and S_f (% v/v) for all retention experiments performed on the laboratory scale coils. Experiments peformed as described in Section 2.4.1.1 using a phase system comprising of hexane/ethyl acetate/methanol/water (1.4/2.0/2.0/1.0 v/v). All coil dimensions provided in Tables 2-3 and 2-4.**

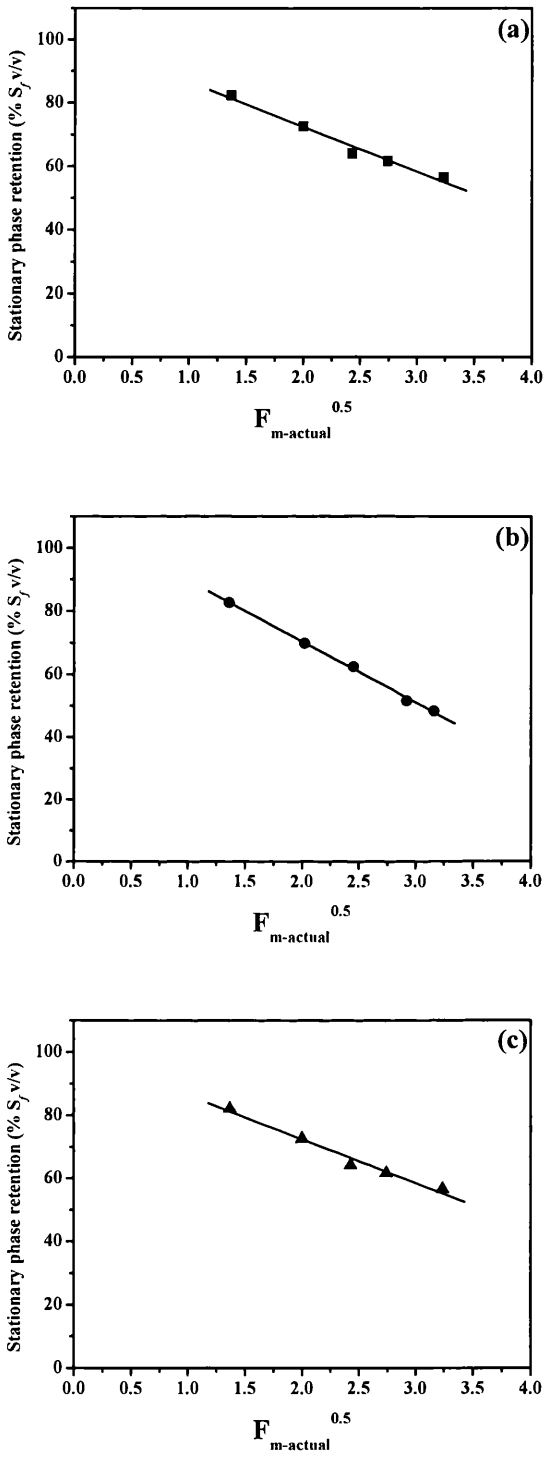

Figure 5-2 **Du plots of percentage stationary phase retention against the square root of mobile phase flow rate (2-10 mL.min^{-1}) using the laboratory scale coils. (a) corresponds to bobbin 7/1 inner. (b) corresponds to bobbin 7/2 outer. (c) corresponds to bobbin 7/2 inner. All experiments performed using a phase system comprising of hexane/ethyl acetate/methanol/water (1.4/2.0/2.0/1.0 v/v) as described in 2.4.1.1. Coil properties described in Section 2.3.1. Solid lines fitted by linear regression.**

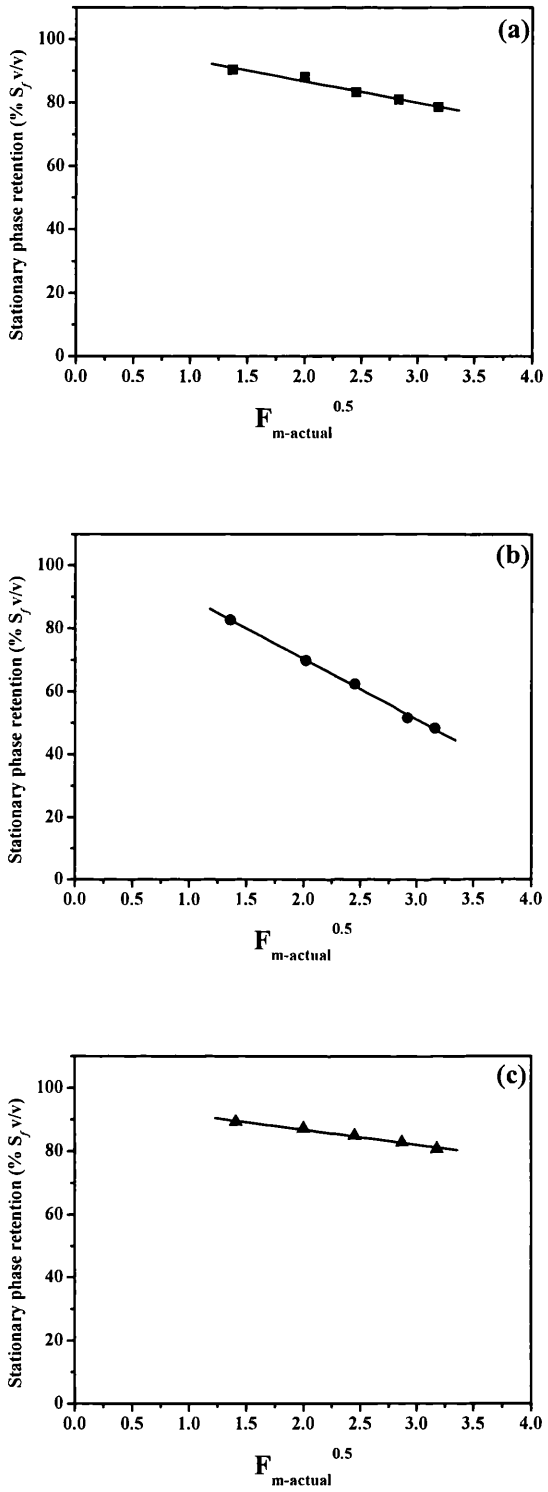

Figure 5-3 **Du plots of percentage stationary phase retention against the square root of mobile phase flow rate (2-10 mL.min^{-1}). (a) corresponds to bobbin 6/1 outer. (b) corresponds to bobbin 6/1 inner. (c) corresponds to bobbin 6/2 outer. All experiments performed using a phase system comprising of hexane/ethyl acetate/methanol/water (1.4/2.0/2.0/1.0 v/v) as described in 2.4.1.1. Coil properties described in Section 2.3.1. Solid lines fitted by linear regression.**

Bobbin number	Stationary phase retention (S_f % v/v)	Correlation coefficient (R^2)
7/1 Inner	$= 100.6 - 14.1.F^{0.5}$	0.989
7/2 Outer	$= 109.0 - 19.4.F^{0.5}$	0.999
7/2 Inner	$= 100.3 - 14.0.F^{0.5}$	0.990
6/1 Outer	$= 100.3 - 6.8.F^{0.5}$	0.988
6/1 Inner	$= 110.4 - 16.4.F^{0.5}$	0.995
6/2 Outer	$= 96.3 - 4.7.F^{0.5}$	0.994

Table 5-5 Regression analysis between stationary phase retention (% S_f) and the square root of mobile phase flow $F_{m\text{-}actual}^{0.5}$ ($mL.min^{-1}$) determined from Du plots in Figures 5-2 and 5-3.

From the results in Table 5-5, for all the laboratory scale coils there is a good correlation ($R^2 \geq 0.988$) between S_f and $F_{m\text{-}actual}^{0.5}$, further supporting those observations of Du *et al.* (1999). As previously discussed for the retention tests with the outer coil on Bobbin 7/1, the intercept on the ordinate is generally above 100% and ranged from 96.3 (coil 6/2 outer) to 110.4 (coil 6/1 inner). This range of C values is similar to those published by Du *et al.* (1999). Recent detailed hydrodynamic investigation of stationary phase retention in the J-Type CCC machine (Personal communication, Wood, 2002) has shown a relationship between eluted stationary phase (V_e) during hydrodynamic phase equilibrium and $F^{0.5}$. Wood (2002) has attributed this observation to the dead volume within the external 'flying leads', or even possibly within the coil itself. During the construction of Du plots, the volumes of inlet and outlet flying lead coils is subtracted from the measured volume of stationary phase eluted, i.e. the $V_{e\text{-}corrected}$ term. Hence, attributing the dead volume within the system to non-active retention of the stationary phase in the external 'flying lead' coils can be neglected.

Comparing the Du plots for PTFE (Figure 5-2(a)-(c)) and SS (Figure 5-3(a)-(c)) coils, the gradient of the regression line for the SS coils is generally less than a comparable PTFE coil (in terms of coil positioning and volume). As a result, with the larger bore SS coils (Table 2-4) over the entire flow rate range (2-10 $mL.min^{-1}$) the S_f values were higher. Sutherland *et al.* (2001b) have shown that tubing material does not significantly affect the S_f value, with the same study investigating the effects of tubing bore on S_f. The results support those observed in this study, demonstrating that with

increasing bore, at a comparable mobile phase flow rate, a higher S_f value would be achieved. For phase systems with similar viscosities, Sutherland *et al.* (2000b) has proposed that by increasing tubing bore, viscous wall effects become less dominant, and as a result viscous drag on the tubing walls would cause an increased stripping of the stationary phase, i.e. reduced S_f. From the data in Tables 2-3 and 2-4, for the outer coils on bobbins 7/2 and 6/2, there is a greater β-ratio range in bobbin 6/2. As discussed in Section 1.2.3 larger β values result in larger generate radial forces acting on phases, and with regard to this work would enable a larger volume of the less dense organic phase (stationary phase) to be retained, i.e. increasing S_f.

5.3. Phase hydrodynamics in the pilot scale machine

This section demonstrates that the linear relationship between $F_{m\text{-}actual}^{0.5}$ and S_f holds over the entire range of mobile phase flow rates studied for the pilot scale coil as described in Section 2.3.2. The results are presented both in a tabular format and as Du plots of stationary phase retention (S_f) against flow ($F_{m\text{-}actual}^{0.5}$). The method by which phase volume measurements were obtained, and subsequent analysed to obtain the required terms for calculating S_f, has been previously described in Section 5.2.1. One key feature of the Brunel pilot scale CCC machine is its ability to rotate at higher rotational speeds, up to a maximum of 1200 rpm. Retention experiments were therefore performed at 800 and 1200 rpm over the mobile phase flow rate range 10-80 $mL.min^{-1}$, with Table 5-6 providing the $F_{m\text{-}actual}^{0.5}$ and corresponding S_f (% v/v).

Rotational speed (rpm)	Mobile phase flow rate ($mL.min^{-1}$)	Actual mobile phase flow rate ($mL.min^{-1}$)	$F_{m\text{-}actual}^{0.5}$	S_f (% v/v)
800	10	9.92	3.15	81.9
	20	20.5	4.53	75.3
	40	40.45	6.36	64.8
	80	81.20	9.01	46.8
1200	10	9.88	3.14	87.4
	20	24.45	4.95	77.5
	40	41.89	6.47	69.5
	80	83.89	9.16	55.8

Table 5-6 **Corrected mobile phase flow rates ($F_{m\text{-}actual}$) , together with the square root of mobile phase flow ($F_{m\text{-}actual}^{0.5}$) and S_f for the pilot scale CCC machine. Experiments performed as described in Section 2.4.2.1.**

The correspond Du plot of the data provided in Table 5-6 is shown in Figure 5-4.

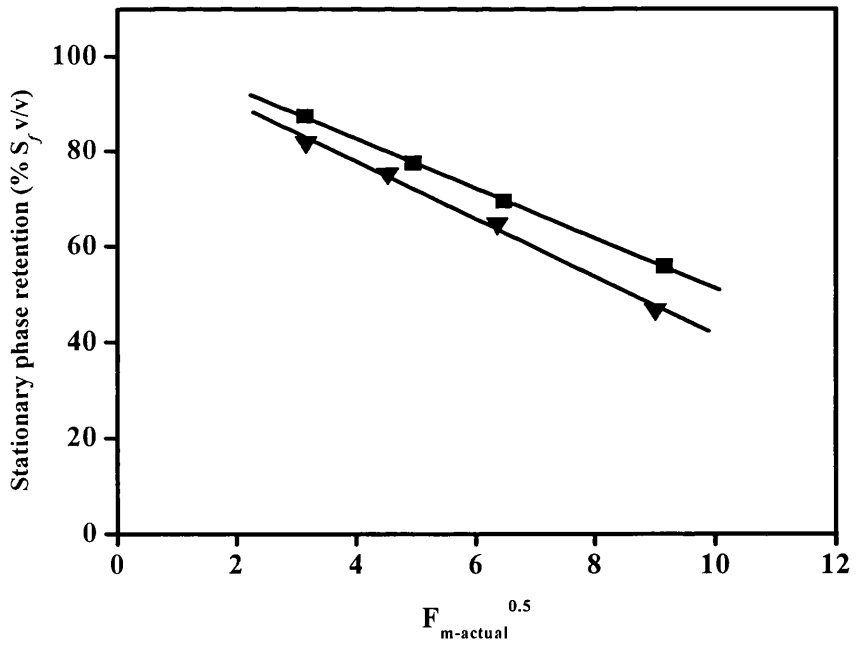

Figure 5-4 **Du plot of percentage stationary phase retention against the square root of mobile phase flow rate (10 – 80 $mL.min^{-1}$) for the pilot scale CCC machine: (▼) N = 800 rpm, (■) N = 1200 rpm.**

The solid lines in Figure 5-4 as with previously illustrated Du plots (Section 5.2.1) were fitted by linear regression. The corresponding linear regression equations are given in Table 5-7.

Rotational speed (rpm)	**Stationary phase retention (S_f % v/v)**	**Correlation coefficient (R^2)**
800	$= 101.9 - 6.0.F^{0.5}$	0.995
1200	$= 103.6 - 5.2.F^{0.5}$	0.999

Table 5-7 Regression analysis between S_f and the square root of mobile phase flow rate ($F_{m\text{-}actual}^{0.5}$; $mL.min^{-1}$) determined from Du plots in Figure 5-4.

5.4. Summary of retention studies

The results in Sections 5.2 and 5.3 have confirmed that there is a linear relationship between S_f and $F_{m\text{-}actual}^{0.5}$ on both the laboratory (PTFE and SS coils) and pilot (SS coils) CCC machines. As described in Section 5.1 this provides a basis for the accurate interpretation of CCC chromatograms, and accurate prediction of EA elution times upon scale-up, as discussed in Chapter 8.

6. Laboratory scale optimisation

6.1. Introduction

In Chapter 4, research demonstrated, under isocratic operating conditions, the successful fractionation of the target compound, EA. The aim of this work is to systematically investigate the effects of key process variables on the CCC separation performance. A number of studies specifically on the separation of antibiotics by CCC have been previously performed (Chen *et al.*, 1988; Oka *et al.*, 2000; Harada *et al.*, 2001). These studies, however, have generally focused on analytical scale fractionations, operating at low mobile phase flow rates and low solute loadings. Very few studies have addressed the issue of how solute throughput affects resolution and product recovery levels. These are obviously vital issues in relation to eventual process scale applications of CCC. In order to increase solute throughput two process variables were studied, the mobile phase flow rate and solute loading.

The majority of the results presented in this Chapter have been published as: Booth A.J. and Lye G.J. (2001). Optimization of the fractionation and recovery of polyketide antibiotics by Countercurrent chromatography. *J. Liq. Chrom. and Rel. Technol.*, 24(11&12): 1841-1861.

6.2. Variation of mobile phase flow rate

Increasing the mobile phase flow rate has the potential to increase solute throughput. The upper limit to which this is possible is determined by the hydrodynamics of the system, i.e. the decrease in stationary phase retention at higher flow rates and consequently the decrease in chromatographic resolution. In order to explore the influence of mobile phase flow rate on CCC performance, a series of separations were performed at flow rates between 2 and 10 $mL.min^{-1}$.

The CCC chromatograms can been seen in Figure 6-1. The CCC chromatogram for the separation performed at a mobile phase flow rate of 2 $mL.min^{-1}$ is already presented in Figure 4-4. All experiments were performed at a fixed solute loading concentration and injection volume of 100 $mg.mL^{-1}$ and 1 mL respectively.

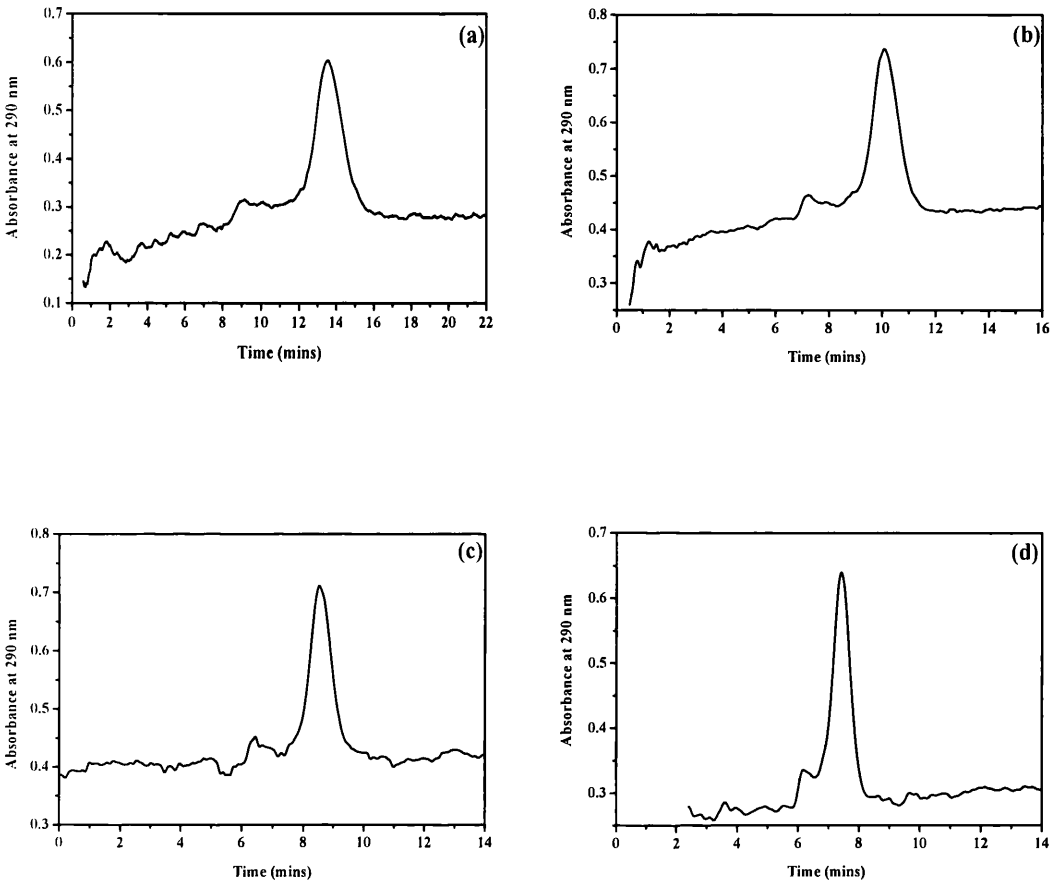

Figure 6-1 CCC chromatograms from experiments performed at mobile phase flow rates of (a) 4 mL.min^{-1}, (b) 6 mL.min^{-1}, (c) 8 mL.min^{-1} and (d) 10 mL.min^{-1}. All experiments performed as described in Sections 2.4.1.1 and 2.4.1.2 using a quaternary phase system comprised of hexane/ethyl acetate/methanol/water (1.4/2.0/2.0/1.0 v/v).

Prior to solute injection, hydrodynamic phase equilibrium was achieved as described in Section 2.4.1.1. The corresponding S_f values are given in Table 6-1. The first stage in analysing the results was to determine the actual elution time of the target product, EA and the other forms of erythromycin. EA was identified from both the offline sulphuric acid assay and HPLC analysis (Sections 2.3.3.4.1 and 2.3.3.4.2) of fractions collected every minute. In all cases the fraction with the maximum EA concentration (EA_{max}) corresponded to the centre of the main peak observed in the CCC chromatograms (a) to (d) in Figure 6-1.

Flow rate ($mL.min^{-1}$)	S_f (% v/v)
2	82
4	71
6	62
8	57
10	51

Table 6-1 **S_f results for flow rate experiments performed between 2 to 10 $mL.min^{-1}$. All CCC operating conditions as described in Figure 6-1.**

An example table (Table 13-4) for both quantitative and qualitative analysis of each erythromycin in collected fractions can be found in Appendix 13.4. The main HPLC results for the fractions containing the different erythromycin analogues are summarised in Table 6-2.

Flow rate ($mL.min^{-1}$)	Fraction (min)	Solute identity	Concentration ($mg.mL^{-1}$)	TMIF (mg)
2	13-15	EC/ED	3.97	15.9
	17-19	EA	8.08	32.3
	21-23	EB/psu-EEA	1.03	12.8
4	11-12	EC/ED	1.14	4.6
	13-14	EA	9.99	40.0
	15-16	EB/psu-EEA	0.37	1.5
6	8-9	EC/ED	0.44	2.6
	10-11	EA	5.98	35.9
	12-13	EB/psu-EEA	0.37	2.2
8	7-8	EC/ED	0.48	3.8
	8-9	EA	7.40	59.2
	9-10	EB/psu-EEA	0.40	3.2
10	6-7	EC/ED	0.35	3.5
	7-8	EA	6.55	65.5
	8-9	EB/psu-EEA	0.25	2.5

Table 6-2 **Identification and quantification of the various forms of the erythromycins from isocratic CCC experiments performed as described in Figure 6-1. EA: erythromycin A, EC: erythromycin C, ED: erythromycin D, EB: erythromycin B, psu-EEA: ring-contracted enol ether of erythromycin A.**

Firstly considering the experiment performed at a mobile phase flow rate of 4 $mL.min^{-1}$, analysis of the HPLC results (Table 6-2) shows the main EA peak eluted between 12 and 13 minutes. The corresponding concentration and total mass in the fraction (TMIF) are 9.99 $mg.mL^{-1}$ and 39.99 mg respectively. This elution time ascertained from off-line HPLC data shows a good correlation with that determined directly from the CCC chromatogram by on-line UV detection (Figure 6-1(a)). However, due to the positioning of the detector, the elution time should be corrected to take into account the connecting tubing required from the outlet of the CCC coil to the inlet of the detector. At this mobile phase flow rate (4 $mL.min^{-1}$), the solute exiting the CCC coil would be detected 0.225 minutes later, hence the actual elution time was calculated to be 13.3 minutes. Generally in chromatographic analysis, the corresponding fraction collection time is presented as being the arithmetic mean between the start and end collection time. Hence, for the experiment at 4 $mL.min^{-1}$, EA, from HPLC analysis could be considered to elute at 12.5 minutes. Table 6-3 provides, for all flow rate experiments performed, the EA elution time determined by both on-line and off-line analyses.

Flow rate ($mL.min^{-1}$)	**EA elution time (min)**		**Error (%)**
	HPLC	**CCC chromatogram**	
2	20	19.4	3.0
4	12.5	13.3	6.0
6	10.5	10.0	4.8
8	8.5	8.5	0.0
10	7.5	7.3	2.7

Table 6-3 Comparison of EA elution times determined from off-line HPLC analysis and directly from CCC chromatograms obtained using on-line UV-Vis detection. Experiments performed as described in Figure 6-1.

Based on the off-line HPLC data, over the range of flow rates, CCC has achieved a good separation between EA and the other forms of erythromycin. Table 6-1 shows the elution time of the main 'process contaminants', i.e. the other minor erythromycin analogues EC/ED and EB/psu-EEA also present in the feed, whose elution profile over the flow rate range remained the same. If focusing on the separation

at 4 mL.min^{-1} (Figure 6-1(a)), the corresponding elution time of the main EA fraction by HPLC was determined to be 12.5 minutes. With a doubling in the mobile phase flow rate, the EA elution time dropped to 8.5 minutes. As the proportion of the mobile phase within the CCC coil (Section 2.4.1.1) increases with increasing mobile phase flow rate, due to a reduction in S_f, a non-linear increase in the mobile phase velocity (u, cm.s^{-1}) would be expected. From knowledge of phase system hydrodynamics in all experiments performed (Table 6-1), the linear mobile phase velocity could be calculated using Equation 3.32. Table 6-4 illustrates the changes in linear mobile phase velocity with mobile phase flow rate. From these results it is apparent that a doubling of the mobile phase flow rate, as considered above, only results in a ~1.3 times increase in 'u'.

Flow Rate (mL.min^{-1})	**V_m (mL)**	**u (cm.sec^{-1})**
2	17.2	10.3
4	25.2	13.1
6	33.2	14.9
8	37.2	17.8
10	42.2	19.6

Table 6-4 **Variation in linear mobile phase velocity with mobile phase flow rate and mobile phase volume at hydrodynamic equilibrium. Experiments performed as described in Figure 6-1. Determination of the mobile phase volume (V_m) achieved using S_f values in Table 6-1 and Equations 3.1-3.5. Mobile phase velocity calculated using Equation 3.32.**

6.2.1. Effect on chromatographic retention factors

The calculated distribution ratio (K) and retention factor (k) of the main EA peak for all experiments shown in Figure 6-1 are presented in Table 6-5. Figure 6-2 illustrates the variation in both K and k with mobile phase flow rate. Firstly it can be seen that with increasing mobile phase flow rate there is a gradual increase in the EA distribution up to a maximum of 0.59 at the mobile phase flow rate of 10 mL.min^{-1}. This increase in K_{EA} (Equation 3.8) is due to the larger reduction in the denominator

term (t_c'). Since the corrected K=1 peak, i.e. t_c', also decreases as the result of an increase in mobile phase flow rate, the available column length for solute distribution to take place (the chromatographic window) is effectively reduced. Hence, the solute during the course of the separation resides for a larger proportion of its time in the mobile phase, experiencing fewer mixing and settling steps. The observed decrease in the retention factor (k) over this flow rate range is to be expected, given the corresponding reduction in the stationary phase retention and the fact that these terms are related as described in Equation 3.10.

Flow rate ($mL.min^{-1}$)	t_c'	t_k'	K_{EA}	k_{EA}
2	41.9	10.4	0.25	1.14
4	17.3	7.2	0.42	1.03
6	10.2	4.5	0.44	0.71
8	7.1	3.9	0.55	0.73
10	5.2	3.1	0.59	0.61

Table 6-5 Variation in the distribution ratio (K_{EA}) and retention factor (k_{EA}) with mobile phase flow rate. Values calculated from chromatograms shown in Figure 6-1, and as described in Sections 3.1.2 – 3.1.4.

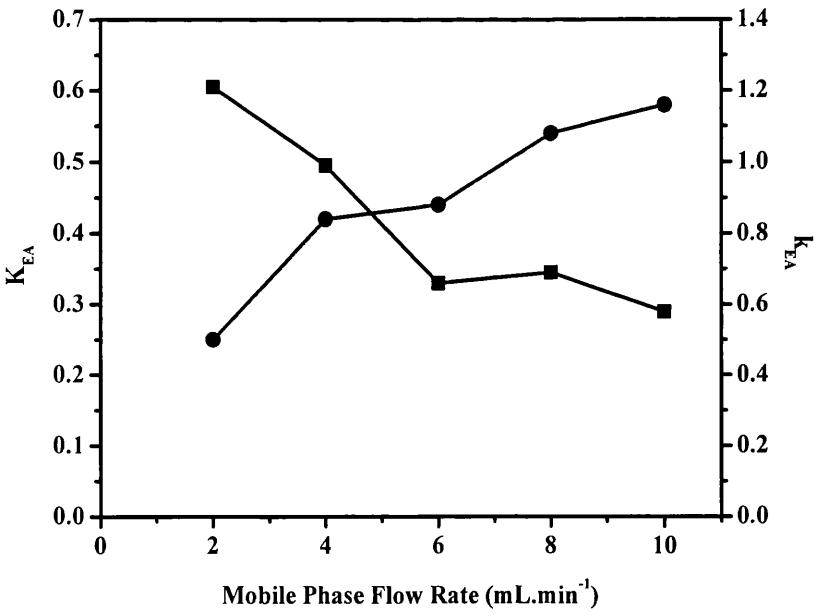

Figure 6-2 Effect of mobile phase flow rate on EA distribution ratio (●) and retention factor (■). Values calculated as described in Table 6-5.

Flow rate ($mL.min^{-1}$)	t_c'	t_k'		$K_{EC/ED}$	$K_{EB/psu-EEA}$	$k_{EC/ED}$	$k_{EB/psu-EEA}$
		EC/ED	EB/psu-EEA				
2	41.5	5.9	13.9	0.14	0.34	0.63	1.55
4	17.3	4.2	8.2	0.24	0.47	0.59	1.15
6	10.2	3.3	6.0	0.33	0.59	0.53	0.96
8	7.1	2.9	4.9	0.40	0.68	0.53	0.90
10	5.2	2.3	4.3	0.44	0.82	0.45	0.85

Table 6-6 Variation in K and k of EC/ED and EB/psu-EEA with mobile phase flow rate. Values calculated from off-line HPLC results shown in Table 6-2, and as described in Sections 3.1.2 – 3.1.4.

The distribution ratio and retention factor can also be calculated for the other erythromycin analogues, EC/ED and EB/psu-EEA, from knowledge of their elution time, identified by HPLC analysis (Table 6-2). This data is presented in Table 6-6. The trend observed for K_{EA} and k_{EA} is also found for the other erythromycin analogues eluting before and after the main EA peak. By plotting this observed variation in the distribution ratio for all the erythromycin analogues against the linear mobile phase velocity (Table 6-4) the following plot is obtained (Figure 6-3). The results of linear regression analysis for the different erythromycin analogues is given in Table 6-7.

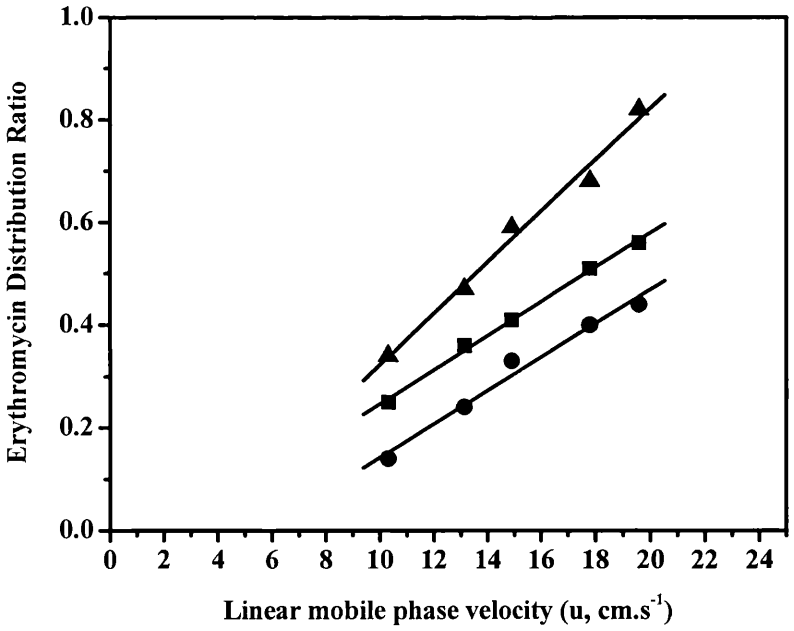

Figure 6-3 Relationship between linear mobile phase velocity (u) and distribution ratios of EC/ED (●), EA (■) and EB/psu-EEA (▲). Solid lines fitted by linear regression. Values calculated as described in Tables 6-4 to 6-6.

Erythromycin	Distribution ratio K_x	Correlation coefficient (R^2)
EC/ED	= 0.03u – 0.19	0.99
EA	= 0.03u – 0.09	1.00
EB/psu-EEA	= 0.05u – 0.18	0.99

Table 6-7 Regression analysis between distribution ratio of the erythromycins (K_x) and linear mobile phase velocity (u, $cm.s^{-1}$). Values calculated from results presented in Figure 6-3.

K_x refers to the solute distribution ratio for a particular erythromycin. As can be seen from the results, for all the different erythromycin analogues there is a linear relationship between the linear mobile phase velocity and their corresponding distribution ratios. This observed linear relationship between K and u, for a fixed phase system composition and under fixed operating conditions, could be used to determine the elution times (peak maxima) of the various components with increasing mobile phase flow rates.

Research by Menet *et al.* (1992) also investigated the effects of S_f on the retention factor (k), finding that with decreasing S_f, the k value also decreased. Similar analysis of our results shows that in plotting k for the different erythromycin components against the corresponding S_f there is a similar trend (Figure 6-4). Regression analysis performed on each of these data sets demonstrates a linear relationship between S_f and the retention factors of the various erythromycin analogues. The corresponding equations are presented in Table 6-8, with the coefficient of linear regression (R^2) being greater than 0.95. Since the retention factor describes the actual solute retention characteristics of the phase system, and can be expressed as a ratio of the solute mass in the stationary phase to that in the mobile phase (Equation 3.9), it provides an indication of solute retention ability of the organic stationary phase within the CCC coil.

The CCC process can be considered as a continuous liquid-liquid distribution process (Conway, 1990), and as such can be subjected to thermodynamic and mass transfer investigation. The thermodynamic process, namely the solute distribution ratio (K), of this separation has been discussed in detail within this section. Mass transfer

determines the rate of separation, and hence the coil length required to achieve an adequate degree of resolution. Since there is a reduction in the available stationary phase within the coil with increase mobile phase flow rate, correspondingly there is reduction in the capacity of the stationary phase for the injected solute. Such effects are considered in the following section.

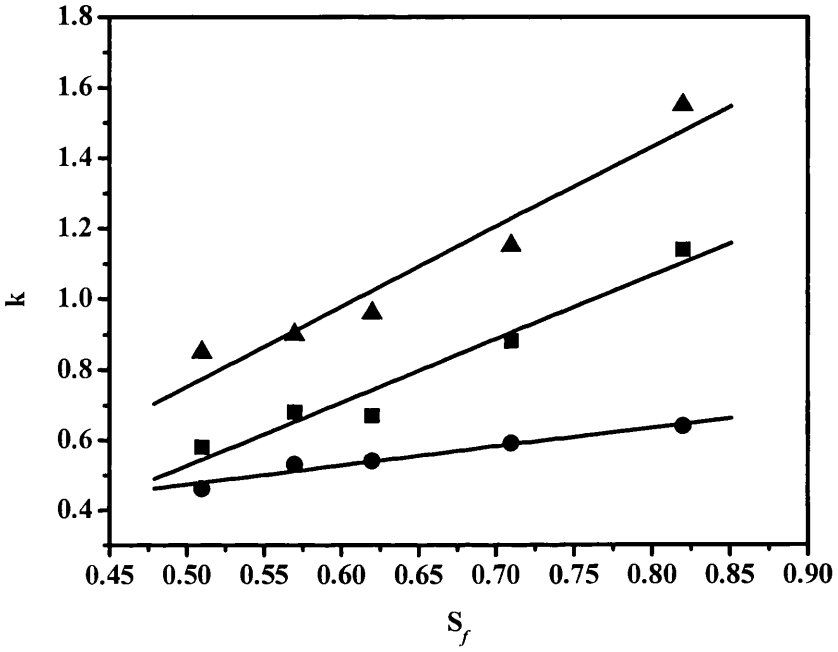

Figure 6-4 **Relationship between S_f and retention factors of EC/ED (●), EA (■) and EB/psu-EEA (▲). Solid lines fitted by linear regression. Values calculated as described in Tables 6-5 and 6-6.**

Erythromycin	Retention factor k_x	Correlation coefficient (R^2)
EC/ED	$= 0.20.S_f + 0.54$	0.97
EA	$= 1.70.S_f - 0.37$	0.98
EB/psu-EEA	$= 2.27.S_f - 0.38$	0.97

Table 6-8 **Regression analysis between the retention factor of the erythromycins (K_x) and S_f. Values calculated from results presented in Figure 6-4.**

6.2.2. Effect on chromatographic performance

In chromatographic separations, the partitioning efficiency of the column can be expressed in terms of column efficiency (N), the separation factor (α). Firstly, column efficiency for all the CCC experiments were calculated for the main erythromycin A peak using both Equations 3.14 and 3.15. Due to the large mobile phase volume (V_m) in CCC compared to solid-phase chromatography, Conway (1990) suggests that overestimations in N can result. Therefore, it has been advocated that N_{eff} is a more representative means of comparing column performance, particularly when the phase volume ratio varies between experiments. The results from column efficiency determination together with mobile phase flow rate and S_f are illustrated in Figures 6-5 and 6-6 respectively.

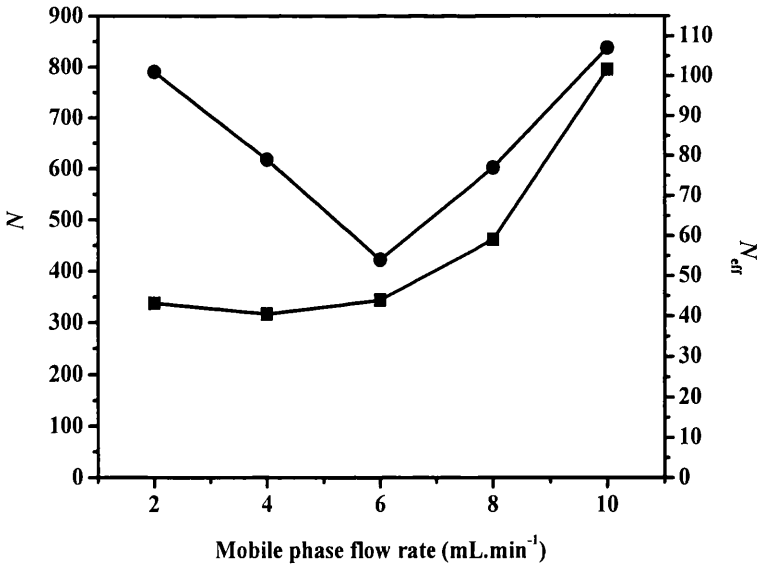

Figure 6-5 Relationship between mobile phase flow rate and column efficiency calculated as N_{eff} (●) and N (■). Column efficiency based on the main EA peak for the CCC chromatograms shown in Figures 4-4 and 6-1, and calculated according to Equations 3.14 and 3.15.

Considering first the variation of N with mobile phase flow, it is initially constant between 2 and 6 mL.min^{-1}. From 6 to 10 mL.min^{-1}, N increases up to a maximum of 795 theoretical plates. A similar trend was observed by Menet *et al.* (1992). In comparison, between 2 and 6 mL.min^{-1} N_{eff} shows a ~50% decrease, increasing to 107 at 10 mL.min^{-1}. These results therefore suggest that it is more favourable to operated at higher mobile phase flow rates. Figure 6-6 illustrates the effect of stationary phase retention on column efficiency (N). Interestingly, at a low S_f value there is a maximum N of 795 theoretical plates which decreases to a between 317 and 344 plates. Research by Oka *et al.* (1992) supports this observation, in that during their study with the same biphasic solvent system, increasing aqueous mobile phase flow rate led to an increase in column efficiency over a similar S_f range.

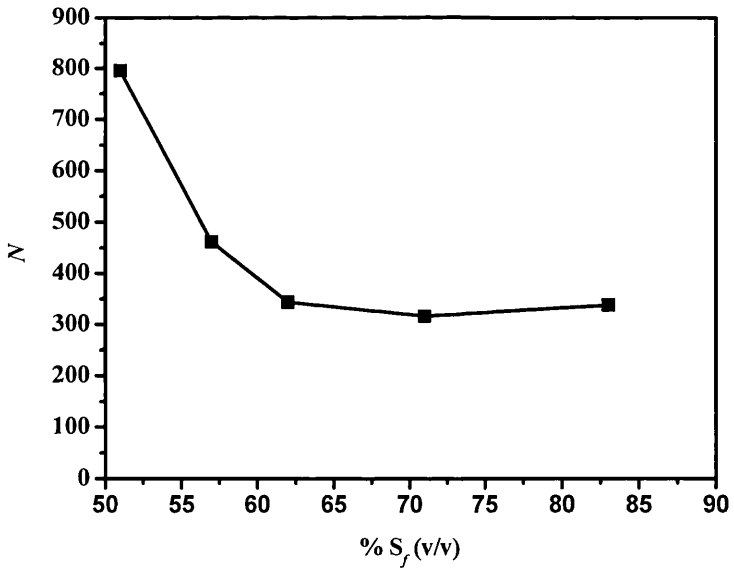

Figure 6-6 Relationship between S_f and column efficiency, N (■). Column efficiency based on the main EA peak for the CCC chromatograms shown in Figures 4-4 and 6-1, and calculated according to Equations 3.14 and 3.15.

The effect of mobile phase flow rate on the separation factor (α) was also determined, with the results shown in Table 6-9. Since the erythromycins EC/ED and EB/psu-EEA analysed by HPLC eluted together under the chosen operating conditions

(Figure 4-3), they are treated as a single peak. These results demonstrate that there is no clear relationship between increasing mobile phase flow and the separation factor.

Considering first the variation in the separation factor between the mobile phase flow rates 2 and 6 $mL.min^{-1}$, for $\alpha_{EC/ED-EA}$ we see a reduction, with $\alpha_{EB/Psu-EEA-EA}$ remaining almost constant. The decreased selectively between EC/ED and EA at the higher flow rate, as implied by Equation 3.11, is due to the difference in the $K_{EC/ED}$ between the two flow rates being proportionally larger than the K_{EA}. At the higher flow rates, i.e. at 8 and 10 $mL.min^{-1}$, $\alpha_{EC/ED-EA}$ becomes constant, whereas $\alpha_{EB/Psu-EEA-EA}$ shows a slight increase.

Since the separation factor is directly related to the selectivity of the phase system, with no effects of variations in phase volume ratio taken into account in the standard calculation (Equation 3.11) using the distribution ratios, its value is thermodynamically dependent (Schoenmakers, 1986). Menet *et al.* (1992) have studied the effects of increased mobile phase flow on the separation factor, choosing to calculate its value using retention factors (k), since they suggest the selectivity of the system is dependent on the phase volume ratio. If determination of α between EA and the other erythromycin components is performed using the corresponding k values instead, between EC/ED and EA there is a decrease going from 2 to 6 $mL.min^{-1}$, with a nominal increase at the higher mobile phase flow rates. Between EB/psu-EEA and EA there is no clear relationship. In chromatography, for adequate separation of two closely eluting components α must be greater than 1, and this is demonstrated over the range of flow rates studied.

Flow rate ($mL.min^{-1}$)	Separation factor (α) using K		Separation factor (α) using k	
	EC/ED – EA	EB/psu-EEA – EA	EC/ED – EA	EB/psu-EEA – EA
2	1.8	1.4	1.8	1.4
4	1.5	1.3	1.8	1.1
6	1.2	1.4	1.3	1.4
8	1.3	1.3	1.4	1.2
10	1.3	1.5	1.4	1.4

Table 6-9 **Variation in separation factor (α) with mobile phase flow rate between both EC/ED - EA and EB/psu-EEA - EA, calculated from distribution ratios and retention factors as shown in Tables 6-5 and 6-6.**

6.2.3. Effect on yield, purity and throughput

The effect of mobile phase flow rate on product yield, purity and predicted throughput are presented in Table 6-10. It can be seen that increasing the mobile phase flow rate reduced the total solute yield by approximately 20% w/w. At all flow rates up to 8 $mL.min^{-1}$ the purity of EA in the main fraction was found to be 100% (w/w), decreasing to 96% (w/w) at a mobile phase flow rate of 10 $mL.min^{-1}$. Based on the total solute yield, the maximum estimated throughput of this CCC separation (Equation 3.16) was calculated to be 0.016 $kg.day^{-1}$.

Flow rate ($mL.min^{-1}$)	**EA purity (% w/w)**	**EA yield (% w/w)**	**Total solute yield (% w/w)**	**Throughput ($kg.day^{-1}$)**
2	100	100	100	0.006
4	100	91	80	0.009
6	100	81	74	0.011
8	100	87	77	0.013
10	96	87	80	0.016

Table 6-10 Variation in performance parameters with mobile phase flow rate for experiments performed as described in Figures 4-4 and 6-1.

6.3. Variation of solute loading

A second means of achieving a higher throughput of processed material is to increase the amount of solute injected onto the CCC column. In the current investigation two loading strategies were considered due to the relatively low solubility of erythromycin in the aqueous mobile phase. Firstly, solute concentration was increased from 100–500 $mg.mL^{-1}$ in a fixed injection volume of 1 mL of the mobile phase. The upper concentration is close to the solubility limit of erythromycin in the mobile phase used. The CCC chromatograms for the range of solute loadings can been seen in Figure 6-7. All experiments were performed at a fixed mobile phase flow rate

of 2 $mL.min^{-1}$, with the corresponding S_f value for all the loading studies found to be 81%. Solute loading was increased further by increasing the injection volume to 2 mL allowing up to 1000 mg of the crude erythromycin preparation to be loaded onto the column. CCC experiments were performed again at a mobile phase flow rate of 2 $mL.min^{-1}$, with the resultant chromatograms illustrated in Figure 6-8. The corresponding S_f value for all the loading studies was found to be 82%.

For all the solute loading experiments, fractions collected every minute were analysed by the off-line HPLC and sulphuric acid assays (Sections 2.3.3.4.1 and 2.3.3.4.2). The results from HPLC analysis for EA, EC/ED and EB/psu-EEA are given in Table 6-11 for solute loading experiments between 200 and 500 mg (V_i = 1 mL) and Table 6-12 for those experiments between 200 and 1000 mg (V_i = 2 mL). Once again, results are given for the peak maxima of the different erythromycin forms, with the corresponding elution time being calculated as the arithmetic mean of the collection period for a particular fraction.

For the solute loading experiments between 200 and 1000 mg (Tables 6-11 and 6-12), focusing initially on the main EA peak, the elution time from the CCC chromatograms (Figures 6-7 (a)-(d); Figures 6-8 (a) – (e)) as shown in Table 6-13 was compared with that determined from off-line HPLC analysis. For all experiments there is a good correlation between the EA retention times determined by the two methods, with a maximum calculated percentage error of 17%. The error is larger at the highest loadings due to an increase in band broadening as the injected mass of solute increases causing greater peak asymmetry. The effect of solute loading on the retention time of the main EA peak shows only small variations between 20.5 and 23.5 minutes.

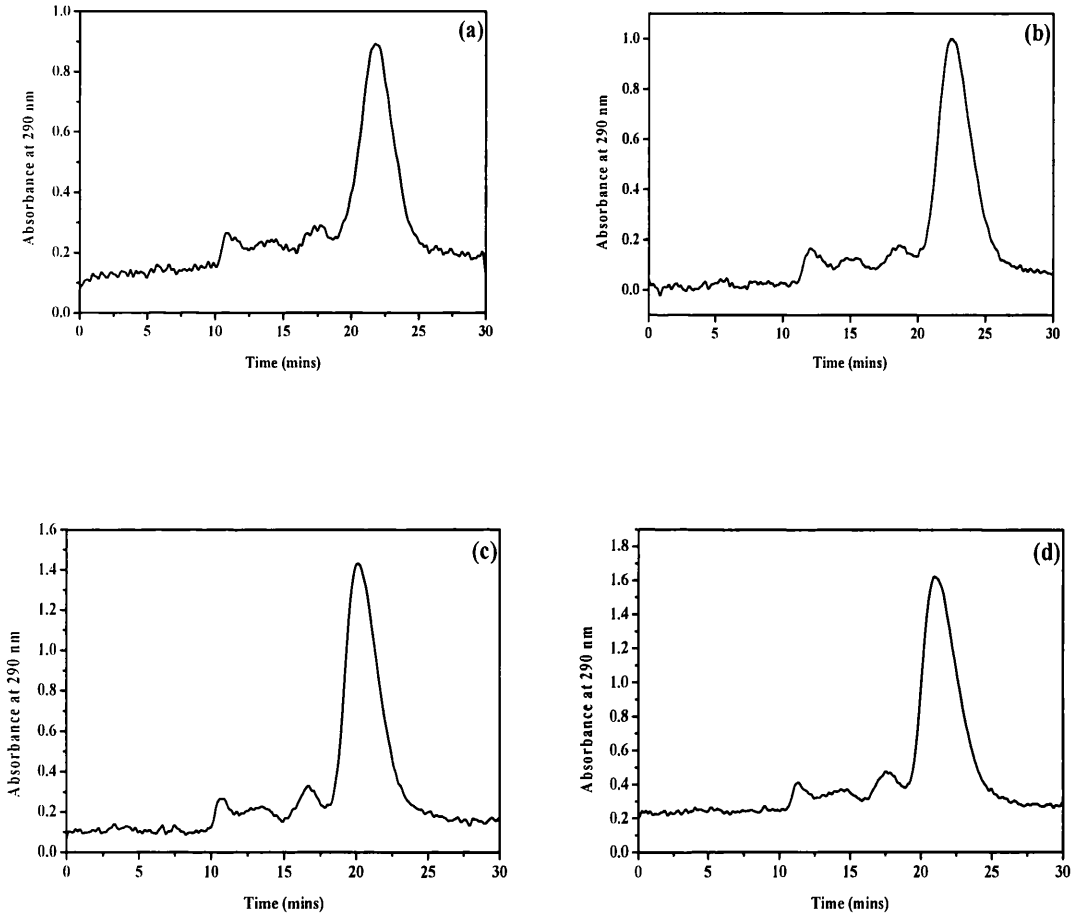

Figure 6-7 **CCC chromatograms from solute loading experiments (V_i = 1 mL) of (a) 200 mg (b) 300 mg (c) 400 mg and (d) 500 mg. All experiments performed as described in Sections 2.4.1.1 and 2.4.1.2 using a quaternary phase system comprising of hexane/ethyl acetate/methanol/water (1.4/2.0/2.0/1.0 v/v).**

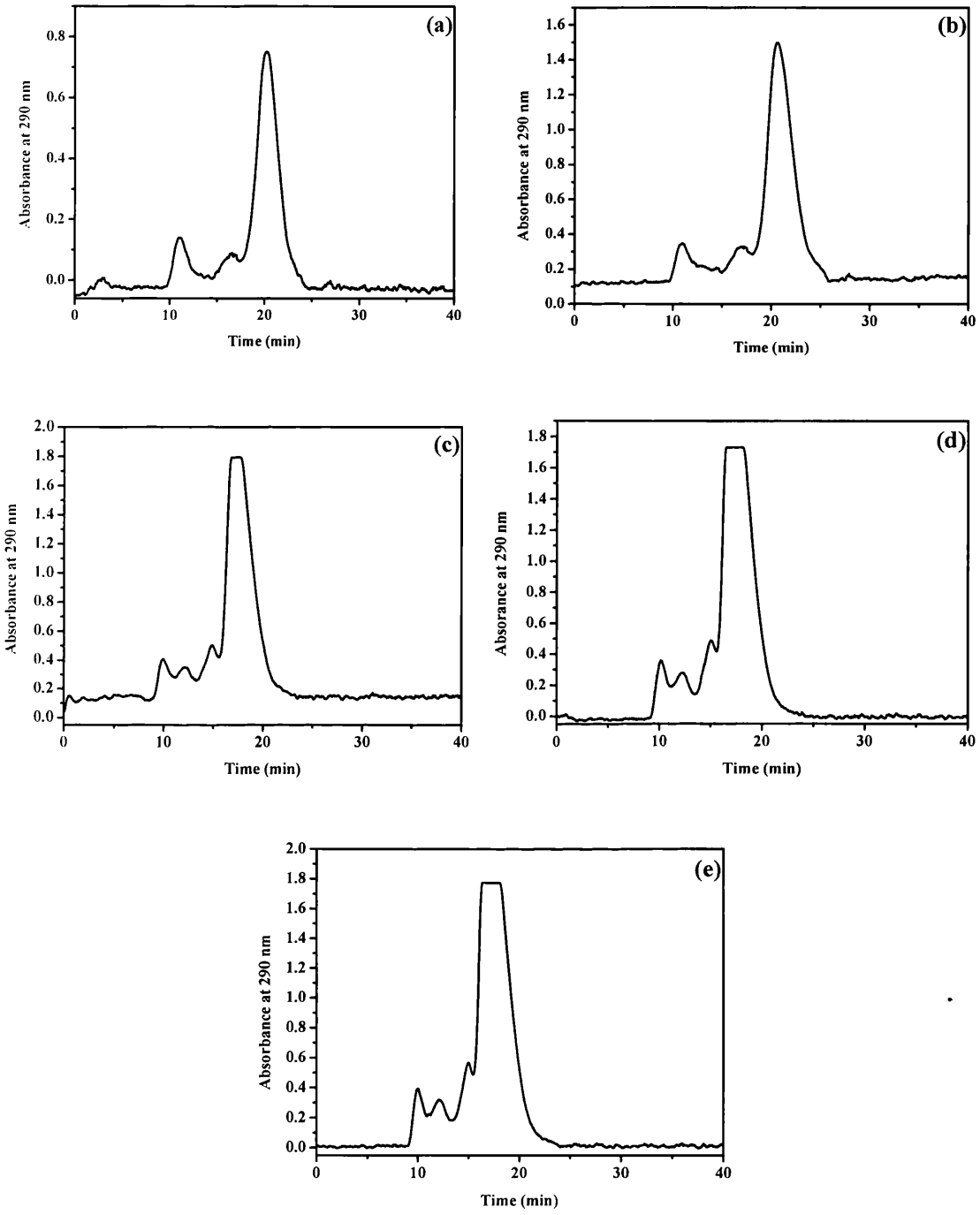

Figure 6-8 **CCC chromatograms from solute loading experiments (V_i = 2 mL) of (a) 200 mg, (b) 400 mg,(c) 600 mg, (d) 800 mg and (e) 1000 mg. All experiments performed as described in Sections 2.4.1.1 and 2.4.1.2 using a quaternary phase system comprising of hexane/ethyl acetate/methanol/water (1.4/2.0/2.0/1.0 v/v).**

Solute loading	Fraction (min)	Solute identity	Concentration ($mg.mL^{-1}$)	TMIF (mg)
200	17.5	EC/ED	1.4	5.6
	21.5	EA	30.1	60.2
	26.5	EB/psu-EEA	0.5	3.2
300	18.5	EC/ED	5.2	10.3
	22.5	EA	30.6	61.2
	27.5	EB/psu-EEA	0.9	1.8
400	16.5	EC/ED	8.9	17.7
	20.5	EA	52.7	105.4
	19.5	EB/psu-EEA	4.9	9.7
500	17.5	EC/ED	9.7	19.3
	21.5	EA	56.7	113.4
	23.5	EB/psu-EEA	1.9	3.7

Table 6-11 **Identification and quantification of the various forms of the erythromycins from isocratic CCC experiments performed as described in Figure 6-7. EA: erythromycin A, EC: erythromycin C, ED: erythromycin D, EB: erythromycin B, psu-EEA: ring-contracted enol ether of erythromycin A.**

Solute loading	Fraction (min)	Solute identity	Concentration ($mg.mL^{-1}$)	TMIF (mg)
200	16.5	EC/ED	4.1	8.2
	20.5	EA	16.8	33.5
	20.5	EB/psu-EEA	11.3	22.6
400	20.5	EC/ED	3.8	7.5
	23.5	EA	44.3	88.6
	26.5	EB/psu-EEA	5.1	10.1
600	17.5	EC/ED	12.7	25.4
	20.5	EA	84.1	168.2
	22.5	EB/psu-EEA	4.2	8.4
800	16.5	EC/ED	10.0	20.0
	20.5	EA	105.1	210.1
	22.5	EB/psu-EEA	7.6	15.1
1000	17.5	EC/ED	16.8	33.5
	20.5	EA	112.9	225.8
	22.5	EB/psu-EEA	7.4	14.8

Table 6-12 **Identification and quantification of the various forms of the erythromycins from isocratic CCC experiments performed as described in Figure 6-8. EA: erythromycin A, EC: erythromycin C, ED: erythromycin D, EB: erythromycin B, psu-EEA: ring-contracted enol ether of erythromycin A.**

Solute loading (mg)	EA elution time (min)		Error (%)
	HPLC	CCC chromatogram	
200	21.5	22.2	3.2
300	22.5	22.2	1.3
400	20.5	19.7	3.9
500	21.5	20.7	3.7
200*	20.5	19.7	3.9
400*	23.5	20.7	11.9
600*	20.5	17.1	16.6
800*	20.5	17.2	16.1
1000*	20.5	16.9	17.6

Table 6-13 Comparison of EA elution times determined from off-line HPLC analysis and directly from CCC chromatograms obtained using on-line UV-Vis detection. Experiments performed as described in Figures 6-7 and 6-8.

6.3.1. Effect on chromatographic retention factors

Chromatographic retention factors for the different erythromycin forms were again calculated for each solute loading as described in Sections 3.1.2 and 3.1.3. The retention times of the various species were determined from off-line HPLC data (Tables 6-11 and 6-12). The effect of solute loading on the distribution ratio (K) of EA, EC/ED and EB/psu-EEA is shown in Table 6-14. Figure 6-9 illustrates the effects of solute loading on the K values for the different erythromycins.

Considering firstly Figure 6-9(a) for all the erythromycins detected, increasing solute loading from 200 to 300 mg sees an increase in K of between 7 and 15%. Increasing solute loading further to 400 mg, in all cases sees a decrease in the distribution ratio of between 14 and 44%. At a solute loading of 500 mg, the K values for all erythromycins increase back up to a maximum of 0.30 for EB/psu-EEA. In addition, the solute loading concentration was altered by varying the injection volume up to 2 mL. Figure 6-9(b) illustrates the variation in the K values for the erythromycins EA, EC/ED, and EB/psu-EEA.

Solute loading (mg)	t_c'	t_k'			K		
		EA	EC/ED	EB/psu-EEA	EA	EC/ED	EB/psu-EEA
200	45.8	11.9	7.9	16.9	0.26	0.17	0.37
300	45.8	12.9	8.9	17.9	0.28	0.20	0.39
400	45.8	10.9	6.9	9.9	0.24	0.15	0.22
500	45.8	11.9	7.9	13.9	0.26	0.17	0.30
200*	42.7	11.6	7.6	11.5	0.27	0.18	0.27
400*	42.7	14.6	11.6	17.6	0.34	0.27	0.41
600*	42.7	11.6	8.6	13.6	0.27	0.34	0.32
800*	42.7	11.6	7.6	13.6	0.27	0.27	0.32
1000*	42.7	11.6	8.6	13.6	0.27	0.27	0.32

Table 6-14 Variation in K of EA, EC/ED and EB/psu-EEA with solute loading. * indicates loading experiments performed using a 2 mL injection volume. Experiments performed as described in Figures 6-7 and 6-8.

Again focusing on the target compound EA, at the solute loading of 200 mg, the corresponding K value was calculated to be 0.27. This K value of 0.27 is extremely close to the K of 0.26 determined for the 200 mg solute injection experiment with 1 mL injection volume. A further comparison of K values between the two 400 mg solute loading experiments is possible. At the 1 mL injection (400 $mg.mL^{-1}$) the corresponding K was found to be 0.24, increasing to 0.34 for the 2 mL injection. This observed increase at the higher injection volume is also true for the other erythromycin analogues. In conclusion, the results demonstrate that solute loading concentration does not have a dramatic effect on retention time and hence K. These observations are supported by a similar study investigating the effects of mass loading on the preparative separation of macrolide antibiotics (Wang-Fan *et al.*, 2001). This group found for the range of mass loadings investigated (12.5 mg to 200 mg) that there was 'almost no effect on peak retention time'.

At this point it is important to stress the potential discrepancy in K value calculations based on the methods by which retention time is determined. The percentage error between EA retention times determined by these two methods is presented in Table 6-13, and as previously discussed shows an increasingly poor correlation with increasing solute loading. Table 6-15 provides K results for EA for the range of solute loading experiments based on retention times determined directly from the CCC chromatograms (Figures 6-7 and 6-8).

Solute loading (mg)	t_c'	t_k' EA	K EA
200	45.8	12.9	0.32
300	45.8	12.9	0.32
400	45.8	10.4	0.25
500	45.8	11.4	0.28
200*	42.7	11.4	0.30
400*	42.7	12.4	0.32
600*	42.7	8.8	0.23
800*	42.7	8.9	0.23
1000*	42.7	8.6	0.22

Table 6-15 **Variation in the K of EA with solute loading (mg) based on retention times determined directly from the corresponding CCC chromatograms as shown in Figures 6-7 and 6-8. Experiments performed as described in Figures 6-7 and 6-8.**

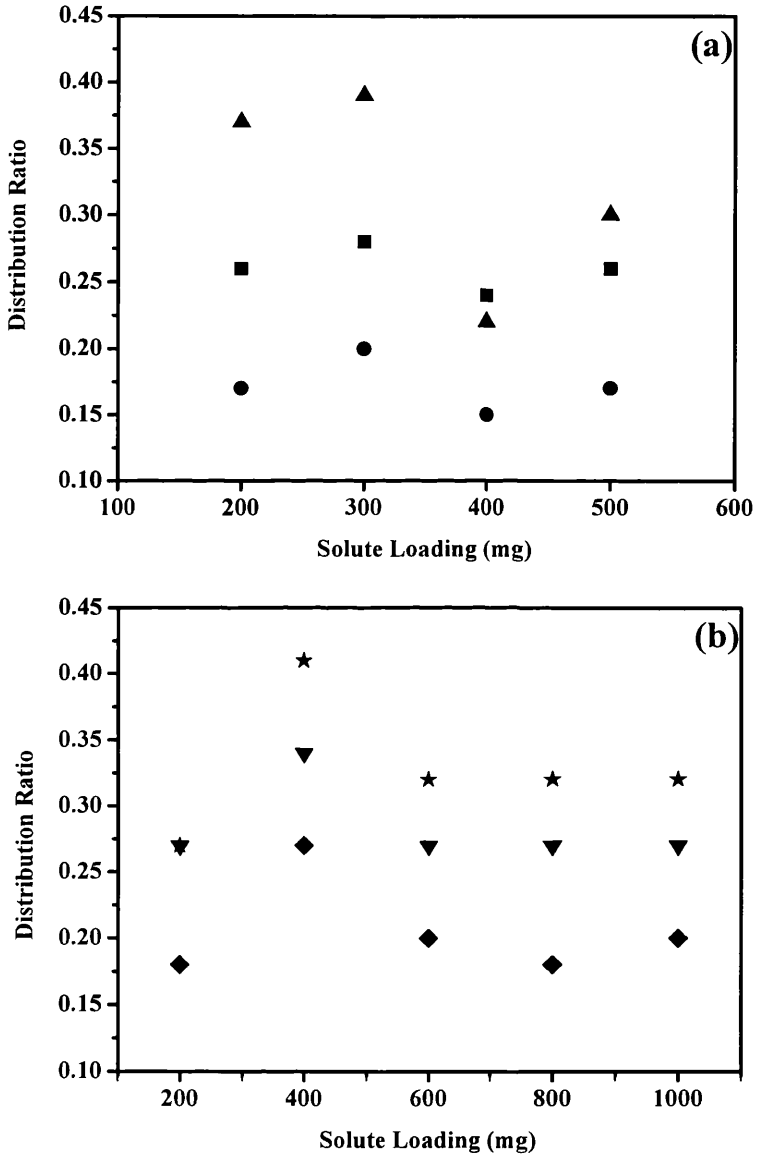

Figure 6-9 **Effect of solute loading on distribution ratios of erythromycins. Plot (a) corresponds to experiments using a 1 mL injection volume, where (■) is EA, (●) is EC/ED, (▲) is EB/psu-EEA. Plot (b) corresponds to experiments using a 2 mL injection volume, where (▼) is EA, (◆) is EC/ED, (★) is EB/psu-EEA. All experiments performed as described in Figures 6-7 and 6-8.**

From the comparison of the K_{EA} results in Tables 6-14 and 6-15, it can be seen that there is, for all loading experiments, a significant deviation in the results. The percentage error was between 4 and 19%. The significance of these K value discrepancies is of importance when attempting to predictably model the separation, either at the same operating scale or larger, i.e. process scale-up.

The effect of increasing solute loading on k_{EA} is shown in Table 6-16 for the solute retention time determined by the two methods described previously. Once again, it is apparent that the k value determined using the two different EA retention times is different for each solute loading. Since, in determining k (Equation 3.10) all K values are multiplied by the same factor, $(S_f / 1 - S_f)$ the percentage errors between the k values was found to be the same as those percentage errors for the K values.

Solute Loading (mg)	k_{EA}	
	HPLC	CCC
200	1.11	1.36
300	1.19	1.36
400	1.02	1.07
500	1.11	1.19
200*	1.23	1.37
400*	1.55	1.46
600*	1.23	1.05
800*	1.23	1.05
1000*	1.23	1.00

Table 6-16 Variation in the k of EA with solute loading (mg) based on retention times determined directly from the corresponding CCC chromatograms and from off-line HPLC analysis. All experiments performed as described in Figures 6-7 and 6-8.

The largest error occurs at the higher solute loadings, again primarily due the increased band broadening and detection limitations of the UV detector. It is therefore more advantageous to use the k_{EA} values determined from HPLC analysis, as this represents the actual elution profile of the EA analogue, as well as the other forms of erythromycin.

The results in Table 6-16 determined by HPLC analysis suggest that at a higher solute loading concentration, i.e. those experiments performed using a 1 mL injection volume, the k_{EA} values and hence the retention time are lower than corresponding

experiments performed at the 2 mL solute loading. The reason for this deviation from the expected trend, as inferred from Equation 3.10, is due to the variation in the V_s/V_m term with S_f.

6.3.2. Effect on chromatographic performance

As with the flow rate studies described in Section 6.2.2, the separation performance with increasing solute loading was evaluated a number of ways. Firstly performance was measured by calculating the number of theoretical plates (N) using Equation 3.14. All efficiency calculations in the first instance were made with the corresponding terms measured directly from the corresponding CCC chromatogram. For both loading volumes the variation in N with increasing solute loading is illustrated in Figure 6-10.

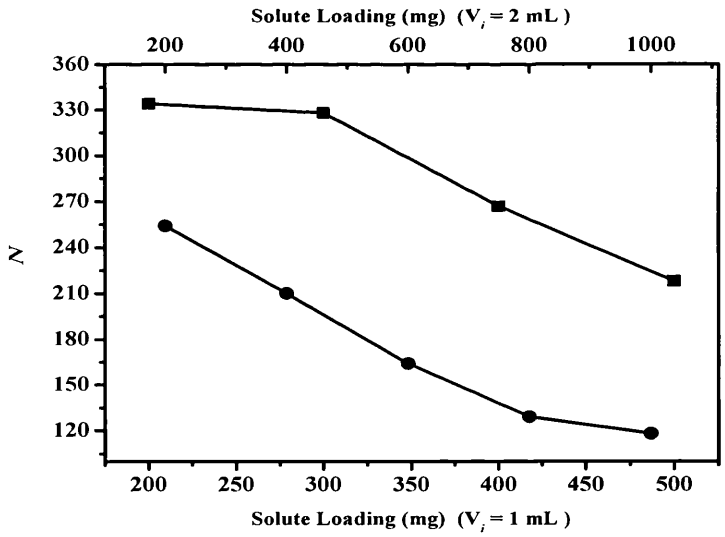

Figure 6-10 Effect of solute loading on column efficiency calculated as N. (■) represents 1 mL loading studies. (●) represents 2 mL loading studies. Column efficiency based on the main EA peak for the CCC chromatograms shown in Figures 6-7 and 6-8 and according to Equation 3.14.

As can be seen from Figure 6-10 for all experiments, there is a decrease in the calculated column efficiency with increasing solute loading. Column efficiency also decreases with increasing injection volume. Closer inspection of the chromatographic data from the CCC chromatograms used in calculating *N*, i.e. R_TEA; $d_{h/2}$ (Equation 3.14) shows that firstly, with regard to the separation performed at the 200 mg loading experiments, the nominator term, d_R, decreases with increasing injection volume (Table 6-13). In addition, the denominator term, $w_{h/2}$, shows a variation between these two loading scales, which increases with increasing loading volume. Similar analysis of the data for the comparison between the 400 mg loading experiments shows a slight variation in the R_TEA values (Table 6-13) of 1 minute, with the variation in the $d_{h/2}$ values being more pronounced, again increasing with increasing loading volume up to ~14%.

This increasing variation in the peak widths for both loadings (200 and 400 mg) signifies the band broadening phenomena in addition to increased fronting and tailing (Hermans-Lokkerbol *et al.*, 1997) and as such is the reason for the decreasing efficiency of the column.

As with the flow rate studies, separation factors between the main component EA and the 'contaminants' eluting either side were calculated and are shown in Figure 6-11. It is clear that the variation in α with increasing solute loading is to be expected in the case of $\alpha_{EC/ED-EA}$ due to the small variations in the retention times over the solute loading range studied (Tables 6-11 and 6-12). However, it is apparent that across the range of solute loadings, $\alpha_{EB/psu\text{-}EEA-EA}$ is consistently lower than the corresponding $\alpha_{EC/ED-EA}$ values, but again remains fairly constant.

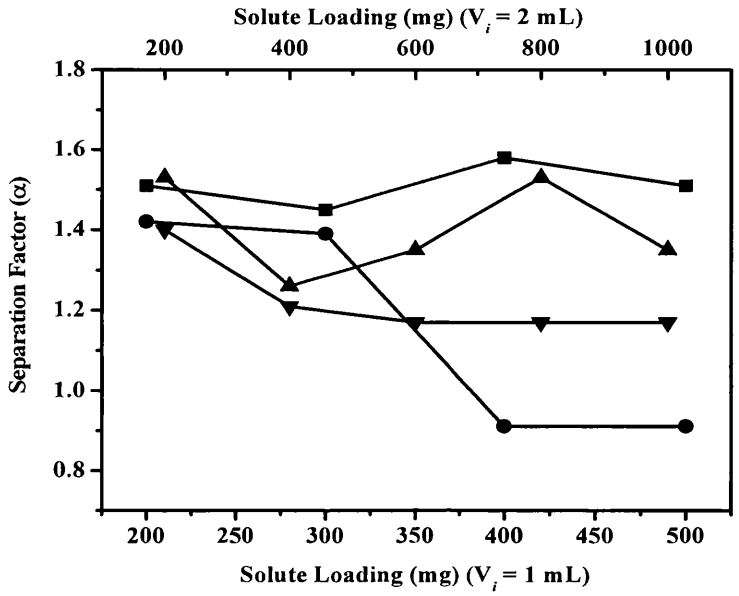

Figure 6-11 Effect of solute loading on the separation factor (α). (■) and (●) represents $\alpha_{EC/ED - EA}$ and $\alpha_{EB/psu-EEA - EA}$ respectively (V_i = 1 mL). (▲) and (▼) represents $\alpha_{EC/ED - EA}$ and $\alpha_{EB/psu-EEA - EA}$ respectively (V_i = 2 mL). Experiments performed as described in Figures 6-7 and 6-8 and calculated according to Equation 3.11.

Due to increasing band broadening that occurs with larger solute and volume loadings (Berthod and Armstrong, 1988) a more applicable means of determining the performance of the separation is to calculate the resolution. The resolution between both EA and the analogues eluting before and after it, i.e. EC/ED and EB/psu-EEA respectively were calculated using Equation 3.12, with solute retention data obtained from off-line HPLC analysis of collected fractions (Tables 6-11 and 6-12). The results are shown in Figure 6-12 and demonstrate an overall trend, in that increasing solute loading leads to a reduction in resolution between EA and the analogues EC/ED and EB/psu-EEA. No data was obtained at the solute loadings of 400 and 500 mg (V_i = 1 mL) due to the coelution of the EB/psu-EEA analogue with the main EA peak.

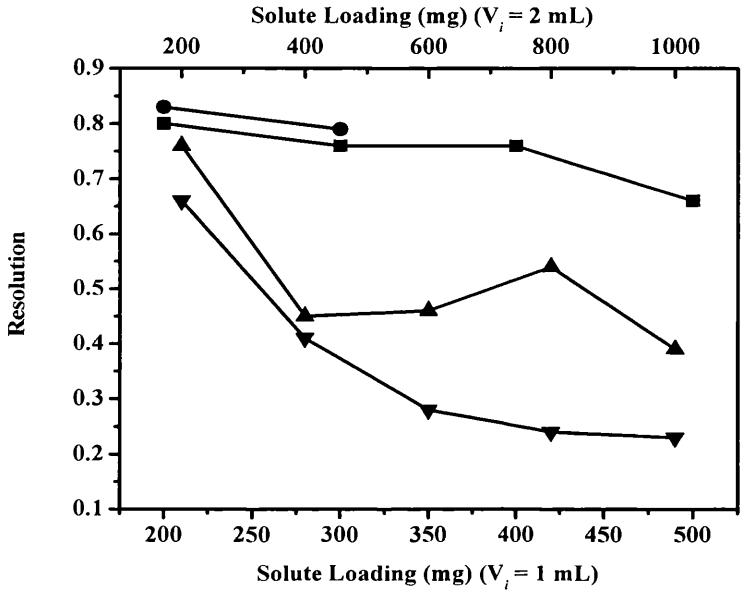

Figure 6-12 Effect of solute loading on resolution (R_s). (■) and (●) represents $R_{s(EC/ED - EA)}$ and $R_{s(EB/psu-EEA - EA)}$ respectively (V_i = 1 mL). (▲) and (▼) represents $R_{s(EC/ED - EA)}$ and $R_{s(EB/psu-EEA - EA)}$ respectively (V_i = 2 mL). Experiments performed as described in Figures 6-7 and 6-8 and calculated according to Equation 3.12.

6.3.3. Effect on product yield, purity and throughput

The effect of solute loading on EA yield, purity and predicted throughput is presented in Table 6-17. It can be seen that increasing solute loading initially at a V_i of 1 mL, reduced the EA purity from 100% (w/w) at a solute loading of 200 mg to 92% (w/w) at a solute loading of 500 mg. The reason for the reduction in the purity of the main EA peak at 500 mg is due to the band broadening effect previously discussed (Section 6.3.1).

Solute loading (mg)	EA purity (% w/w)	EA yield (% w/w)	Total solute yield (% w/w)	Throughput ($kg.day^{-1}$)
200	100	100	98	0.011
300	100	92	88	0.015
400	93	95	98	0.023
500	92	90	93	0.024
200*	100	90	100	0.011
400*	95	93	97	0.018
600*	98	88	87	0.025
800*	98	92	90	0.033
1000*	98	89	89	0.041

Table 6-17 Variation in performance parameters with solute loading. * indicates the 2 mL loading volume. Experiments performed as described in Figures 6-7 and 6-8.

6.4. Optimisation of CCC operation

Based on the results in Sections 6.2 and 6.3 an initial optimisation of the two operating strategies was attempted. The conditions chosen were a solute loading of 600 mg and a mobile phase flow rate of 8 $mL.min^{-1}$. The resultant CCC chromatogram is shown in Figure 6-13(a). The presence of two main peaks can be seen between 5.5 and 8.4 minutes. The increased loading and mobile phase flow rate used resulted in the erythromycin analogues EC/ED (72 mg), EB/psu-EEA (8 mg) and the target product EA (144 mg) to begin to co-elute. Off-line HPLC analysis of the fraction corresponding to the main CCC peak between 7 and 8 minutes (Figure 6-13(b)) shows the presence of mainly EA (420 mg) with a very small amount of EB/psu-EEA (8 mg). For a comparable fractionation at 8 $mL.min^{-1}$ (Figure 6-1(c)) it can be seen that the retention time of the main EA peak decreases when the solute loading increases from 0.2 g to 0.6 g. The increase in the solute loading further accounts for the reduction in the values of the EA distribution ratio (K_{EA}) and the retention factor (k_{EA}) (0.32 and 0.46 respectively). Despite the low calculated column efficiency (N = 23), a high degree of EA purity and total solute yield was achieved in the main fraction (97% w/w and 100% w/w respectively) with a maximum throughput estimated to be 0.097 $kg.day^{-1}$.

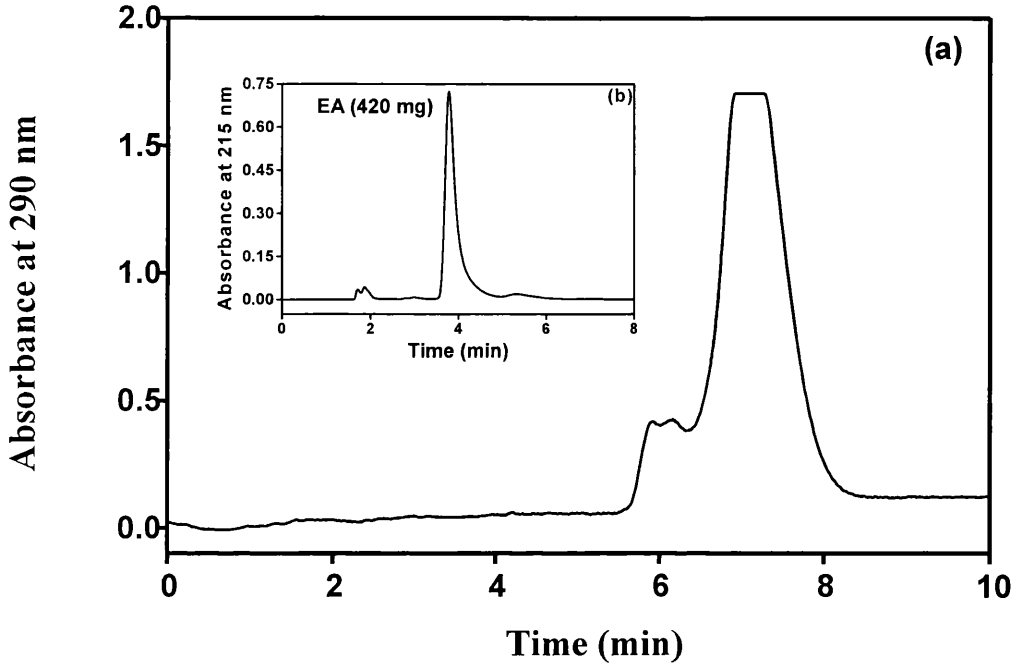

Figure 6-13 **(a) CCC chromatogram of optimised erythromycin fractionation (600 mg) at a mobile phase flow rate of 8 mL.min^{-1} (S_f = 59% v/v). Retention time of main EA peak was at 7.1 minutes. (b) The main peak fraction between 7-8 minutes analysed by HPLC shows the target compound EA (420 mg) at a purity of 97% (w/w).**

6.5. Summary

The results presented in this chapter have shown efficient separation of EA from closely related analogues can be achieved over a range of operating conditions. Increasing mobile phase flow rate (Section 6.2) leads to a reduction in the total solute yield by approximately 20% w/w, but still provides a satisfactory separation of EA from its analogues, even at the highest flow rates. Increasing solute loading leads to a reduction in the column efficiency, but despite this a satisfactorily high yield and purity of the target solute, EA, was achieved at the highest injected solute concentration.

Having established an understanding of how CCC operating variables influence the separation of a crude erythromycin preparation, the work described in the next Chapter will examine the separations of erythromycin A from real fermentation broths.

7. Laboratory scale fractionation of fermentation broth derived erythromycins

7.1. Introduction

For the successful integration of CCC into new as well as existing and well established purification processes, the technology will need to meet a number of criteria, such as ease of method development (Chapter 4), scale-up (Chapter 8) and also it must be able to successfully handle crude feed streams. For the purification of antibiotics by CCC in the majority of cases the material loaded onto the CCC column has undergone a large degree of pre-purification prior to injection (Brill *et al.*, 1985; Chen *et al.*, 1988). This was the impetus for the range of systematic 'real system' experiments described in this Chapter, with the aim being to examine the feasibility of using CCC for the purification of fermentation broth derived erythromycins. The majority of the results presented in this Chapter forms the basis of a manuscript: Booth A.J., Ngiam S.H., Titchener-Hooker N.J and Lye G.J (submitted): Antibiotic purification from fermentation broths by counter-current chromatography: analysis of product purity and yield trade-offs.

7.2. Fermentation characterisation

The main aim of the fermentation studies was to obtain an industrially representative matrix from which the target product, EA, could be purified. This will enable the effects of broth impurities on the separation performance of CCC to be studied. The fermentations were performed as described in Section 2.2, with a representative example of the outcome of on-line monitoring for dissolved oxygen concentration (DOT), oxygen uptake rate (OUR) and off-line dry cell weight (DCWT) analyses during the operating period shown in Figure 7-1. As can be seen from the on-line profiles, during the course of the fermentation there was a gradual increase in both the OUR and CER, from 0 to 40 hours, with a corresponding increase in biomass concentration during this time

period, representing the exponential growth phase. The maximum biomass concentration of ~12 $g.L^{-1}$ was achieved at 49 hours, and remained approximately constant until the end of the fermentation (70 hours). Davies *et al.* (2000) have shown a similar growth profile using the same soluble complex media and micro organism. With increasing growth of *S. erythraea* up to 40 hours, the dissolved oxygen tension (DOT) within the fermenter decreased to a minimum of 80% during the exponential phase and tended back towards 100% during the 'deceleration phase'. The respiratory quotient (RQ), the ratio of the number of moles of carbon dioxide produced by the organism, to the number of moles of oxygen utilised, recorded a value of ~0.8, where it remained constant till the end of the fermentation (70 hours) indicating the utilisation of carbohydrates as the main carbon energy source.

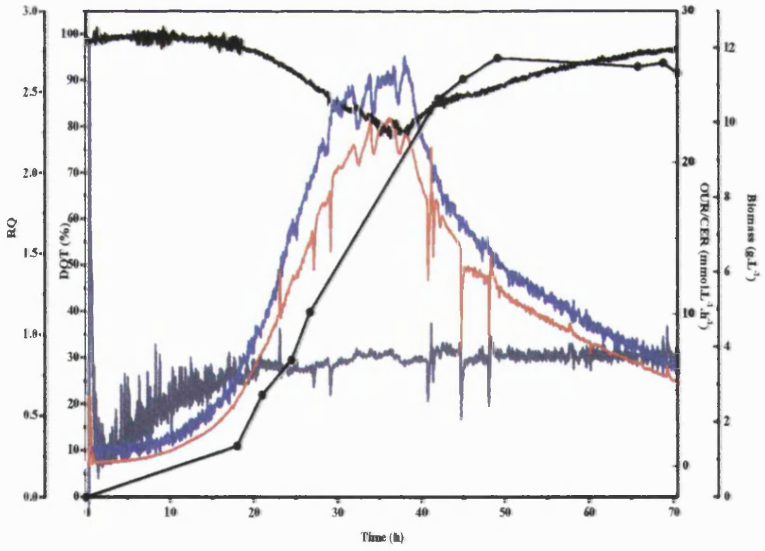

Figure 7-1 **Growth profiles of *S.erythraea* on a soluble complex medium. (—) oxygen-uptake rate (OUR). (—) carbon dioxide evolution rate (CER). (—) dissolved oxygen tension. (—) respiratory quotient (RQ). (—•—) dry cell weight (DCWT). Fermentation and on-line monitoring peformed as described in Section 2.2.3. DCWT analysis peformed as described in Section 2.2.3.1.**

7.3. Application of an Evaporating Light Scattering Detector

Before examining the effect of feed composition on the fractionation of erythromycin by CCC, due to the presence of unused nutrients, such as glucose or yeast extract, and undefined impurities, such as unwanted metabolites and surfactants (Section 1.1.6.4.1, Table 1-3) the resulting clarified broth was pigmented. Detection of such a complex matrix eluting from the CCC machine by UV absorbance masked the elution of the target compound EA. To overcome this limitation, an evaporative light scattering detector (ELSD) (Section 2.3.3.2) was employed in this work to evaporate off any volatiles that could potentially interfere with the detection of the target compound. For comparison to the earlier work, Figure 7-2 illustrates an on-line ELSD trace from a CCC separation of a crude model erythromycin preparation (as used in Chapters 4 and 6) performed at a mobile phase flow rate of 2 $mL.min^{-1}$ (S_f = 81.5%). HPLC analysis (Section 2.3.3.4.2) confirmed the main peak between 19 and 20 minutes consisted of EA. This observed elution profile (Figure 7-2) showed an exact correlation with previous CCC experiments performed under the same operating conditions using on-line UV detection (Figure 4-4) therefore providing an assurance of the peak composition.

7.4. Effect of degree of pre-purification on erythromycin separation

7.4.1. Effect on solute retention

The first stage of the study investigated the effect of feed composition on the erythromycin fractionation. The aim of this was to establish where in a post-clarification recovery process CCC could be effectively employed to provide a reproducible separation of the target compound, EA, from its analogues. Based on the range of solvent extraction stages used in industrial erythromycin recovery (Verrall, 1992) the feed material to be injected onto the CCC column was firstly clarified (clarified broth), then underwent a forward extraction step (forward extract) and finally a back extraction step (back extract) as described in Section 2.2.4. Due to the low erythromycin levels produced

by the fermentation, typically in the region of 230 $mg.L^{-1}$ (Davies *et al.*, 2000), and the need to maintain operating conditions comparable to those used in Chapter 6, the mobile phase was spiked with the crude erythromycin used during the model system studies.

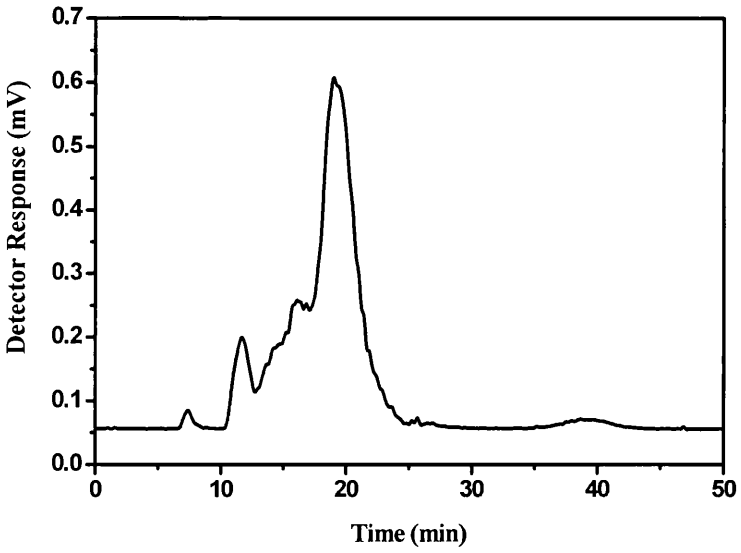

Figure 7-2 Laboratory scale CCC chromatogram of a crude erythromycin fractionation (100 mg) at a mobile phase flow rate of 2 $mL.min^{-1}$ (S_f = 81.5%) using the ELSD. Experiments performed as described in Section 2.4.1.1 and 2.4.1.2 using a quaternary solvent system comprising of hexane/ethyl acetate/methanol/water (1.4/2.0/2.0/1.0 v/v).

Figure 7-3(a) illustrates an example CCC chromatogram of a crude erythromycin separation that had been resuspended in 1 mL of the clarified broth (Section 2.2.4.1). The fractionation was performed under the standard laboratory scale operating conditions, i.e. a mobile phase flow rate of 2 $mL.min^{-1}$ and 100 $mg.mL^{-1}$ loading. The solid line represents the on-line ELSD trace of the mobile phase eluant, clearly showing a similar elution profile to that in Figure 7-2. The bars shown in Figure 7-3(a) correspond to mass balance data from off-line HPLC analysis of fractions collected at 1 minute intervals for the different erythromycin analogues. It can be seen that the main peak from the ELSD trace corresponds to EA, with the smaller peaks just before and after corresponding to the erythromycins C/D and EB/psu-EEA respectively.

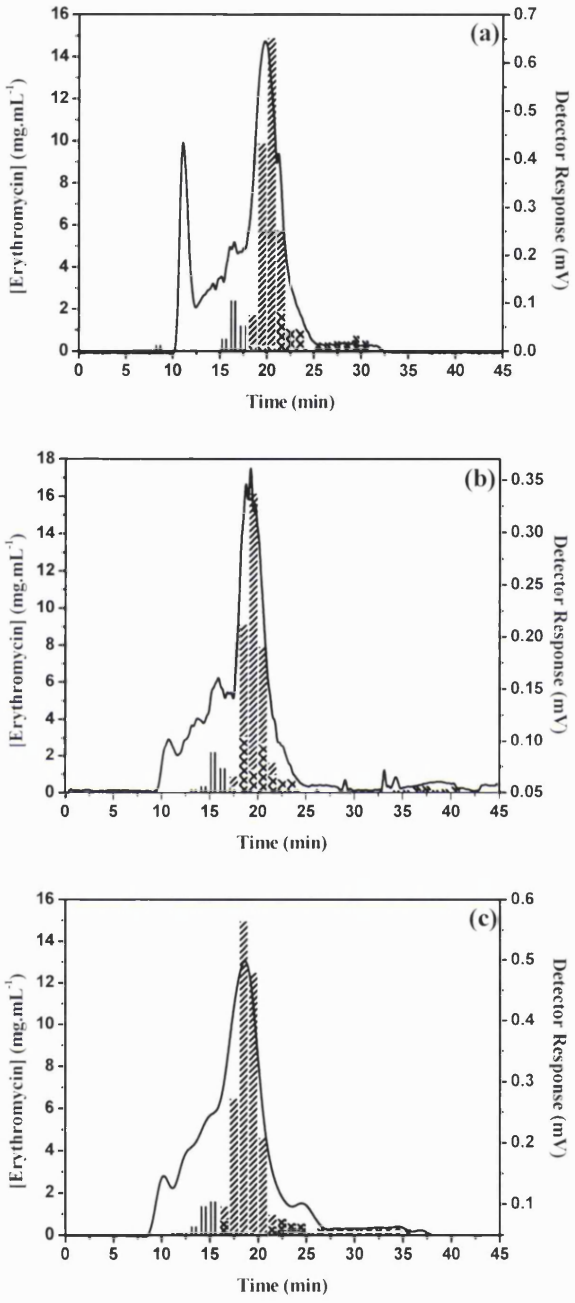

Figure 7-3 **Laboratory scale CCC chromatograms of erythromycin fractionation (100 mg) and corresponding off-line HPLC data of the various erythromycin analogue concentrations, using (a) clarified broth, (b) forward extract, (c) back extract. (‖) = EC/ED. (///) = EA. (xx) = EB/psu-EEA. (\\\) = EEA. Solid line represents the detector response from the ELSD. Experiments performed at a mobile phase flow rate of 2 mL.min^{-1} as described in Sections 2.4.1.1 and 2.4.1.2.**

Secondly, clarified fermentation broth underwent a forward solvent extraction step into butyl acetate, as described in Section 2.2.4.2. After entrained solvent removal by vacuum drying, the resultant feed material was resuspended in the aqueous mobile phase used for CCC. The mobile phase feed was then spiked with the crude erythromycin to a concentration of 100 $mg.mL^{-1}$. Figure 7-3(b) illustrates a dual plot of the on-line ELSD trace of the eluting mobile phase and the corresponding concentrations of the erythromycins EC/ED, EA, and EB/psu-EEA determined by HPLC. From the results separation between the erythromycins EC/ED and EA was achieved, and to a lesser extent between EB/psu-EEA and EA. The final stage involved performing a back extraction stage, from the butyl acetate rich phase into an aqueous phosphate buffer as described in Section 2.2.4.2.

Once again, to ensure direct comparisons between corresponding experiments could be made, the resultant back extracted feed, once resuspended in the aqueous CCC mobile was spiked with the crude erythromycin to a concentration of 100 $mg.mL^{-1}$. The mobile phase eluant was again monitored using ELSD and collected fractions analysed by HPLC, with the dual plot presented in Figure 7-3(c). From the ELSD traces in Figures 7-3(a) to 7-3(c), the most noticeable difference is the absorbance of the peak eluting at 10 minutes, which is approximately 3 times greater in Figure 7-3(a) than the corresponding peaks shown in Figures 7-3(b) and (c). This is indicative of the relative impurity levels present in the feed streams used, i.e. greater amounts of broth impurities in the clarified broth compared to the solvent extracts. While these components can not be identified explicitly, the fact that they elute early, i.e. being non-retained material, hence having a distribution ratio of 0, and are not as prevalent in the forward extract suggests they are hydrophilic in nature.

The CCC chromatograms presented in Figures 7-3(a) to 7-3(c) were used to calculate the distribution ratio (K) and retention factor (k) for the main EA peak in each case, with the results presented in Table 7-1.

Feed type	t_c'	t_k'	K_{EA}	k_{EA}
CB	38.4	11.8	0.31	1.35
FE	38.6	10.9	0.28	1.27
BE	38.3	10.1	0.25	1.13

Table 7-1 **Variation in the distribution ratio (K_{EA}) and retention factor (k_{EA}) with feed type. CB: clarified broth, FE: forward extract, BE: back extract. Values calculated from Figures 7-3(a) to (c) and as described in Sections 3.1.2 and 3.1.3.**

As can be seen from the results in Table 7-1, there is a decrease in K_{EA} from 0.31 (clarified broth), to 0.28 (forward extract) and finally to 0.25 (back extract). Since the stationary phase retention for each of the experiments remained approximately constant, being 81.5% (CB), 81.8% (FE) and 81.1% (BE), the calculated phase ratios, i.e. V_s and V_m, could be determined, allowing the retention factor (k) to be calculated. With lower impurity levels in the feed, i.e. moving from the clarified broth to the back extract, there is a corresponding decrease in the retention factor (Table 7-1). This suggests that feed impurities cause a reduction in solute mass transfer and hence the product resides for longer periods in the stationary phase. From the HPLC results in Figures 7-3(a) to 7-3(c), the retention time of the EA peak was determined to be 20.5 minutes (CB), 19.5 minutes (FE) and 19 minutes (BE), supporting the calculated k_{EA} results. The effect of feed type on the retention factors, K and k, for the other erythromycin analogues of interest, were calculated and are shown in Table 7-2.

Feed type	t_c'	t_k'		K		k	
		EC/ED	EB/psu-EEA	EC/ED	EB/psu-EEA	EC/ED	EB/psu-EEA
CB	38.4	7.4	12.5	0.19	0.32	0.85	1.43
FE	38.6	6.5	10.5	0.17	0.27	0.75	1.22
BE	38.3	6.3	14.5	0.17	0.38	0.71	1.63

Table 7-2 **Variation in K and k of EC/ED and EB/psu-EEA with feed type. Retention times determined directly from HPLC results. CB: clarified broth, FE: forward extract, BE: back extract. Values calculated from Figures 7-3(a) to (c), and as described in Sections 3.1.2 and 3.1.3.**

From these results for EC/ED and EA reducing the proportion of broth impurities leads to a reduction in K. In the case of the erythromycin analogue, EB/psu-EEA, this previously described trend is observed between the clarified and forward extract, but increases when using the back extract feed. For all feed types, EC/ED is well resolved from EA. However, the CB and FE feeds compared to the BE feed do not appear to resolve EB/psu-EEA from EA to the same degree. For an industrial purification process, this degree of attainable distribution between the target product and its closely related contaminants is an important attribute to ensure a high degree of product purity.

7.4.2. Effect on chromatographic performance

As with the previous model system studies (Section 6.2.2), the effect of feed type on column performance was calculated. Firstly, based on the distribution ratio (K) values for EA, EC/ED and EB/psu-EEA, as shown in Tables 7-1 and 7-2, the separation factor between both EC/ED and EA ($\alpha_{EC/ED-EA}$) and EB/psu-EEA and EA ($\alpha_{EB/psu-EEA-EA}$) was calculated and is shown in Table 7-3. It can be seen that feed type has little effect on $\alpha_{EC/ED-EA}$, but the separation factor is influenced to a greater degree by feed type between EB/psu-EEA and EA, with the BE feed attaining the highest separation factor. Another measure of chromatographic performance is the number of theoretical plates (N). The theoretical plate number was again calculated based on the main EA peak and using Equation 3.14. Column efficiency for EA increased with the degree of pre-purification from 415 (CB) to 421 (FE) and 583 (BE).

Solute loading (mg)	Separation factor (α)	
	EC/ED – EA	EB/psu-EEA - EA
CB	1.53	1.10
FE	1.68	0.96
BE	1.59	1.44

Table 7-3 **Variation in the separation factor (α) with feed type between both EC/ED - EA and EB/psu-EEA - EA. CB: clarified broth, FE: forward extract, BE: back extract. Values calculated from distribution ratio values in Tables 7-1 and 7-2, and as described in Section 3.1.4.**

7.5. Influence of repeated sample loading

7.5.1. Effect on solute retention

Based on the results from the initial experiments (Section 7.4), the decision was made to concentrate further experimentation on using forward and back extracts since with these feed types the separation of EA from its analogues was closest to the model system (Section 4.1.3.2; Figure 4-4). Prior to initial optimisation studies, the effect of repeat injections using forward and back extracted broth feed was performed to identify which feed type would provide a reproducible separation during long term operation. Solute loading concentrations (100 $mg.mL^{-1}$; 1 mL injection volume) were kept constant during subsequent injections, with the separation being performed at a mobile phase flow rate of 2 $mL.min^{-1}$ in all cases. Figure 7-4 illustrates the effect of repeated feed injection using a forward extracted feed on the CCC chromatogram. The first feed injection resulted in an EA elution time of 19.1 minutes. For the second feed injection, the chromatogram has shifted to the right giving an increased EA elution time to 19.7 minutes. Results from off-line HPLC analysis of collected fractions for each of the CCC runs are provided in Table 7-4.

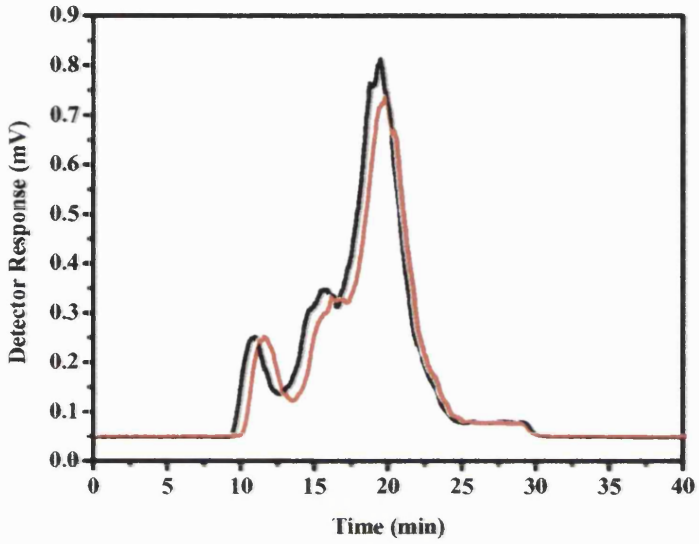

Figure 7-4 **CCC chromatograms showning the effect of repeated feed injections using FE feed on retention characteristics of erythromycin A. (▬) first feed injection. (▬) second feed injection. Solid line represents the detector response (mV) from the ELSD. Experiments performed at a mobile phase flow rate of 2 mL.min^{-1} and a solute loading of 100 mg (V_i = 1 mL) as described in Sections 2.4.1.1 and 2.4.1.2.**

Another important observation that can be made from the CCC chromatogram in Figure 7-4 is that the beginning of the eluting peak was determined to be ~9.1 minutes. From knowledge of S_f prior to the first injection, calculated to be 81.8% (v/v), the corresponding value of t_m could be calculated using Equation 3.7. Based on the actual measure mobile phase flow rate of 1.89 mL.min^{-1}, t_m was calculated to be equal to the first eluting peak. This time correlation indicates the feed components eluting in the initial peak have a K of 0, and can therefore be used to accurately calculate the relative

volumes of the phases within the coil for the second feed injection. The reason for the observed shift in the K = 0 and EA peaks is due to the reduction in the amount of stationary phase retained in the coil as a result of a small amount of 'stationary phase stripping' during the initial separation. This could possibly have been caused by surface active components in the feed reducing the interfacial tension between the two immiscible phases. By using the previously stated K = 0 peak for the second CCC chromatogram (Figure 7-4) the phase volumes, and hence S_f were determined. The correspond K = 0 peak for the second feed injection run occurred at 9.9 minutes. With a constant mobile phase flow rate of 1.89 $mL.min^{-1}$, the mobile phase volume within the coil is 18.71 mL, with a corresponding stationary phase volume of 75.59 mL. Using Equation 3.5, S_f was therefore calculated to be 80.2%.

The product collection times presented in Table 7-4 were again, from HPLC analysis used to identify the elution times. As can be seen for the EA time determined by the two methods, i.e. directly from the CCC chromatogram and HPLC derived chromatograms, there is a slight discrepancy in the values. However, the main observed peak from the CCC chromatogram corresponds to EA.

FE feed injection number	Fraction (min)	Solute identity	Concentration ($mg.mL^{-1}$)	TMIF (mg)
1	16.5	EC/ED	1.7	3.3
	19.5	EA	14.4	28.7
	19.5	EB/psu-EEA	2.3	4.6
2	16.5	EC/ED	1.2	2.5
	19.5	EA	23.2	49.1
	20.5	EB/psu-EEA	1.7	3.3

Table 7-4 **Identification and quantification of fractions corresponding to the various forms of the erythromycins from repeated feed injection experiments using forward extract feed. Experiments performed as described in Figure 7-4. EA: erythromycin A, EC: erythromycin C, ED: erythromycin D, EB: erythromycin B, psu-EEA: ring-contracted enol ether of erythromycin A.**

CCC experiments were also performed using repeated back extract feed injections. The CCC chromatograms from these studies are shown in Figure 7-5. The retention times of EA (the main peak) were, for the first and second feed injections, found to be 18.7 and 18.9 minutes respectively. The S_f values for the first and second CCC runs were 80.8% and 79.6% (v/v) respectively, demonstrating that due to the lower impurity levels in the BE feed it had less of an effect on the phase hydrodynamics. Once again, from collected fractions for both runs analysed by HPLC (Table 7-5), the peak maxima for EA, EC/ED and EB/psu-EEA, were determined. The elution times determined indicate that the main peaks in Figure 7-5 correspond to EA, with the peaks just before and after corresponding to EC/ED and EB/psu-EEA respectively.

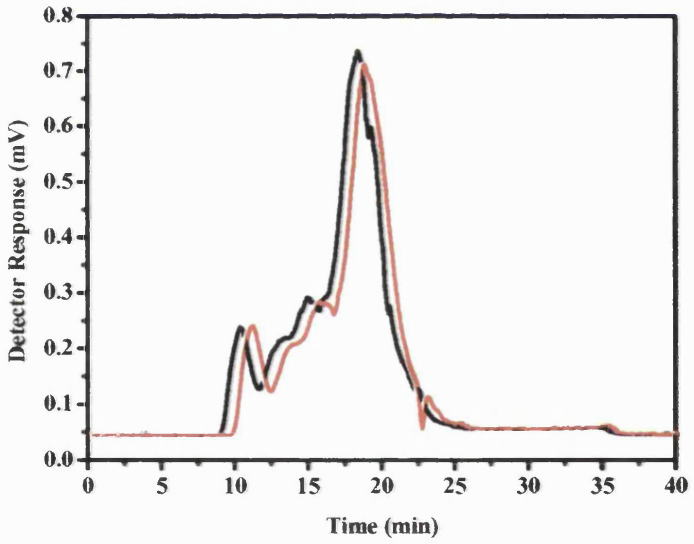

Figure 7-5 **CCC chromatograms showning the effect of repeated feed injections using BE feed on retention characteristics of erythromycin A. (—) first feed injection. (—) second feed injection. Experiments performed at a mobile phase flow rate of 2 mL.min^{-1} and a solute loading of 100 mg (V_i = 1 mL) as described in Sections 2.4.1.1 and 2.4.1.2. Solid line represents the detector response (mV) from the ELSD.**

BE feed injection number	Fraction (min)	Solute identity	Concentration ($mg.mL^{-1}$)	TMIF (mg)
1	15.6	EC/ED	2.4	4.8
	18.7	EA	15.7	31.4
	19.03	EB/psu-EEA	1.0	2.0
2	15.6	EC/ED	2.4	4.8
	18.9	EA	14.7	29.4
	19.9	EB/psu-EEA	1.0	2.0

Table 7-5 Identification and quantification of fractions corresponding to the various forms of the erythromycins from repeated feed injection experiments using back extract feed. Experiments performed as described in Figure 7-5. EA: erythromycin A, EC: erythromycin C, ED: erythromycin D, EB: erythromycin B, psu-EEA: ring-contracted enol ether of erythromycin A.

Based on these retention results in Tables 7-4 and 7-5, the K and k values for the different erythromycins were calculated, with the results presented in Table 7-6. From the distribution ratio (K) values firstly for EA with the repeated FE feed injection experiments there is an increase from 0.27 up to 0.29. This trend in increasing K also occurs with the other erythromycins. For repeated injection experiments using the BE feed, K_{EA} and $K_{EC/ED}$ values remain constant. The $K_{EB/psu\text{-}EEA}$ value is seen to slightly increase, but is not as well resolved from EA. The retention factor (k) for the different erythromycins is given (Table 7-6) and again shows the same trend as the K values.

Feed Type and injection number	K			k		
	EA	EC/ED	EB/psu-EEA	EA	EC/ED	EB/psu-EEA
FE (1)	0.27	0.20	0.34	1.22	0.91	1.53
FE (2)	0.29	0.25	0.39	1.29	1.14	1.75
BE (1)	0.25	0.16	0.25	0.98	0.65	1.02
BE (2)	0.25	0.16	0.28	0.99	0.65	1.12

Table 7-6 Variation in K and k of EA, EC/ED and EB/psu-EEA with repeated injections of FE and BE extracts. Retention times determined directly from data in Tables 7-4 and 7-5. FE and BE represents forward and back extracts respectively. (1) and (2) represents the first and second feed injections respectively.

7.5.2. Effect on chromatographic performance

The effect of the number of feed injections on separation efficiency of the erythromycins EA, EC/ED and EB/psu-EEA was determined, with the results presented as separation factors, column efficiency and resolution in Table 7-7. The separation factor between EA and EC/ED, with the FE feed, showed a decrease between the first (α = 1.39) and second (α = 1.17) injection runs, but with the BE feed between the first and second injections was comparatively larger and remained almost constant. Considering $\alpha_{EB/psu\text{-}EEA\text{-}EA}$, for the FE and BE feed experiments there is an observed increase between the first and second feed injections, with a larger attainable α with the FE feed. Resolution results with this particular set of experiments were less conclusive, but did indicate that between EC/ED and EA a consistent degree of separation could be achieved using the BE feed.

Feed Type and Injection Number	*N*	**Separation factor (α)**		**Resolution (R_s)**	
		EC/ED – EA	**EB/psu-EEA - EA**	**EC/ED – EA**	**EB/psu-EEA - EA**
FE (1)	562	1.39	1.21	1.03	0.41
FE (2)	357	1.17	1.31	0.42	0.51
BE (1)	347	1.60	0.97	0.66	0
BE (2)	375	1.57	1.09	0.89	0.11

Table 7-7 **Variation in the separation factor (α) and resolution (R_s) of EA, EC/ED and EB/psu-EEA with repeated injections of FE and BE extracts. Column efficiency (*N*) determined directly from EA peak. FE and BE represents forward and back extracts respectively. (1) and (2) represents the first and second feed injections respectively. Values calculated as described in Sections 3.1.4 to 3.1.6.**

The process benefits of using the BE feed are that a number of sample injections can be performed, with an assurance of a continuously predictable separation, an important prerequisite for process validation. In addition, for CCC to demonstrate its ability to successfully process real feed streams, its performance was evaluated with a select number of optimisation experiments.

7.6. Effects of operating conditions of erythromycin fractionation and throughput

To enable further comparisons between previous model (Chapter 6) and broth derived CCC experiments performed, based previous experiments (Section 7.5), a select number of experiments were performed to increase throughput. These experiments investigated the effect of mobile phase flow (5 and 10 $mL.min^{-1}$) and solute loading (500 and 1000 mg) using back extract feed.

7.6.1. Effect of mobile phase flow rate on solute retention

Flow rate studies were performed at a solute loading concentration of 100 $mg.mL^{-1}$ in all cases. As with the model system experiments (Chapter 6) S_f values were obtained prior to solute injection. For the 5 and 10 $mL.min^{-1}$ experiments the corresponding S_f values were 73.3% and 43.6% respectively. The resultant CCC chromatograms are provided in Figure 7-6, with K and k values for the erythromycins EC/ED, EA, and EB/psu-EEA shown in Table 7-8.

The first notable variation is the width and magnitude of larger peak, which, from HPLC analysis was shown to be EA. In Figure 7-6(a), the peak width, determined from the CCC chromatogram, was found to be 2.58 minutes, with an EA retention time of 10.90 minutes. The EA retention time and corresponding peak width for the 10 $mL.min^{-1}$ experiment (Figure 7-6(b)) were found to be 6.51 and 1.48 minutes respectively.

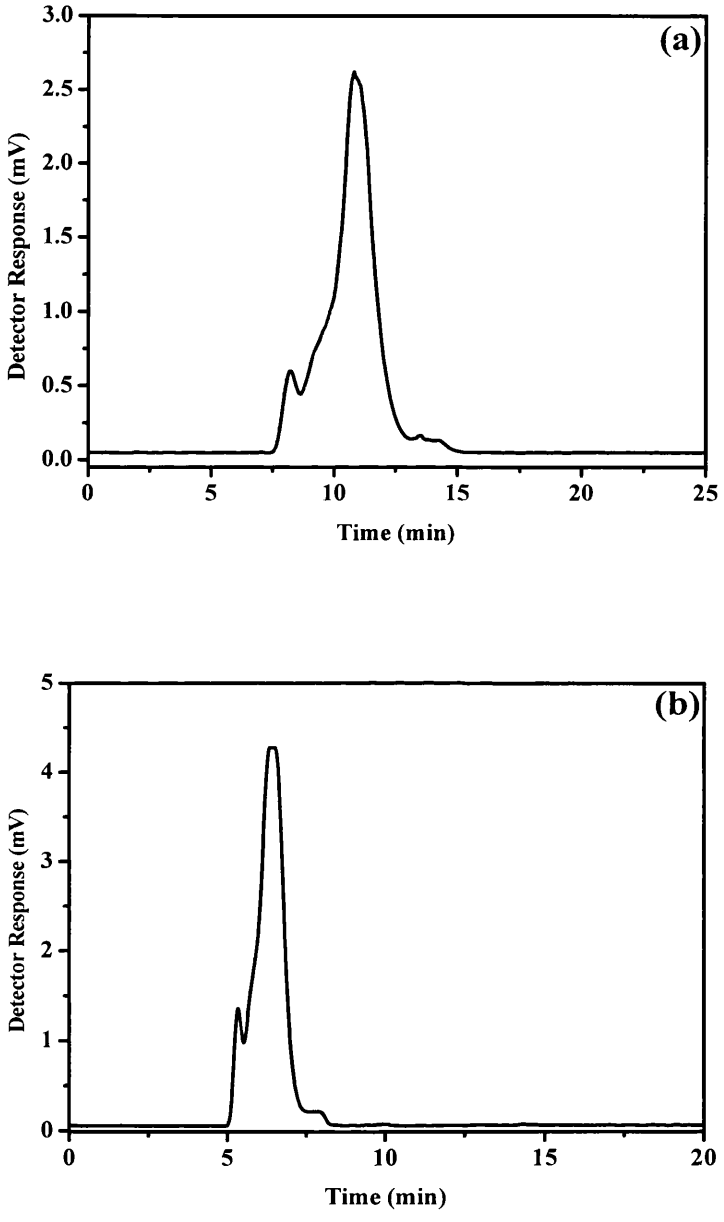

Figure 7-6 **CCC chromatograms from increasing mobile phase flow rate experiments. (a) and (b) correspond to mobile phase flow rate operation at 5 and 10 mL.min^{-1} respectively. Experiments performed at a solute loading of 100 mg (V_i = 1 mL) as described in Sections 2.4.1.1 and 2.4.1.2.. Solid line represents the detector response (mV) from the ELSD.**

The EA retention times for both flow rate studies obtained directly from the CCC chromatograms show a good correlation with those obtained using chromatograms generated from the corresponding off-line HPLC data, which were found to be 11.08 and 6.49 minutes respectively. In addition, the peaks before and after the main EA peak, with increasing mobile phase flow rate become narrower, and as shall be shown later, result in reduced chromatographic resolution.

The K and k values for the peaks shown in Figure 7-6 were determined as described in Sections 3.1.2 and 3.1.3 and are shown in Table 7-8. The calculated distribution ratio of EA over this mobile phase range up to 5 $mL.min^{-1}$ shows an increase from 0.25 at 2 $mL.min^{-1}$ up to 0.44 at 5 $mL.min^{-1}$. This trend also occurs with the different erythromycins, and is similar to that observed with the model system experiments (Section 6.2.1). However, in contrast to the model system experiment, at the higher flow rate of 10 $mL.min^{-1}$ for all the erythromycins a drop in K was observed. In addition, due to the decrease in S_f from 73.3% at 5 $mL.min^{-1}$ to 43.6% at 10 $mL.min^{-1}$, there was a related decrease in the retention factor at the higher flow rates.

Mobile phase flow rate ($mL.min^{-1}$)	**K**			**k**		
	EA	**EC/ED**	**EB/psu-EEA**	**EA**	**EC/ED**	**EB/psu-EEA**
5	0.44	0.34	0.54	1.20	0.89	1.48
10	0.29	0.32	0.28	0.22	0.14	0.22

Table 7-8 Variation in K and k of EA, EC/ED and EB/psu-EEA with increasing mobile phase flow rate using BE feed at a solute loading concentration of 100 $mg.mL^{-1}$. Values calculated from the chromatograms in Figure 7-6 and as described in Sections 3.1.2 and 3.1.3.

7.6.2. Effect of mobile phase flow rate on chromatographic performance

Based on the chromatograms from the off-line HPLC data, the column efficiency (*N*), separation factor (α) and resolution (R_s) between EC/ED – EA and EB/psu-EEA – EA were calculated, as shown in Table 7-9. From the results in Table 7-9 an increased mobile phase flow rate results in an apparent increase in the both the theoretical plate number, *N*, and $\alpha_{EC/ED - EA}$. The $\alpha_{EB/psu\text{-}EEA - EA}$ value however, with the doubling in the mobile phase flow rate, was seen to decrease from 1.23 to 0.98. The calculated resolution between EA and EC/ED over this flow rate range was found to be 0.51 (5 $mL.min^{-1}$), decreasing to 0.15 (10 $mL.min^{-1}$), and between EA and EB/psu-EEA, it was 0.5 at 5 $mL.min^{-1}$ and 0 at 10 $mL.min^{-1}$.

Despite a calculated resolution between EA and EB/psu-EEA at a mobile phase flow rate of 10 $mL.min^{-1}$ of 0, from off-line HPLC data of corresponding fractions collected (Table 7-10) it is apparent that the co-eluting EB/psu-EEA peak accounts for only 0.5% (w/w) of the total recovered solute mass in the specific fraction. The corresponding recoverable EA mass in this fraction was 59.7 mg, 96.7% (w/w) of the total in the main fraction. The remaining constituent of this fraction was EC/ED, at a solute mass and percentage composition of 1.8 mg and 2.9% (w/w) respectively. In comparison, similar flow rate studies with the model system (Chapter 6) yielded both higher column efficiencies and higher separation factors.

These results however do demonstrate that despite the lower column efficiency and selectivity over the flow rate range studied, a good separation of EA from its analogues was achieved.

Mobile phase flow rate (mL.min^{-1})	*N*	α		R_s	
		EC/ED – EA	EB/psu-EEA - EA	EC/ED – EA	EB/psu-EEA - EA
5	151	1.35	1.23	0.51	0.50
10	177	1.52	0.98	0.15	0

Table 7-9 **Variation in the separation factor (α) and resolution (R_s) of EA, EC/ED and EB/psu-EEA with mobile phase flow rate using the BE extract as the feed. Column efficiency (*N*) determined directly from EA peak. Experiments performed with a 100 mg solute loading as described in Figure 7-6. Values calculated as described in Sections 3.14 to 3.16.**

Flow rate (mL.min^{-1})	Collection time (min)	Product type	Concentration (mg.mL^{-1})	TMIF (mg)
5	9.5	EC/ED	0.6	3.1
	11.5	EA	8.3	41.7
	12.5	EB/psu-EEA	0.3	1.3
10	6.5	EC/ED	0.2	1.8
	6.5	EA	6.0	59.7
	6.5	EB/psu-EEA	0.03	0.3

Table 7-10 **Identification and quantification of fractions corresponding to the various forms of the erythromycins from corresponding flow rate experiments using back extract feed at a erythromycin loading of 100 mg. Experiments performed as described in Figure 7-6. EA: erythromycin A, EC: erythromycin C, ED: erythromycin D, EB: erythromycin B, psu-EEA: ring-contracted enol ether of erythromycin A.**

7.6.3. Effect of solute loading on solute retention

The second means of increasing throughput, as with the model system experiments (Section 6.3) was to increase the solute loading. Two experiments were performed at solute loadings of 500 and 1000 mg, constituting a 1 and 2 mL injection volume respectively. The resultant CCC chromatograms are shown in Figure 7-7. From off-line HPLC analysis of fractions collected at 1 minute intervals, the K values for the erythromycin analogues were calculated and are given in Table 7-11. For each experiment S_f values were calculated to be 81.3% and 82.4% respectively. From known phase volumes, i.e. V_s and V_m derived from the calculated S_f values, the k (retention factor) values were calculated and are shown in Table 7-11.

Solute loading (mg)	K			k		
	EA	EC/ED	EB/psu-EEA	EA	EC/ED	EB/psu-EEA
500	0.24	0.17	0.34	1.04	0.73	1.51
1000	0.41	0.34	0.54	1.89	1.60	2.50

Table 7-11 Variation in K and k of EA, EC/ED and EB/psu-EEA with increasing solute loading using BE feed at a mobile phase flow rate of 2 mL.min^{-1}. Values calculated from the chromatograms in Figure 7-7 and as described in the Sections 3.1.2 and 3.1.3.

From these results up to a solute loading of 500 mg the distribution ratios of all the erythromycins remain close to those at 100 mg (Tables 7-1 and 7-2), hence demonstrating a similar separation. In comparison with the model system experiments, at a solute loading of 500 mg the K values for all the erythromycins are close to those obtained with the model system. However at the 1000 mg solute loading with the real system the K value of all erythromycins increased, but were observed to decrease at the same solute loading in the model system experiment.

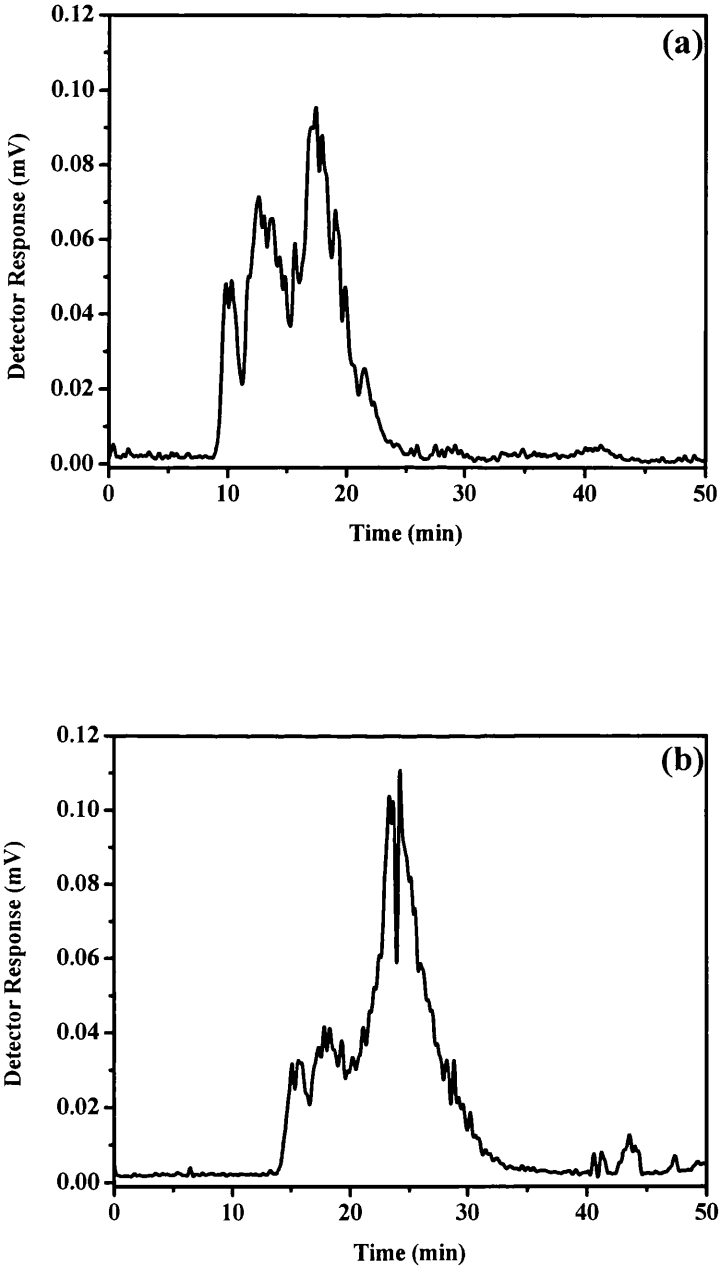

Figure 7-7 **CCC chromatograms from increasing solute loading mass experiments, (a) and (b) corresponds to operation at 500 and 1000 mg respectively. Experiments performed at a mobile phase flow rate of 2 mL.min^{-1} described in Sections 2.4.1.1 and 2.4.1.2.. Solid line represents the detector response (mV) from the ELSD.**

7.6.4. Effect on chromatographic performance

Based on the chromatograms generated from off-line HPLC data, the column efficiency (*N*), based on the main EA peak, the separation factor (α) and resolution (R_s) between EC/ED – EA and EB/psu-EEA – EA, were all calculated, with the results shown in Table 7-12. From the results doubling solute loading firstly leads to a reduction in column efficiency, from 267 plates (500 mg) to 245 plates (1000 mg). This decrease in column efficiency is due to the lower $d_R/d_{h/2}$ term in Equation 3.14. Closer inspection of the corresponding EA peak measurement, i.e. d_R and $d_{h/2}$ from both experiments demonstrates a ~4% decrease in the $d_R/d_{h/2}$ term with a doubling in the injected solute mass.

The reduction in the systems capacity with increasing loading, as expected, resulted in a reduction in the degree of selectivity (α). This is particularly apparent between EA and EC/ED, where compared to an $\alpha_{EA\text{-}EC/ED}$ value of 1.59 (Table 7-3) at 500 mg, and 1000 mg there is a decrease to 1.42 and 1.18 respectively.

With this reduction in the separation factor (α), in addition to band broadening, illustrated from column efficiency measurements, there is an expected decrease in the resolution. The reduction in resolution is more pronounced between EC/ED and EA resulting in a ~32% decrease, supported by the larger decrease in the α values between these two loadings. Comparing these results to similar loading experiments with the model system (Section 6.3.2) they indicate the process, in terms of fractionating EA from its analogues, performs better.

Solute loading (mg)	*N*	α		R_s	
		EC/ED – EA	**EB/psu-EEA - EA**	**EC/ED – EA**	**EB/psu-EEA - EA**
500	267	1.42	1.45	0.63	0.79
1000	245	1.18	1.32	0.43	0.71

Table 7-12 **Variation in separation factor (α) and resolution (R_s) of EA, EC/ED and EB/psu-EEA with solute loading using the BE extract as the feed. Column efficiency (*N*) determined directly from EA peak. Values calculated as described in Sections 3.1.4 to 3.1.6.**

7.7. EA purity, yield and throughput

This section provides values for achievable EA purity, total solute yield and throughput for the range of 'real system' experiments discussed in detail within Sections 7.4 to 7.6. The results are presented in Table 7-13 illustrating the impact of the numerous operational variables on the chosen performance measures.

Firstly, it is clear that for experiments 1 to 7 a large degree of solute recovery (> 93% w/w) is achievable. With increasing mobile phase flow rate (Experiments 8 and 9) there is a significant decrease in total solute recovery, down to 51% (w/w) at 10 $mL.min^{-1}$. With regard to the EA purity in the main peak fraction it was greater than 97% (w/w) in most cases. Those experiments using the FE feed (2, 4a and 4b) all resulted in lower EA purity values of between 93 and 94% (w/w).

Throughput values, determined using Equation 3.16, for the feed experiments (Experiments 1 to 3) did not show a large variation. For the repeat injection experiments using both FE and BE feeds (Section 7.5), there was also no noticeable difference in the achievable total solute throughput values. With increasing solute loading, from 500 to 1000 mg the throughput was seen to almost double from 0.015 to 0.029 $kg.day^{-1}$, with a high degree of achievable EA purity (>99% w/w). Finally, with an increase in the mobile

phase flow rate from 5 to 10 mL.min^{-1} (Experiments 8 and 9), there was only a nominal increase in the total solute throughput due to the decrease in the total solute recovered. Compared with the 'standard separation conditions' (mobile phase flow rate of 2 mL.min^{-1}; solute loading mass of 100 mg (Experiment 3)) a 5 times increase in the mobile phase flow rate, i.e. up to 10 mL.min^{-1}, led to only a doubling in the total solute throughput, but a 3% reduction in the attainable EA purity.

Conversely, with a 10 times increase in the solute loading over the 'standard separation' conditions, i.e. up to 1000 mg, there was a 7 times increase in total solute throughput, with a high degree of EA purity maintained (>99%). This therefore demonstrates that from an operational perspective, it is more favourable to operated at higher solute loadings than at higher mobile phase flow rates.

Experiment number	**Total solute yield (% w/w)**	**Purity of EA (% w/w)**	**Throughput (kg.day^{-1})**
1	100	98	0.005
2	100	93	0.003
3	100	~100	0.004
4a	98	94	0.005
4b	100	94	0.005
5a	100	99	0.005
5b	100	99	0.005
6	93	~100	0.015
7	100	99	0.029
8	72	99	0.006
9	51	97	0.008

Table 7-13 **Variation in performance parameters with operational variables. (1 – 3) corresponds to real system experiments performed using CB, FE and BE feeds (Section 7.4). (4a and 4b) and (5a and 5b) correspond to repeated FE and BE feed injection experiments respectively (Section 7.5). (6 and 7) and (8 and 9) correspond to solute loading and flow rate optimisation experiments respectively (Section 7.6).**

Compared to model system studies (Chapter 6), firstly for the flow rate studies, at 2 $mL.min^{-1}$ there are comparable EA purity and throughput values. With increasing flow rate the purity of EA is higher with the back extract feed, but due to low solute recovery values, the throughput is lower. Comparing the solute loading experiments, at a loading of 100 mg, both model and real systems provided comparable EA purity, yield and throughput values. At the solute loadings of 500 and 1000 mg the back extract feed provides the highest EA yields, solute yields and throughputs.

7.8. Summary

The results presented in this Chapter have identified the degree of pre-purification required to achieve a good separation of EA from its analogues. The effects of mobile phase flow rate and solute loading with the chosen back extract feed was examined, and has shown that a comparable, in certain case better separation to corresponding model system experiments could be achieved. Together with the results from Chapter 6, this provides an encouraging basis for investigating the scale-up of this technology with both the model and broth derived systems as discussed in Chapter 8.

8. Predictive scale-up of CCC separations

8.1. Introduction

In the previous Chapters 6 and 7, the separation of EA from its analogues was, from both model and broth-derived feeds, shown to be feasible. In this Chapter, the aim is to evaluate the scale-up of CCC for both the model and real systems by (a) investigating the effects of feed impurity, mobile phase flow rate, solute loading and column rotational speed on the separation performance and (b) demonstrating the predictive nature of the technology upon scale-up by the application of a model to enable the determination of product elution times over a range of operating conditions. Firstly, the fractionation of EA from its analogues on a novel pilot scale J-Type CCC machine (V_c = 928 mL) showing how the variation of key operational variables influence the achievable purity and yield of the target compound is presented. Then, based on knowledge of the distribution ratio of the target component (obtained on the laboratory scale CCC machine) and the hydrodynamics of the pilot scale machine, both the elution time and width of the target erythromycin peak can be satisfactorily predicted as described in Section 3.2.

The results presented in this Chapter form the basis of the manuscripts: Booth, Sutherland and Lye, 2002: Modeling the performance of pilot-scale countercurrent chromatography: Scale-up predictions and experimental verification of erythromycin separation, *Biotechnol. Bioeng.* (in press); and Booth A.J., Ngiam S.H., and Lye G.J (submitted): Antibiotic purification from fermentation broths by counter-current chromatography: analysis of product purity and yield trade-offs.

8.2. Scale-up of model system separation

Having determined the distribution ratio of EA and its analogues at the laboratory scale (Section 4.1.3.2) the first step in the scale-up methodology, as described in Section 3.2.1 is to examine the hydrodynamic characteristics of the pilot scale CCC machine. The degree of stationary phase retention in the pilot scale CCC coil was thus determined with the same quaternary solvent system over a range of rotational speeds and mobile phase flow rates as described in Section 5.3. The resulting Du plots (Figure 5-4) indicate the expected linear relationship between S_f and the square root of mobile phase flow at both rotational speeds (800 and 1200 rpm) with the intercept on the ordinate at ~100% S_f. Figure 5-4 also shows a favourable increase in stationary phase retention with increasing rotational speed. For each CCC experiment however, prior to solute injection it is important that hydrodynamic phase equilibrium is established and the corresponding S_f value accurately calculated in order to achieve reliable scale-up predictions, as described in Section 3.2.1.

The operating conditions used during the laboratory scale CCC fractionation (Figure 4-4) can be scaled up on the basis of a proportional mobile phase flow rate (based on the ratio of the coil internal diameters) with an equivalent solute loading and injection volume at the same rotational speed. The calculated mobile phase flow rate for the pilot scale separation, based on a laboratory scale mobile phase flow rate of 2 $mL.min^{-1}$ (as shown in Figure 4-4), was 10.58 $mL.min^{-1}$. The solute injection volume was 10 mL, with a corresponding solute mass loading of 1000 mg. The rotational speed was maintained at 800 rpm. Figure 8-1 illustrates the resultant CCC chromatogram for such a pilot scale separation, with the corresponding mass balance data provided in Appendix 13.4 (Table 13-6). Qualitatively this is similar to the elution profile seen for the laboratory scale separation (Figure 4-4), with the main EA peak now eluting at 40.5 minutes. Off-line HPLC analyses of fractions collected after 31, 41 and 51 minutes, are shown in Figure 8-2, and indicate the presence of the erythromycins EC/ED, EA and EB/psu-EEA respectively.

Based on accurate knowledge of the EC/ED, EA and EB/psu-EEA elution times of 29.5, 40.5 and 48.5 minutes respectively, in addition to phase volume ratios (V_s and V_m) in Section 5.2, the K and k values were calculated as described in Sections 3.1.2 and 3.1.3. The K values for EA, EC/ED, and EB/psu-EEA were calculated to be 0.26, 0.09, and 0.37 respectively. The k values for EA, EC/ED, and EB/psu-EEA were calculated to be 1.58, 0.55, and 2.27 respectively. The calculated distribution ratio of EA (K_{EA}) of 0.26 is in good agreement with that found for the laboratory scale CCC separation (K_{EA} = 0.25) shown in Figure 4-4. The increased EA elution time of 40.5 minutes at the pilot scale is due to the approximate doubling in the coil length (47.6 and 91.2 metres on the laboratory scale and pilot scale CCC machines respectively).

The separation performance at the pilot scale was determined by calculating α and R_s between EA and the other erythromycins EC/ED and EB/psu-EEA, in addition to the column efficiency, *N*. The calculated column efficiency for the pilot scale CCC fractionation was found to be 1219 theoretical plates, over 3.5 times greater than the corresponding laboratory scale CCC fractionation. With the increased theoretical plate number, the α values between EA and EC/ED and EA and EB/psu-EEA were found to be 2.89 and 1.42 respectively. Compared to the laboratory scale CCC experiment, the $\alpha_{EC/ED\text{-}EA}$ increased, with the $\alpha_{EA\text{-}EB/psu\text{-}EEA}$ remaining almost constant. The resolution between EA-EC/ED and EA-EB/psu-EEA at the pilot scale were calculated to be 1.6 and 1.1 respectively. These results show that this CCC separation can be readily scaled up, giving an improved separation at the larger scale due to the increased coil length available for chromatography, and hence an increase in the generated theoretical plate number (*N*).

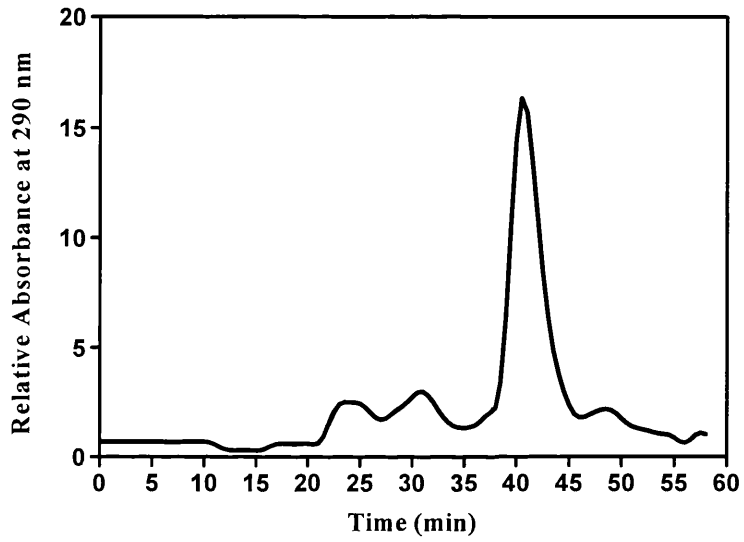

Figure 8-1 **Linear scale-up of the laboratory scale separation shown in Figure 4-4 to the pilot scale CCC machine. ω = 800 rpm, 1000 mg loading, 10 mL.min^{-1}, S_f = 86%). Retention time of the main EA peak was 40.5 minutes. Experiments performed as described in Section 2.4.2. On-line monitoring of eluting mobile phase and construction of the CCC chromatograms in all cases was performed as described in Sections 2.3.3.1 and 2.3.3.3.**

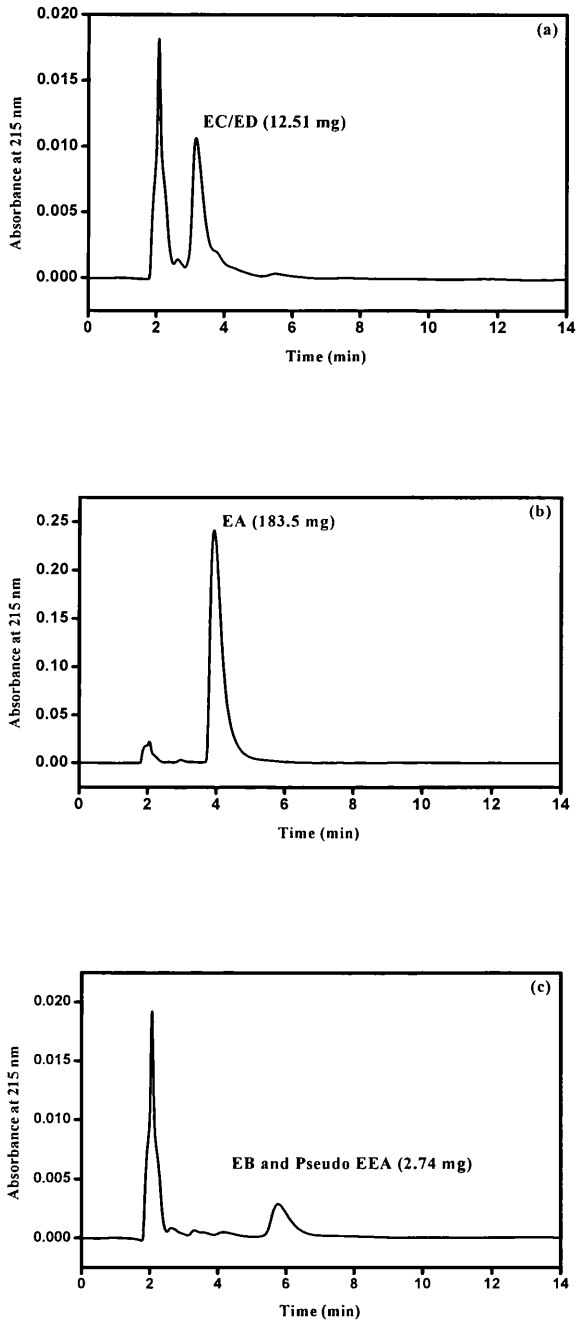

Figure 8-2 **Analytical HPLC chromatograms of selected fractions collected from the pilot scale CCC fractionation of erythromycin shown in Figure 8-1. Chromatograms (a)-(c) correspond to mobile phase fractions collected after 31, 41 and 51 minutes respectively. The peak eluting after 2 minutes is the solvent front. Experiments performed as described in Section 2.3.3.4.2.**

8.2.1 Effect of operating conditions on pilot scale CCC performance

Having successfully scaled up the standard laboratory scale CCC separation, erythromycin fractionation was examined as a function of column rotational speed, mobile phase flow rate, and solute loading volume on the pilot scale CCC machine. The full range of experiments performed are summarised in Table 8-1.

The corresponding CCC chromatograms for experiments 1 and 2 (Table 8-1) are illustrated in Figure 8-3. For the experiments performed at a rotational speed of 1200 rpm, the corresponding CCC chromatograms are shown in Figure 8-4.

Experiment number	N (rpm)	F ($mL.min^{-1}$)	Loading volume (mL)	Solute mass (g)
1	800	20	10	1
2	800	20	100	10
3	1200	10	10	1
4	1200	40	10	1

Table 8-1 Operating conditions for the optimisation experiments performed on the pilot scale CCC machine.

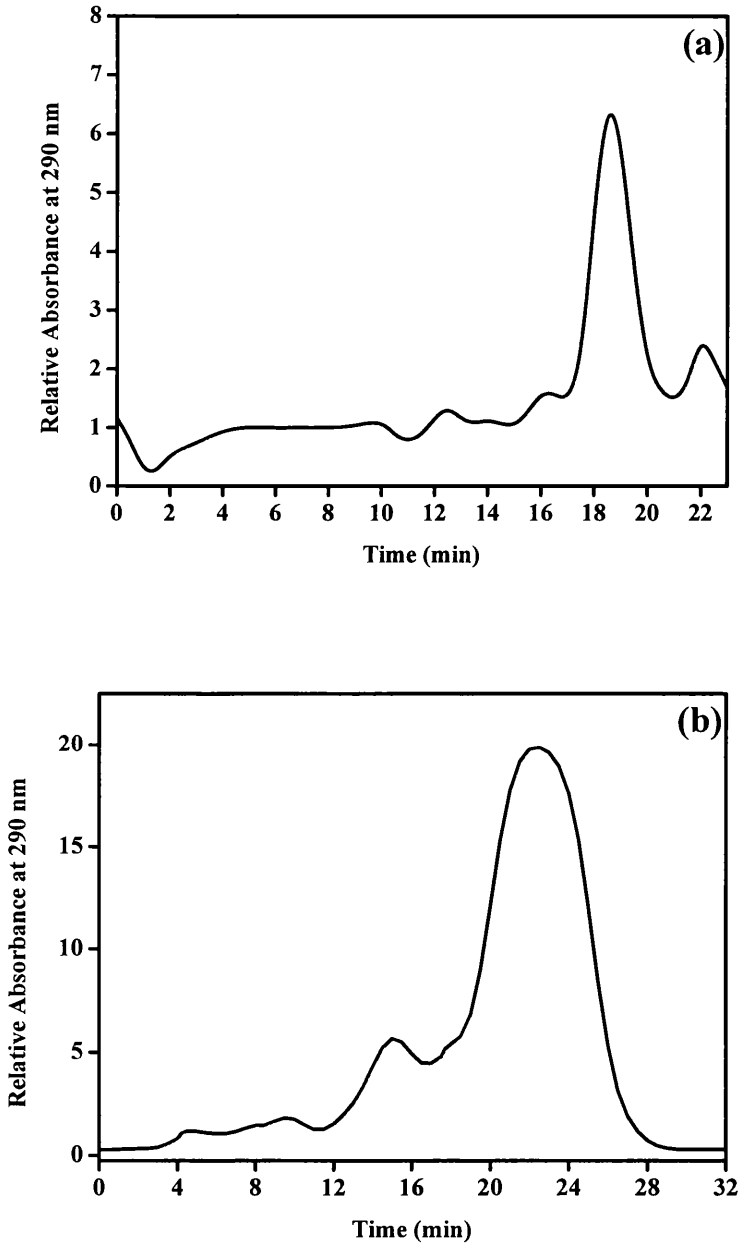

Figure 8-3 **(a) Pilot scale CCC chromatogram of erythromycin fractionation performed at a mobile phase flow rate of 20 mL.min^{-1} (Experiment 1: 1 g loading; S_f = 78.2%). Retention time of the main EA peak was 18.6 minutes. (b) Pilot scale CCC chromatograms of erythromycin fractionation performed at a solute loading of 10 g (Experiment 2: 20 mL.min^{-1}; S_f = 76.2%). Retention time of the main EA peak was 22.5 minutes. Experiments performed as described in Section 2.4.2.**

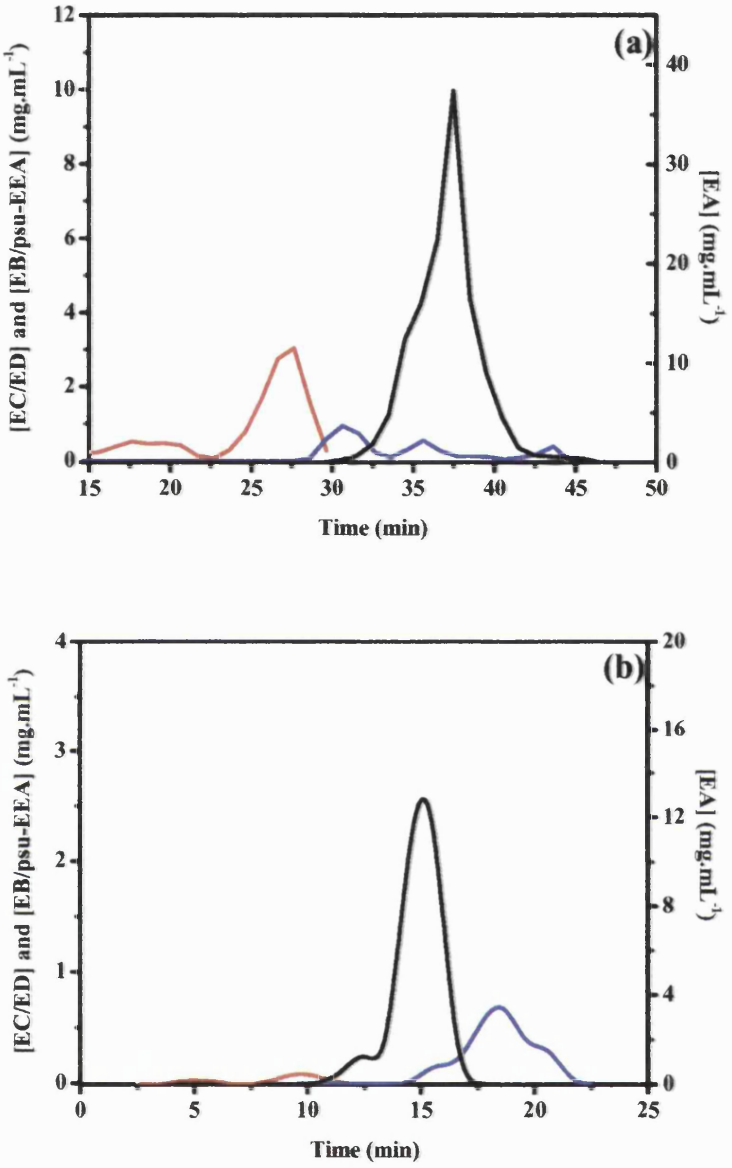

Figure 8-4 **(a) Pilot scale CCC chromatogram of erythromycin fractionation performed at a mobile phase flow rate of 10 mL.min^{-1} (Experiment 4: 1 g loading; S_f = 88.4%). Retention time of the main EA peak was 37.5 minutes. (b) Pilot scale CCC chromatogram of erythromycin fractionation performed at a mobile phase flow rate of 40 mL.min^{-1} (Experiment 5: 1g loading; S_f = 70.6%). Retention time of the main EA peak was 15.5 minutes.(—) EC/ED. (—) EB/psu-EEA. (—) EA. Experiments performed as described in Section 2.4.2.**

8.2.1.1. Effect on both solute retention time and factors

The effect of mobile phase flow rate, solute loading and bobbin rotational speed on solute retention was studied on the pilot scale machine. Table 8-2 contains solute retention times and the corresponding retention factors, K and k from the chromatograms shown in Figures 8-3 and 8-4. Firstly, at a rotational speed of 800 rpm, keeping the solute loading mass constant, the mobile phase flow rate was increased from 10 to 20 $mL.min^{-1}$ (Table 8-1, Experiment 1). As can be seen from the corresponding CCC chromatogram (Figure 8-3(a)) there is an expected reduction in the solute elution times. The elution time of the main EA component occurred at 18.5 minutes. EC/ED and EB/psu-EEA as determined from off-line HPLC analysis eluted at 16.1 and 21.5 minutes respectively. From the data in Table 8-2, a doubling in the mobile phase flow rate led to a decrease in the K values of EA and EB/psu-EEA. The corresponding k values for EA and EB/psu-EEA almost halved, with $k_{EC/ED}$ remaining almost constant. Increasing solute loading (Experiment 2) led to a decrease in the K and k values for EC/ED and EA, but increased for EB/psu-EEA.

Experiment number	K			k		
	EA	EC/ED	EB/psu-EEA	EA	EC/ED	EB/psu-EEA
1	0.23	0.17	0.32	0.83	0.60	1.13
2	0.22	0.15	0.38	0.71	0.50	1.22
3	0.32	0.19	0.45	2.43	1.45	3.43
4	0.53	0.43	0.69	1.26	1.03	1.66

Table 8-2 Variation in K and k of EA, EC/ED and EB/psu-EEA at the pilot scale. Operating conditions as described in Table 8-1, related by experiment numbers. Values calculated from CCC chromatograms in Figures 8-3 and 8-4, and as described in Sections 3.1.2 and 3.1.3.

Focusing on the experiments performed at the higher rotational speed of 1200 rpm (Experiments 3 and 4) the higher stationary phase retention at a given flow rate (Figure 5-4) would be expected to improved product separation. Comparing Experiment 3 with that described in Section 8.2, there is an observed increase in the both the distribution ratio and retention factor. With a doubling in the mobile phase flow rate i.e. up to 40 mL.min^{-1} (Experiment 4), the distribution ratios in all cases continued to increase. However, due to the reduction in the percentage S_f value at this flow rate (70.6%), the retention factor is seen to decrease. These results demonstrated that at the larger scale a good separation of EA from its closely eluting analogues can be achieved over the range of operating variables studied.

8.2.1.2. Effect on chromatographic performance

For the experiments described in Section 8.2, chromatographic performance was evaluated by calculating both α and R_S between EC/ED – EA and EB/psu-EEA – EA. Column efficiency was also determined, again based on the main EA peak. All results are presented in Table 8-3.

The resolution (R_S) at a mobile phase flow rate of 10 mL.min^{-1} (N = 800 rpm) between EA and EC/ED, as well as EA and EB/psu-EEA was found to be 1.6 and 1.1 respectively. This degree of resolution is attributed to the larger S_f values obtained at lower flow rates (Figure 5-4). As expected, α and R_S were found to decrease with a higher mobile phase flow rate and hence lower S_f values. As with HPLC, the peak asymmetry that occurs is due to an overloading of the column, can in turn significantly compromise column efficiency (N). This was seen to decrease from 600 to 89 (Experiments 2 and 3) and significantly reduce the achievable resolution due to co-elution of EC/ED and EB/psu-EEA either side of the main EA peak. The achievable resolution at a rotational speed of 1200 rpm and a mobile phase flow rate of 40 mL.min^{-1} (Experiment 4) is equal to that obtained at rotational speed of 800 rpm and a mobile phase flow rate of 20 mL.min^{-1} (Experiment 1).

Experiment number	*N*	α		R_s	
		EC/ED – EA	EB/psu-EEA – EA	EC/ED – EA	EB/psu-EEA - EA
1	600	1.35	1.39	0.7	0.8
2	89	1.47	1.73	ND	ND
3	1138	1.68	1.41	2.0	ND
4	1051	1.23	1.30	0.7	0.8

Table 8-3 **Variation in α and R_s of EA, EC/ED and EB/psu-EEA with mobile phase flow rate and solute loading. Column efficiency (*N*) determined directly from EA peak. Operating conditions as described in Table 8-1, related by experiment numbers. ND indicates values that could not be calculated due to overlapping peaks.**

8.2.1.3. Effect on yield, EA purity and throughput

The effect of solute loading on yield, purity and predicted throughput was studied, with the results presented in Table 8-4. From the results presented in Table 8-4, in most cases a high degree of EA purity was achieved. From Experiment 3, the achievable EA purity was calculated to be ~92% (w/w). The other 8% comprised of the 'minor contaminant' EC/ED, with a solute mass of 99.1 mg. The maximum solute throughput was calculated to be 0.411 $kg.day^{-1}$. Furthermore, as previously stated, the achievable resolution at a rotational speed of 1200 rpm and a mobile phase flow rate of 40 $mL.min^{-1}$ (1200 rpm) is equal to that obtained at rotational speed of 800 rpm and a mobile phase flow rate of 20 $mL.min^{-1}$. This confirms that it is beneficial to operate at the higher rotational speed, where significantly higher throughputs (~16%) can be obtained.

Experiment number	Purity of EA (% w/w)	EA Yield (% w/w)	Total solute yield (% w/w)	Throughput ($kg.day^{-1}$)
1	~100	~83	100	0.026
2	~100	~95	96	0.046
3	~92	~28	100	0.411
4	~100	~56	87	0.023
5	~100	~47	100	0.060

Table 8-4 **Variation in performance parameters with operational variables. Experiment number 1 and 2 correspond to CCC operation at a mobile phase flow rate of 10 and 20 $mL.min^{-1}$ respectively: solute loading and rotational speed was 1 g and 800 rpm respectively. Experiment number 3 corresponds to a mobile phase flow rate and solute loading of 20 $mL.min^{-1}$ and 10 g respectively (ω = 800 rpm). Experiment numbers 4 and 5 correspond to experiments performed at the mobile phase flow rates of 10 and 40 $mL.min^{-1}$ respectively (solute loading = 1 g; ω = 1200 rpm).**

8.3. Real system scale-up

As with the previous model system scale-up studies (Section 8.2), the same procedure for scaling up the real system separation on the pilot scale CCC machine was adopted. Based on the results from previous laboratory scale studies (Sections 7.4 – 7.5) the back extract feed was chosen for the scale-up studies. The conditions used during the laboratory scale CCC fractionation (Figure 7-3(c)) were initially used to scale-up on the basis of a proportional mobile phase flow rate (based on the ratio of the coil internal diameters), an equivalent solute loading and injection volume at the same rotational speed. The calculated mobile phase flow rate, based on a laboratory scale mobile phase flow rate of 2 $mL.min^{-1}$, for the pilot scale separation in this case was 10.58 $mL.min^{-1}$. The solute injection volume was 10 mL, with a corresponding solute mass loading of 1000 mg. The rotational speed was maintained at 800 rpm. Due to the high flow rates used, the construction of the corresponding CCC chromatogram was achieved from off-line HPLC data, plotted as

erythromycin concentration against time and is shown in Figure 8-5. From the chromatogram shown in Figure 8-5, the elution time of EA, EC/ED and EB/psu-EEA were determined to be 43.5, 36.5 and 51.5 minutes respectively. Based on knowledge of the EC/ED, EA and EB/psu-EEA elution times, in addition to phase volume ratios (V_s and V_m), from knowledge of the stationary phase retention (S_f = 84%), the K and k values were calculated and are shown in Table 8-5.

The calculated column efficiency for the pilot scale CCC fractionation was found to be 30% lower than the corresponding laboratory scale CCC fractionation (Figure 7-3(c)) at 408 theoretical plates. The calculated α values between EA-EC/ED and EA-EB/psu-EEA were found to 1.29 and 1.23. The corresponding R_s values between EA-EC/ED and EA-EB/psu-EEA were calculated to be both 0.97. The corresponding total solute and EA yield (at a purity of ~100% w/w) were calculated to be ~100% (w/w) and ~91% (w/w) respectively.

Flow rate ($mL.min^{-1}$)	**K**			**k**		
	EA	**EC/ED**	**EB/psu-EEA**	**EA**	**EC/ED**	**EB/psu-EEA**
10	0.37	0.28	0.45	1.90	1.46	2.33

Table 8-5 **Variation in K and k of EA, EC/ED and EB/psu-EEA at the pilot scale, with a mobile phase flow rate of 10 $mL.min^{-1}$, rotational speed of 800 rpm and back extract solute loading mass of 1000 mg (100 $mg.mL^{-1}$; V_i = 10 mL). Values calculated from the CCC chromatogram in Figure 8-5, and as described in Sections 3.1.2 and 3.1.3.**

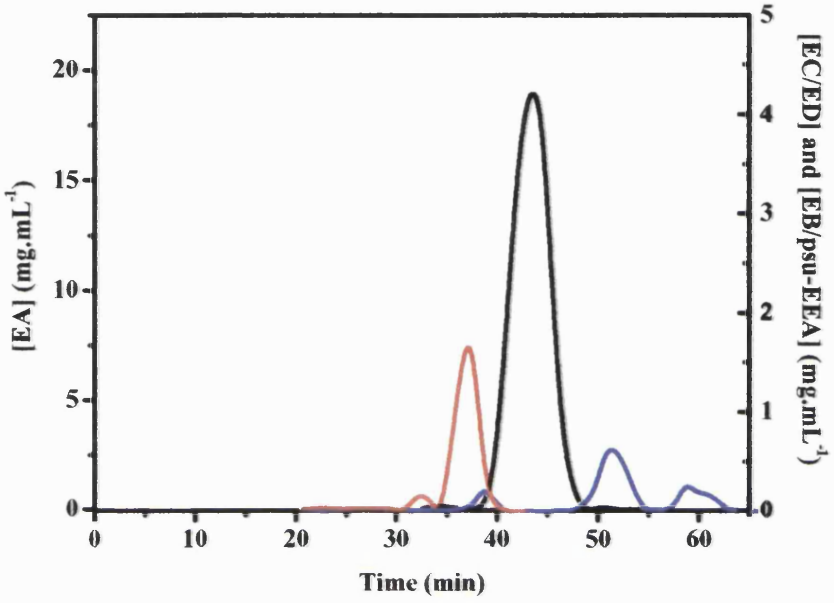

Figure 8-5 **Pilot scale CCC chromatograms of erythromycin fractionation with back extract feed performed at a mobile phase flow rate of 10 mL.min^{-1}; 1 g loading (S_f = 84%). Retention time of the main EA peak was 43.5 minutes. (—) EC/ED. (—) EB/psu-EEA. (—) EA. Experiments performed as described in Section 2.4.2.**

8.3.1. Effect of operating variables on pilot scale CCC performance

As with the pilot scale model system studies, experiments were performed to investigate the effects of increasing mobile phase flow rate and solute loading on the separation performance with a back extract feed. The experiments performed (Table 8-6) as will be discussed later in Section 8.4, enabled comparisons between the pilot scale studies with model (Section 8.2) and real feeds. CCC chromatograms from all experiments described in Table 8-6 were generated as previously described in Section 8.2. Figure 8-6 illustrates the CCC chromatograms corresponding to Experiments 1 and

2 (Table 8-6). Figure 8-7 illustrates the CCC chromatogram corresponding to Experiment 3 (Table 8-6).

Experiment number	*N* (rpm)	F ($mL.min^{-1}$)	Loading volume (mL)	Solute mass (g)
1	800	20	10	1
2	"	40	10	1
3	"	20	100	10

Table 8-6 Operating conditions for experiments performed on the pilot scale CCC machine using a back extract feed. Experiments performed as described in Section 2.4.2.

8.3.1.1. Effects on solute retention

As with the pilot scale model system studies, the effects of increased operating variables, i.e. mobile phase flow rate and solute loading on solute retention time and factors was studied, and illustrated in Table 8-7. From the results presented in Table 8-7, with a doubling in the mobile phase flow rate from 10 to 20 $mL.min^{-1}$ there is no significant change in the K values for any of the erythromycins. The k values for these corresponding mobile phase flow rate experiments decrease as expected. Further increasing the mobile phase flow rate up to 40 $mL.min^{-1}$ sees an increase in the K value in all cases, again with an expected decrease in the respective k values.

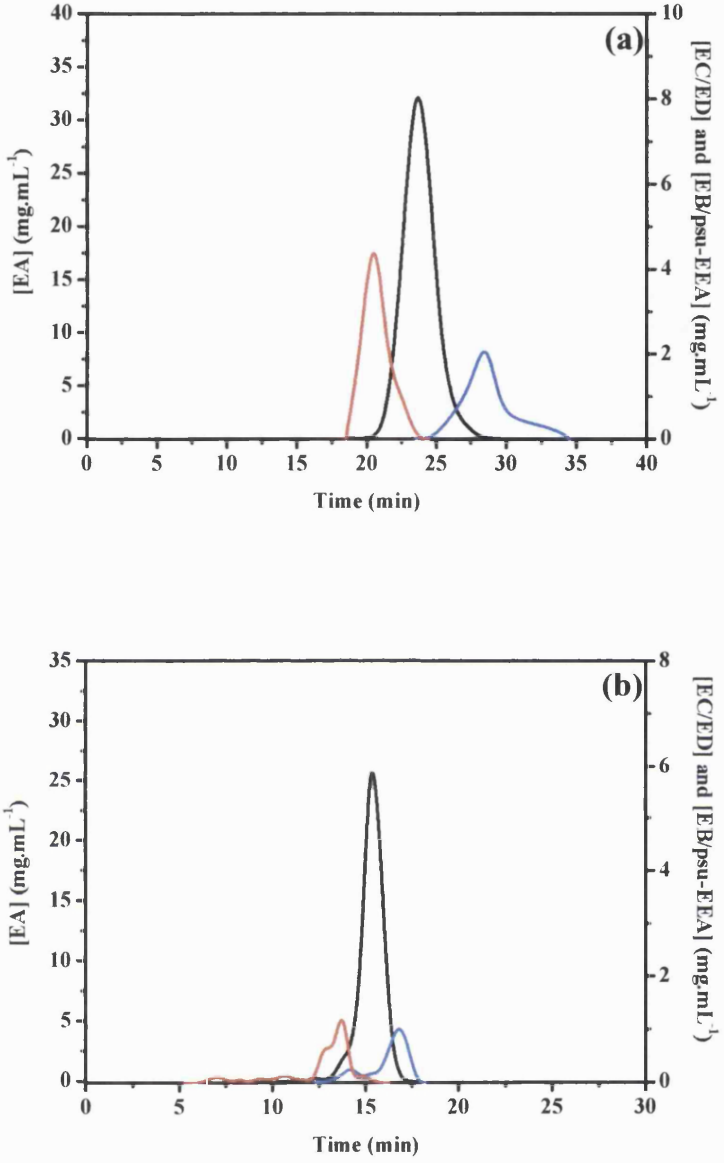

Figure 8-6 **(a) Pilot scale CCC chromatogram of erythromycin fractionation performed using a back extract feed at a mobile phase flow rate of 20 mL.min^{-1} (Experiment 1: 1 g loading; S_f = 75.6%). Retention time of the main EA peak was 23.5 minutes. (b) Pilot scale CCC chromatogram of erythromycin fractionation performed at a mobile phase flow rate of 40 mL.min^{-1} (Experiment 2: 1 g loading; S_f = 64.6%). Retention time of the main EA peak was 15.3 minutes. (—) EC/ED. (—) EB/psu-EEA. (—) EA. Experiments performed as described in Section 2.4.2.**

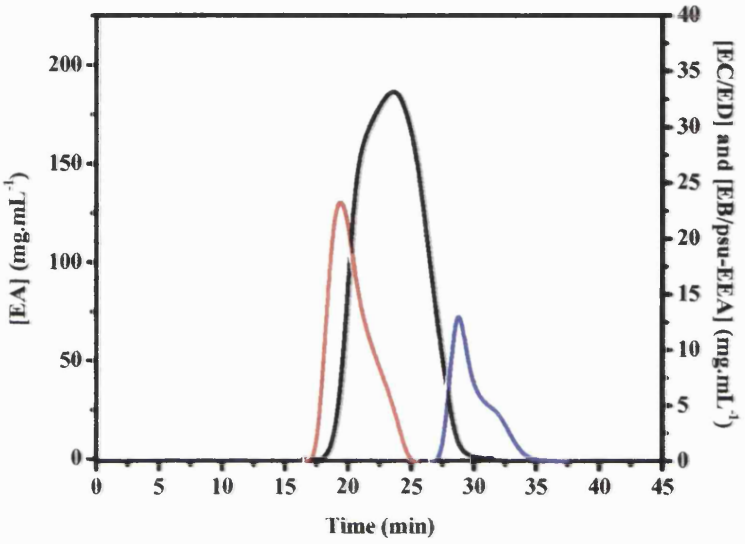

Figure 8-7 **Pilot scale CCC chromatograms of erythromycin fractionation performed using a back extract feed at a mobile phase flow rate of 20 mL.min^{-1} and solute loading of 10 g (Experiment 3; S_f = 75.6%). Retention time of the main EA peak was 23.5 minutes. (—) EC/ED. (—) EB/psu-EEA. (—) EA.**

Experiment number	K			k		
	EA	EC/ED	EB/psu-EEA	EA	EC/ED	EB/psu-EEA
1	0.36	0.26	0.49	1.13	0.83	1.55
2	0.48	0.37	0.57	0.88	0.67	1.04
3	0.32	0.26	0.50	0.99	0.70	1.55

Table 8-7 **Variation in K and k of EA, EC/ED and EB/psu-EEA at the pilot scale. Operating conditions as described in Table 8-6, related by experiment numbers. K and k values calculated as described in Sections 3.1.2 and 3.1.3.**

8.3.1.2. Effects on chromatographic performance

For the scale-up studies (Table 8-6), chromatographic performance was evaluated by calculating both α and R_s between EC/ED – EA and EB/psu-EEA – EA. Column efficiency was also determined, again based on the main EA peak. All results are provided in Table 8-8. Analysis of the results indicates that a doubling in mobile phase flow rate (10 to 20 mL.min^{-1}) results in a decrease in N, with a small increase in both $\alpha_{EC/ED - EA}$ and $\alpha_{EB/psu-EEA - EA}$. The resolution between EC/ED and EA at these flow rates did not show a notable variation, but interestingly showed a slight increase between EB/psu-EEA and EA. Increasing the flow rate further (40 mL.min^{-1}) resulted in a larger calculated N, with both α and R_s between EA, EC/ED and EB/psu-EEA decreasing in all cases. The decrease in α and R_s between EA and EB/psu-EEA was more pronounced.

It can be seen that with a ten fold increase in solute loading (Experiment 3) there is a marked reduction in the column efficiency. Despite the reduced column efficiency, the α values between EA and the contaminants are higher than would be expected. However, the impact of increased solute loading on separation performance is more noticeable from the corresponding R_s values. Between both EC/ED – EA and EB/psu-EEA – EA there is a marked reduction, compared to the R_s values for Experiment 1.

Experiment number	N	α		R_s	
		EC/ED – EA	EB/psu-EEA - EA	EC/ED – EA	EB/psu-EEA - EA
1	265	1.35	1.37	0.90	1.21
2	1251	1.32	1.18	0.89	0.62
3	79	1.41	1.57	0.43	0.80

Table 8-8 **Variation in α and R_s of EA, EC/ED and EB/psu-EEA at the pilot scale with mobile phase flow rate and solute loading using the BE extract as the feed. Column efficiency (N) determined directly from the EA peak. Operating conditions as described in Table 8-6, related by experiment numbers. Experiments performed as described in Figures 8-6 and 8-7. Values calculated as described in Sections 3.1.4 to 3.1.6.**

8.3.1.3. Effects on yield, EA purity and throughput

Table 8-9 illustrates the effects of increasing the operating variable, mobile phase flow rate and solute loading on the achievable EA purity, total solute yield and predicted throughputs. As can be seen, for all experiments a higher EA purity in the main fraction was achieved (>97% w/w). The maximum estimated throughput was determined to be 0.400 $kg.day^{-1}$.

Experiment Number	Purity of EA (% w/w)	EA Yield (% w/w)	Total Solute Yield (% w/w)	Throughput ($kg.day^{-1}$)
1	100	~71	95	0.039
2	99	~74	100	0.069
3	97	~64	100	0.400

Table 8-9 Variation in performance parameters with operational variables. Experiment numbers correspond to those given in Table 8-6.

8.4. Comparison of model and real system performance

8.4.1. Comparison of chromatographic retention factors and performance

The variation in K_{EA} and k_{EA} over the corresponding range of operating conditions between the model and real systems, for all operating conditions studied, firstly demonstrates that the K_{EA} values determined using the real system were all higher. This indicates that with the impure feed EA resides for a longer period in the stationary phase as a result of reduced mass transfer kinetics. With an increase in the solute loading (20 $mL.min^{-1}$; 10 g loading) for both feed types there was an observed decrease in the K_{EA} values, with it being more pronounced with the real feed. The k_{EA} values show a

similar trend to the K_{EA} values. With the back extract (real system) feed, the EA elution time was seen to increase, with the exception of the experiment at 40 mL.min^{-1}. The reason for the lower k_{EA} value in this case was primarily due to the higher rotational speed used with the model system. At this higher rotational speed, as previously illustrated (Figure 5-4) for a given mobile phase flow rate, the corresponding S_f value will be higher, i.e. a smaller volume of mobile phase (V_m) present within the coil at hydrodynamic equilibrium. Since the K_{EA} values at 40 mL.min^{-1} for both the model and real system are almost equal, the ~30% variation in the k_{EA} values is due to the larger V_s/V_m of Equation 3.10 at the higher rotational speed, as a result of the smaller denominator (V_m) value.

Comparisons between the α and R_s values are illustrated in Figure 8-8(a) and (b) respectively for both pilot scale studies. Firstly from the results presented in Figure 8-8(a) large variations in the $\alpha_{EC/ED - EA}$ and $\alpha_{EB/psu-EEA - EA}$ were observed initially at 10 mL.min^{-1}. With an increase in the flow rate there was very little observed variation in α values. At the increased solute loading (20 mL.min^{-1}; 10g), the $\alpha_{EC/ED - EA}$ between the model and real systems showed little variation. In comparison, under the same operating conditions, a larger variation in $\alpha_{EB/psu-EEA - EA}$ between the model and real systems was observed. As illustrated in Figure 8-8(b), in terms of $R_{s\,(EC/ED - EA)}$ and $R_{s\,(EB/psu-EEA - EA)}$ with increasing mobile phase flow rate, a similar trend to that observed with the α values previously described was seen. However, in contrast for the experiments at the higher flow rates the model system was less able to resolve EC/ED from EA than the real system. Resolution calculations for the increased solute loading experiment with the model system could not be calculated due to co-elution of EA, EC/ED and EB/psu-EEA, but was calculated in the real system experiment.

Figure 8-9 illustrates the variation in the calculated column efficiencies between the model and real systems. In almost all cases, the model system attains a higher theoretical plate number than the corresponding real system experiment. In terms of EA purity (Tables 8-4 and 8-9) between the two feed types, with regard to the flow rate

studies, there was no variation in the achievable EA purity. At the higher solute loading, with the real system feed there was a 7% increase in the EA purity. Throughput comparisons indicate a higher predicted throughput with the model system would be obtainable, mainly due the faster product elution time, and hence larger number of operational runs possible in a given time.

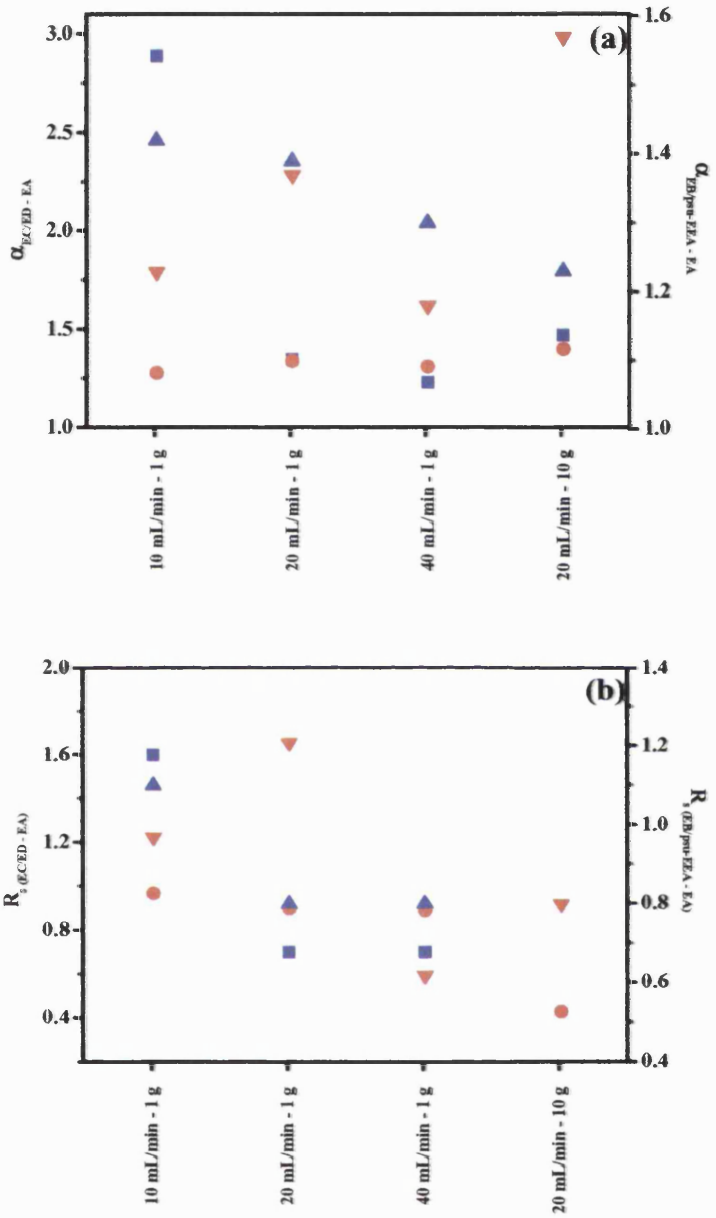

Figure 8-8 **(a) Comparison of α between pilot scale studies with the model and real systems over the range of operating variables investigated. (b) Comparison of R_s between model and real system pilot scale studies. In all case (■) and (▲) correspond to either α or R_s for the model system between EC/ED - EA and EB/psu-EEA – EA respectively. (●) and (▼) correspond to either α or R_s for the real system between EC/ED - EA and EB/psu-EEA – EA respectively. Data from Tables 8-3 and 8-8.**

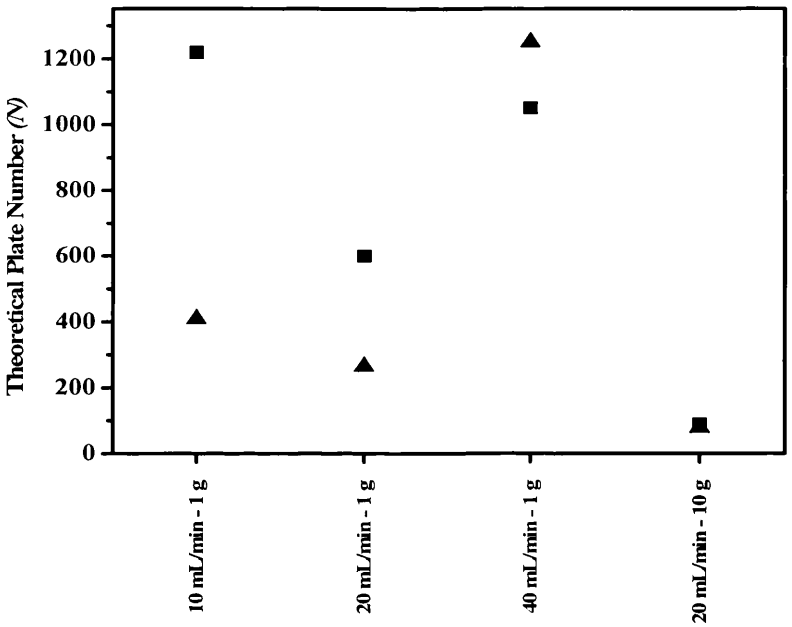

Figure 8-9 **Variation in column efficiency (*N*) at the pilot scale between the model (■) and real (▲) systems over a range of operating conditions. Data from Tables 8-3 and 8-8.**

8.5. Predictive scale-up of CCC separations

As previously described in Section 3.2 it is possible to predict scale-up of both the elution time and width of the target EA peak accurately, based on knowledge of the distribution ratio of the target component, EA (obtained on the laboratory scale CCC machine) and the phase hydrodynamics on the pilot scale machine. The predictive scale-up model was applied to both model and real system separations.

8.5.1. Predictive scale-up of the model system

8.5.1.1. Laboratory to pilot scale predictions

The first stage in the scale-up procedure described in Section 3.2.1 was to perform a fractionation of the crude erythromycin preparation at the laboratory scale (Figure 4-4). The distribution ratio calculated for the main EA peak (K) was found to be 0.25. The K values for the beginning ($K_{A\text{-}start}$) and the end ($K_{A\text{-}end}$) of the peak as illustrated in Figure 8-10, were calculated as described in Section 3.2.1, and found to be 0.207 and 0.322 respectively.

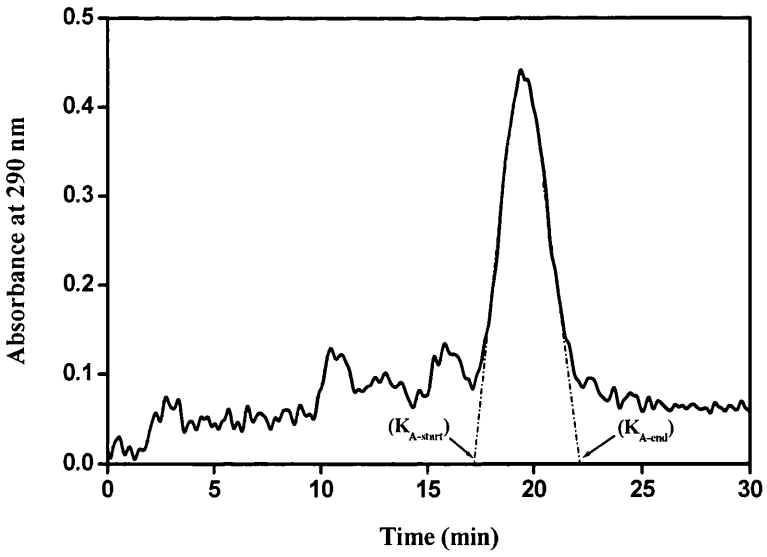

Figure 8-10 Laboratory scale CCC chromatogram of a model erythromycin fractionation (100 mg) at a mobile phase flow rate of 2 mL.min^{-1} (S_f = 82 %) illustrating the $K_{A\text{-}start}$ and $K_{A\text{-}end}$ points used for scale-up predictions. Experiments performed as described in Figure 4-4.

As previously discussed in Section 8.2, the separation was experimentally scaled-up based on the ratio of the coil internal diameters, maintaining the same relative injection volume and solute loading. The elution times (t_{kA}, $t_{kA\text{-start}}$, $t_{kA\text{-end}}$) of the EA peak at the pilot scale can be predicted from knowledge of the stationary phase retention in the pilot scale coil (S_f = 86%; Figure 5-4) and by using Equation 3.18. Table 8-10 shows the measured (from Figure 8-1) and predicted values of t_{kA}, $t_{kA\text{-start}}$ and $t_{kA\text{-end}}$ at both the laboratory and pilot scale. These results demonstrate that accurate predictions of EA elution can be achieved to within ~5% based on the simple linear scale-up of the laboratory scale CCC operating conditions.

	Lab Scale CCC			**Pilot Scale CCC**		
	t_{kA} (min)	$t_{kA\text{-start}}$ (min)	$t_{kA\text{-end}}$ (min)	t_{kA} (min)	$t_{kA\text{-start}}$ (min)	$t_{kA\text{-end}}$ (min)
Measured	19.4	17.3	22.1	40.5	38.3	45.8
Predicted	-	-	-	42.4	39.0	48.2
Error (%)	-	-	-	4.6	1.8	5.0

Table 8-10 Comparison of predicted and experimental erythromycin A elution times for model system CCC scale-up from laboratory to pilot scale. Scale-up performed as described in Section 8.2. Predictions calculated using Equation 3.18.

8.5.1.2. Predictions at the pilot scale with increasing operating conditions

Having shown that accurate scale-up predictions are possible based on a 'standard' set of operating conditions, the next step was to determine if similarly accurate predictions could be made for separations with increased mobile phase flow rates and injection volumes at the pilot scale. The results from Experiment 1 (Table 8-1) were used to test the model's ability to predict EA elution with increasing mobile phase flow rate. The K_{EA} values for the start, centre and end of the peak were again taken from the standard laboratory scale separation. Once again, with knowledge of the S_f value at the

pilot scale (78.2% v/v) at this mobile phase flow rate (20 mL.min^{-1}), and using Equation 3.18, EA peak elution times were predicted, with the values given in Table 8-11. As can be seen from the results presented in Table 8-11, there is a good correlation between the predicted and measured values for the main EA peak, i.e. the start, centre and end of EA elution, with the maximum error of ~7%.

	Lab scale CCC			Pilot scale CCC		
	t_{kA} (min)	$t_{kA\text{-start}}$ (min)	$t_{kA\text{-end}}$ (min)	t_{kA} (min)	$t_{kA\text{-start}}$ (min)	$t_{kA\text{-end}}$ (min)
Measured	19.4	17.3	22.1	18.6	16.6	21.1
Predicted	-	-	-	19.4	17.8	22.1
Error (%)	-	-	-	4.0	6.7	4.3

Table 8-11 Comparison of predicted and experimental erythromycin A elution times for model system CCC scale-up at the increased mobile phase flow rate of 20 mL.min^{-1} (1 g loading). Scale-up performed as described in Section 8.2. Predictions calculated using Equation 3.18.

Secondly, the application of the model to predict EA elution times with increasing solute loading was investigated. The experiments used to test these predictions were performed at injection volumes of 10 mL and 100 mL (Experiments 1 and 3 respectively; Table 8-1) representing solute loadings of 1 and 10 grams respectively, with a constant solute concentration of 100 mg.mL^{-1}. The resultant CCC chromatograms are shown in Figure 8-11. Considering first chromatogram A, the stationary phase retention (S_f) was calculated to be 78.2%, with a resultant t_m of 9.8 minutes. The values of $t_{kA\text{-start}}$, t_{kA} and $t_{kA\text{-end}}$ were taken to be 16.6, 18.6 and 21.1 minutes respectively. The predicted elution times of $t_{kB\text{-start}}$, t_{kB} and $t_{kB\text{-end}}$ at the higher loading (chromatogram B) could be calculated using Equations 3.19 to 3.21 (Section 3.2.2). It was observed however that, with all other conditions held constant, there was a slight decrease in the S_f, resulting in an increase in t_m to 10.9 minutes (chromatogram B). This variation can readily be taken into account as described by Equations 3.22 to 3.24 (Section 3.2.2). Table 8-12 shows the predicted and measured elution times. Allowing for changes in t_m between runs, all predictions can be made to within ~13% of the measured value.

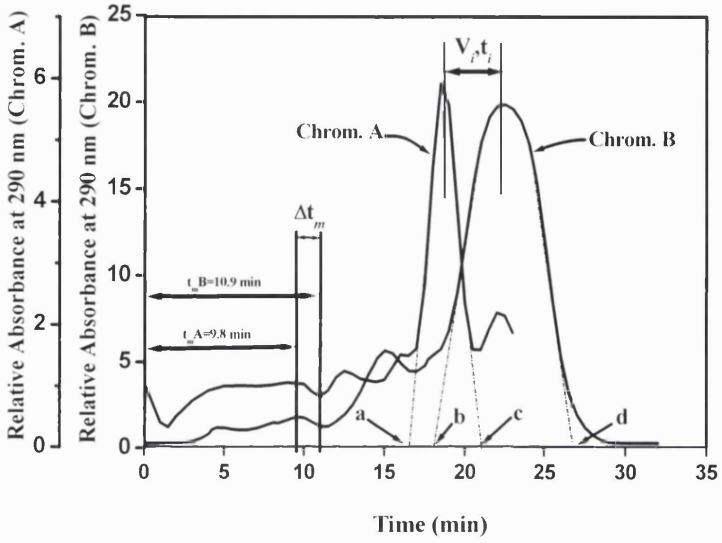

Figure 8-11 **Pilot scale CCC chromatograms illustrating the effect of increased injection volume, V_i, on erythromycin separation. Chromatogram A corresponds to a separation performed at a mobile phase flow rate of 20 mL.min^{-1} (S_f = 78.2%; ω = 800 rpm; V_i = 10 mL). Chromatogram B corresponds to a separation performed at a mobile phase flow rate of 20 mL.min^{-1} (S_f = 76.4%; ω = 800 rpm; V_i = 100 mL). Points (a) and (c) correspond to the start ($t_{kA\text{-}start}$) and finish ($t_{kA\text{-}end}$) of the main peak in chromatogram A. Points (b) and (d) correspond to the start ($t_{kB\text{-}start}$) and finish ($t_{kB\text{-}end}$) of the main peak in chromatogram B.**

	Chromatogram A			Chromatogram B		
	t_{kA} (min)	$t_{kA\text{-}start}$ (min)	$t_{kA\text{-}end}$ (min)	t_{kA} (min)	$t_{kA\text{-}start}$ (min)	$t_{kA\text{-}end}$ (min)
Measured	18.6	17.1	21.6	22.4	18.2	26.9
Predicted	-	-	-	23.6	15.8	25.0
Error (%)	-	-	-	5.0	13.2	7.0

Table 8-12 **Comparison of predicted and experimental erythromycin A elution times for different injection volumes. Chromatograms and loadings as shown in Figure 8-11. Predictions calculated using Equations 3.22 to 3.24.**

The scale-up model was also used to predict the EA elution time at the higher rotational speed of 1200 rpm. Scale-up predictions were again made using both the K_{EA} values obtained from the laboratory scale CCC chromatogram (Figure 4-4) and Equation 3.1.8, with the results presented in Table 8-13.

	10 mL.min^{-1}			**40 mL.min^{-1}**		
	t_{kA} (min)	$t_{kA\text{-start}}$ (min)	$t_{kA\text{-end}}$ (min)	t_{kA} (min)	$t_{kA\text{-start}}$ (min)	$t_{kA\text{-end}}$ (min)
Measured	37.4	31.4	42.5	15.5	13.1	16.7
Predicted	31.6	28.1	37.6	11.0	10.3	12.2
Error (%)	15.4	10.5	11.6	29.0	21.1	26.8

Table 8-13 Comparison of predicted and experimental erythromycin A elution times for different mobile phase flow rates at a rotational speed of 1200 rpm. Chromatograms as shown in Figure 8-4. Predictions calculated using Equation 3.18.

From the results in Table 8-13 the error in the predicted value increased up to around 29%. This is due primarily to the difference in the measured and assumed values of K (Table 8-2) arising from the fact that the laboratory scale CCC machine could not be operated at a rotational speed greater than 800 rpm.

8.5.2. Predictive scale-up of the real system

As previously demonstrated with a model system, the scale-up of the erythromycin fractionation from knowledge of the distribution ratio at the laboratory scale, and system hydrodynamics at the pilot scale, can be predicted to within 13% depending upon mobile phase flow rate and sample injection volume. The future industrial acceptance of this separation technology, as an alternative to currently employed high-resolution chromatographic techniques, will be dependent not only on its ability to processing crude feeds, but predicatively scale-up these separations. This perceived process requirement was the impetus for the application of the previously described predictive scale-up model to real systems.

8.5.2.1. Laboratory to pilot scale predictions

As with the model system scale-up predictions, the K_{EA} value was first determined from an laboratory scale CCC chromatogram (Figure 7-3(c)) and found to be 0.25, with corresponding $K_{EA\text{-start}}$ and $K_{EA\text{-end}}$ values of 0.194 and 0.318 respectively. From knowledge of the S_f value (84% v/v) for the linearly scaled pilot CCC run (Figure 8-5) the corresponding start ($t_{kA\text{-start}}$), centre (t_{kA}) and end ($t_{kA\text{-end}}$) were predicted using Equation 3.18. Table 8-14 shows the comparison between the measured (directly from the CCC chromatogram in Figure 8-5) and predicted EA peak elution times. As can be seen from the results in Table 8-14, there is a good agreement between predicted and experimentally measured EA peak elution time, with a maximum calculated error of 6%.

	Lab scale CCC			**Pilot scale CCC**		
	t_{kA} (min)	$t_{kA\text{-start}}$ (min)	$t_{kA\text{-end}}$ (min)	t_{kA} (min)	$t_{kA\text{-start}}$ (min)	$t_{kA\text{-end}}$ (min)
Measured	19	16.3	21.1	43.4	39.7	47.2
Predicted	-	-	-	44.9	40.6	50.2
Error (%)	-	-	-	3.3	2.1	6.0

Table 8-14 Comparison of predicted and experimental erythromycin A elution times for real system CCC scale-up from laboratory to pilot scale. Pilot scale experiment performed as described in Figure 8-5. Predictions calculated using Equation 3.18.

8.5.2.2. Predictions at the pilot scale with increasing operating conditions

Once again, as with the model system predictions, the model's ability to accurately predicted EA elution times with increasing mobile phase flow rates and solute loadings was investigated. The mobile phase flow rates used were 20 and 40 $mL.min^{-1}$ (100 mg loading). Table 8-15 illustrates the experimentally measured and predicted EA elution times for both flow rate studies investigated.

	20 mL.min^{-1}			40 mL.min^{-1}		
	t_{kA} (min)	$t_{kA\text{-start}}$ (min)	$t_{kA\text{-end}}$ (min)	t_{kA} (min)	$t_{kA\text{-start}}$ (min)	$t_{kA\text{-end}}$ (min)
Measured	23.8	21.4	25.7	15.5	14.4	16.5
Predicted	25.3	23.3	27.6	14.5	13.7	15.5
Error (%)	5.8	8.1	7.1	6.5	4.9	6.3

Table 8-15 Comparison of predicted and experimental erythromycin A elution times for real system CCC scale-up with increased mobile phase flow rate. Experiments performed as described in Figure 8-6. Predictions calculated using Equation 3.18.

Finally, EA elution times were predicted and experimentally verified between 1 and 10 grams solute loadings at a mobile phase flow rate of 20 mL.min^{-1}. Figure 8-12 illustrates the comparison between the two CCC chromatograms in question, with the comparison between the predicted and measured EA elution results presented in Table 8-16.

The results in Tables 8-14 to 8-16 demonstrate the model's ability to predict EA elution times to with ~10% with an increase in the both the mobile phase flow rate and solute loading. These results are comparable with the scale up predictions from Sutherland *et al.* (2001a), where for a similar mobile phase flow rate and solute loading their predictions were to within ~5%.

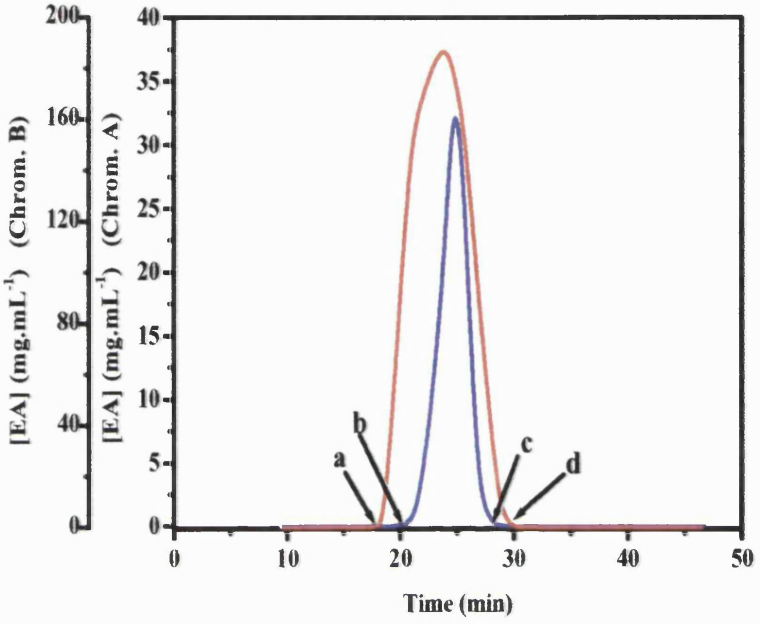

Figure 8-12 **Pilot scale CCC chromatograms illustrating the effect of increased injection volume, V_i, on erythromycin separation. Chromatogram A (—) corresponds to a separation performed at a mobile phase flow rate of 20 mL.min^{-1} (S_f = 78.2%; N = 800 rpm; V_i = 10 mL). Chromatogram B (—) corresponds to a separation performed at a mobile phase flow rate of 20 mL.min^{-1} (S_f = 76.4%; N = 800 rpm; V_i = 100 mL). Points (b) and (c) correspond to the start ($t_{kA\text{-}start}$) and finish ($t_{kA\text{-}end}$) of the main peak in chromatogram A. Points (a) and (d) correspond to the start ($t_{kB\text{-}start}$) and finish ($t_{kB\text{-}end}$) of the main peak in chromatogram B.**

	Chromatogram A			Chromatogram B		
	t_{kA} (min)	$t_{kA\text{-}start}$ (min)	$t_{kA\text{-}end}$ (min)	t_{kA} (min)	$t_{kA\text{-}start}$ (Min)	$t_{kA\text{-}end}$ (min)
Measured	23.8	21.4	25.7	22.6	19.5	28.6
Predicted	25.3	23.3	27.6	24.3	21.6	26.5
Error (%)	5.8	8.1	7.1	7.1	9.8	7.4

Table 8-16 **Comparison of predicted and experimental erythromycin A elution times for different injection volumes. Chromatograms and loadings as shown in Figure 8-12. Predictions calculated using Equations 3.19 to 3.21.**

8.5.3. Comparison between model and real systems predictions

Finally, the accuracy of the predictive model is illustrated by parity plots for the main EA peak, t_{kEA} (Figure 8-13) from both model and real systems.

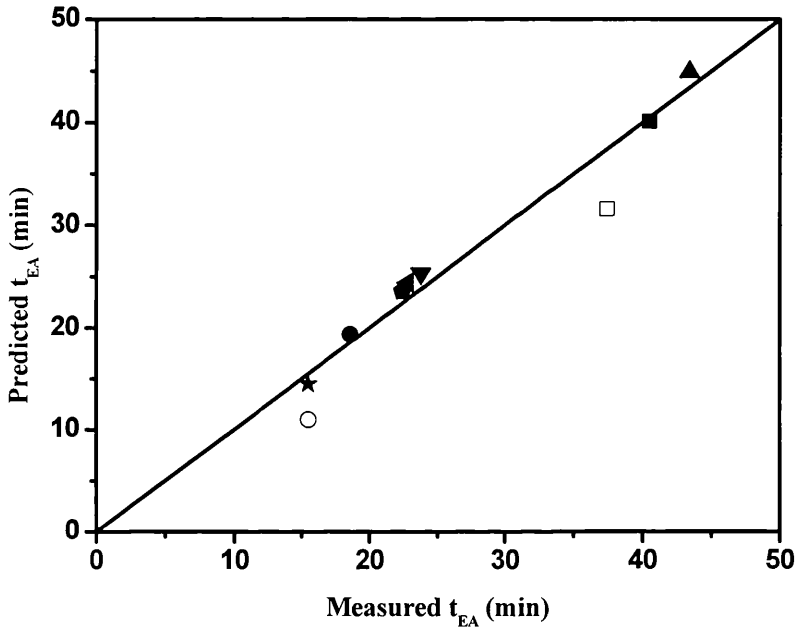

Figure 8-13 **Parity plot of measured and predicted pilot scale elution times of erythromycin A for both model and real system experiments. Both model and real predictions made assuming a constant K value of 0.25 obtained from a corresponding laboratory scale CCC experiment. (■) = Model system experiment at 10 mL.min^{-1}. (●) = Model system experiment at 20 mL.min^{-1}. (⬟) = Model system experiment at 20 mL.min^{-1} (10 g loading). (▲) = Real system experiment at 10 mL.min^{-1}. (▼) = Real system experiment at 20 mL.min^{-1}. (◀) = Real system experiment at 20 mL.min^{-1} (10g loading). All experiments performed at a rotational speed of 800 rpm. (□) and (○) correspond to model system experiments performed at 10 and 40 mL.min^{-1} respectively at a rotational speed of 1200 rpm.**

8.6. Summary

In this Chapter the performance, upon scale-up, of a novel pilot scale CCC machine for the fractionation of EA from its structurally similar analogues in both model and real systems has been studied. With an increase in mobile phase flow rate and solute loading, for both feed types (Sections 8.2.1 and 8.3.1) a satisfactory separation of EA from its analogues was achieved, with a maximum estimated throughput for the model and real system of 0.41 $kg.day^{-1}$ and 0.40 $kg.day^{-1}$ respectively. More importantly, results have shown that with both model and real systems the scale-up of CCC from knowledge of a single laboratory scale separation is linear and predictable. Predictions of EA elution time at the pilot scale were accurate, for the model and real systems, to within 5% and ~7% respectively. Changes in the mobile phase flow rate and injection volume could also be accounted for to within ~13% for the model system, and ~10% for the real system.

In the final results Chapter, the feasibility of using a fractionation diagram approach to investigate the trade-offs between product purity and total yield with changes in operating conditions will be presented.

9. Analysis of product purity and yield trade-offs for CCC separations

9.1. Introduction

The stringent regulations imposed by regulatory authorities require manufacturing industries to produce pharmaceuticals at reproducible levels of quality and efficacy. Also in an economic context, for processes to perform at optimal performance levels of yield and/or purity, precise and predictive controls are required to be in place. A basic requirement for good manufacturing practice (GMP) is the 'control and validation of changes to the manufacturing process' (Sherwood, 1996). The prediction of chromatographic performance to changes in operating conditions have previously been evaluated directly from on-line chromatograms, but are not visually that informative in quantifying the consequences for performance and sensitivity of a given chromatographic separation to changes in operational conditions (Ngiam *et al.*, 2001). The ultimate aim of any chromatographic model is to enable accurate prediction of target peak elution times. Hence a model should therefore enable the determination of the cut points, i.e. to consistently identify the start and end points for sample collection to obtain the target product at the maximum purity and yield.

Research within our laboratories has focused on the development of a novel fractionation diagram approach, initially to investigate fractional protein precipitation (Richardson *et al.*, 1989, 1990), and more recently as a graphical method for determining chromatographic performance in terms of the process trade-off between purity and yield (Ngiam *et al.*, 2001). The theory behind the construction of fractionation and PF_{max} vs yield diagrams is presented in detail in Section 3.3. In this chapter the application of this graphical method to CCC aims to demonstrate, with the real system, the effects of feed type and operating variables on the degree of fractionation and yield at both the laboratory and pilot CCC scales, and ultimately identify the optimal trade-off between product purity and solute yield, together with respective cut-point determinations.

The results presented in this chapter form the basis of the manuscript: Booth A.J., Ngiam S.H., and Lye G.J (submitted): Antibiotic purification from fermentation broths by counter-current chromatography: analysis of product purity and yield trade-offs.

9.2. Effects of feed type at the laboratory CCC scale

In relation to the laboratory scale studies described in Section 7.4, that investigated the effects of feed type, i.e. clarified broth (CB), forward extract (FE) and back extract (BE) on the CCC separation performance, Figure 9-1 illustrates the resultant fractionation diagram. The point Y>0 for each curve represents initial product elution (Y), with complete product elution occurring at the point Y = 1. The corresponding X values (Cum. fraction EA + imp.) at Y = 1 are given in Table 9-1. From these values the corresponding gradient of the linear portion of the fractionation curves do not show any significant difference.

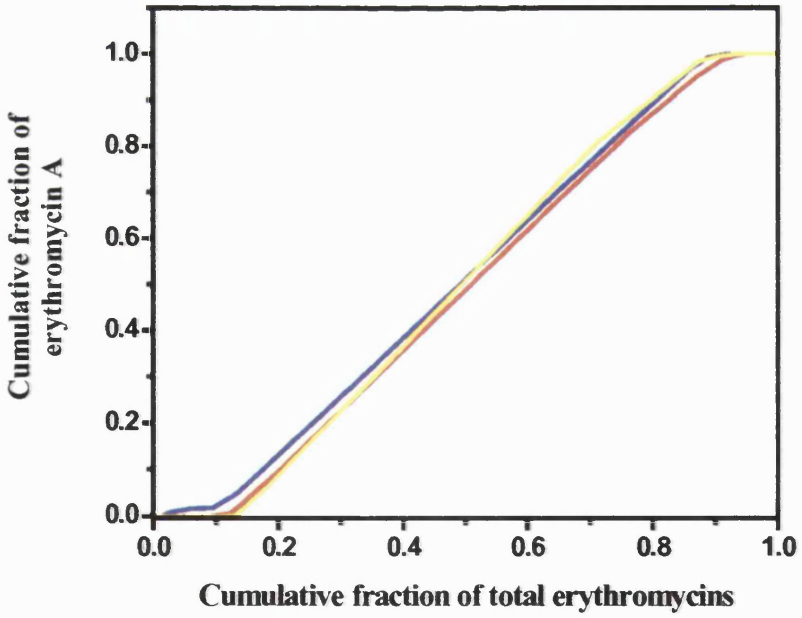

Figure 9-1 Fractionation diagrams illustrating the purification of Erythromycin A from spiked clarified ( ), forward ( ) and back ( ) extracted feeds. Fractionation diagrams constructed as described in Section 3.3.1 using data from Figures 7-3 (a), (b) and (c) respectively.

Operating variable		X at Y > 0	X at Y = 1
Feed	CB	0.13	0.94
	FE	0.10	0.91
	BE	0.09	0.87

Table 9-1 Variation in the cumulative fraction of total erythromycins eluted (X) at Y > 0 and Y = 1 for the fractionation diagrams illustrated in Figure 9-1.

The next stage in cut point determination is the construction of the Purification factor (PF) versus yield graph. This is achieved by calculating, from the relevant fractionation diagram, both the gradient of the tie line between any combination of two points, and the corresponding total EA yield value for any combination of fraction cutpoints over the entire CCC chromatogram (see Section 3.3.2). Figure 9-2 is an example of a PF versus yield diagram, from analysis of the fractionation curve corresponding to the BE experiment, illustrating the range of possible PF and yield (% w/w) combinations available.

A 'searching-type computer algorithm' can then be applied to identify, for each given yield on a PF versus yield diagram (Figure 9-2), the corresponding maximum purification factor (PF_{max}). The resultant PF_{max} versus yield diagram, as illustrated in Figure 9-3, demonstrates how, despite small variations in the fractionation diagram curves (Figure 9-1) there are large differences between the operational runs in terms of chromatographic performance.

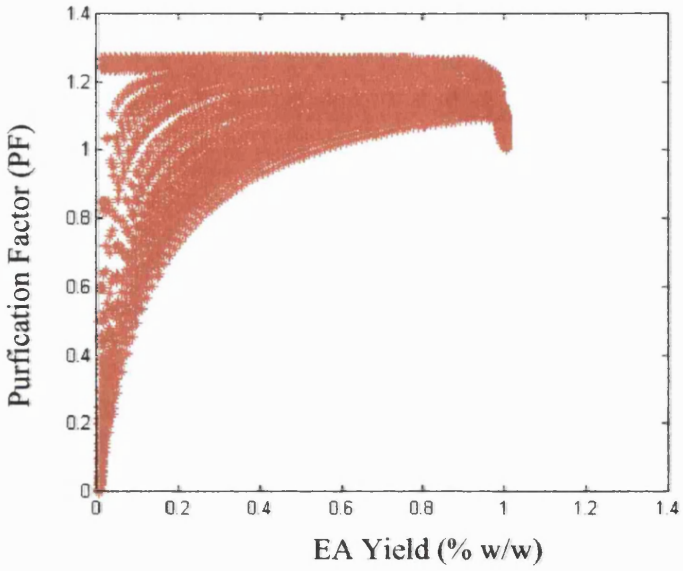

Figure 9-2 **MatLab generated PF versus yield diagram for Erythromycin A separation from a BE feed at the laboratory CCC scale. Diagram illustrates the range of possible combinations of PF and yield values and constructed as described in Section 3.3.2 from the fractionation diagram in Figure 9-1.**

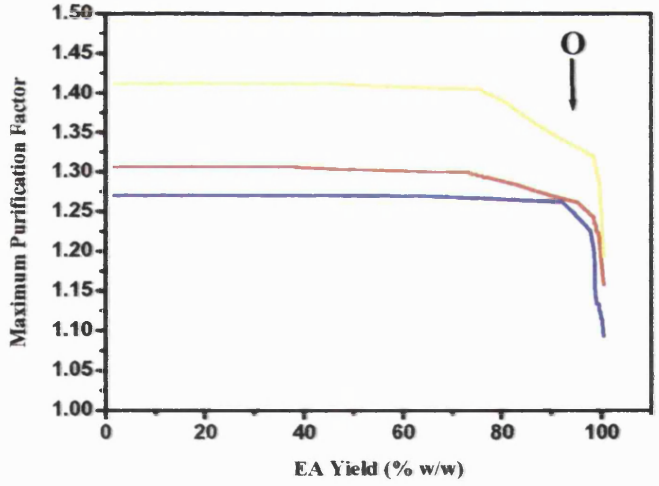

Figure 9-3 **Maximum PF versus yield diagram illustrating the comparisons between spiked clarified (—), forward (—) and back (—) extracted feeds for Erythromycin A purification using the laboratory scale CCC. O represents optimal point for trade off between purity and yield. Diagrams constructed as described in Section 3.3.2 using data from figures similar to Figure 9-2.**

Examination of the PF_{max} versus yield lines in Figure 9-3 at a 1% yield value, i.e. where the PF_{max} value is at its greatest, indicates a larger PF_{max} value for both the CB and FE feed in comparison to the BE feed. The larger PF_{max} values for the CB and FE feeds is due to a larger proportion of broth impurities present, i.e. the proportion of the target product, EA, to its 'contaminates' is far lower, hence a larger PF_{max} value is required to attain the corrected EA purity values.

In addition to the construction of the PF_{max} versus yield diagrams a range of PF_{max} values with their corresponding yield values are generated. Table 9-2 is an example, from the BE feed experiment of cut point determination at a range of solute yields together with their corresponding PF_{max} values. The PF_{max}, 1.271, is attainable up to a total solute yield of 60.9%. In terms of final EA purity this represents ~100% (w/w). Relating the optimal trade-off between EA purity and total solute yield to the corresponding PF_{max} versus yield diagram, it has been suggested that fraction collection should occur at the point immediately prior to inflection, labelled as O on Figure 9-3 (Ngiam *et al.* 2001). For the data shown in Figure 9-3 the point O has a corresponding yield value of 92.7% (w/w).

Maximum purification factor	Total solute yield (% w/w)	Cut 1	Cut 2	t_1 (min)	t_2 (min)
1.271	10.2	0.435	0.515	18.1	18.4
1.271	50.8	0.255	0.655	16.5	19.0
1.271	60.9	0.255	0.734	16.5	19.4
1.268	70.3	0.255	0.809	16.5	20.0
1.265	80.6	0.221	0.858	16.7	20.5
1.263	90.6	0.141	0.858	16.5	20.5
1.241	95.2	0.111	0.878	16.0	21.2
1.120	99.7	0.011	0.905	12.5	22.5

Table 9-2 Example of start (t_1) and end (t_2) sample collection times (cut-points) corresponding to different PF and yield values for Erythromycin A purification from a back extract feed at the laboratory CCC scale. Cut-points determined as described in Section 3.3.2 using data from Figure 9-3.

As a means of comparison between the various types of feed stream used for laboratory scale CCC experiments, the final yield value was fixed at 92.7% (w/w), corresponding, in this example, to the optimal yield with the BE feed. Table 9-3 provides the PF_{max} values at a solute yield of 92.7% (w/w) for all experiments performed. From these results (Table 9-3) there is an observed reduction in the PF_{max} value moving from the CB to BE feed. In addition, Table 9-3 also provides final EA purity values ($PurEA_{final}$) , present in the determined fractions, demonstrating the BE feed enables an optimal trade-off between product purity (EA = 99% w/w) and solute yield. Finally, data generated during the construction of the PF_{max} versus yield diagrams is used to select appropriate sample collection times to obtain a required degree of purity and total solute yield.

Feed type	PF_{max}	$PurEA_{final}$ (% w/w)	Cut point (min)	
			t_1	t_2
CB	1.339	67	17.5	21.2
FE	1.266	79	17.3	20.7
BE	1.257	99	14.5	18.9

Table 9-3 Summary of attainable PF_{max} values and final EA purities ($PurEA_{final}$) for clarified broth (CB), forward extract (FE) and back extract (BE) together with corresponding cut points. PF_{max} values identified correspond to a yield value of 92.7% (w/w). Cut points determined as described in Section 3.3.2 using data from corresponding tables, such as that illustrated in Table 9-2.

With reference to the optimal PF and yield values identified in Table 9-3, the corresponding start (t_1) and end (t_2) cut points, for the back extracted feed run are t_1 = 14.5 minutes and t_2 = 18.9 minutes. These points are illustrated in Figure 9-4 on the original CCC chromatogram.

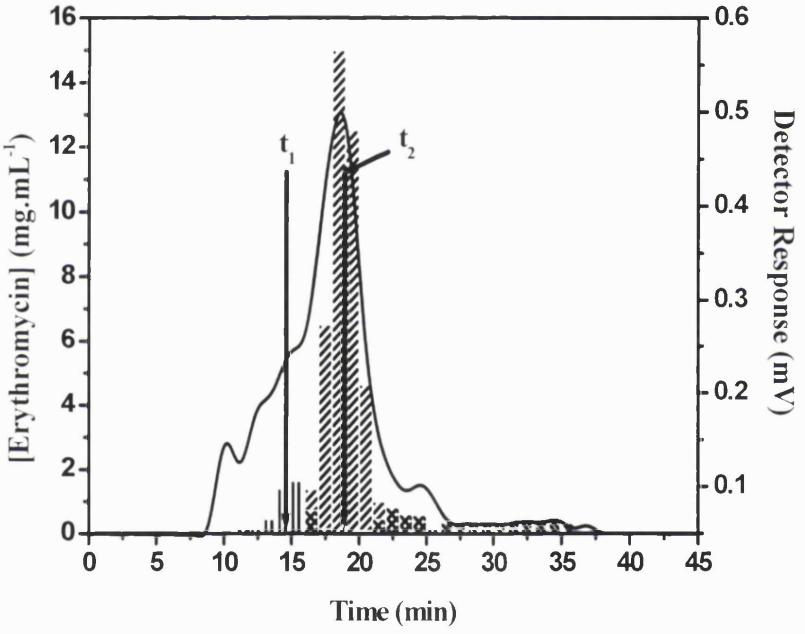

Figure 9-4 **Laboratory scale CCC chromatogram from BE feed separation illustrating the cut points, t_1 and t_2 required to achieve an EA purity of 99% (w/w) and yield of 92.7% (w/w). Cut points determined as described in Table 9-3.**

9.3. Effects of operating variables at the laboratory CCC scale

The graphical approach described in Section 9.2 to visually determine product purity and yield trade-offs was also applied to the real system experiments performed at increased mobile phase flow rates and solute loadings as described in Section 7.6. The same procedure described in Section 9.2 was followed, with results presented as fractionation and PF_{max} versus yield diagrams and corresponding cut point tables.

9.3.1. Effects of increasing mobile phase flow rate

Figure 9-5 illustrates the fractionation diagrams for the 2 and 5 $mL.min^{-1}$ mobile phase flow rate experiments with the BE feed (solute injection = 100 mg). Visually the 2 $mL.min^{-1}$ experiment generates the steeper gradient of the line, indicating that operating at the lower flow rate will enable a higher purity and yield to be achieved. The next stage of the simulation generated the PF_{max} versus yield diagram as illustrated in Figure 9-6.

From Figure 9-6 the lower mobile phase flow rate (2 $mL.min^{-1}$) enables, for any given yield, a higher PF_{max} value, and hence a higher final EA purity to be obtained. To enable the comparison between the two flow rates, the required solute yield was set to the in the optimal region of the Figure labelled O, corresponding to 92.7% (w/w). The corresponding PF_{max} values for 2 and 5 $mL.min^{-1}$ found to be 1.261 and 1.109 respectively. Based on these PF_{max} values, the final EA purity ($PurEA_{final}$) values for the 2 and 5 $mL.min^{-1}$ experiments were calculated from experimental data and using Equation 3.29 to be 100% (w/w) and 88% (w/w) respectively.

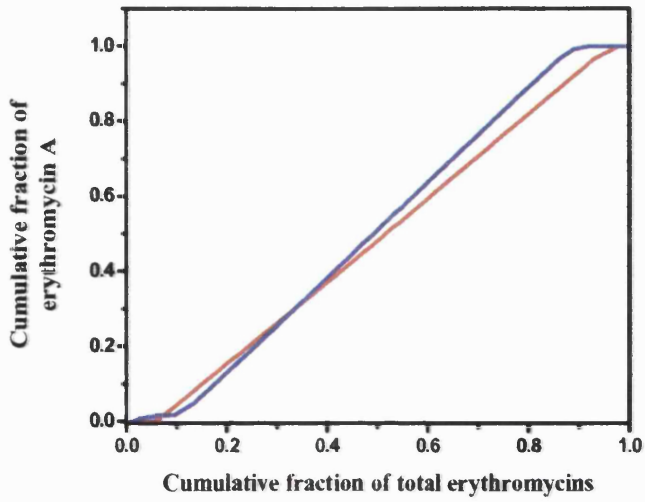

Figure 9-5 **Fractionation diagrams illustrating the purification of Erythromycin A from the 2 (—) and 5 (—) mL.min^{-1} mobile phase flow rate experiments with the BE feed. Fractionation diagrams constructed as described in Section 3.3.1 using data from Figures 7-6(a) and (b) respectively.**

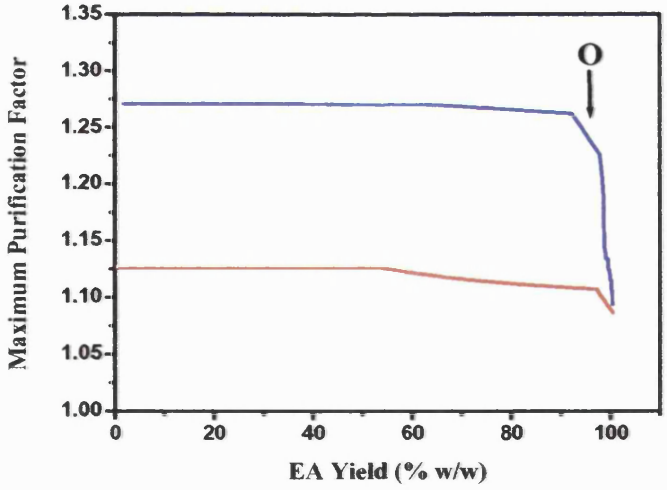

Figure 9-6 **Maximum PF versus yield diagrams illustrating the comparisons between 2 (—) and 5 (—) mL.min^{-1} for Erythromycin A purification using the laboratory scale CCC. O represents optimal point for trade off between purity and yield. Diagrams constructed as described in Section 3.3.2 using data from figures similar to Figure 9-2.**

9.3.2. Effects of increasing solute loading

Finally, this technique was applied to the solute loading experiments performed as described in Section 7.6. The corresponding fractionation curves for the 100, 500 and 1000 mg solute loading experiments are illustrated in Figure 9-7. From the fractionation diagrams in Figure 9-7, there is an observed decrease in the gradient of the line with the increasing solute loadings, and as previously stated, one would therefore expect a reduction in achievable $PurEA_{final}$ values with larger amounts of injected solute. This assumption based on these results (Figure 9-7) is supported by the corresponding PF_{max} versus yield plots as illustrated in Figure 9-8. Focusing on the O point, where the required total solute yield was fixed at 92.7% (w/w) the corresponding PF_{max} values for the 100, 500 and 1000 mg experiments was 1.257, 1.216 and 1.182 respectively. Based on these stated PF_{max} values, there is a decrease in EA purity from 99% (100 mg) to 96% (500 mg) and finally 93% (1000 mg), with the corresponding cut points provided in Table 9-4.

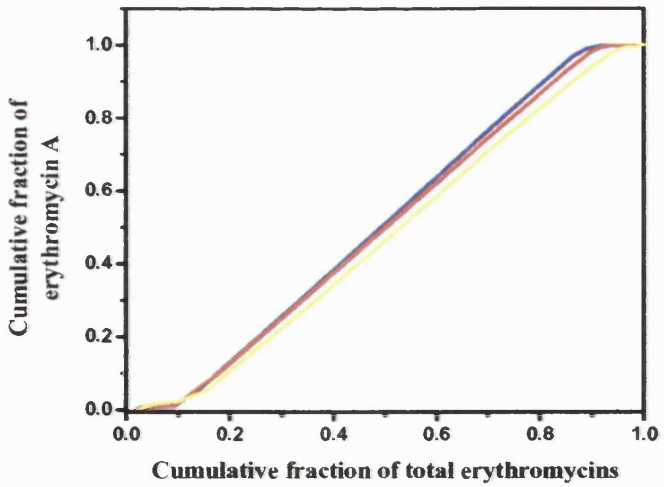

Figure 9-7 Fractionation diagrams illustrating the purification of Erythromycin A from the 100 (—), 500 (—) and 1000 mg (—) experiments with the BE feed. Fractionation diagrams constructed as described in Section 3.3.1 using data from Figures 7-7 (a) and (b) respectively.

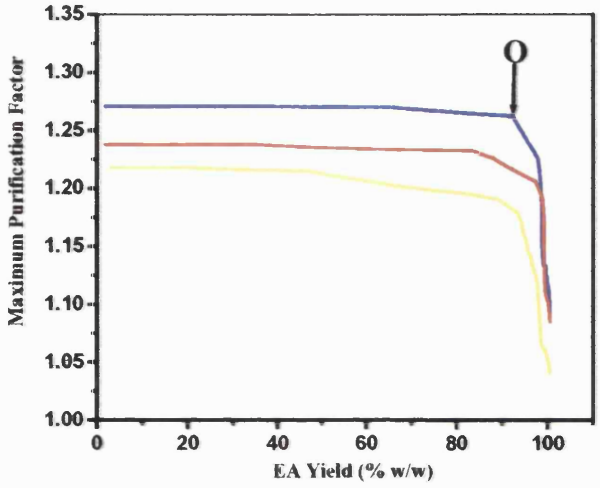

Figure 9-8 **Maximum PF versus yield diagrams illustrating the comparisons between 100 mg (▬), 500 mg (▬) and 1000 mg (▬) back extracted feeds at a mobile phase flow rate of 2 mL.min^{-1} for Erythromycin A purification using the laboratory scale CCC. O represents optimal point for trade off between purity and yield. Diagrams constructed as described in Section 3.3.2 using data from figures similar to Figure 9-2.**

Operating variable		Cut point (min)	
		t_1	t_2
Flow rate	2	14.5	18.9
	5	9.6	11.5
Loading	500	16.4	21.5
	1000	22.5	28.5

Table 9-4 **Summary of fraction cut-points for the range of mobile phase flow rate and solute loading experiments performed.**

9.4. Use of PF_{max} versus yield diagrams in optimising EA purity

Obviously, for a human therapeutic, such as that used during this project, stringent regulatory requirements dictated a high and consistent degree of final product purity over a range of operational parameters, i.e. comparable optimal EA purity levels must be obtainable over the range of operational variables investigated. This section aims to show that greater EA purities under specified operating conditions can be achieved, but at the sacrifice of product yield.

Considering first the 500 mg solute loading experiment (Section 9.3.2), by direct reference to similar yield, PF_{max} and cut point data to that shown in Table 9-2, the attainment of an identical final EA purity to that achieved with a 100 mg solute loading (>99% w/w) occurs at a PF_{max} of 1.227, with a calculated $PurEA_{final}$ of 99.01% (w/w). The corresponding cut-points are at 16.5 and 20.5 minutes. The total solute and EA yield were found to be 87.7% (w/w) and 89.9% (w/w) respectively. For the 1000 mg solute loading experiment, in order to achieve a comparable $PurEA_{final}$ (>99% w/w) a PF_{max} value of 1.217 is required. At this PF_{max} value the corresponding cut points on Figure 7-7 (b) are between 23.95 and 25.5 minutes, with a total solute and EA yield of 34.1% (w/w) and 39.9% (w/w) respectively.

From these results it is apparent that at higher solute loadings, the trade-off between product purity and EA yield is far less favourable. In the first instance, at the 1000 mg loading, it can be seen that despite a marked reduction in both total solute and EA yield over the optimal conditions discussed above, only a ~3% increase in EA purity was achievable. Relating this EA purity value of ~3% (w/w) to EA yield, under the specified operational conditions, for every 1% (w/w) increase in EA purity, there is a 17.4% (w/w) decrease in EA yield. Comparatively, for the 500 mg solute loading experiment, similar analysis of the data shows that for every 1% (w/w) increase EA purity there is a corresponding 1% (w/w) decrease in EA yield. In terms of predicted throughput, at the higher loading throughput, if an EA purity of 99% (w/w) was required, would decrease from 0.027 $kg.day^{-1}$ to 0.010 $kg.day^{-1}$. These results therefore demonstrate that in terms of

both process economics and more importantly maximising the purity of the target product, EA, it is far more favourable to operate at the lower solute loading concentration.

9.5. Application of fractionation diagram theory at the pilot scale

9.5.1. Effects of increasing mobile phase flow rate

As with laboratory scale studies, the fractionation diagram approach was also applied to pilot scale real system experiments performed (Section 8.3). Figure 9-9 illustrates for the flow rate studies the corresponding fractionation diagrams.

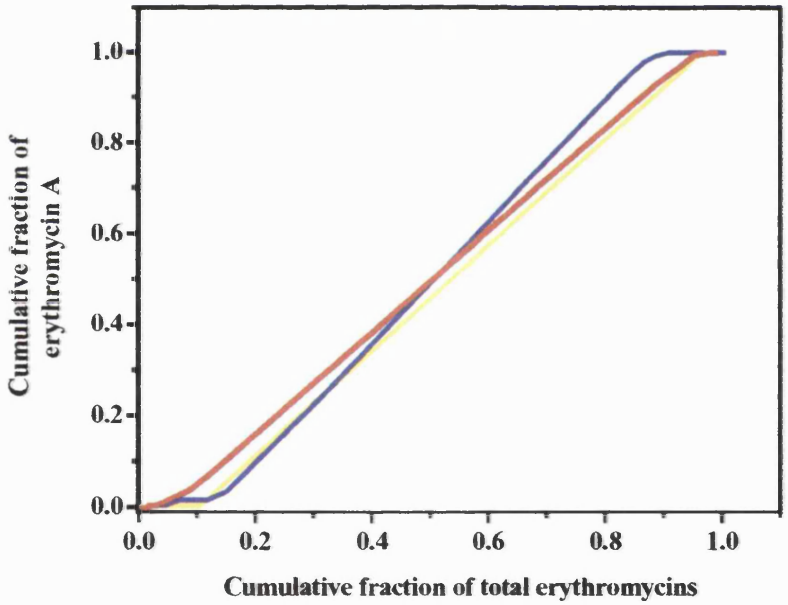

Figure 9-9 Fractionation diagrams illustrating the purification of Erythromycin A for the 10 (—), 20 (—) and 40 mL.min^{-1} (—) experiments with the BE feed (Section 8.3.1). Fractionation diagrams constructed as described in Section 3.3.1 using data from Figures 8-5, 8-6 (a) and (b) respectively.

From the fractionation diagrams in Figure 9-9, there is very little immediate difference between the 10 and 20 mL.min^{-1} experiments. However, at the 40 mL.min^{-1} mobile phase flow rate, the gradient of the corresponding fractionation curve is lower in comparison to the other curves, indicating the impact the higher operational flow rate has on product purity.

Figure 9-10 illustrates the corresponding PF_{max} versus yield for the range of flow rates investigated and demonstrates that at the highest flow there would be an expected reduction in the achievable EA purity upon processing ($PurEA_{final}$). In fixing the required yield to 92.7% (w/w), as with laboratory scale studies (Sections 9.2 and 9.3), the corresponding PF_{max} values were found to be 1.132 (10 mL.min^{-1}), 1.318 (20 mL.min^{-1}), and 1.107 (40 mL.min^{-1}). Based on these PF_{max} values there is a marginal decrease in EA purity from 100% (10 mL.min^{-1}) to 98.9% (20 mL.min^{-1}) and finally 97.6% (40 mL.min^{-1}).

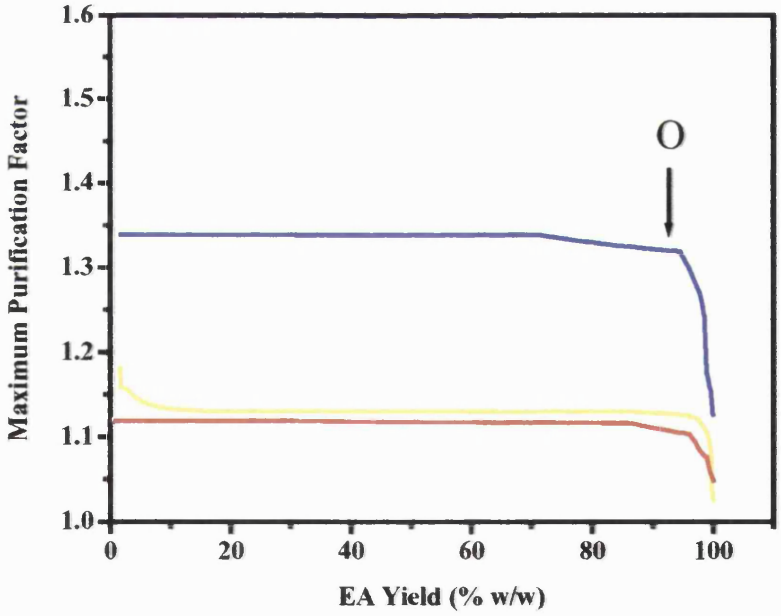

Figure 9-10 Maximum PF versus yield diagrams illustrating the comparisons between 10 (—), 20 (—) and 40 mL.min^{-1} (—) back extracted feeds at a solute loading of 1 g for Erythromycin A purification using the pilot scale CCC. O represents optimal point for trade off between purity and yield. Diagrams constructed as described in Section 3.3.2 using data from figures similar to Figure 9-2.

9.5.2. Effects of increasing solute loading

The fractionation diagram theory, in addition, was applied to pilot scale studies investigating the effects of solute loading on separation performance (Section 8.3), the corresponding fractionation diagrams are illustrated in Figure 9-11. From the fractionation diagrams (Figure 9-11), firstly it is visible that compared to the smaller solute loading volume, at the larger loading volume (100 mL) product elution begins earlier. However, where as in previous fractionation diagrams, one could identify which operating condition could enable higher EA purities to be obtained, in this particular case both curves have similar gradients. The variation, in terms of achieving optimal trade-offs between product purity and yield, becomes more apparent when constructing the PF_{max} versus yield diagram, as illustrated in Figure 9-12.

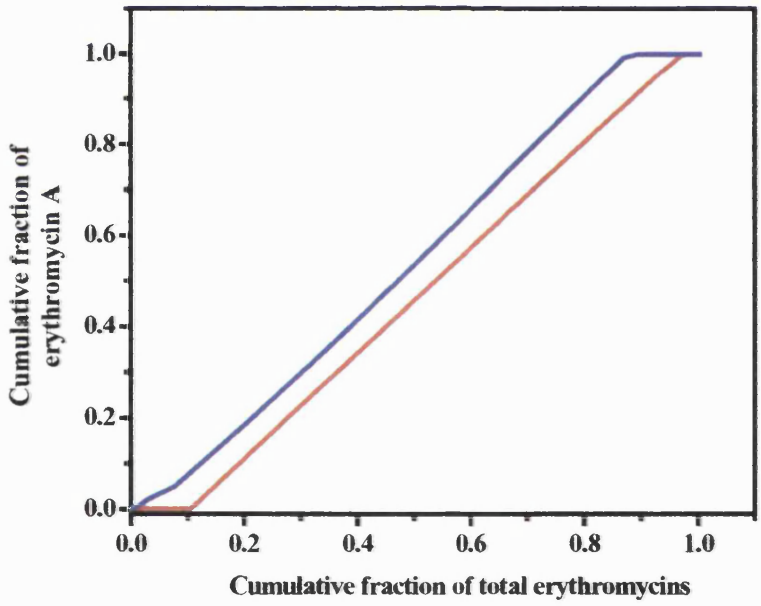

Figure 9-11 Fractionation diagrams illustrating the purification of Erythromycin A for the 10 mL loading volume (—) and 100 mL loading volume (—) experiments with the BE feed. Solute concentration set at 100 mg.mL^{-1} and a fixed mobile phase flow rate of 20 mL.min^{-1} in all cases. Fractionation diagrams constructed as described in Section 3.3.1 using data from Figures 8-6 (b) and 8-7 respectively.

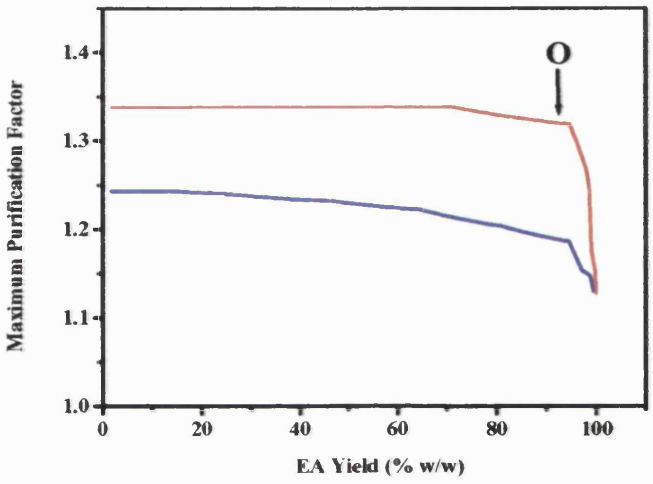

Figure 9-12 Maximum PF versus yield diagrams illustrating the comparisons between 10 mL (—) and 100 mL (—) loading experiments using BE feeds at a mobile phase flow rate of 20 mL.min^{-1} for Erythromycin A purification using the pilot scale CCC. O represents optimal point for trade off between purity and yield. Diagrams constructed as described in Section 3.3.2 using data from figures similar to Figure 9-2.

Once again, at a fixed solute yield of 92.7%, the corresponding PF_{max} values for the 10 and 100 mL loading volumes were measured to be 1.319 and 1.187 respectively. The $PurEA_{final}$ values, based on a starting EA purity of 74.5% (10 mL) and 88.7% (100 mL), were calculated to be 98.5% and 96.5% respectively. The PF_{max} versus yield diagrams (Figure 9-10 and 9-12) provide an indication of the reduction in the achievable yield under the more unfavourable operating conditions, i.e. increased mobile phase flow rate and solute loading required to ensure a high attainable EA purity ($PurEA_{final}$). Firstly, focusing on the flow rate studies, at 40 mL.min^{-1}, in order to achieve a $PurEA_{final}$ value of 99% (w/w), there must be a reduction in the solute yield to 86.4%. Based on previous $PurEA_{final}$ and solute yield values (Section 9.5.1) a 1.4% increase in the $PurEA_{final}$ value requires a 5.7% decrease in the total solute yield. In comparison, for the 1000 mg loading study, in order to achieve a $PurEA_{final}$ value of 99% (w/w), there must be a 20.5% reduction in the solute yield.

From an operational perspective, in comparison to the 40 $mL.min^{-1}$ experiment, the ~4 times increase in solute yield reduction at the higher loading volume (100 mL) would effectively result in a 20.5% decrease in the initial injected solute value, i.e. 10 grams. Hence, based on throughput results discussed in Sections 8.3.1.3, for the 100 mL loading experiment the predicted throughput decreased from 0.400 $kg.day^{-1}$ to 0.309 $kg.day^{-1}$.

9.6. Comparison between laboratory and pilot scale CCC

Finally, Figure 9-13(a) and (b) illustrates the comparative fractionation and PF_{max} versus yield diagrams respectively between the laboratory (2 $mL.min^{-1}$; 100 mg solute loading) and pilot scale (10 $mL.min^{-1}$; 1000 mg loading) operations. Detailed analysis of the PF_{max} versus yield diagram in the optimal region for maximum purity and yield, illustrated by the point O (yield = 92.7% w/w), shows that for the laboratory and pilot scales, the corresponding PF_{max} values are 1.257 and 1.153 respectively. The larger presented maximum PF_{max} for the laboratory scale should not be interpreted as an indication of a greater achievable EA purity, but is a facet of the computer simulation, in that the simulation, depending upon the calculated initial purity of the target product, adjusts the PF_{max} value accordingly to achieve corrected $PurEA_{final}$ values, .i.e. at the maximum PF_{max} value, the $PurEA_{final}$ value will be 100% (w/w). Therefore at the laboratory and pilot scales, the $PurEA_{final}$ values were ~100% (w/w) and 99% (w/w) respectively, demonstrating a comparable separation. Cut points at the pilot scale, for the specified yield and purity values, were between 39.5 and 45.4 minutes (Figure 8-5), with a corresponding EA yield of ~89% (w/w).

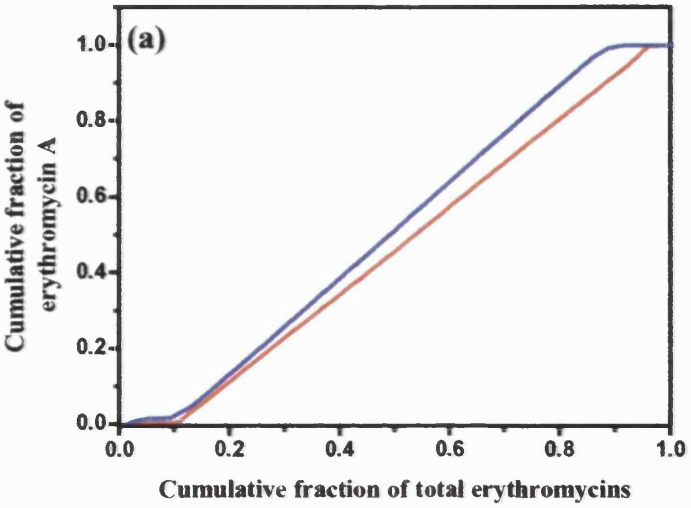

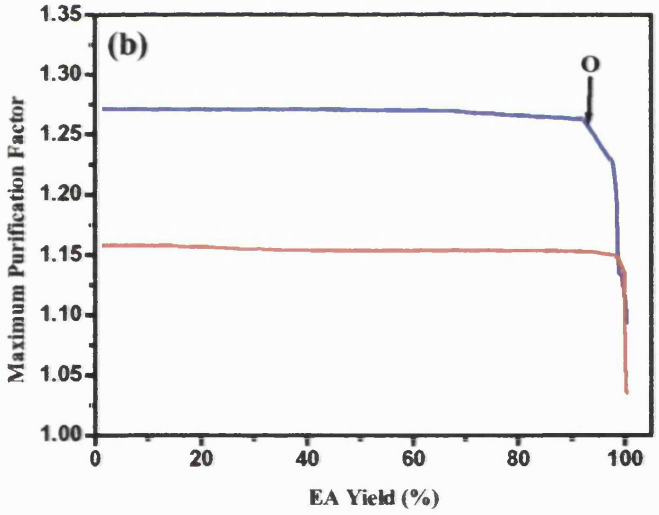

Figure 9-13 **(a) Fractionation diagrams (b) Maximum PF versus yield diagrams; illustrating the comparison between a laboratory scale (100 mg; 2 mL.min^{-1}) represented by (▬) and pilot scale (1000 mg; 10 mL.min^{-1}) represented by (▬) CCC purification of Erythromycin A using in both cases a spiked BE feed. O represents optimal point for trade off between purity and yield. Diagrams constructed as described in Section 3.3.2 using data from figures similar to Figure 9-2.**

9.7. Summary

In this Chapter results have demonstrated the successful application of the 'Fractionation diagram theory' to CCC, enabling, for all operating variables investigated with the BE feed, the identification of fraction collection points for a required degree of EA purity and total solute yield. This graphical technique has also demonstrated its effectiveness in identifying the required trade-off between purity and yield to optimising the EA purity for a given separation.

10. Comparison of CCC and HPLC

10.1. Introduction

For industrial processing, engineers aim to develop simple and hence cost effective purification schemes. If a high degree of resolving power is required, techniques such as high performance liquid chromatography would commonly be employed. This section aims to identify the process advantages of CCC over HPLC, and a proposed means of making performance comparison by the construction of the Van deemter curve.

10.2. Process benefits and drawbacks of CCC

The qualitative advantages and disadvantages of CCC over HPLC are well documented (Gunawardana and McAlpine, 1999) and include:

1) No irreversible adsorption or degradation of the target compound associated with solid phase interactions.
2) The ability to load relatively crude samples (even containing some particulates).
3) Use of the same phase systems at all scales of operation, enabling reliable scale-up and good column to column reproducibility.
4) A higher loading capacity since the separation takes place throughout the total volume of the stationary phase, rather than at the surface.

The current drawbacks of this technique, hindering wider industrial acceptance include:

1) The selection of a suitable solvent system, i.e. method development, in comparison to other LC method development strategies remains less defined, and as a result has been problematic to users (Berthod, 1991).
2) Processing times are longer, due to the lower number of generated theoretical plates in CCC.
3) The scalability of the technology, particularly from analytical to pilot to process scale has not, to the same degree as HPLC, received a great deal of research interest, and hence would not be considered an established and validatible operation.
4) CCC does not possess the same degree of equipment sophistication as seen in HPLC, and due to the lack of automation is labour intensive. A recently marketed CCC system, developed from the collaboration of Amersham Biosciences and Tauto Biotech (ShenZhen Tauto Biotech Co. Ltd, China) has successfully coupled an integrated gradient pumping unit (0.01 – 100 $mL.min^{-1}$), UV/VIS detector, a fraction collector and CCC machine (V_c = 1 L) together with Windows™ based controlling software. The development of such an integrated process unit has come some way to providing a feasible solution to this particular technological drawback.

10.3. Experimental and economic comparisons between CCC and HPLC

An experimental comparison between CCC and preparative HPLC (Menet and Thiebaut, 1999) has highlighted the process advantages of this technology using an antibiotic mixture. Their results have demonstrated the greater processing efficiency of hydrodynamic CCC in terms of volumetric yield compared to HPLC, and in addition 'taking into account the time required for purification steps before preparative HPLC, the productivity of CCC is higher than that of HPLC'.

Industrial based interest in CCC in the U.K. has led to research (Graham *et al.*, 2001) investigating the processing performance of CCC for the purification of an active pharmaceutical ingredient (API). This study investigated the initial laboratory scale

separation, primarily concerned with method development, followed by scale-up. In addition, this group have proposed estimated outputs from the pilot scale CCC machine in comparison to HPLC and have shown them to be comparable. The solvent consumption of CCC was determined to be 25% of that required for HPLC.

An economic evaluation of the Brunel laboratory scale CCC machine versus various scales of HPLC device has been proposed in terms of solvent flows and yields, together with corresponding hardware costs (Sutherland *et al.*, 1998) as shown in Table 10-1. This comparison between CCC and HPLC, in terms of operational and economic data illustrates the potential for cost savings, with respect to initial start up costs, such as hardware, e.g. columns, pumping systems, and operational costs, e.g. solvent consumption and product recovery from the eluant stream.

	Column o.d (mm)	**Flow ($mL.min^{-1}$)**	**Yield (g)**	**Hardware costs (£K)**
Analytical HPLC	1-5	1-10	<0.005	5-20
Lab prep HPLC	5-20	4-50	0.005-0.1	20-100
Pilot Prep HPLC	20-150	50-800	0.1-10	100-1,000
Lab prep CCC	3	1-10	0-10	25
Process Prep HPLC	150-1000+	800-7000+	10-100,000	1,000+

Table 10-1 Comparison between Lab prep CCC and range of HPLC scales of operation in terms of mobile phase flows, processing yields and initial hardware (capital) costs (from Sutherland *et al.*, 1998).

10.4. Performance comparisons between CCC and HPLC

Due to the observed variations in separation performance between corresponding HPLC columns, as a result of such factors as the packing procedure and differences in the physicochemical properties of the packing material used, e.g. particle diameter, a number of experimental techniques are used to evaluate their performance (Berthod and Billardello, 2000). The performance of a column can be expressed in terms of the theoretical plate

number (*N*) and selectively, methods used during the course of this project. However, due to excessive band broadening which can occur during a given separation as a result of changes in operational variables, such as increased solute loading and mobile phase flow rate, the van Deemter plot of the height equivalent to a theoretical plate (HETP or H) against mobile phase velocity aids in identifying the optimal mobile phase velocity (Section 3.4).

In solid-phase liquid chromatography, from the van Deemter plot, one can determine how well a column is packed, the quality of the packing material used, and whether the system used was correctly chosen for a given separation challenge (Scholozovà, 2000). Chromatographic studies by Scholozovà (2000) have resulted in the generation of these curves for erythromycin separations on a large scale Prochrom HPLC column (18cm x 6cm), packed using Amerchrom CG-300 (300Å) 35 micron polymer material, and operated in the reverse phase mode. The injected erythromycin mass was 20 $g.L^{-1}$ (20 $mg.mL^{-1}$), and the mobile phase composition was 45% ACN:55% phosphate buffer (pH 9; 0.2 M).

Initially, the effects of solute injection volume and mobile phase flow rate on column efficiency were studied, demonstrating a decrease in the achievable *N* with increasing flow rates, a trend observed to a lesser extent with our solute loading studies (Section 6.3). Based on these results, the H/*v* curves identified the optimal mobile phase flow rate to be 4.8 $mL.min^{-1}$, with a corresponding reduced h value of ~7. In detail, these plots over the flow rate range studied (10-145 $mL.min^{-1}$), showed a gradual increase in the H value up to 120 $mL.min^{-1}$. Above this flow rate, a steeper increase in the h value signified an increase in the band broadening, and hence a decrease in the column efficiency.

The determination of optimal mobile phase flow rate in CCC through the construction of van Deemter plots has been attempted, firstly by Menet *et al.* (1992), and then Du *et al.* (2001). Prior to the construction of van Deemter plots, due to the liquid-liquid solute partitioning mechanism by which chromatographic separations are achieved,

a pre-requisite for efficient, high resolution separations, is the attainment of a high stationary phase volume (S_f). Despite the similarity between CCC and RP-HPLC, in terms of the elution profile of our model erythromycin system, the most noticeable difference is the chromatographic dependent variable, i.e. the proportion of the column occupied by the chosen stationary phase during its operation. Considering first the CCC system, hydrodynamic studies at both scales of operation, i.e. laboratory and pilot (Sections 5.1 and 5.2) illustrate the relationship between S_f (% v/v) and $F^{0.5}$, which linearly decreases with increasing mobile phase flow.

The implications of this reduction in S_f on the generation of van Deemter plots, as discussed by Menet *et al.* (1992), is a reduction in the retention factor (k), as observed during our investigations (Figure 6-4), due to a reduced V_s/V_m term (Equation 3.10). In solid-phase chromatography this V_s/V_m term can be assumed to remain constant (packing matrix swelling or compression during operation would be negligible), hence in an efficient system, where a solute K_s remains constant, i.e. at each theoretical plate complete solute equilibrium is achieved, the corresponding retention factor (k_s) over a range of mobile phase flow rate range would remain constant.

In CCC, as a result of this variation in the k values with reductions in S_f, the generation of van Deemter plots would become ineffectual in identifying the 'u' term for a maximum *N*. Du *et al.* (2001) proposed that by fixing the stationary phase volume prior to separation, one would effectively fix the V_s/V_m term in Equation 3.10, hence enable meaningful generation of H/u plots. This technique was applied to the separation using a crude erythromycin A mixture (Sigma Chemicals), at a loading concentration of 100 $mg.mL^{-1}$ over the flow rate range 0.5 to 6 $mL.min^{-1}$ using the outer coil on bobbin 7/1 (V_c = 94.3 mL). The experimental procedure adopted, together with raw experimental data required, i.e. H and u is presented in Appendix 13.5. To ensure a fixed volume of stationary phase was maintained over the previously stated flow rate range, a minimum hydrodynamic phase equilibrium (S_f) of ~41% was achieved using the standardised method described in Section 5.2. From the generated CCC chromatograms, column efficiency was calculated using both peak width (as performed by Du *et al.*,

2001) and peak width at half height (Equation 3.14), together with linear mobile phase velocity calculated using Equation 3.32. The resulting van Deemter plot together with determined K_{EA} values (Section 3.1.2) is illustrated in Figure 10-1 and shows the general trend associated with the generated CCC van Deemter plots (Du et *al.*, 2001), i.e. the curve passes through a minimum. This minimum point corresponds to a u of 2.1 $cm.s^{-1}$ (using W_b) or 1.8 $cm.s^{-1}$ (using $W_{h/2}$), with a H_{min} value of ~4.1 cm/plate in both cases. Increasing the mobile phase velocity up to ~6 $cm.s^{-1}$ results in an increase in H up to a maximum of 10.4 cm/plate. With further increases in the mobile phase velocity the H value begins to decrease, signifying an increase in the column efficiency. In comparison in HPLC, increasing the mobile phase velocity results in a decrease in column efficiency (Scholozovà, 2000).

Focusing on the area of the plot providing the maximum efficiency, the corresponding mobile phase flow rate, calculated by rearranging Equation 3.32 in terms of the mobile phase flow (F), is 1.4 $mL.min^{-1}$ (using W_b) and 1.2 $mL.min^{-1}$ (using $W_{h/2}$). Under either of these optimal flow rates, using a K of ~0.3, determined from the corresponding CCC chromatogram (as described in Section 3.1.2), elution of the main EA fraction would occur at 48 minutes, with a column efficiency, based on the main EA peak, of ~1028 theoretical plates.

The main consideration in determining the optimal mobile flow rate for a maximum column efficiency, through the generation of the van Deemter plot in CCC method previously described, has been highlighted by Bousquet *et al.* (1991). From their experimental observations they identified that the maximum efficiency in their CCC system occurred at a flow rate around 2 $mL.min^{-1}$, and concluded that 'efficiency is better for lower flow rates and higher volumes of the mobile phase, which means for lower linear velocities'. They also identified that the phase volume ratio within the CCC coil plays an important role in column efficiency, suggesting that at an approximately equal phase volume ratio, i.e. $V_s \approx V_m$, better mass transfer may occur.

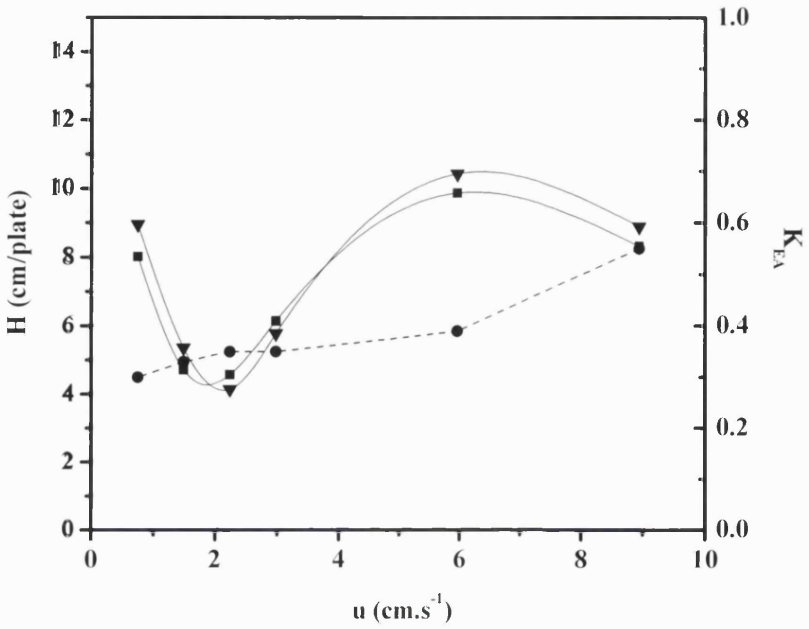

Figure 10-1 Van deemter plots for determining optimal mobile phase flow rate. h/u curves generated from *N* calculated from $W_{h/2}$ (Equation 3.30) illustrated as (■) and W_h (▼). ū calculated using Equation 3.32. Column length (L) = 47.6m (Table 2-3). (●) corresponds to K_{EA} determined as described in Section 3.1.2. Experiments performed as described in Appendix 13.5.

This proposed optimal operating situation, i.e. where it is more favourable to operate at higher mobile phase flow rates, with an increased mobile phase volume in a laboratory or industrial scale separation, would only be viable if resolution was not an important factor. Under reduced S_f conditions, i.e. a reduced volume of stationary phase available for solute partitioning, there would be a reduction in the retention factor (k), as observed during our laboratory scale studies (Section 6.2.1). This reduction in the k value indicates a reduction in the stationary phase capacity. With increased solute loadings, as discussed in Section 6.3, any further reduction in the stationary phase capacity would result in an increased degree of band broadening, with a corresponding observed decrease in column efficiency (Section 6.3.2). The consequence of this would be a detrimental loss of resolution, and hence a reduction in the purity of the target product (EA).

In conclusion, for the separation of a complex feed by CCC, where the highest resolving power of the system is required, the chosen solvent system and operating conditions must be maximised, i.e. adequate distribution of the k_s values and maximum S_f for a given set of operating conditions (mobile phase flow rate and solute loading) must be achieved.

10.5. Towards process scale separations

This section aims, if this CCC technology is to be utilised in an industrial purification scheme, to identify the safety and design issue together with environmental issues associated with the safe recovery of volatile solvents used.

Scale-up is a term usually used to describe an increase in the output of a target product from a given unit operation or process. In this work the alteration of two process variables, the mobile phase flow rate and quantity of solute injected, to optimise the throughput of erythromycin through our CCC column have been examined. This led to a ~17 fold increase in throughput over the initial conditions. To increase throughput still further, it may be possible to perform multiple injections of the feed material onto the column. For this to be viable, detailed knowledge of the distribution ratios and thus the retention times of the various solutes would be required to develop a suitable injection schedule. The major considerations in this case would firstly be the critical level of any impurity build-up in the stationary phase before it is necessary to pump out and refill the CCC column, and any reduction in the phase volume ratio (stationary phase stripping) between subsequent feed injections, which, from a process robustness, and, hence, validation point of view would be unacceptable (Graham *et al.*, 2001). It is therefore speculated that this may increase throughput further by a factor of 2 to 3.

For further scale-up one could look at redesigning the CCC machine itself. This could be achieved by increasing either the column length or bore. Compared to conventional liquid chromatography, where solute separation or exchange occurs at the surface of the solid support, in CCC separation occurs throughout the entire volume of the stationary phase. This has the benefit of enabling the CCC column to have a higher

capacity (loadability) than a comparable LC column. Therefore, increasing the volume by either increasing the column length or bore will increase the retention still further (Sutherland *et al.*, 2001b), provided that the mechanical engineering issues can be overcome.

Finally, as with the scale-up of any operation, there are a number of other important factors that must be considered in parallel to the development of the process. In the case of large scale CCC these will include the safe design, installation and operation of the rotating equipment, the minimisation of explosion risks when using organic solvents and the simplification of the solvent system used in order to aid recovery and recycling and minimise the environmental impact of the process.

11. Conclusions and future work

11.1. Conclusions

The overall objective of this research has been to evaluate CCC as a novel chromatographic technique for the fractionation and recovery of the polyketide antibiotic, erythromycin A, from its structurally similar analogues in a model and broth-derived feed, at the laboratory and pilot scales. With the industrial scale application of this technology in mind, a number of operational issues were addressed experimentally.

Firstly, due to the complexity of solvent system selection for a given purification challenge, the research, as discussed in Chapter 4, has demonstrated the ability of a generic method development strategy in rapidly identifying an effective medium polarity quaternary phase system consisting of hexane/ethyl acetate/methanol/water (1.4/2.0/2.0/1.0 v/v) and isocratic, reverse phase, run mode. At a mobile phase flow rate of 2 $mL.min^{-1}$, the separation and recovery of EA was achieved in 30 minutes with an EA purity of 100% (w/w) and total solute yield of 100% (w/w). Under these conditions, throughput was predicted to be 0.0058 $kg.day^{-1}$.

Based on the successful fractionation of EA from its structurally similar analogues under the isocratic conditions identified, the second project aim was two fold. Firstly, using the 'model system', as discussed in Chapter 6, in order to increase process throughput, the operating variables, mobile phase flow rate and solute loading, were studied in terms of their effects on CCC performance. The results successfully identified, over the range of variables studied, the upper operating limits at which the separation would be considered viable, i.e. an acceptable level of EA purity achieved. Under optimised operating conditions a maximum estimated throughput of 0.097 $kg.day^{-1}$, with a EA purity of 97% (w/w) and total solute yield of 100% (w/w) was achieved at a solute

loading of 0.6 g and a mobile phase flow rate of 8 $mL.min^{-1}$. Secondly, the application of the CCC system, i.e. the chosen solvent system and run mode, to real broth-derived feed streams, as discussed in Chapter 7, identified the degree of broth impurity removal required to ensure reproducible separation performance, in terms of reproducible K_{EA} values, that being operating using a back extract feed. The maximum predicted throughput was calculated to be 0.029 $kg.day^{-1}$, at a solute loading of 1000 mg and a mobile phase flow rate of 2 $mL.min^{-1}$.

This research, as discussed in Chapter 8, then addressed firstly the scalability of the separation, showing it to be both linear and feasible over a range of operating conditions, and has demonstrated the first application of a 'predictive scale-up model' to both 'model' and 'real' systems. In addition, a modified predictive scale-up equation has been proposed and experimentally verified, to account for 'stationary phase stripping' during extended operation with subsequent feed injections. Predictions of EA elution time at the pilot scale were accurate, for the model and real systems, to within 5% and ~7% respectively. Changes in the mobile phase flow rate and injection volume could also be accounted for to within ~13% for the model system, and ~10% for the real system.

The need for an accurate method to rapidly identify the trade-offs between product purity and solute yield, as discussed in Chapter 9, has been addressed by the first application of 'fractionation diagram theory' to CCC, resulting in accurate cut-point determination for a required degree of product purity and yield. The results demonstrate that firstly the back extract feed enables, upon processing, the highest degree of EA purity to be achieved (99% w/w). With increasing mobile phase flow rate at the laboratory scale, for a corresponding total solute yield (92.7% w/w) a 12% reduction in EA purity was observed over the 2 $mL.min^{-1}$ separation. With increasing solute loading at the analytical scale over the loading range investigated (100 – 1000 mg), a 6% decrease in achievable EA purity was observed.

At the pilot scale, results demonstrate that over the flow rate (10 – 40 $mL.min^{-1}$) and solute loading (10 and 100 mL) ranges, there is a 2.4% and 2% decrease in EA purity.

11.2. Future Work

The proposed generic method development strategy, as shown during the course of this study, did successfully identify a robust phase system and run mode. However, further research in this area of method development should focus on further optimisation of the solvent system, with the primary goals being to:

- Increase process performance, by increasing the achievable resolution between the target product and it contaminants. The means by which this could be achieved would be to increase the distribution ratio of the target product, focussing it around the K = 1 point.
- From an environment and process safety standpoint, due to the large volumes of organic solvents used, solvent system simplification should be studied, ensuring that a corresponding level of EA purification to that achieved using the current solvent system is maintained. As observed during our initial partition studies, the distribution of the erythromycin molecule is greatly affected by aqueous phase pH, and hence the application of a pH gradient may yield an acceptable and comparable separation. However, a number of requirements, such as phase settling time and hence the degree of the stationary phase retention would need to be determined, in addition to other process issues, such as the process scalability, predictions of product elution and the ability to process broth-derived feed streams, if it were to be a viable option.

- At the laboratory scale, with the chosen phase system, all studies were performed using a nominal coil volume of 100 mL, thus limiting, at any one time, the mass injected onto the coil due to system capacity limitations. To increase product throughput still further, whilst maintain an acceptable level of product purity, the increase in coil volume and hence stationary phase capacity should be investigated.
- For the real system studies, research could focus on the use of *Sacchropolyspora erythraea* strains that over express EA, so as to vary the product to contaminant ratio levels, providing more realistic industrial process conditions. In parallel, future work should further look at the application/validation of the 'Fractionation diagram theory' with these complex feed streams over a wider range of operating variables.
- From pilot scale studies performed, this research has demonstrated the potential of the technology for scale-up, both with model and real systems. The applied predictive scale-up model has been experimentally verified, but due to financial and time constraints on the project, detailed evaluation of both the pilot scale CCC machine, and hence the model, was not possible. Further pilot scale research should therefore focus on validating the predictive scale-up model over a wider range of process variables, such as solute loadings, multiple feed injections and mobile phase flow rates (S_f dependent). In addition the model could be developed further to enable a complete process scale scenario to be planned by predicting the distribution ratio of the target solute in a given phase system, and from this product elution times over a range of realistic operating variables at all scales of operation.
- Engineering and safety analysis of the use of the pilot/process scale CCC machines in industry.

12. References

Acton, N., Klayman, D.L., Rallman, I.J., and Novotny, J.F. (1986). Isolation of artemisinin (quinghaosu) and its separation from artemisitene using the Ito multilayer coil separator-extractor and isolation of arteannium B, *J. of Chromatog.*, **355**: 448-450.

Adams, D.A. (1971). Apparatus for providing energy communication between a moving and stationary terminal. U.S Patent, no. 3,586,413.

Berthod, A., and Armstrong, D.W. (1988). Centrifugal partition chromatography for preparative sample purification and partition-coefficient determination, *J. of Liq. Chromatog.*, **11(6)**: 1187-1204.

Berthod, A. (1991). Practical approach to high-speed counter-current chromatography. *J. of Chromatog.*, **530**: 677-693.

Berthod, A., Talabardon, K., Caravieelhes, S., and De Bellefon, C. (1998). Original use of the liquid nature of the stationary phase in counter-current chromatography – II. A liquid-liquid reactor for catalytic reactions, *J. of Chromatog. A.*, **828**: 523-530

Berthod, A., and Billardello, B. (2000). Test to evaluate countercurrent chromatographs – Liquid stationary phase retention and chromatographic resolution, *J. of Chromatog. A.*, **902**: 323-335.

Bousquet, O., Foucault, A.P., and Le Goffic, F. (1991). Efficiency and resolution in countercurrent chromatography, *J. Liq. Chromatog.*, **14(18)**: 3343-3363.

Braithwaite A., and Smith, F.J. (1996). Chromatographic methods, 5th Ed. Chapman and Hall, Great Britain.

Brisson-Noel, A., Trieu-Cuot, P., and Courvalin, P. (1988). Mechanism of action of spiramycin and other macrolides, *J. Antimicrobial Chemother.*, **22(Supp. B)**: 13-33.

Brill, G.M., McAlpine, J.B., and Hochlowski, J.E. (1985). Use of coil planet centrifuge in the isolation of antibiotics, *J. of Liq. Chromatog.*, **8(12)**: 2259-2280.

Brockmann, H., and Henkel, W. (1950). Pikromycin ein bitter schmerckendes antibiotikum aus Actinomycenten, *Chem. Ber.*, **84**: 284-288.

Brown, L. (1998). Personal communication. AECS, P.O Box 80, Bridgend, Wales, U.K. CK31 4XZ.

Carreras, C.W., and Santi D.V. (1998). Engineering of modular polyketide synthases to produce novel polyketides, *Current Opin. in Biotechnol.*, **9**, 403-411.

Carrington, R. (1986). A review of antibiotic isolation techniques: 45-58. In: Stowell, J.D., Bailey, P.J., and Winstanley, D.J, eds. Bioactive microbial products 3: Academic Press, London, U.K.

Chen, R.H., Hochlowski, J.E., McAlpine, J.B., and Rasmussen R.R. (1988). Separation and purification of macrolide antibiotics using the Ito Multi-Layer Horizontal Coil Planet Centrifuge, *J. Liq. Chromatog.*, **11**: 191-201.

Conway, W.D., and Ito, Y. (1984). Phase distribution of liquid-liquid systems in spiral and multilayer helical coils on a centrifugal countercurrent chromatograph. Presented at Pittsburgh Conference, Atlantic City, N.J., U.S.A.

Conway, W.D. (1990). Counter Current Chromatography: Apparatus, Theory and Applications: VCH Publishers, New York, U.S.A.

Cornish, R.E., Archibald, R.C., Murphy, E.A., and Evans, H.M. (1934). Purification of vitamins, *Ind. Eng. Chem.*, **26**: 397-406.

Coulson, J.M., and Richardson, J.F. (1991). Drying, Chapter 16: 690-744. From Chemical Engineering, Vol 2, 4th Ed. Pergamon Press Ltd, Oxford, England.

Danielson, N.D., Holeman, J.A., Bristol, D.C., and Kirzner D.H. (1993). Simple methods for the qualitative identification and quantitative determination of macrolide antibiotics, *J. Pharmaceut. and Biomed. Anal.*, **11(2)**: 121-130.

Davies, J.L., Baganz, F., Ison, A.P., Lye, G.J. (2000). Studies on the interaction of fermentation and microfiltration operations: Erythromycin recovery from Saccharopolyspora erythraea fermentation broths, *Biotechnol. Bioeng.*, **69(4)**: 429-439.

Drogue, S., Rolet, M. –C., Thiébaut, D., and Rosset, R. (1991). Improvement of on-line detection in high-speed counter-current chromatography: UV absorptiometry and evaporative light scattering detection, *J. of Chromatog.*, **538**: 91-97.

Du, Q., Wu, C., Quian, P., Ito, Y. (1999). Relationship between flow rate of the mobile phase and retention of the stationary phase in counter-current chromatography, *J. of Chromatog. A*, **835**: 231-235.

Du, Q., Wu, C., Ito, Y. (2000). Van deemter plots in high-speed countercurrent chromatography with a fixed volume of stationary phase, *J. Liq. Chrom. & Rel. Technol.*, **23(19)**: 2929-2935.

Elks, J., and Ganellin, C.R. (eds) (1991). Dictionary of drugs: Chapman and Hall, London, U.K.

Ford, J.H., Prescott, G.C., Hinman, J.W., and Louis Caron, E. (1953). Colorimetric determination of erythromycin, *Anal. Chem.*, **25(8)**: 1195-1198.

Foucault, A.P., and Chevolot, L. (1998). Review - Counter-current chromatography: instrumentation, solvent selection and some recent applications to natural product purification, *J. of Chromatog. A*, **808**: 3-22.

Giddings, J.C. (1965). Dynamics of chromatography: Part I, Principles and theory. Marcel Dekker, New York, U.S.A.

Gilbert, M., Morosoli, R., Shareck, F., and Kluepfel, D. (1995). Production and secretion of proteins by Streptomycetes. *Critical reviews in biotechnology*. **15(1)**: 13-39.

Goodfellow, M., Williams, S.T. and Mordarski, M. (1983). The biology of the Actinomycetes. Academic Press, London.

Graham, A.S., McConvey, I.F., and Shering, P. (2001). An evaluation of the performance of a preparative CCC machine for the separation of an active pharmaceutical ingredient. *J. Liq. Chrom. & Rel. Technol.*, **24(11 & 12)**: 1811-1825.

Gunawardana, G., and McAlpine, J. (1999). Preparative scale separations of natural products by countercurrent chromatography: 251-252. In: Menet J-M and Thiébaut D, eds. Countercurrent chromatography. Chromatographic Science Series, Vol. 82. : Marcel Dekker, New York, U.S.A.

Hahn, F.E. (1967). Erythromycin and oleandomycin. In: Antibiotics: Mechanism of action. Vol 1. eds Gottlieb, D., and Shaw, P.D. Springer-Verlag, New York, U.S.A.

Harada, K., Kimura, I., Yoshikawa, A., Suzuki, M., Kakazawa, H., Hattori, S., Komori, K., and Ito, Y. (1990). Structural investigation of the antibiotic sporaviridin. Preparative- scale purification of sporaviridin components by HSCCC, *J. Liq. Chromatog.*, **13**: 2373-2388.

Harada, K., Suzuki, M., Kato, A., Fujii, K., Oka, H., and Ito, Y. (2001). Separation of WAP-8294A, a novel anti-methicillin resistance Staphylococcus aureus antibiotic, using high-speed counter-current chromatography, *J. of Chromatog. A.*, **932**: 75-81.

Hata, T., Sano, Y., Ohki, N., Yokoyama, Y., Matsumae, A., and Ito, Y. (1953). Leucomycin, a new antibiotic. *J. Antibiot. Ser. A.*, **6**: 87-89.

Hermans-Lokkerbol, A. C. J., Hoek, A. C., and Verpoorte, R. (1997). Preparative separation of bitter acids from hop extracts by centrifugal partition chromatography, *J. of Chromatog. A.*, **771(1&2)**: 71-79.

Hilderbrand, J.H., and Scott, R.L. (1962). Regular Solutions. Prentice Hall. N.J. U.S.A.

Hochlowski, J.E., Mullally, M.M., Brill, G.M., Whittern, D.N., Buko, A.M., Hill, P., and McAlpine, J.B. (1991). Dunaimycins, a new complex of spiroketal 24-membered macrolides with immunosuppressive activity. II. Isolation and elucidation of structures, *J. Antibiot.*, **39**: 1318-1330.

Holt, J.G., Krieg, N.R., Sneath, P.H.A., Staley, J.T., and Williams, S.T. (1994). Bergey's manual of determinative bacteriology, 9th edn. Williams and Wilkins, Baltimore, U.S.A.

Ito, Y., Harada, R., Weinstein, M.A., Aoki, I., Harada, R., Kimura, E., and Nunogaki, K. (1966). The coil planet centrifuge, *Nature*, **212**: 985-987.

Ito, Y., and Bowman, R.L. (1970). Countercurrent chromatography: Liquid-liquid partition chromatography without a solid support, *Science*, **167**: 281-283.

Ito, Y., Suaudeau, J., and Bowman, R.L. (1975). New flow-through centrifuge without rotating seals applied to plasmapheresis, *Science*, **189**: 999-1000.

Ito, Y., and Bowman, R.L. (1978). Preparative countercurrent chromatography with horizontal flowthrough coil planet centrifuge, *J. of Chromatog.*, **147**: 221-231.

Ito, Y., Carmeci, P., and Sutherland, I.A. (1979). Nonsychronous flow-through coil planet centrifuge applied to cell separation with physiological solution, *Anal. Biochem.*, **94**: 249-252.

Ito, Y., Sandlin, J., and Bowers, W.G. (1982). High speed preparative countercurrent chromatography (CCC) with a coil planet centrifuge, *J. of Chromatog.*, **244**: 247-258.

Ito, Y., and Bhatnagar, R. (1984). Improved scheme for preparative countercurrent chromatography with a rotating coil assembly. *J. Liq. Chromatog.* 7: 257-273.

Ito, Y. (1991). Review – Recent advances in counter-current chromatography, *J. of Chromatog.*, **538**: 3-25.

Ito, Y. (1992). Speculation on the mechanism of unilateral hydrodynamic distribution of two immiscible solvent phases in the rotating coil, *J. Liq. Chromatog.*, **15(15&16)**: 2639-2675.

Ito, Y. (1996). Principle, apparatus, and methodology of high-speed countercurrent chromatography: 3-44. In: eds. Ito, Y., and Conway, W.D. High speed countercurrent chromatography, **132.** Chemical analysis series, John Wiley & Sons, New York, U.S.A.

Jantzen, E. (1932). Das frackitonierte destillieren und dar fractioerte verteilen als methoden zur tiennug von staffgemischen, Verlag Chemie, Berlin.

Kanfer, I., Skinner, M.F., and Walker, R.B. (1998). Review – Analysis of macrolide antibiotics, *J. of Chromatog. A*. **812**: 255-286.

Kao, C.M., Katz, L., Khosla, C. (1994). Engineering biosynthesis of a complete macrolactone in a hetrologous host, *Science*, **265**: 509-512.

Kavangh, F., and Dennin, L.J. (1963). Analytical microbiology, Academic Press, New York, U.S.A.

Kendall, D., Booth, A.J., Levy, M.S., Lye, G.J. (2001). Separation of supercoiled and open-circular plasmid DNA by liquid-liquid counter-current chromatography, *Biotech. Letters*, **23**: 613-619.

Kies, M.W., and Davis, P.L. (1951). A new procedure for fractionation of mixtures by solvent distribution, *J. Biol. Chem.*, **189**: 637-650.

Knight, M., Ito, Y., Sandlin, J.L., and Kask, A.M. (1986). Preparative purification of peptides by countercurrent chromatography on the Ito coil planet centrifuges, *J. of Liq. Chromatog.*, **9**: 791-802.

Labeda, D.P. (1987). Transfer of the type strain of *Streptomyces erythreus* (Walksman, 1923) Waksman and Henrici (1948) to the genus *Sacchropolyspora* (Lacey and Goodfellow, 1975) as *Sacchropolyspora erythraea sp-nov*, and designation of a neotype strain for *Streptomyces erythreus*, *Int. J. of Syst. Bac.*, **37(1)**: 19-22.

Liew, M.K.H., Fane, A.G., and Rogers, P.L. (1997). Fouling of microfiltration membranes by broth-free antifoam agents, *Biotechnol. Bioeng.*, **56**: 89-98.

Lye, G.J., and Woodley, J.M. (1999). Application of *in situ* product removal techniques to biocatalytic processes, *Trends Biotechnol.*, **17**, 395-402.

Maillard, M., Marston, A., and Hostettmann, K. (1996). High-speed countercurrent chromatography of natural products: 179-223. In: eds. Ito, Y., and Conway, W.D. High speed countercurrent chromatography, **132.** Chemical analysis series, John Wiley & Sons, New York, U.S.A.

Marston, A., Hostettmann, K. (1994). Countercurrent Chromatography as a Preparative Tool – Applications and Perspectives. *J. Chromatog. A.*, **658**: 315-341.

Martin, A.J.P., and Synge, R.L.M. (1941). A new form of chromatogram employing two phases, *Biochem. J.*, **35**: 1358-1368.

Martin, D.G., Biles, C., and Peltonen, R.E. (1986a). Countercurrent chromatography in the fractionation of natural products, *Amer. Lab.*, **18(10)**: 21-26.

Martin, D.G., Peltonen, R.E., and Nielsen, J.W. (1986b). Preparative resolution of an actinomycin complex by countercurrent chromatography in the coil planet centrifuge, *J. of Antibiot.*, **39**: 721-723.

Maryutina, T.A., Fedotov, P.S., and Spivakov, Ya. B. (1999). Application of countercurrent chromatography in inorganic analysis: 192-219. In: Menet J-M and Thiébaut D, editors. Countercurrent chromatography. Chromatographic Science Series, Vol. 82. Marcel Dekker. New York: U.S.A.

McGuire, J.M., Bunch, R.L., Anderson, R.C., Bonz, H.E., Flyon, E.H., Powell, H.M., and Smith, J.W. (1952). "Llotycin" a new antibiotic, *Antibiot. Chemother.*, **2**: 281-283.

Menet, J. –M., Rolet, M. –C., Thiebaut, D., Rosset, R., and Ito, Y. (1992), Fundamental chromatographic parameters in countercurrent chromatography: influence of the volume of stationary phase and the flow-rate, *J. Liq. Chromatog.*, **15(15&16)**: 2883-2908.

Menet, J. –M., and Thiebaut, D. (1999). Preparative purification of antibiotics for comparing hydrostatic and hydrodynamic mode counter-current chromatography and preparative high-perfomance liquid chromatography, *J. of Chromatog. A.*, **831**: 203-216.

Mercardo, T.I., Ito, Y., Strickler, M.P., and Ferrans, V.J. (1988). Countercurrent chromatography of an anti-trypanosomal factor from Psuedomonas fluorescens, *J. Liq. Chromatog.*, **11**: 203-226.

Ngiam, S.H., Zhou, Y.H., Turner, M.K., Titchener-Hooker, N.J. (2001). Graphical method for calculation of chromatographic performance in representing the trade-off between purity and recovery, *J. of Chromatog. A.* **937**: 1-11.

Oka, F., Oka, H., and Ito, Y. (1991). Systematic search for suitable two-phase solvent systems for high-speed counter-current chromatography, *J. of Chromatog.*, **538**: 99-108.

Oka, H., Ikai, Y., Hayakawa, J., Harada, K., Nagase, K., Suzuki, M., Nakazawa, H., and Ito, Y. (1992). Discrepancy between the theoretical plate number (N) and peak resolution (Rs) for optimizing the flow rate in countercurrent chromatography, *J. of Liq. Chromatog.*, **15(15&16)**: 2707-2719.

Oka, H., Ikai, Y., Hayakawa, J., Harada, K.-I., Suzuki, M., Shimizu, A., Hayashi, K., Takeba, H,, Nakazawa, Y., and Ito, Y. (1996). Separation of ivermectin components by high-speed counter-current chromatography, *J. of Chromatog. A.*, **723**: 61-68.

Oka, H., Harada, K., Ito, Y., and Ito, Y. (1998). Review - Separation of antibiotics by counter-current chromatography, *J. Chromatog. A.*, **812**: 35-52.

Oka, H., Harada, K., Suzuki, M., and Ito, Y. (2000). Separation of spiramycin components using high-speed counter-current chromatography, *J. of Chromatog. A.*, **903**: 93-98.

Paesen, J., Khan, K., Roets, E., and Hoogmartens, J. (1994). Study of the stability of erythromycin in neutral and alkaline solutions by liquid chromatography on poly(styrene-divinylbenzene), *Int. J. of Pharmaceu.*, **113**: 215-222.

Pinnert-Sindico, S., Ninet, L., Preud'homme, J., and Coar, C. (1955). A new antibiotic, Spiramycin, *Antibiot. Annu.*, **55**: 724-727.

Queener, S.W., Day, L.E., and Gunsalus, I.C. (1986). The Bacteria: A Treatise on Structure and Function, Vol IX: Antibiotic producing Streptomyces. Academic Press, London, U.K.

Reichardt, C. (1988). Solvents and solvent effects. In: Orgainc Chemistry, VCH, Weinheim.

Richardson, P., Hoare, M., Dunnill, P. (1989). Optimization of fractional precipitation for protein purification. *Chem. Eng. Res. Des.*, **67**: 273- 277.

Richardson, P., Hoare, M., Dunnill, P. (1990). A new biochemical engineering approach to the fractional precipitation of proteins, *Biotechnol. Bioeng.*, **36**: 354-366.

Rohrschneider, L. (1973). Solvent characterization by gas-liquid partition coefficients of selected solutes, *Anal. Chem.*, **45**: 1241-1247.

Sandlin, J.L., and Ito, Y. (1985). Large-scale preparative countercurrent chromatography with a coil planet centrifuge, *J. of Liq. Chromatog.*, **8**: 2153-2172.

Schaufelberger, D.E., McCloud, T.G., and Beutler, J.A. (1991). Laser-light-scattering detection for high-speed counter-current chromatography, *J. of Chromatog.*, **538**: 87-90.

Schaufelberger, D.E. (1996). Theoretical aspects of countercurrent chromatography: 45-70. In: eds. Ito, Y., and Conway, W.D. High speed countercurrent chromatography, **132.** Chemical analysis series, John Wiley & Sons, New York, U.S.A.

Schoenmakers, P.J. (1986). Optimization of chromatographic selectivity – a guide to method development. Elsevier Science Publishers B.V. Amsterdam, Netherlands.

Scholtzovà, A. (2000). The scale up and modelling of high performance liquid chromatography. PhD Thesis. University of London.

Schuler, M.L. (1987). Bioprocess engineering: From Encyclopedia of Physical Science and Technology, **2**, ed. Meyer, R.A., Academic Press, Orlando, U.S.A.

Sherwood, D. (1996). GMP and quality control: 329-346. In: ed Verall, M.S. Downstream Processing of Natural Products. John Wiley & Sons. England.

Shibusawa, Y.; and Ito, Y. (1998). Purification of proteins with aqueous two-phase solvent systems by countercurrent chromatography, *Prep. Biochem. & Biotechnol.*, **28(2)**: 99-136.

Sobin, B.A., English, A.R., and Celmer, W.D. (1955). PA 105, a new antibiotic, *Antibiot. Annu.*, **56**: 827-830.

Stecher, P.G. (1968). The Merck Index, 8th ed., Merck and Co.

Sutherland, I.A., Brown, L., Forbes, S., Games, G., Howes, D., Hostettman, K., McKerrel, E.H., Marston, A., Wheatley, D., Wood, P. (1998). Countercurrent chromatography (CCC) and its versatile application as an industrial purification and production process, *J. Liq. Chrom. & Rel. Technol.*, **21(3)**: 279-298.

Sutherland, I.A. (2000a). Relationship between retention, linear velocity and flow for counter-current chromatography, *J. of Chromatog. A*, **886**: 283-287.

Sutherland, I.A., Muytjens, J., Prins, M., and Wood, P. (2000b). A new hypothesis on phase distribution in countercurrent chromatography, *J. Liq. Chrom. & Rel. Technol.*, **23(15)**: 2259-2276.

Sutherland, I.A., Brown, L., Graham, A.S., Guillon, G.G., Hawes, D., Janaway, L., Whiteside, R., Wood, P. (2001a). Industrial scale-up of countercurrent chromatography: Predictive scale-up, *J. of Chromatographic Science*, **39**: 21-28.

Sutherland, I.A., Booth, A.J., Brown, L., Kemp, B., Kidwell, H., Games, D., Graham, A.S., Guillon, G.G., Hawes, D., Hayes, M., Janaway, L., Lye, G.J., Massey, P., Preston, C., Shering, P., Shoulder, T., Strawson, C., and Wood. P. (2001b). Industrial scale-up of countercurrent chromatography, *J. Liq. Chrom. & Rel. Technol.*, **24(11 & 12)**: 1533-1553.

Synder, L.R., and Kirkland, J.J. (1979). Introduction to Modern Liquid Chromatography, 2nd ed. John Wiley & Sons. New York. U.S.A.

Tanimura, T., Pisano, J.J., Ito, Y., and Bowman, R.L. (1970). Droplet countercurrent chromatography, *Science*, **169**: 54-56.

Tavel, P.V., and Bollinger, W. (1968). Die frakionierung von serumproteinen mit flussingen phasenpaaren einc zentrifuge fur gengenstromverteilung, *Helv. Chim. Acta.*, **51**: 278-293.

Van Der Wielen, L.A.M., Potters, J.J.M., Straathof, A.J.J., and Luyben., K.Ch.A.M. (1990). Integration of bioconversion and continuous product separation by means of countercurrent adsorption, *Chemical Engineering Science*, **45**: 2397-2404.

Verrall, M.S. (1992). Liquid-liquid partitioning in the pharmaceutical industry. In: ed. Thornton, J.D. Science and practice of liquid-liquid extraction – Process chemistry and extraction operations in the hydrometallurgical, nuclear, pharmaceutical, and food industries, Vol. 2: Clarendon Press, Oxford, U.K.

Wang-Fan, W., Küsters, E., Lohse, O., Mak, C., and Wang, Y. (1999). Application of centrifugal counter-current chromatography to the separation of macrolide antibiotic analogues, I. Selection of solvent systems based on solubility and partition coefficient investigations, *J. of Chromatog. A*, **864**: 69-76.

Wang-Fan, W., Küsters, E., Mak, C., and Wang, Y. (2001). Application of centrifugal counter-current chromatography to the separation of macrolide antibiotic analogues, III. Effects of flow-rate, mass load and rotation speed on the peak resolution, *J. of Chromatog. A*, **925**: 139-149.

Wood, P.L., and Sutherland, I.A. (2001). Mixing, settling, and the movement of the interface between the mobile and stationary phases in CCC, *J. Liq. Chrom. & Rel. Technol.*, **24(11&12)**: 1699-1710.

Wood, P.L. (2002). Personal Communication. Brunel Institute for Bioengineering, Brunel University, Uxbridge, UB8 3PH, U.K.

Zhang, W., Park, B.G., Chang, Y.K., Chang, H.N., Yu, X.J., Yuan, Q. (1998). Factors affecting membrane fouling in filtration of Saccaromyces cerevisiae in an internal ceraminfilter bioreactor, *Bioproc. Eng.* **18**: 317-322.

13. Appendices

13.1. Calibration curves

This section provides calibration curves for the colorimetric and HPLC assays used for the construction of mass balances and identification of erythromycin analogues. All assays were performed in triplicate with the average value used in all cases.

13.1.1. Colorimetric calibration curves

Presented in Figures 13-1 and 13-2 are typical calibration curves for the initial equilibrium distribution studies (Section 4.1.1) and CCC studies (Section 4.1.3.2 and Section 6) respectively. Experiments performed as described in Section 2.3.3.4.1.

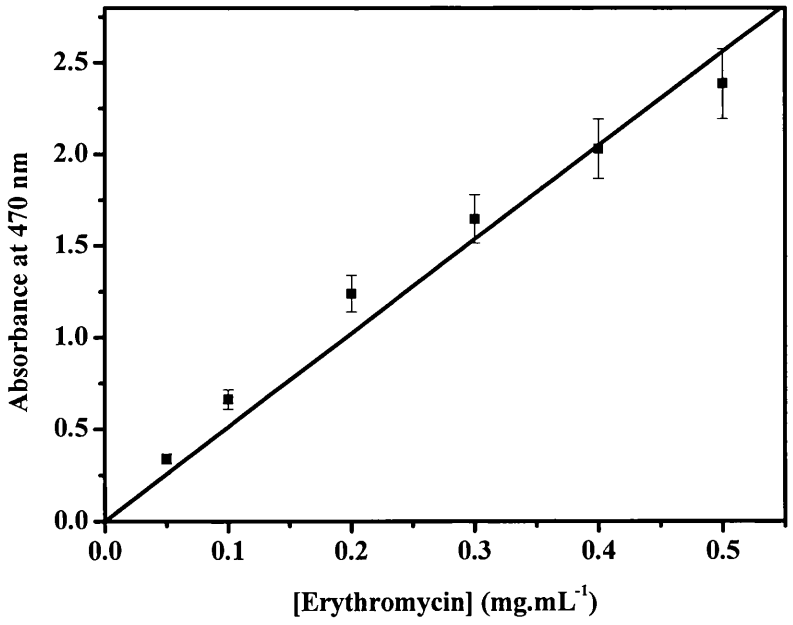

Figure 13-1 Typical calibration curve for quantification of total erythromycin using the colorimetric sulphuric acid assay as described in Section 2.3.3.4.1 for use in equilibrium distribution studies (Section 4.1.1). Line fitted by linear regression; [Erythromycin] = Abs/5.1195 (R^2 = 0.994).

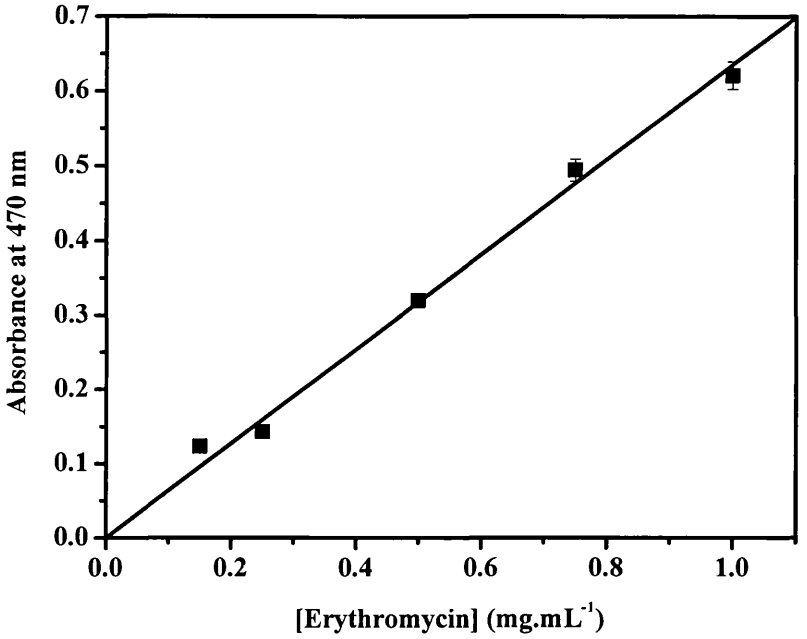

Figure 13-2 Typical calibration curve for quantification of total erythromycin using the colorimetric sulphuric acid assay as described in Section 2.3.3.4.1 for use in CCC studies (Sections 4.1.3.2 and 6). Line fitted by linear regression; [Erythromycin] = Abs/0.635 (R^2 = 0.997).

13.1.2. HPLC calibration curves

Figure 13-3(a) to (d) illustrates typical HPLC calibration curves constructed for the different erythromycin analogues. Experiments performed as described in Section 2.3.3.4.2.

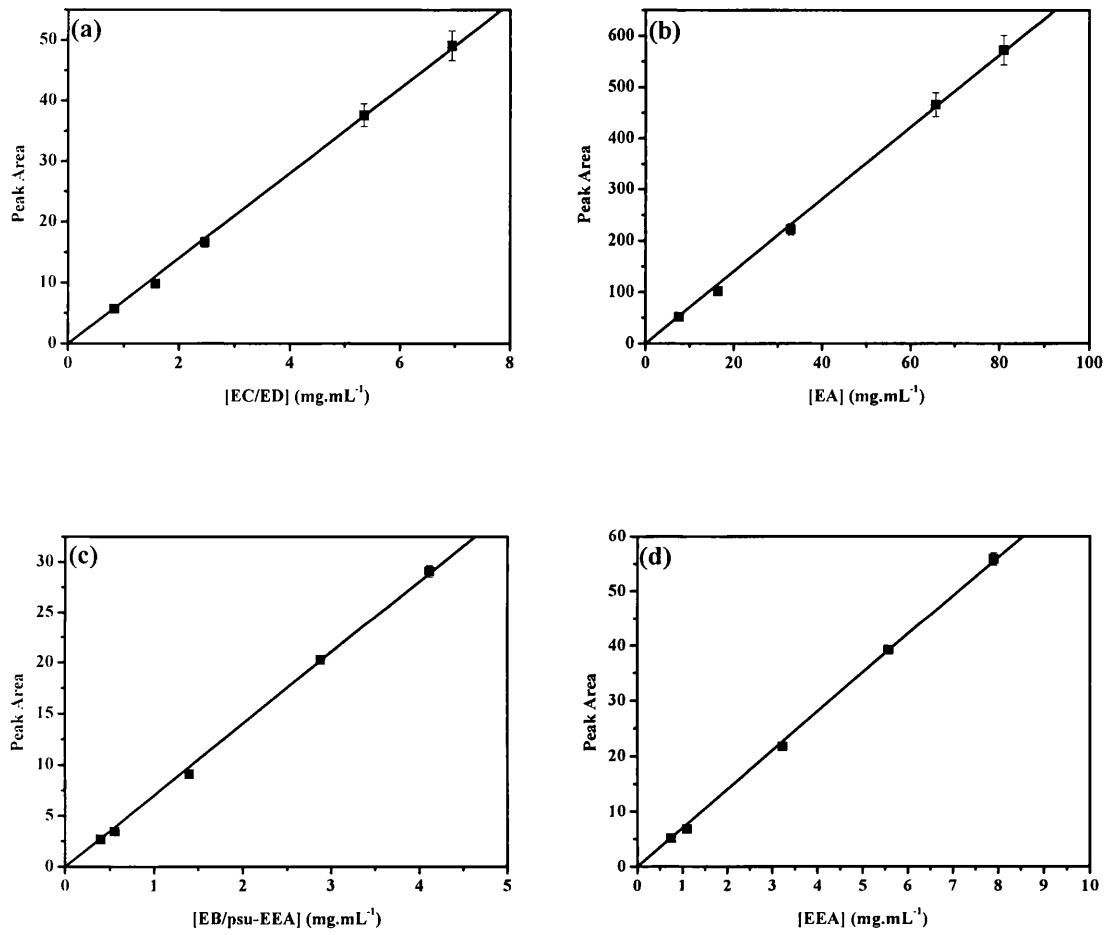

Figure 13-3 Typical calibration curves for quantification and identification of the various erythromycin using the HPLC assay as described in Section 2.3.3.4.2 for use in CCC studies (Sections 4.1.3.2, 6, 7 and 8). All lines fitted by linear regression, with equation of lines and the correlation coefficients (R^2) being as follows: (a) = [EC/ED] = Abs/7.008 (R^2 = 0.997); (b) [EA] = Abs/7.031 (R^2 = 0.999); (c) [EB/psu-EEA] = Abs/7.009 (R^2 = 0.999); (d) [EEA] = Abs/7.016 (R^2 = 0.999).

13.2. Calculation of Rohrschneider solvent system polarity

The procedure for the generation of the Rohrschneider polarity indexing scheme for the range of phase systems studied during the initial method development is presented in stages with the corresponding raw data.

STAGE 1

The first stage involves the determination of percentage compositions of solvents from the corresponding integer ratios, with the results are presented in Table 13-1.

Phase system number	Phase system integer ratios				Total	Percentage composition			
	Hex	EtOAc	MeOH	H_2O		Hex	EtOAc	MeOH	H_2O
1	1.4	0.1	0.5	1.0	3	46.7	3.3	16.7	33.3
2	1.4	0.6	1.0	1.0	4	35.0	15.0	25.0	25.0
3	1.4	4.5	1.0	1.0	7.9	17.7	57.0	12.7	12.7
4	1.4	0.6	3.5	1.0	6.5	21.5	9.2	53.9	15.4
5	1.4	2.0	0.1	1.0	4.5	31.1	44.4	2.2	22.2
6	1.4	2.0	2.0	1.0	6.4	21.9	31.3	31.3	15.6
7	1.4	2.0	3.5	1.0	7.9	17.7	25.3	44.3	12.7
8	1.4	0.6	2.0	1.0	5	28.0	12.0	40.0	20.0
9	1.4	0.6	1.0	1.0	4	35.0	15.0	25.0	25.0

Table 13-1 Raw data of percentage compositions of individual solvents in the quaternary phase system used during method development studies.

STAGE 2

The next stage involves the determination of the pure solvent polarities based on the volumetric composition of the individual solvents from corresponding solvent fraction (the integer ratios), together with the Rohrschinder pure solvent polarity values (P′) provided in Table 4-2, with the data presented in Table 13-2.

	Volumetric composition (8 mL)				Pure solvent polarity				
Phase System	**Hex**	**EtOAc**	**MeOH**	**H_2O**	**Hex**	**EtOAc**	**MeOH**	**H_2O**	**Solvent mix polarity**
1	3.7	0.3	1.3	2.7	0.4	1.2	6.8	27.2	43.6
2	2.8	1.2	2.0	2.0	0.3	5.3	10.2	20.4	44.2
3	1.4	4.6	1.0	1.0	0.1	20.1	5.2	10.3	43.7
4	1.7	0.7	4.3	1.2	0.2	3.3	22.0	12.6	45.9
5	2.5	3.6	0.2	1.8	0.3	15.6	0.9	18.1	42.9
6	1.8	2.5	2.5	1.3	0.2	11.0	12.8	12.8	44.7
7	1.4	2.0	3.5	1.0	0.1	8.9	18.1	10.3	45.5
8	2.2	1.0	3.2	1.6	0.2	4.2	16.3	16.3	45.1
9	2.8	1.2	2.0	2.0	0.3	5.3	10.2	20.4	44.2

Table 13-2 Raw data of volumetric composition of individual solvents in the quaternary phase system used during method development studies with a system volume of 8 mL, together with calculated pure solvent polarities and the resulting solvent mixture polarity. Pure solvent polarities calculated using Equation 4.1.

13.3. Stationary phase retention data

This section illustrates the method by which raw volumetric data was collated to enable the construction of stationary phase retention diagrams presented in Chapter 5. Table 13-3 is a representative data collection chart from the 2 $mL.min^{-1}$ laboratory scale experiment used to record incremental increases in both the stationary and mobile phases during hydrodynamic equilibrium.

Time (min)	T_0	T_2	T_4	T_6	T_8	T_{10}	T_{12}	T_{14}	T_{16}
Total/Stat (mL)	42/12	44/14	48/18	52/20	56/22	60/22	64/22	68/22	72/22
Mobile (mL)	30	30	30	34	36	38	42	46	50

Table 13-3 Data collection chart illustrating measured volumes of stationary and mobile phases eluting from the CCC column during the establishment of hydrodynamic equilibrium for use in determining the stationary phase retention (S_f). T_0 corresponds to time zero (minutes) with all other subscript numbers correspond to real time values. Experiments performed as described in Section 5.2.1. S_f calculated as described in Section 3.1.1.

13.4. Mass balance data

This section provides representative qualitative and quantitative mass balance data from off-line HPLC analyses of collected CCC fractions for a range of operating conditions and scales of operation. Table 13-4 corresponds to mass balance data from a laboratory scale CCC experiment performed at 2 $mL.min^{-1}$ (100 mg solute loading) with the model system, as described in Section 4.1.3.2. Table 13-5 corresponds to mass balance data from the laboratory scale CCC experiment performed using the back extract (BE) feed at a mobile phase flow rate and solute loading of 2 $mL.min^{-1}$ and 100 mg respectively, as described in Section 7.4. Table 13-6 corresponds to mass balance data from the pilot scale CCC experiment with the model system at a mobile phase flow rate and solute loading of 10 $mL.min^{-1}$ and 1000 mg respectively (ω = 800 rpm), as described in Section 8.2.

Collection time (min)	Erythromycin concentration ($mg.mL^{-1}$)				TMIF (mg)	Purity of EA (% w/w)
	EC/ED	EA	EB/psu-EEA	EEA		
9-11	0.70	0.00	0.00	0.00	1.69	0.0
11-13	1.01	0.00	0.00	0.00	2.44	0.0
13-15	3.97	0.00	0.00	0.00	15.9	0.0
15-17	2.07	3.01	0.00	0.00	20.3	59.3
17-19	0.00	8.08	0.00	0.00	32.3	100.0
19-21	0.00	4.91	0.00	0.00	19.6	100.0
21-23	0.00	2.16	1.03	0.00	12.8	68.8
23-25	0.00	0.00	0.30	0.00	1.20	0.0
25-27	0.00	0.00	0.00	0.00	0.00	0.0
27-29	0.00	0.00	0.00	0.00	0.00	0.0

Table 13-4 **Quantitative mass balance data for the 2 $mL.min^{-1}$ laboratory scale CCC separation of erythromycin A using the model system. Initial solute concentration determined by HPLC to be 106 mg, giving a total solute yield of ~100% (w/w). Experiments performed as described in Section 4.1.3.2. TMIF represents the total mass of the erythromycins in each fraction (mg).**

Collection time (min)	Erythromycin concentration ($mg.mL^{-1}$)				TMIF (mg)	Purity of EA (% w/w)
	EC/ED	EA	EB/psu-EEA	EEA		
8-9	0.04	0.00	0.00	0.00	0.08	0.0
9-10	0.05	0.00	0.00	0.00	0.10	0.0
10-11	0.06	0.00	0.00	0.00	0.12	0.0
11-12	0.08	0.00	0.00	0.00	0.16	0.0
12-13	0.14	0.00	0.00	0.00	0.28	0.0
13-14	0.43	0.37	0.00	0.00	1.60	46.3
14-15	1.38	0.32	0.00	0.00	3.40	18.8
15-16	1.61	0.04	0.00	0.00	3.30	2.4
16-17	0.00	1.38	0.00	0.00	2.76	100.0
17-18	0.00	6.49	0.00	0.00	12.98	100.0
18-19	0.00	15.00	0.00	0.00	30.00	100.0
19-20	0.00	12.52	0.00	0.00	25.04	100.0
20-21	0.00	4.64	0.11	0.00	9.50	97.7
21-22	0.00	1.00	0.45	0.00	2.90	70.0
22-23	0.00	0.25	0.80	0.00	2.10	23.8
23-24	0.00	0.06	0.59	0.00	1.30	9.2
24-25	0.00	0.01	0.57	0.00	1.16	1.7
25-26	0.00	0.00	0.10	0.14	0.48	0.0
26-27	0.00	0.00	0.02	0.33	0.70	0.0
27-28	0.00	0.00	0.00	0.28	0.56	0.0
28-29	0.00	0.00	0.00	0.32	0.64	0.0
29-30	0.00	0.00	0.00	0.34	0.68	0.0
30-31	0.00	0.00	0.00	0.27	0.54	0.0
31-32	0.00	0.00	0.00	0.37	0.74	0.0
32-33	0.00	0.00	0.00	0.33	0.66	0.0
33-34	0.00	0.00	0.00	0.39	0.78	0.0
34-35	0.00	0.00	0.00	0.47	0.94	0.0
35-36	0.00	0.00	0.00	0.31	0.62	0.0
36-37	0.00	0.00	0.00	0.00	0.00	0.0
37-38	0.00	0.00	0.00	0.00	0.00	0.0

Table 13-5 **Quantitative mass balance data for the 2 $mL.min^{-1}$ laboratory scale CCC separation of erythromycin A using the back extract feed. Initial solute concentration determined by HPLC to be ~106 mg, giving a total solute yield of ~100% (w/w). Experiment performed as described in Section 7.4. TMIF represents the total mass of the erythromycins in each fraction (mg).**

Collection time (min)	Erythromycin concentration ($mg.mL^{-1}$)				TMIF (mg)	Purity of EA (% w/w)
	EC/ED	EA	EB/psu-EEA	EEA		
24-25	0.00	0.00	0.00	0.00	0.00	0.0
25-26	0.18	0.00	0.00	0.00	1.80	0.0
26-27	0.14	0.00	0.00	0.00	1.40	0.0
27-28	0.50	0.00	0.00	0.00	5.00	0.0
28-29	0.88	0.00	0.00	0.00	8.80	0.0
29-30	1.47	0.00	0.00	0.00	14.70	0.0
30-31	1.14	0.00	0.00	0.00	11.40	0.0
31-32	0.77	0.00	0.00	0.00	7.70	0.0
32-33	0.50	0.00	0.00	0.00	5.00	0.0
33-34	0.43	0.34	0.00	0.00	7.70	44.2
34-35	0.23	0.72	0.00	0.00	9.50	75.8
35-36	0.07	1.03	0.00	0.00	11.00	93.6
36-37	0.00	1.40	0.00	0.00	14.00	100.0
37-38	0.00	2.67	0.00	0.00	26.70	100.0
38-39	0.00	4.71	0.00	0.00	47.10	100.0
39-40	0.00	20.43	0.00	0.00	204.30	100.0
40-41	0.00	30.58	0.00	0.00	305.80	100.0
41-42	0.00	18.00	0.00	0.00	180.00	100.0
42-43	0.00	12.61	0.00	0.00	126.10	100.0
43-44	0.00	6.18	0.10	0.00	62.80	98.4
44-45	0.00	3.03	0.33	0.00	33.60	90.2
45-46	0.00	0.83	0.50	0.00	13.30	62.4
46-47	0.00	0.45	0.64	0.00	10.90	41.3
47-48	0.00	0.35	1.04	0.00	13.90	25.2
48-49	0.00	0.19	1.19	0.00	13.80	13.8
49-50	0.00	0.00	1.04	0.00	10.40	0.0
50-51	0.00	0.00	0.46	0.00	4.60	0.0
51-52	0.00	0.00	0.29	0.00	2.90	0.0
52-53	0.00	0.00	0.48	0.00	4.80	0.0
53-54	0.00	0.00	0.62	0.00	6.20	0.0

Table 13-6 **Quantitative mass balance data for the 10 $mL.min^{-1}$ pilot scale CCC separation of erythromycin A using the model feed (1000 mg). Initial solute concentration determined by HPLC to be ~1031 mg, giving a total solute yield of ~100% (w/w). Experiment performed as described in Section 8.2. TMIF represents the total mass of the erythromycins in each fraction (mg).**

13.5. Construction of Van deemter curves

This section demonstrates the experimental stages in the construction of the Van deemter curves, as illustrated in Section 10.4, together with the corresponding raw data.

STAGE 1

This involves the CCC separation of the crude erythromycin mixture, with the generation of the on-line trace of eluting mobile phase. An example CCC chromatogram from such an experiment is illustrated in Figure 13-4.

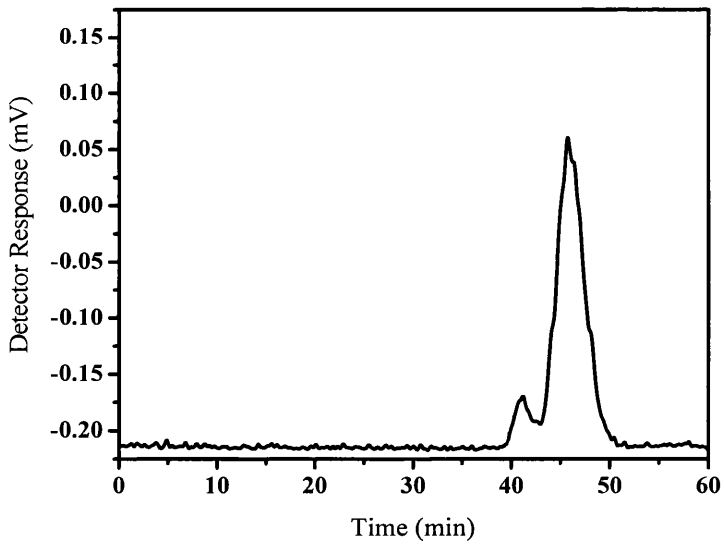

Figure 13-4 Representative laboratory scale CCC chromatogram of a crude erythromycin fractionation (100 mg) at a mobile phase flow rate of 2 mL.min^{-1} (S_f = 41.5%) using the ELSD for use in the construction of the Van deemter curve. Experiments performed as described in Section 2.4.1.1 and 2.4.1.2 using a quaternary solvent system comprising of hexane/ethyl acetate/methanol/water (1.4/2.0/2.0/1.0 v/v).

STAGE 2

From the CCC chromatogram, similar to that illustrated in Figure 13-1, the column efficiency was calculated using Equation 3.14. The values d_R and w_b in Equation 3.1.4 were determined directly from the CCC chromatogram for the main erythromycin A peak. Secondly the height equivalent to a theoretical plate (HETP) and the average linear mobile phase velocity ($\bar{u}$) were calculated as described in Section 3.4. Table 13-7 illustrates, for the range of experiments performed, the HETP and $\bar{u}$ values used in the construction of the Van deemter curve illustrated in Figure 10-1 (Section 10.4).

Flow rate ($mL.min^{-1}$)	Erythromycin A peak measurements		*N*	HETP or H (cm/plate)	$\bar{u}$ ($cm.s^{-1}$)
	d_R (min)	$d_{h/2}$ (min)			
0.5	131.8	12.7	594	8.01	0.75
1.0	67.5	5.0	1009	4.71	1.49
1.5	45.7	3.3	1040	4.58	2.24
2.0	34.4	2.9	775	6.14	2.98
4	17.5	1.9	483	9.86	5.96
6	12.5	1.2	573	8.31	8.94

Table 13-7 Data used in the construction of the Van deemter curve as illustrated in Figure 10-1. d_R and $d_{h/2}$ obtained directly from corresponding CCC chromatograms. Column efficiency (*N*) calculated using Equation 3.14. HETP calculated as described in Section 3.4, with $\bar{u}$ calculated using Equation 3.32.